

AD-A145 115

PIEZOELECTRIC AND ELECTROSTRICTIVE MATERIALS FOR  
TRANSDUCER APPLICATIONS(U) PENNSYLVANIA STATE UNIV  
UNIVERSITY PARK MATERIALS RESEARCH LAB

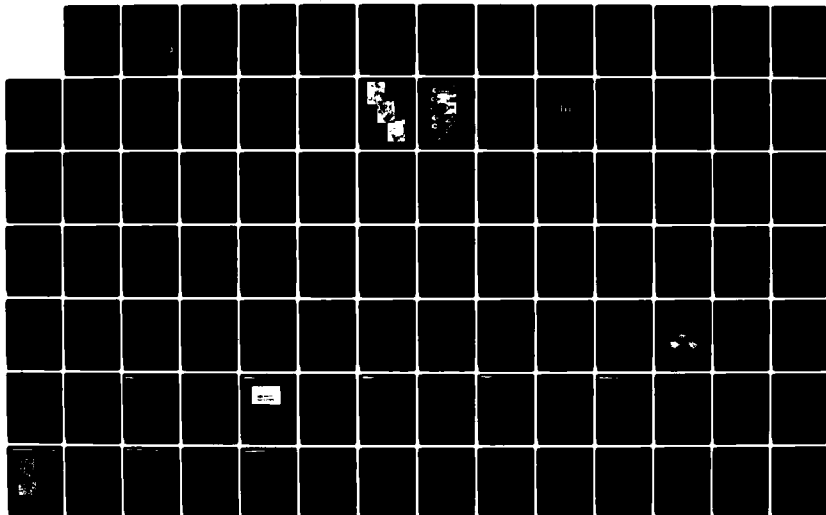
1/4

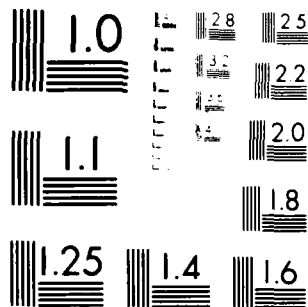
UNCLASSIFIED

L F CROSS ET AL MAY 84 N00014-82-K-0339

F/G 20/3

NL





MICROCOPY RESOLUTION TEST CHART  
 NATIONAL BUREAU OF STANDARDS-1963-A

(12)

**PIEZOELECTRIC AND ELECTROSTRICTIVE MATERIALS  
FOR TRANSDUCER APPLICATIONS**

**Annual Report to  
OFFICE OF NAVAL RESEARCH**

**Contract No. N00014-82-K0339**

**APPROVED FOR PUBLIC RELEASE - DISTRIBUTION UNLIMITED**

**Reproduction in whole or in part is permitted for  
any purpose of the United States Government**

**L.E. Cross  
R.E. Newnham  
G.R. Barsch  
J.V. Biggers**

**May, 1984**

**DTIC**  
**S** **AUG 3 0 1984** **D**  
**H**

**DTIC FILE COPY**



**THE MATERIALS RESEARCH LABORATORY**

**THE PENNSYLVANIA STATE UNIVERSITY**

**UNIVERSITY PARK, PENNSYLVANIA**

**84 08 28 006**

## TABLE OF CONTENTS


	<u>Page</u>
1. INTRODUCTION. . . . .	1
2. SUMMARY OF ACCOMPLISHMENTS. . . . .	1
2.1 Piezoelectric Composites . . . . .	1
2.2 Electrostriction . . . . .	3
2.3 Conventional Piezoelectrics. . . . .	4
3. COMPOSITE MATERIALS . . . . .	13
3.1 Transversely Reinforced 1-3 and 1-3-0 PZT: Polymer Composite. .	13
3.2 PZT:Polymer Composites with 3:1 and 3:2 Connection . . . . .	16
3.3 Finite Element Calculations of the Stress Distribution in 3:1 Perforated PZT:Polymer Composites. . . . .	19
3.4 Fresnoite: Oriented Polar Glass Ceramics for Hydrophone Applications . . . . .	24
4. ELECTROSTRICTION STUDIES. . . . .	25
4.1 Theoretical Studies. . . . .	25
4.1.1 Static Lattice Calculations for $KZnF_3$ and $KMnF_3$ . . . . .	25
4.1.2 Temperature Dependence of Electrostriction in $SrTiO_3$ . . .	25
4.2 Experimental Electrostriction. . . . .	27
4.2.1 Measurements by the Direct Method . . . . .	27
4.2.2 Measurements by the Converse Method . . . . .	28
4.2.3 Electrostriction in High Permittivity Crystals. . . . .	29
4.2.3.1 Introduction . . . . .	29
4.2.3.2 Instrumentation. . . . .	32
4.2.3.3 Measurements on $BaTiO_3$ . . . . .	34
4.2.3.4 Electrostriction in the Uniaxial Ferroelectric $Sr_{0.61}Ba_{0.39}Nb_2O_6$ . . . . .	35
4.2.3.5 Practical Electrostrictors . . . . .	38
5. CONVENTIONAL PIEZOELECTRIC CERAMICS . . . . .	39
5.1 Introduction . . . . .	39
5.2 Low Temperature Measurements . . . . .	40
5.3 Diffraction Studies. . . . .	41
5.3.1 Neutron Diffraction of $Pb(Zr_{0.6}Ti_{0.4})O_3$ . . . . .	41
5.3.2 High Temperature X-ray Studies. . . . .	41
5.4 Poling Studies . . . . .	43
5.4.1 Continuous Poling . . . . .	43
5.4.2 Curie Point Poling of PZT 501A. . . . .	43



6. PREPARATIVE STUDIES . . . . .	43
6.1 Reaction Sequence in the Formation of Lead Zirconate:Lead Titanate . . . . .	43
6.2 Molten Salt Synthesis. . . . .	44
6.2.1 Preparation of Lead Metaniobate . . . . .	44
6.2.2 Grain Oriented $\text{PbBi}_2\text{Nb}_2\text{O}_9$ . . . . .	44
6.3 Synthesis of $\text{PbTiO}_3\text{:BiFeO}_3$ Solid Solution. . . . .	44
6.4 Relaxor Ferroelectrics . . . . .	45
6.5 Crystal Growth . . . . .	46
6.5.1 Perovskite Halides. . . . .	46
6.5.2 $\text{Pb}_{1-x}\text{Ba}_x\text{Nb}_2\text{O}_6$ . . . . .	46
REFERENCES. . . . .	48
APPENDICES. . . . .	50

UNCLASSIFIED

SECURITY CLASSIFICATION OF THIS PAGE (When Data Entered)

REPORT DOCUMENTATION PAGE		READ INSTRUCTIONS BEFORE COMPLETING FORM																				
1. REPORT NUMBER	2. GOVT ACCESSION NO.	3. RECIPIENT'S CATALOG NUMBER																				
4. TITLE (and Subtitle) PIEZOELECTRIC AND ELECTROSTRICTIVE MATERIALS FOR TRANSDUCER APPLICATIONS		5. TYPE OF REPORT & PERIOD COVERED																				
		6. PERFORMING ORG. REPORT NUMBER																				
7. AUTHOR(s) L.E. Cross, R.E. Lewnham, G.R. Barsch and J.V. Biggers		8. CONTRACT OR GRANT NUMBER(s) N00014-82-K0339																				
9. PERFORMING ORGANIZATION NAME AND ADDRESS Materials Research Laboratory The Pennsylvania State University University Park, PA 16802		10. PROGRAM ELEMENT, PROJECT, TASK AREA & WORK UNIT NUMBERS																				
11. CONTROLLING OFFICE NAME AND ADDRESS Office of Naval Research Room 619 Ballston Tower, 800 N. Quincy St. Arlington, VA 22217		12. REPORT DATE																				
		13. NUMBER OF PAGES May, 1984																				
14. MONITORING AGENCY NAME & ADDRESS (if different from Controlling Office)		15. SECURITY CLASS. (of this report)  UNCLASSIFIED																				
		15a. DECLASSIFICATION/DOWNGRADING SCHEDULE																				
16. DISTRIBUTION STATEMENT (of this Report)  Reproduction in whole or in part is permitted for any purpose of the United States Government																						
17. DISTRIBUTION STATEMENT (of the abstract entered in Block 20, if different from Report)																						
18. SUPPLEMENTARY NOTES		 <table border="1"> <tr> <td colspan="2">Accession For</td> </tr> <tr> <td>NTIS GRA&amp;I</td> <td><input checked="" type="checkbox"/></td> </tr> <tr> <td>DTIC TAB</td> <td><input type="checkbox"/></td> </tr> <tr> <td>Unannounced</td> <td><input type="checkbox"/></td> </tr> <tr> <td>Justification</td> <td></td> </tr> <tr> <td colspan="2">By</td> </tr> <tr> <td colspan="2">Distribution/</td> </tr> <tr> <td colspan="2">Availability Codes</td> </tr> <tr> <td>Dist</td> <td>Avail and/or Special</td> </tr> <tr> <td>A-1</td> <td></td> </tr> </table>	Accession For		NTIS GRA&I	<input checked="" type="checkbox"/>	DTIC TAB	<input type="checkbox"/>	Unannounced	<input type="checkbox"/>	Justification		By		Distribution/		Availability Codes		Dist	Avail and/or Special	A-1	
Accession For																						
NTIS GRA&I	<input checked="" type="checkbox"/>																					
DTIC TAB	<input type="checkbox"/>																					
Unannounced	<input type="checkbox"/>																					
Justification																						
By																						
Distribution/																						
Availability Codes																						
Dist	Avail and/or Special																					
A-1																						
19. KEY WORDS (Continue on reverse side if necessary and identify by block number)																						
20. ABSTRACT (Continue on reverse side if necessary and identify by block number)  (See Back of this page.)																						

This report covers work accomplished during the first year of a new 3-year contract No. N00014-82-K0339 for the study of "Piezoelectric and Electrostrictive Materials for Transducer Applications." The work reported covers a rather wide range of topics and for convenience, it is divided into four major sections.

(1) > COMPOSITE MATERIALS FOR TRANSDUCER APPLICATIONS;

This covers new work on the 3:1 and 3:2 connected perforated PZT:polymer composites, forming hydrophone transducer materials of excellent sensitivity and stability. A refined study of 1:3 and 1:3:0 connected transversely reinforced PZT-polymer systems which show the highest sensitivity for low hydrostatic static pressures. Finite element theoretical methods have been used to calculate the stress distribution and sensitivity of the 3:1 configuration with excellent agreement to experiment. This year a new family of polar glass ceramics has been evaluated for hydrophone application, showing good sensitivity with excellent stability and no aging.

(2) ~ELECTROSTRICTION;

Work has included extension of atomistic calculations of electrostriction constants to the fluoride perovskites and to the temperature dependence of electrostriction in  $\text{SrTiO}_3$ . Experimentally problems of measuring alkali halide crystals by the direct method have been traced to the charged dislocation structure and a new equipment has been built to make measurements of the converse effect, and applied successfully to measure  $\text{CaF}_2$ . Temperature dependence of the  $Q_{ijk}$  constants has been determined for  $\text{BaTiO}_3$  and for  $\text{Ba}_{0.39}\text{Sr}_{0.61}\text{Nb}_2\text{O}_6$  giving clear evidence of the importance of polarization fluctuations at temperatures close to  $T_c$  in the uniaxial ferroelectrics.

(3) ~CONVENTIONAL PIEZOELECTRICS;

Low temperature measurements are being continued and are compared to basic phenomenological calculations to separate intrinsic and extrinsic contributions to the dielectric and piezoelectric behavior in pure and in doped PZTs. X-ray methods have been used to examine heterogeneity in the Zr:Ti distribution for PZTs from several different Navy sources.

(4) ~PREPARATIVE STUDIES.

Work has ranged through calcining studies of PZTs, fabrication of grain oriented  $\text{PbNb}_2\text{O}_6$  and  $\text{PbBi}_2\text{Nb}_2\text{O}_6$ , preparation of new high c/a ratio powders in the  $\text{PbTiO}_3\text{:BiFeO}_3$  solid solutions and the growth of single crystals of halide perovskites for electrostriction studies and of  $\text{Pb}_{0.6}\text{Ba}_{0.4}\text{Nb}_2\text{O}_6$  bronze ferroelectrics for single crystal study of a model morphotropic phase boundary.

Over the contract year, 33 papers relating to work on the contract have been published in refereed journals and 39 presentations have been given at National and International meetings. One Ph.D., 3 M.S. and 4 B.S. theses topics were stimulated from contract studies.

## 1. INTRODUCTION

This report covers work which has been accomplished during the first year of a new ONR Contract No. N00014-82-K-0339 for the study of 'Piezoelectric and Electrostrictive Materials for Transducer Applications'. A number of the topics covered represent development and extension of studies accomplished on our earlier contract 'Targeted Basic Studies of Piezoelectric and Electrostrictive Materials for Transducer Applications' and have capitalized on the momentum generated in the earlier studies. A number, however, are also completely new topics.

Since the work to be reported covers a rather wide range of materials and device applications, it has been divided for convenience into four major sections.

- (1) COMPOSITE MATERIALS FOR TRANSDUCER APPLICATION
- (2) ELECTROSTRICTION
- (3) CONVENTIONAL PIEZOELECTRICS
- (4) PREPARATIVE STUDIES

Following previous practice in earlier piezoelectric report, a brief narrative description is given of current on going work. Completed topics are included as preprints or reprints of published papers.

## 2. SUMMARY OF ACCOMPLISHMENTS

2.1 In the piezoelectric composites, important progress has been made in:

- (a) 3:1 and 3:2 Perforated PZT:Polymer Composites.

These materials exhibit very high sensitivity with  $d_{hg_h}$  products of up to  $40,000 \times 10^{-15} \text{ m}^2/\text{V}$  and very little change of sensitivity under hydrostatic pressure. This work has now been largely completed and is discussed in detail in the Ph.D thesis of Dr. A. Safari<sup>(1)</sup>.

(b) 1:1:1:3 Transverse Reinforced Composites. .

The highest sensitivities to date, with  $d_{hg}h$  products up to  $150,000 \times 10^{-15} \text{ m}^2/\text{V}$  have been achieved in the foamed transversely reinforced 1:3 composites. Mr. M. Hann completed this study for his M.S. thesis in Solid State Science<sup>(2)</sup>. His results have recently been confirmed by similar studies at Plessey Company in the United Kingdom and published in a recent paper by Shorrocks, Brown, Whatmore and Ainger<sup>(3)</sup>.

(c) The first finite element calculations of the stress distribution in 1:3 PZT polymer composites have been carried out. The predicted stress distributions appear reasonable and the calculated sensitivities are in good agreement with A. Safari's measured values.

(d) The fresnoite glass ceramics which were being developed as polar composites for pyroelectric application have been shown to exhibit both high sensitivity ( $d_{hg}h \sim 1,000 \times 10^{-15} \text{ m}^2/\text{V}$ ) and extreme stability in measurements by Ting<sup>(4)</sup> at Orlando. The polar glass ceramic can show no aging and appears very stable to exceedingly high hydrostatic pressures.

(e) Following the work of Banno<sup>(5)</sup> in NGK, a new water quenching technique has been used to develop  $\text{PbTiO}_3$  and  $\text{PbTiO}_3:\text{BiFeO}_3$  powders for 0:3 composites.

(f) In a joint program with North American Philips Laboratories, a detailed analysis of the resonant modes of 1:3 PZT:epoxy composites has been carried out. The results follow closely the expected performance as a function of scaling for the thickness modes and confirm the advantage of the composite (suitably scaled) for electromedical transduction<sup>(6)</sup>.

A cooperative study with Dr. Auld and his group at Stanford<sup>(7)</sup> has revealed a most interesting spectrum of transverse modes, and Dr. Auld has developed a two dimensional lattice theory which explains the observed spectra<sup>(8)</sup>.

## 2.2 Electrostriction

### (a) Basic Theory

Calculations of the hydrostatic electrostriction constant  $Q_h$  and of the third order elastic constant  $c_{111}$  have been made for the non-ferroelectric fluoride perovskite  $KZnF_3$  and the values are in excellent agreement with the experimental measurements of K. Rittenmyer<sup>(9)</sup>.

A new derivation has been made of the temperature dependence of the  $Q_h$  in  $SrTiO_3$  which now takes proper account of the soft mode behavior and gives much better agreement with experimental values.

### (b) Basic Experiments

Problems which have plagued us for more than 5 years in our attempts to make direct dilatometric measurements of the separated electrostriction constants  $Q_{ij}$  in NaCl have been traced to the dislocation structure in the crystals. Pinning the dislocations by intense neutron irradiation gives much better values, but does not remove all frequency dependence for  $Q_{11}$ .

A new equipment has now been completed for measurements of the uniaxial stress dependence of the dielectric permittivity which is the converse of the electrostrictive effect. Measurements on  $CaF_2$  yield high reproducibility and appear completely consistent with phenomenological correlation.

### (c) Practical Electrostrictors

Measurements in the PLZT family suggest that the slim loop 9.5:65:35 material is a superparaelectric comparable in most properties to  $PbMg_{1/3}Nb_{2/3}O_3:PbTiO_3$ . The 8.5:65:35 composition is more sensitive than the PMN:10% PT, but probably a little slower in electrostrictive response.

### 2.3 Conventional Piezoelectrics

(A) A combination of the thermodynamic data of A. Amin<sup>(10)</sup>, and the low temperature data of Chen, Zhang, Schulze and Cross<sup>(11)</sup> has been used to separate extrinsic (domain and phase boundary motion) from intrinsic single domain contributions to  $\epsilon_{33}$ ,  $d_{31}$  and  $d_{33}$  in pure and in commercial doped PZTs.

(b) Preliminary x-ray studies at temperatures above the Curie temperature  $T_c$  have verified that Navy type PZTs from different manufacturers do have distinguishably different degrees of x-ray line broadening suggesting differing degrees of heterogeneity in the Zr:Ti distribution.

### 2.4 Processing Studies

(a) New high strain  $\text{PbTiO}_3\text{:BiFeO}_3$  solid solutions have been developed and powders of these materials generated by water quenching.

(b) A wide range of solid substitutions are being explored in the  $\text{PbMg}_{1/3}\text{Nb}_{2/3}\text{O}_3\text{:PbTiO}_3$  and in the  $\text{PbMg}_{1/3}\text{Nb}_{2/3}\text{O}_3\text{:PbFe}_{1/2}\text{Nb}_{1/2}\text{O}_3$  solid solution relaxor systems. This work is jointly with the Dielectric Center programs as these materials are interesting both for electrostrictive and for their high dielectric constants.

(c) In single crystal growth large crystals of the non-oxide perovskite  $\text{KMnF}_3$  have been grown for electrostriction and non-linear elastic constant measurements.

In cooperation with Rockwell Science Center solid solutions in the  $\text{Pb}_{1-x}\text{Ba}_x\text{Nb}_2\text{O}_6$  at compositions close to the morphotropic boundary at  $x = 0.6$  have been grown into single crystals. The interest in Rockwell is in the high electro-optic  $r_{41}$ ,  $r_{52}$  and in the possibility for temperature compensated SAW application.

For this program, the interest is in generating a single crystal material upon which the nature of the field induced morphotropic change may be explored

by simple optical techniques and the full tensor properties measured upon oriented crystal samples.

Over the period of the contract from January 1, 1983, to December 31, 1983, the following papers were published.

- (1) A. Safari, 'Perforated PZT-Polymer Composites with 3-1 and 3-2 Connectivity for Hydrophone Applications.' Ph.D. Thesis in Solid State Science, The Pennsylvania State University (December, 1983).
- (2) M. Haun, 'Transversely Reinforced 1:3 and 1:3:0 PZT:Polymer Piezoelectric Composites with Glass Fibers.' M.S. Thesis in Solid State Science, The Pennsylvania State University (December, 1983).
- (3) E. Galgochi, 'Polymer:PZT Fiber Composites.' M.S. Thesis in Polymer Science, The Pennsylvania State University (August, 1983).
- (4) M.J. Haun, P. Moses, T.R. Gururaja, W.A. Schulze and R.E. Newnham, 'Transversely Reinforced 1-3 and 1-3-0 Piezoelectric Composites.' *Ferroelectrics* 49:259 (1983).
- (5) R.E. Newnham and J. Runt, 'Polymer:Piezoelectric Ceramics.' *Polymer News* (in press).
- (6) J. Runt and E.C. Galgochi, 'Piezoelectric Composites of PZT and Some Semi-Crystalline Polymers.' *Materials Research Bulletin* 19:253 (1984).
- (7) J. Runt and E.C. Galgochi, 'Polymer/Piezoelectric Ceramic Composites: Polystyrene and Poly (methyl methacrylate) with PZT.' *Journal of Applied Polymer Sciences* 29:611 (1984).
- (8) T.R. Gururaja, W.A. Schulze, L.E. Cross, B.A. Auld, Y.A. Shui and Y. Wang, 'Resonant Modes of Vibration in Piezoelectric PZT:Polymer Composites with Two Dimensional Periodicity.' *Ferroelectrics* 54:183-186 (1984).
- (9) W. Schulze, 'The Incorporation of Rigid Composites into a Conformal Hydrophones.' *Ferroelectrics* 50:359 (1983).



- (10) M. Shishineh, 'A New Technique for Measuring Electrostriction Coefficients at Elevated Temperature.' M.S. Thesis in Electrical Engineering, The Pennsylvania State University (December, 1983).
- (11) C.L. Sundius, 'Determination of Temperature Dependence of Electrostriction Coefficients in Strontium Barium Niobate.' M.S. Thesis in Solid State Science, The Pennsylvania State University (December, 1983).
- (12) K. Rittenmyer, A.S. Bhalla, Z.P. Chang and L.E. Cross, 'Electrostriction and Its Relation to Other Properties in Perovskite Type Crystals.' *Ferroelectrics* 50:535-543 (1983).
- (13) M. Shishineh, C.L. Sundius, T. Shrout and L.E. Cross, 'Direct Measurement of Electrostriction in Perovskite Type Ferroelectrics' *Ferroelectrics* 50:219-224 (1983).
- (14) Yao Xi, Chen Zhili and L.E. Cross, 'Polarization and Depolarization Behavior of Hot Pressed Lead Lanthanum Zirconate Titanate Ceramics.' *Ferroelectrics* 54:163-166 (1984).
- (15) Chen Zhili, Yao Xi and L.E. Cross, 'Depolarization Behavior and Reversible Pyroelectricity in Lead Scandium tantalate Ceramics under D.C. Bias.' *Ferroelectrics* 49:213-217 (1983).
- (16) K. Uchino, S. Nomura and L.E. Cross, 'Anomalous Temperature Dependence of Electrostrictive Coefficient in  $K(\text{Ta}_{0.55}\text{Nb}_{0.45})\text{O}_3$ .' *J. Phys. Soc. Jpn.* 51:3242 (1982).
- (17) Chen Zhili, Yao Xi and L.E. Cross, 'Reversible Pyroelectric Effect in  $\text{Pb}(\text{Sc}_{1/2}\text{Ta}_{1/2})\text{O}_3$  Ceramics Under D.C. Bias.' *Ferroelectrics Letters* 44:271 (1983).
- (18) Yao Xi, Chen Zhili and L.E. Cross, 'Polarization and Depolarization Behavior of Hot Pressed Lead Lanthanum Zirconate Titanate Ceramics.' *J. Appl. Phys.* 54(6):3399 (1983).

- (19) T.R. Shrout, H. Chen and L.E. Cross, 'Dielectric and Piezoelectric Properties of  $Pb_{1-x}Ba_xNb_2O_6$  Ferroelectric Tungsten Bronze Crystals.' *Ferroelectrics Letters* 44:325 (1983).
- (20) T. Kimura, M. Machida, T. Yamaguchi and R.E. Newnham, 'Products of Reaction Between  $PbO$  and  $Nb_2O_5$  in Molten  $KCl$  and  $NaCl$ . *J. Amer. Ceram. Soc.* 66:C195 (1983).
- (21) S. Lin, S.L. Swartz, W.A. Schulze and J.V. Biggers, 'Fabrication of Grain Oriented  $PbBi_2Nb_2O_9$ .' *J. Amer. Ceram. Soc.* 66(12):881-884 (1983).
- (22) A. Halliyal, A. Safari, A.S. Bhalla and R.E. Newnham, 'Grain Oriented Glass Ceramics: New Materials for Hydrophone Applications.' *Ferroelectrics* 50:45-50 (1983).
- (23) R.Y. Ting, A.G. Halliyal and A. Bhalla, 'Polar Glass Ceramics for Sonar Transducers.' *Appl. Phys. Letters* 44:852-854 (1984).
- (24) A. Halliyal, A. Safari, A.S. Bhalla, R.E. Newnham and L.E. Cross, 'Grain Oriented Glass Ceramics for Piezoelectric Devices.' *J. Amer. Ceram. Soc.* 67(5):305 (1984).
- (25) K. Uchino and L.E. Cross, 'Longitudinal Piezoelectric Strain Measurements of Poly (vinylidene fluoride) Films.' *J. Polymer Sci.* 21:765 (1983).
- (26) X.L. Zhang, Z.X. Chen, L.E. Cross and W.A. Schulze, 'Dielectric and Piezoelectric Properties of Modified Lead Titanate Zirconate Ceramics from 4.2 to 300°K.' *J. Mat. Sci.* 18:968 (1983).
- (27) T.R. Gururaja, D. Christopher, R.E. Newnham and W.A. Schulze, 'Continuous Poling of PZT Fibers and Ribbons and Its Application to New Devices.' *Ferroelectrics* 47:193 (1983).
- (28) A. Amin and L.E. Cross, 'The Ferroic Phase Transition Behavior of  $Pb(Zr_{0.6}Ti_{0.4})O_3$ .' *Ferroelectrics* 50:237-241 (1983).

- (29) T.R. Shrout, A. Safari and W.A. Schulze, 'Low Field Poling of Soft PZTs.' *Ferroelectrics Letters* 44:227 (1983).
- (30) B.V. Haremath, A. Kington and J.V. Biggers, 'Reaction Sequences in the Formation of Lead Zirconate:Lead Titanate Solid Solutions: Role of Raw Materials.' *J. Amer. Ceram. Soc.* 66(11):790 (1983).
- (31) A.S. Bhalla, C.S. Fang, L.E. Cross and Yao Xi, 'Pyroelectric Properties of Modified Triglycine Sulphate (TGS) Single Crystals.' *Ferroelectrics* 14:151-154 (1984).
- (32) C.S. Fang, Yao Xi, A.S. Bhalla and L.E. Cross, 'The Growth and Properties of a New Alanine and Phosphate Substituted Triglycine Sulphate (ATGSP) Crystal.' *Ferroelectric* 51:669-673 (1983).
- (33) S.T. Liu and A.S. Bhalla, 'Some Interesting Properties of Dislocation-Free Single Crystals for Pure and Modified  $\text{Sr}_{0.5}\text{Ba}_{0.5}\text{Nb}_2\text{O}_6$ .' *Ferroelectrics* 51:707-711 (1983).

Over the year, the following papers relevant to work on this contract, were presented at National and International Meetings.

PAPERS PRESENTED AT THE INTERNATIONAL SYMPOSIUM ON APPLICATIONS OF  
FERROELECTRICS ISAF 83 N.B.S., WASHINGTON, DC, JUNE, 1983

- (1) 1B-1 Ferroelectric Composites (invited) - R.E. Newnham.
- (2) 7B-1 Electrostriction (invited) - L.E. Cross.
- (3) 4B-6 Transversely Reinforced 1-3 Piezoelectric Composites - M.J. Haun,  
T.R. Gururaja, W.A. Schulze and R.E. Newnham.
- (4) 4B-5 Perforated PZT Composites for Hydrophone Applications - A. Safari,  
S. DaVanzo and R.E. Newnham.
- (5) 5B-7 Glass-Ceramics: New Materials for Hydrophone Applications - A.  
Halliyal, A. Safari and A.S. Bhalla.

- (6) 4B-2 Measurement of Plantar Pressures Under the Human Foot Using Piezoelectric Ceramics (invited) - P.R. Cavanagh and N. Macmillan.
- (7) 7B-6 Electrostriction and Its Relationship to Other Properties in Perovskite-Type Crystals - K. Rittenmyer, A.S. Bhalla, Z.P. Chang and L.E. Cross.
- (8) 7B-5 The Effects of Various B-Site Modifications on the Dielectric and Electrostrictive Properties of Lead Magnesium Niobate Ceramics - D.J. Voss, S.L. Swartz and T.R. Shrout.
- (9) 7B-7 Direct Measurement of Electrostriction in Perovskite Type Ferroelectrics - M. Shishineh, C. Sundius, T. Shrout and L.E. Cross.
- (10) 4A-5 Pyroelectric Property of  $\text{Pb}(\text{Sc}_{1/2}\text{Ta}_{1/2})\text{O}_3$  Ceramics Under DC Bias - C. Zhili, Y. Xi and L.E. Cross.
- (11) 8A-2 The Ferroic Phase Transition Behavior of  $\text{Pb}(\text{Zr}_{0.6}\text{Ti}_{0.4})\text{O}_3$  - A. Amin and L.E. Cross.
- (12) 4A-2 Low Temperature Pyroelectric Properties - A.S. Bhalla and R.E. Newnham.
- (13) 10A-2 The Growth and Properties of a New Alanine and Phosphate Substituted Triglycine Sulphate (ATGSP) Crystal - C.S. Fang, Y. Xi, Z.X. Chen, A.S. Bhalla and L.E. Cross.
- (14) 10A-8 Some Interesting Properties of Dislocation Free Single Crystals of Pure and Modified  $\text{Sr}_{0.5}\text{Ba}_{0.5}\text{Nb}_2\text{O}_6$  - S.T. Liu and A.S. Bhalla.

PAPERS PRESENTED AT THE EUROPEAN MEETING

ON FERROELECTRICS EMF5, BENALMADENA, SPAIN, 1983

- (16) P1D10 Electrical Poling and Depoling Studies of the Relaxor Ferroelectric 8:65:35 PLZT - Z. Chen, Y. Xi and L.E. Cross

- (17) P1D16 PZT:Polymer Composite Transducers for Ultrasonic Medical Applications - T.R. Gururaja, W.A. Schulze, L.E. Cross, S.A. Auld, J. Wang and Y.A. Shui
- (18) P1D7 Pyroelectric Properties of Modified Triglycine Sulphate (TGS) - A.S. Bhalla, C.S. Fang, L.E. Cross and Yao Xi
- (19) P1D18 A New Family of Grain Oriented Glass Ceramics for Piezoelectric and Pyroelectric Applications - A. Halliyal and A.S. Bhalla
- (20) P4B4 Pyroelectric and Piezoelectric Properties of SbSI:Composites - A.S. Bhalla and R.E. Newnham
- (21) P4B18 Dielectric and Piezoelectric Properties of Tungsten Bronze Lead Barium Niobate ( $\text{Pb}_x\text{Ba}_{1-x}\text{Nb}_2\text{O}_6$ ) Single Crystals - T.R. Shrout, H.C. Chen and L.E. Cross

PAPERS PRESENTED AT THE FALL MEETING OF THE ELECTRONICS

DIVISION OF THE AMERICAN CERAMIC SOCIETY, GROSSINGERS, NEW YORK, 1983

- (22) 2E83F Relaxor Ferroelectrics - L.E. Cross
- (23) 37E83F Piezoelectric Composites - R.E. Newnham
- (24) 39E83F Pyroelectric and Piezoelectric Properties of SbSI:Composites - A.S. Bhalla and R.E. Newnham
- (25) 40E83F Effects of  $\text{Sm}_2\text{O}_3$  on Electromechanical Properties of  $\text{PbTiO}_3$  Ceramics - W.R. Ine, W. Schulze and R.E. Newnham
- (26) 44E83F Perforated PZT Composites for Hydrophone Applications - A. Safari, S. DeVanzo and R.E. Newnham
- (27) 18E83 Processing Effects in  $\text{PbNb}_2\text{O}_6$  Ceramics - M. Bliss, R.E. Newnham and L.E. Cross
- (28) 20E83 Dielectric Properties in the  $\text{PbFe}_{1/3}\text{Nb}_{2/3}\text{O}_3$ : $\text{PbNi}_{1/3}\text{Nb}_{2/3}\text{O}_3$  Solid Solution System - M.J. Haun, S.L. Swartz and T.R. Shrout

- (29) 58E83    The Ferroelectric Properties of  $\text{Pb}_{1-2x}\text{K}_x\text{M}_x^{3+}\text{Nb}_2\text{O}_6$  M = La or Bi -  
J.R. Oliver, R.R. Neurgaonkar and L.E. Cross
- (30) 59E83    Growth and Properties of Li Doped TGS Crystals - C.S. Fang, Z.X.  
Chen, L.E. Cross and A. Bhalla
- (31) 63E83    Strength of Agglomerated Zirconia Powder - W.R. Xue, B.V.  
Hiremath and J.V. Biggers
- (32) 35E83    Piezoelectric Transducers - L.E. Cross

PAPERS PRESENTED AT IEEE ANNUAL MEETING ON

SONICS AND ULTRASONICS, ATLANTA, 1983

- (33)            Piezoelectric Composites - L.E. Cross and R.E. Newnham

PAPERS PRESENTED AT THE ANNUAL MEETING OF

THE MATERIALS RESEARCH SOCIETY, BOSTON, NOVEMBER, 1983

- (34) B6.1      Design of Composite Materials for Electro-Mechanical and Electro-  
Thermal Applications - L.E. Cross
- (35) X.3.2      Structure-Property Relations in Electronic Ceramics - R.E.  
Newnham

PAPERS PRESENTED AT US:CHINA SEMINAR ON CERAMIC, SHANGHAI, 1983

- (36)            Ferroelectric and Piezoelectric Effects in Crystalline  
Dielectrics - L.E. Cross

AMERICAN CRYSTALLOGRAPHIC ASSOCIATION MEETING, SNOWMASS, COLORADO, 1983

- (37)            Influence of Hydrostatic Pressure on Morpnic PZT Compositions -  
A. Amin, R.E. Newnham and L.E. Cross
- (38)            Primary and Secondary Pyroelectricity in Crystals, Ceramics and  
Composites - A.S. Bhalla and R.E. Newnham

INTERNATIONAL SYMPOSIUM ON PIEZOELECTRIC POLYMERS AND THEIR  
BIOMEDICAL APPLICATIONS, PISA, ITALY, 1983

(39)            Piezoelectric Composites - R.E. Newnham

During the contract year, the following University degrees have been earned by graduate and undergraduate students working upon the program.

GRADUATE DEGREES - M.S., Ph.D.

Ahmad Safari	Ph.D., Solid State Science - December, 1983 'Perforated PZT-Polymer Composites with 3-1 and 3-2 Connectivity for Hydrophone Application'
Michael Haun	M.S., Ceramic Science - December, 1983 'Transverse Reinforced 1-3 and 1-3-0 PZT-Polymer Piezoelectric Composites with Glass Fibers'
Mojtaba Shishineh	M.S., Electrical Engineering - December, 1983 'A New Technique for Measuring Electrostriction Coefficients at Elevated Temperatures'
Carole L. Sundius	M.S., Solid State Science - December, 1983 'Determination of the Temperature Dependence of Electrostriction Coefficients in Strontium Barium Niobate'

UNDERGRADUATE THESIS PROJECT - B.S.

Daniel Armbrust	B.S., Ceramic Science and Engineering - May, 1983 'Bismuth Tungstate Ferroelectrics'
R. Michelle Gedrjiewski	B.S., Ceramic Science and Engineering - May, 1983 'Composites for Vibration Absorbers'
Deborah Murphy	B.S., Ceramic Science and Engineering - May, 1983 'Morphotropic Phase Boundary in the $\text{PbTiO}_3\text{:BiFeO}_3\text{:LaFeO}_3$ System'
Lisa Veitch	B.S., Ceramic Science and Engineering - May, 1983 ' $\text{Pb}(\text{NiNb})\text{O}_3$ Ceramics for Low Temperature Electrostrictive Applications'
James Walch	B.S., Ceramic Science and Engineering - May, 1983 'X-Ray Line Broadening Studies of PZTs'

During the Summer of 1983, the Office of Naval Research again provided support for a Summer Apprentices Program in Applied Sciences to permit minority

students who were considering Science as a vocation to have 'hands on' experience in a basic research laboratory. The students, Cheryl Y. Price and Lucius Smart, were potential entrants to the University Science College through the 'Upward Bound' Program in their high school in Philadelphia and the coordinator in Penn State. Bridget Chadwick is a State College girl now enrolled in our College of Engineering in the Electrical Engineering Program.

Each student was attached to one of our more senior graduate students for immediate supervision. Some indication of their involvements with computer aided measurements, mechanical design of test specimens and optical characterization of composites can be seen in Figure 1.

We are proud and pleased to be able to participate in this most useful 'outreach' program and are convinced that the benefits both to the students and the program justifies the small cost.

Work on this program was again recognized for its excellence in the University wide Xerox Awards for Research Excellence for the 1982-83 academic year. David Christopher who took the award for Research Accomplishment for an Undergraduate was doing his thesis project upon this ONR program. Keven G. Ewsuk an M.S. recipient made extensive use of the H.I.P. equipment and was a regular participant in group meetings, though his support came from another program. James Laughner one of the Ph.D. awardees was a long standing member of the ferroelectrics group whose work was supervised by R.E. Newnham (Figure 2).

### 3. COMPOSITE MATERIALS

#### 3.1 Transversely Reinforced 1-3 and 1-3-0 PZT: Polymer Composites

Early very simple calculations have suggested that the sensitivity figure of merit  $d_{33}$  could be as high as  $300,000 \times 10^{-15} \text{ m}^2/\text{N}$ , for a composite with 5 vol% PZT. Model systems have, however, been limited to sensitivities of at



Sponsored by the Office of Naval Research  
under contract numbered N00014-82-K-0339



Cheryl Y. Price



Bridget A. Chadwick



Lucius Smart

Materials Research Laboratory  
The Pennsylvania State University

Figure 1.

PARTICIPANTS DURING THE SUMMER OF 1983 IN THE APPLIED SCIENCES  
APPRENTICESHIP PROGRAM OF THE CENTER FOR DIELECTRIC STUDIES



Tom Juska

Best Published Work or  
Thesis by a Ph.D. Candidate

Dr. Evan J. Felty

Manager,  
Materials Science Laboratory  
XEROX-Webster Research Center

Keven G. Ewsuk

Best Published Work or  
Thesis by an M.S. Candidate

James W. Laughner

Best Published Work or  
Thesis by a Ph.D. Candidate

Ranbir Singh

Best Published Work or  
Thesis by an M.S. Candidate

David Christopher

Best Research Accomplishment  
by an Undergraduate

Figure 2.

WINNERS OF THE XEROX AWARDS FOR RESEARCH EXCELLENCE FOR THE 1982-83 ACADEMIC YEAR

most  $40,000 \times 10^{-15} \text{ m}^2/\text{N}$ , and we have for some time known that the major limiting factor was the effect of the poisson ratio of the polymer which converts part of the transverse stress into a reverse longitudinal stress along the PZT rods (Fig. 3).

Studies completed this year by M. Haun have demonstrated that using transversely reinforcing glass fibers foamed polyurethane matrix composites can be formed with figures of merit up to  $150,000 \times 10^{-15} \text{ m}^2/\text{N}$  for a 6 vol% PZT. More refined theoretical calculations taking better account of the poisson ratio effects suggest a proper theoretical value near  $180,000 \times 10^{-15} \text{ m}^2/\text{N}$  which in view of the many approximations involved is in quite good agreement.

It is probable that materials with such high coefficients may be too much influenced by hydrostatic pressure for all but very small submergence hydrophones. However, the trends of the data with increasing reinforcement (fiber volume) are quite clear (Table 1). Certainly, it is possible to fabricate materials with a range of sensitivity and stability properties to suite a wide variety of potential applications. The materials which are the component phases are exceedingly inexpensive, the challenge now is to find automated techniques for fabrication and assembly so as to make large size sheets available for general testing and development.

A detailed account of the 1:3:0 transversely reinforced PZT:polymer composites is given in the M.S. thesis by M. Haun. The abstract for this thesis is included as Appendix 1.

### 3.2 PZT:Polymer Composites with 3:1 and 3:2 Connection

An alternative approach for a large area segmented hydrophone may be afforded by the perforated PZT 3:1 and 3:2 connection composites. This structure which uses drilled or in other ways perforated PZT offers the

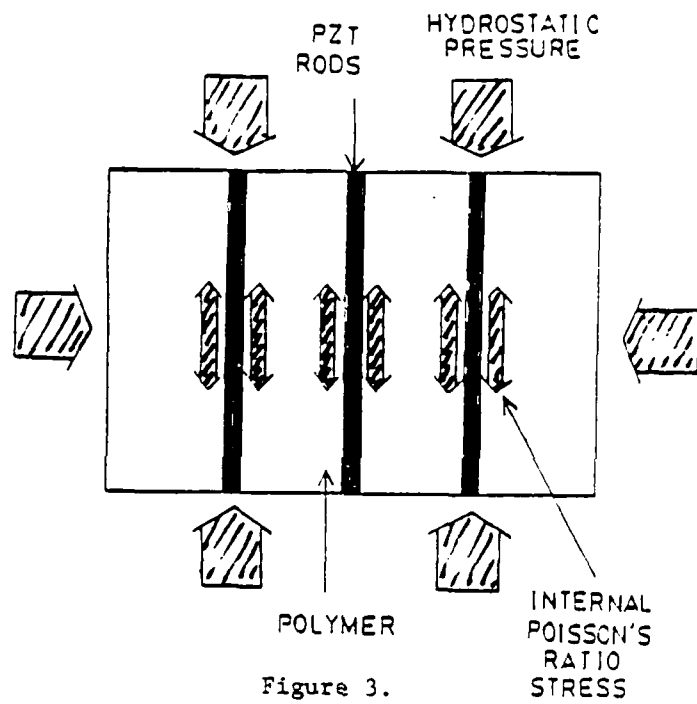


Figure 3.

3-1 Connectivity with Internal Stress.

Table 1.  
Experimental Data for Encapsulated Foamed Polyurethane Samples.

Sample	Z Glass	Z PZT	$\bar{k}_{33}^*$ (pC/N)	$\bar{d}_{33}$ (pC/N)	$\bar{d}_h^{**}$ (pC/N)	$\bar{g}_h$ ( $\times 10^{-3} \frac{Vm}{N}$ )	$\overline{d_{gh}}$ ( $\times 10^{-15} \frac{m}{N}$ )	$-\bar{d}_{31}$ (pC/N)
1	0	6	68	209	106	165	17,500	52
2	0	6	88	332	162	250	40,600	80
3	4	6	49	165	132	344	45,300	16
4	4	6	62	191	202	480	97,000	-6
5	8	6	46	105	169	565	95,400	-32
6	8	6	58	128	188	441	82,800	-30
7	14	6	50	122	167	542	90,600	-22
8	20	6	51	128	224	668	150,000	-48
9	0	8	87	250	143	174	24,900	58
10	0	8	81	267	124	161	20,000	72
11	4	8	79	215	153	200	30,700	8
12	4	8	66	199	129	201	26,000	35
13	0	13	173	322	202	129	26,000	60
14	4	13	158	312	246	173	42,500	33
15	4	13	135	255	204	192	39,100	26
15	20	13	122	213	257	280	72,100	-22

\*These measurements were made before hydrostatic testing. The  $\bar{g}_h$  coefficients were calculated from the dielectric constants determined at 100 psi during hydrostatic testing.

\*\*The Ramp method.

advantage of being much more robust than the 1:3:0 composite, and again by varying the size and spacing of the holes (Fig. 4) and the mode in which the holes are filled or capped a very wide range of trade-offs can be achieved in density, sensitivity, robustness, pressure range, etc. (Table 2).

Perhaps the only significant disadvantage is that the 3:1 and 3:2 modes of connectivity give the structure the mechanical rigidity of the PZT, however, it should be possible to articulate large sheets of 3:1 or 3:2 units in a flexible elastomer.

A second feature of this structure is the protected space inside each active element which on current scaling would be ample for the encapsulation of a miniature semiconductor integrated circuit. For these materials, we believe it should be possible to convert the local pressure information into a modulation on an electromagnetic carrier, to then put many element signals down common wires and still recover individual pressure and phase information in a central processor.

A detailed analysis of the behavior of a range of 3:1 and 3:2 PZT:polymer composites has been given by A. Safari in his Ph.D. thesis. The abstract from that thesis is included as Appendix 2 to this report.

### 3.3 Finite Element Calculations of the Stress Distribution in 3:1 Perforated PZT:Polymer Composites

In the finite element method, a solid of complex shape is divided up into an interconnected network of small 'finite elements.' Using the hookian elastic properties and the continuity relations required, the elastic stress distribution at the nodes of the network can be calculated. For composite materials involving elastic or even visco-elastic properties, the method is particularly powerful and permits detailed evaluation of the stress distributions in each phase provided the elastic boundary conditions can be

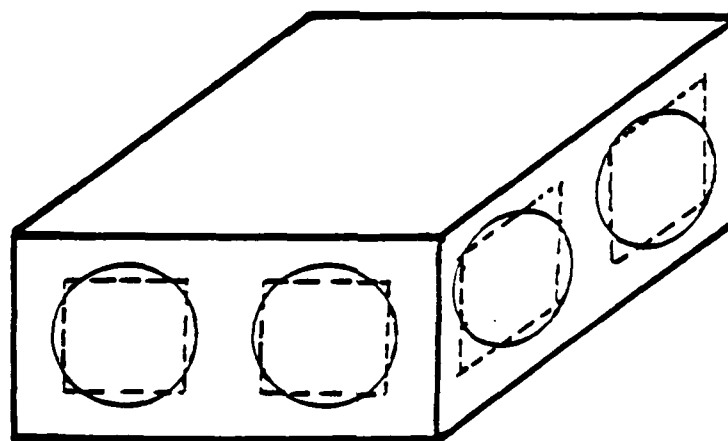
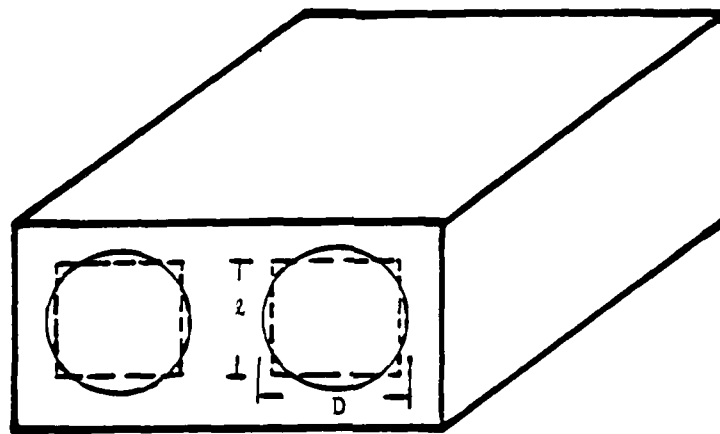


Figure 4.  
 Approximated model for perforated (a) 3-1 and (b) 3-2  
 composites with circular holes.

Table 2.

Optimized Dielectric and Piezoelectric Properties of Perforated Composites

	3-1	3-1-0	3-2	3-2-0
x (mm)	3.5	3.5	4.2	4.2
t (mm)	4.0	4.0	5.0	5.0
D (mm)	3.0	3.0	3.0	3.0
$\rho$ (kg/m <sup>3</sup> )	2500	2600	2500	2300
Vol.% PZT	35	35	45	45
$\bar{\epsilon}_{33}$	650	650	375	360
tan $\delta$	0.03	0.013	0.03	0.02
$\bar{d}_{33}$ (pC/V)	410	430	350	370
$\bar{g}_{33}$ (x10 <sup>-3</sup> Vm/N)	70	75	100	115
$\bar{g}_h$ (x10 <sup>-3</sup> Vm/N)	30	35	60	70
$\bar{d}_h$ (pC/V)	170	200	200	220
$\bar{g}_h \bar{d}_h$ (x10 <sup>-15</sup> m <sup>2</sup> /N)	5000	7000	12000	15000



adequately specified. Clearly for such methods, the precision with which the continuous stress distributions can be calculated will increase as the mesh size for the finite elements is reduced but, of course, at the cost of rapidly increasing computation time and expense.

For the case of the piezoelectric composites, the FEM is used to calculate the stress distribution in the PZT phase, then from the known macroscopic piezoelectric coefficients the distribution of electric polarization can be determined. The polarization for the composite is then determined using simple series and parallel connection models. From the composite polarization it is then simple to calculate the composite  $d_h$  coefficient.

The method is currently being applied to a calculation of the hydrostatic piezoelectric coefficient  $d_h$  for a 3:1 perforated PZT:polymer composite with a square hole configuration as shown in Figure 5. At a hydrostatic pressure level of 100 psi, using bulk constants for a PZT 5 and a SPURS epoxy polymer, the phases used by A. Safari in similar 3:1 composites, preliminary calculations are in excellent agreement with the experimental data of Safari. For a 3-1 composite with a hole size of 2.5 mm, for example, the calculated  $d_h$  was  $120 \times 10^{-12}$  C/N as compared to a measured value of  $130 \times 10^{-12}$  C/N.

Other published papers relevant to the PZT:polymer composite studies are included in Appendices 3-10.

For a limited FEM set, the technique is expected to underestimate the stress values converging to an exact solution as the number of elements is increased, so that in our calculation, it is expected that the FEM value slightly underestimate the stress, and thus the  $d_h$  as is in fact observed.

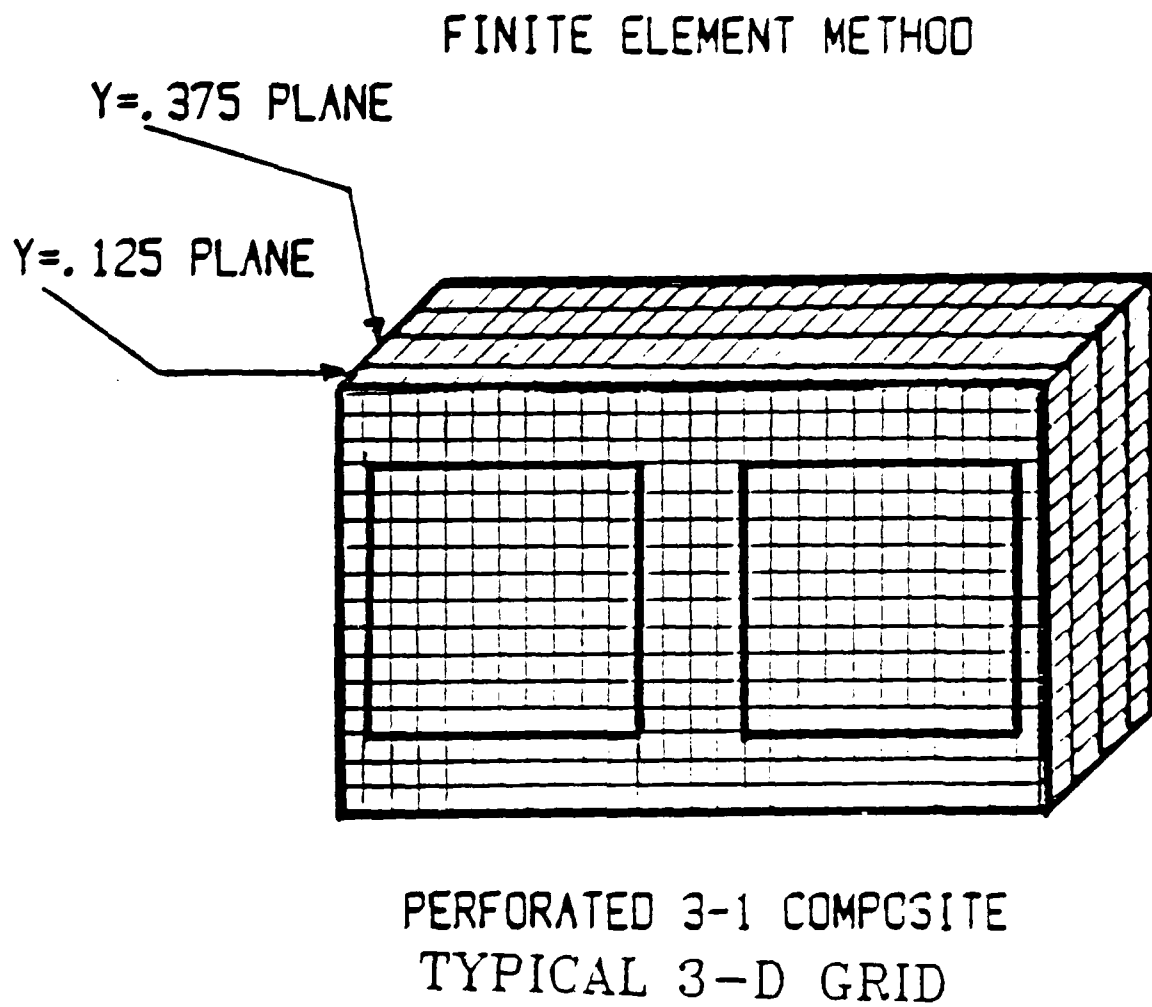


Figure 5. Typical finite element grid for 3:1 composite with square holes.

### 3.4 Fresnoite: Oriented Polar Glass Ceramics for Hydrophone Applications

Over the last four years, a very extensive study has been made of the dielectric, piezoelectric and elastic properties of a new family of polar glass ceramics. Starting from appropriate glass compositions, we have demonstrated that by re-crystallization from a planar surface in a strong normal temperature gradient, highly polar oriented crystallites can be generated in the  $\text{Ba}_2\text{TiSi}_2\text{O}_8$ ,  $\text{Ba}_2\text{TiGe}_2\text{O}_8$ ,  $\text{Sr}_2\text{TiSi}_2\text{O}_8$ ,  $\text{Li}_2\text{Si}_2\text{O}_5$  and  $\text{Li}_2\text{B}_4\text{O}_7$  families. These are all in polar crystal structures, but are non ferroelectric, so that the original orientation initiated when the crystallites grow cannot be destroyed except by physical destruction of the sample.

During the four year period, techniques have been evolved for combining more than one crystalline phase in the composite and for engineering combinations which can be strongly pyroelectric but non piezoelectric, or conversely strongly piezoelectric and non pyroelectric. Combinations of properties which are clearly impossible and forbidden by symmetry in single phase systems.

A practical application which looks most promising for the glass ceramic is as a piezoelectric hydrophone material. In the  $\text{Ba}_2\text{TiSi}_2\text{O}_8$  and analog  $\text{Ba}_2\text{TiGe}_2\text{O}_8$  glass ceramics, a combination of high  $g_h$  and high  $d_h g_h$  comparable to the polymer PVDF, but in a material with zero aging and extremely stable properties holds real promise to generate a new standard for calibration purposes.

Work on the composites is continuing with effort currently focused upon generating larger samples for study and improving the integrity and uniformity of the re-crystallized films. Recent publications on transducer applications of glass ceramics are given in Appendices 11-13.

#### 4. ELECTROSTRICTION STUDIES

##### 4.1 Theoretical Studies

##### 4.1.1 Static Lattice Calculations for $\text{KZnF}_3$ and $\text{KMnF}_3$

Harmonic and first-order anharmonic properties at the zone center have been calculated for two perovskite fluorides on the basis of the shell model. The harmonic part of the model used is equivalent to Cowley's model<sup>(12)</sup>. The 14 harmonic model parameters are determined from the room temperature values of the elastic and dielectric constants and from the zone-center optic mode frequencies. Anharmonic contributions from coulomb interactions and from short range two-body central forces between cation-fluorine nearest neighbors and fluorine-fluorine second neighbors are included. The corresponding model parameters are either determined empirically or by assuming the Born-Mayer potential form. Good agreement between calculated and available room temperature values is found for the electrostriction constants and for the third-order elastic constants. The good agreement indicates only weak coupling between the soft  $R_{15}$  mode and these zone center first order anharmonic properties, and is a clear indication of the adequacy of the shell model employed. For these non-ferroelectric perovskite crystals with only weak  $R_{15}$  mode softening, thermal effects at the zone center can be described by weakly temperature dependent model parameters and do not enter explicitly into the calculation.

##### 4.1.2 Temperature Dependence of Electrostriction in $\text{SrTiO}_3$

Expressions for the electrostriction ( $Q_{ij}$ ) coefficients at finite temperature  $T$  have been derived from anharmonic perturbation theory by using the thermodynamics one-phonon Green's functions. A one-to-one correspondence of all individual terms with the long wavelength method pertaining to the static crystals has been established. The  $Q$  coefficients are given by linear

combinations of third order coupling parameters (C.P.'s) in the static reference state, and on the temperature dependent renormalized zone center frequencies which in turn depend on the third and higher order C.P.'s. The separate mode softening problem and the uncertainties in determining consistent higher than third order C.P.'s may therefore be by passed by using experimental values of the temperature dependence of zone center frequencies as input. Numerical application of this procedure to  $\text{SrTiO}_3$  based on a shell model with coulomb and short range anharmonicity included gives good agreement with the measured temperature dependence of the hydrostatic ( $Q_h$ ) electrostriction coefficient.

For these calculations, it must be remembered that for ionic crystals, at the zone center, there are two ways of defining the dynamical matrix and the Green's function, namely with the macroscopic electric field included ( $D_+$  and  $G_+$ ) and with the field deleted ( $G_-$  and  $D_-$ ). Experimental optic mode phonon frequencies are given by the Eigenvalues of  $D_+$  (or poles of  $G_+$ ), but dielectric constant and electrostriction depend on the Eigenvectors and Eigenfrequencies of  $D_-$ . For transverse optic (TO) modes in perovskite compounds Eigenvalues of  $D_+$  and  $D_-$  are identical, but Eigenvectors of  $D_+$  and  $D_-$  are different. In anharmonic many-body perturbation theory all contributions to electrostriction depend on constant Eigenvectors of  $D_-$  corresponding to the static crystal, and upon the temperature dependent renormalized frequencies (poles of  $G_-$ ). Hence, the possibility to use experimental (temperature dependent) frequencies and theoretical Eigenvectors of the static crystal (corresponding to  $D_-$ ).

## 4.2 Experimental Electrostriction

### 4.2.1 Measurements by the Direct Method

Using a modified and improved version of the capacitance ultradilatometer originated by Uchino and Cross<sup>(13)</sup>. Kurt Rittenmyer has just completed a very extensive sequence of measurements upon single crystals of the alkali halides (KCl and NaCl) and upon the fluorite structure crystal ( $\text{CaF}_2$ ). A full account of this work is given in the Ph.D. thesis of Rittenmyer. The abstract of the thesis is included as Appendix 14 to this report.

Major conclusions from the work may be summarized as follows.

In both KCl and NaCl, the measured values of  $Q_{11}$  show a marked dispersion over the frequency range 5 Hz to 500 Hz. We believe that this dispersion is related to the charged dislocation structure in the alkali halides since: (1) crystals which have been plastically deformed to a polycrystal form and are mechanically much stronger show grossly ENHANCED electrostriction with constants more than an order of magnitude larger than the single crystal. (2) Crystals which have been neutron irradiated at very high doses, so as to pin the dislocations show much reduced constants with reduced dispersion. In view of the above observations, it is the contention of this work that currently accepted values of the constants which have been measured by the direct method are distinctly suspect. It is perhaps not surprising that theoretical calculations do not agree with current measured values.

For the fluorite structure crystals  $\text{CaF}_2$ , the values obtained measuring 100, 110 and 111 oriented crystals give a mutually self-consistent set. There is no significant dispersion for  $Q_{11}$  (measured in 100), and only very slight dispersion for 111 orientation but again the values are larger than would be expected from simple theory and about a factor of five larger than values obtained by the converse method of measurement.

It has been suspected for some time that part of the problem in making direct measurements of electrostriction parameters stems from the mounting of the crystal. Evidently it is not possible to obtain the thickness change by monitoring at a single point on the surface, and it is essential to glue the crystal firmly in place to obtain any reproducibility in the strain measurement. Very recent optical dilatometer measurements by Chen<sup>(14)</sup> suggest that even in non piezoelectric crystals and ceramics, flexure modes can be excited. Possibly surface space charge fields give rise to weakly piezoelectric surface layers and thus an induced bimorph mode.

In future work we will re-design the dilatometer to eliminate these possible flexure modes.

#### 4.2.2 Measurements by the Converse Method

Over the first year of the current contract period, a completely new equipment for measuring the dielectric response of single crystals of low permittivity solids under pure uniaxial stress, has been constructed. In this uniaxial compressometer, the stress is applied to sample using a simple lever arm to provide high load at the center point of a piston of hardened steel. To avoid poisson ratio perturbation of the stress system, the anvils in contact with the crystal are made of the same crystalline material cut in the same orientation as the sample under test.

For dielectric measurement, the sample in the form of a thin disk, is equipped with sputtered metal electrodes and a full three terminal guard ring system. Contacts to both guard and electrodes are made by pressure pads in the perimeter of the metal mounting cylinder which are themselves fully guarded.

Measurements of the capacitance under load were carried out using a General Radio 1620 measuring system which is capable of resolving changes of

order  $10^{-18}$  Farads. Temperature control was effected by the very large thermal mass of the holder and stressing jig, and slow temperature drift effects were eliminated by measuring the changes induced by stress on both loading and unloading.

Data for the stress dependence of permittivity for 100, 110 and 111 cuts of  $\text{CaF}_2$  are shown in Figure 6. A more detailed account of this work is given in Appendix 15.

#### 4.2.3 Electrostriction in High Permittivity Crystals

4.2.3.1 Introduction. Two topics have been of major interest in their importance to the basic understanding of electrostriction in high permittivity solids. In single crystals barium titanate ( $\text{BaTiO}_3$ ), there are two earlier sets of measurements of the temperature dependence of electrostriction<sup>(15,16)</sup> which give completely different trends for the coefficient  $Q_{11}$ . If as is suggested by the data of Beige and Schmidt<sup>(15)</sup> the constant  $Q_{11}$  is a linearly decreasing function of temperature passing through zero at a temperature close to the Curie Weiss point  $T_c$ , then the whole Devonshire phenomenological theoretical explanation of the spontaneous deformations of the ferroelectric phases is suspect. If on the other hand  $Q_{11}$  is only a weakly decreasing linear function of  $T$  as suggested by the data of Huijbregtse et al.<sup>(16)</sup>, the Devonshire phenomenology is clearly adequate to describe the elasto-dielectric properties of the ferroelectric phases.

In view of the importance of the phenomenological approaches to many of the efforts, we have been and are now making to untangle intrinsic and extrinsic contributions to ferroelectric properties, it appeared most desirable to equip ourselves to make direct measurement of electrostriction at higher temperature and resolve the current controversy once and for all.



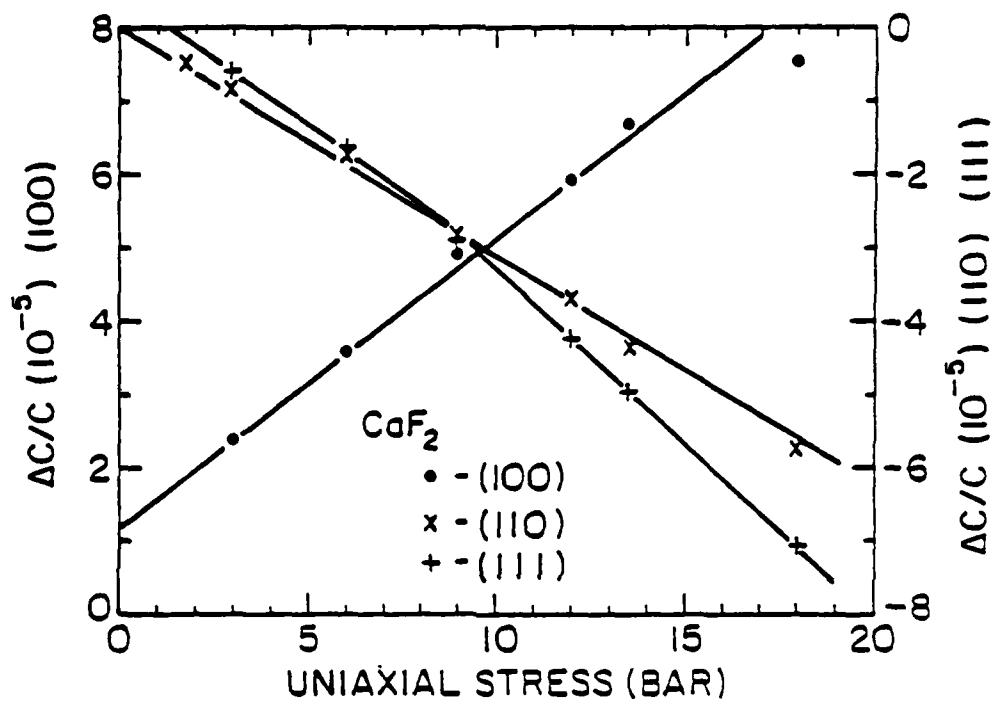


Figure 6. Using a value of  $M_h = 1.017 \times 10^{-21} \text{ m}^2/\text{v}^2$  the data in Figure 6 yields

$$\begin{aligned}
 M_{11} &= -0.132 \times 10^{-20} \text{ m}^2/\text{v}^2 \\
 M_{12} &= +0.117 \times 10^{-20} \text{ m}^2/\text{v}^2 \\
 M_{44} &= +0.507 \times 10^{-20} \text{ m}^2/\text{v}^2 \\
 (M_{1212} &= +0.128 \times 10^{-20} \text{ m}^2/\text{v}^2).
 \end{aligned}$$

Having constructed and calibrated a thermal expansion compensated dilatometer which would perform satisfactorily at high temperature, our attention became focused on the interesting problem of electrostriction in a uniaxial paraelectric. In L.G.D. theory, the average polarization  $\bar{P}$  is zero even for temperatures very close to the Curie Point  $T_c$ , however, the theory cannot speak to the dynamical situation and close to  $T_c$  one expects large thermal fluctuations of  $\pm P$  and thus a non-zero value of  $\bar{P}^2$ . Since in a uniaxial crystal (unique axis along 3) the strain is given by

$$x_{33} = Q_{33}P_3^2$$

If  $\bar{P}_3^2$  is non-zero, electric polarization induced strain must begin to appear well above  $T_c$ .

Clearly, in measuring now the induced strain due to the application of field above  $T_c$ , the measured value of  $Q_{33}$  will depend on the make up of the induced average change of  $P_3$ . One may in general expect at least two components.

$P_{a(3)}$  due to regions whose polarization is changed from zero, and  $P_{b(3)}$  due to the modulation by the field of the thermal fluctuations, which already exist.  $P_{a(3)}$  will contribute to strain in the normal manner, however because electrostriction depends on  $P^2$ ,  $+P$  and  $-P$  produce equal strain and modulating the pre-existing fluctuations will not modulate the strain, i.e.

$$P_3 = P_{a(3)} + P_{b(3)}$$

the induced strain will be

$$x_{33} = Q_{33}P_{a(3)}^2.$$

If, however, we measure only the total polarization, we shall find for the induced strain

$$x_{33} = Q_{33}^1 P_3^2$$

where  $Q_{33}^1$  is an apparent electrostriction constant such that

$$\frac{Q_{33}^1}{Q_{33}} = \frac{P_a^2(3)}{P_3^2} = \frac{[P_3 - P_b(3)]^2}{P_3^2}$$

As  $T \rightarrow T_c$  we expect  $P_b(3) \rightarrow P_3$  and thus  $Q_{33}^1 \rightarrow 0$ .

From the manner in which  $Q_{33}$  decreases as  $T \rightarrow T_c$  we may then expect to gain information as to the importance of fluctuations in the total polarization process.

**4.2.3.2 Instrumentation.** To permit the direct measurement of electrostriction over a wide temperature range, our original capacitance ultradilatometer has been modified to reduce the sensitivity and to compensate the mechanical measuring circuit for the thermal expansion of the sample support system.

A schematic drawing of the measuring cell is given in Figure 7. Insulation of the sensing capacitor is now by glass ceramic for the higher temperature. The outer container is split so that the support is partly of brass and partly of low thermal expansion inconel a sliding ring permits a tuning of the expansion of the outer support so as to match sample and standard (quartz) and the glass ceramic support of the inner structure.

By careful balance of this mechanical bridge structure, it is possible to reduce the thermal effects so that the capacitance bridge can be worked at high enough sensitivity to detect and measure the AC capacitance changes induced by driving the standard and by driving the paraelectric sample under measurement with reasonable AC field levels.

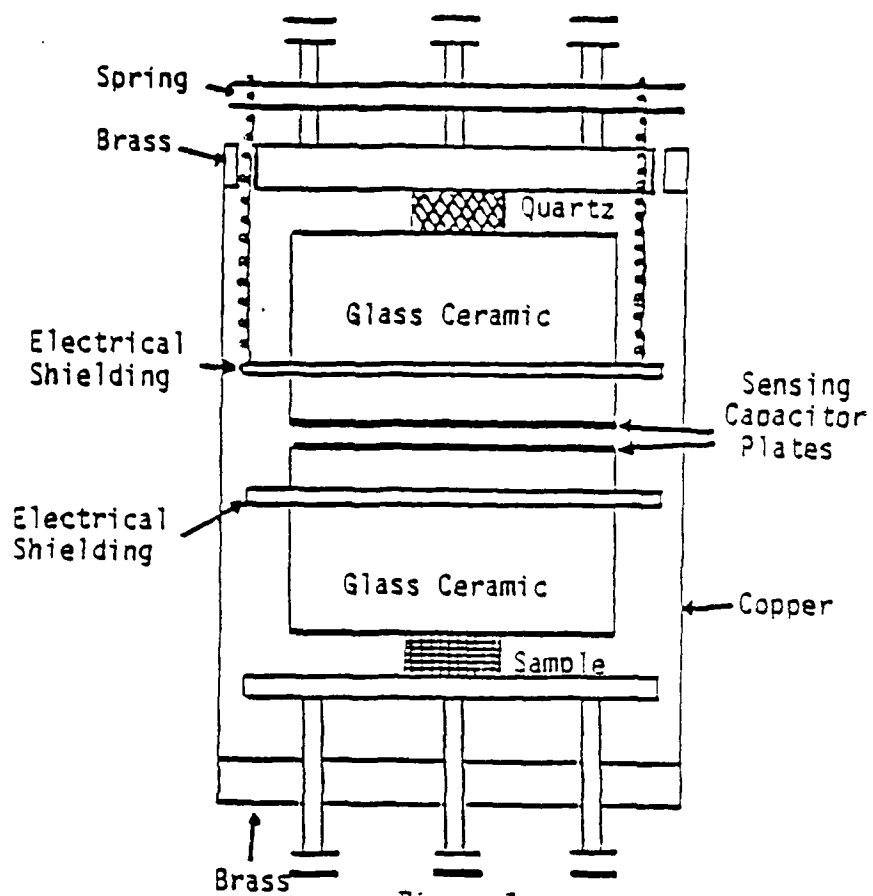


Figure 7.

Schematic representation of A.C. capacitance dilatometer.

For the range from 20°C to 200°C, the dilatometer is capable of resolving AC displacements at frequencies up to 25 Hz of order of  $0.05 \text{ \AA}$  ( $5 \times 10^{-12}$  meters). A complete description of the development, calibration and measurements using this AC dilatometer is given in the MS thesis of Mojtaba Shishineh, 'A Simplified Temperature Compensated AC Dilatometer for Electrostriction Measurements.' The abstract for the thesis is included as Appendix 16.

4.2.3.3 Measurements on BaTiO<sub>3</sub>. The major problem in this work was not the dilatometer or the difficulty of measurement but the problem of obtaining adequate crystals of BaTiO<sub>3</sub> for this work. Remeika type samples were too thin and plate like to give reproducible displacements. It was not possible to obtain new melt grown crystals from Saunders Associates whose available crystals were not of adequate quality. Best results were obtained using crystals from Tyco Co. which had been produced by edge defined growth.

After annealing at 1250°C to remove internal stress, these crystals showed good optical extinction, a Curie point  $T_c$  at 124°C and a Curie Weiss constant  $C = 1.56 \times 10^5$  in good agreement with accepted values.

For measurements in the range 124 to 140°C,  $Q_{11}$  values were in close agreement with the data of Huibregtse et al. showing only a weak negative temperature coefficient, and falling in close agreement with values calculated in the ferroelectric phase from  $P_s$  and spontaneous strain.

Above 150°C, measured values begin to rise rapidly due to inhomogeneity in the field distribution produced by increasing current. Annealing in oxygen was tried to extend the measurable range but without success.

Very recently Roleder in Poland<sup>(17)</sup> has used a compensated capacitance dilatometer to extend measurements of  $Q_{11}$  to 170°C. Up to 150°C his data is in excellent agreement with this work. Apparently, however, his crystals were

of higher resistivity and up to 170°C the weak negative temperature coefficient is found to persist.

It would therefore appear certain now that the data of Beige and Schmidt is in error and that as expected,  $Q_{11}$  is only a weak linear function of temperature and is continuous through the Curie Point  $T_c$ .

4.2.3.4 Electrostriction in the Uniaxial Ferroelectric  $\text{Sr}_{0.61}\text{Ba}_{0.39}\text{Nb}_2\text{O}_6$ . Strontium Barium Niobate (SBN) crystallizes in the tetragonal tungsten bronze structure with 4/mmm point symmetry in the paraelectric phase. The four-fold axis of the prototype is a unique non-polar axis so that the ferroelectric species 4/mmm (1) D4F 4mm in Shuvalov's notation is uniaxial with only 2 available orientation states  $\pm$  along the 4 axis.

In earlier studies in MRL, Shrout<sup>(18)</sup> developed the complete L.G.D. phenomenology for SBN. For the 4/mmm symmetry, the non-zero  $Q_{ij}$  in matrix form are  $Q_{11} = Q_{22}$ ,  $Q_{12} = Q_{21}$ ,  $Q_{13} = Q_{23}$ ,  $Q_{31} = Q_{32}$ ,  $Q_{33}$ ,  $Q_{44} = Q_{55}$  and  $Q_{66}$

$Q_{11}$	$Q_{12}$	$Q_{13}$	0	0	0
$Q_{12}$	$Q_{11}$	$Q_{13}$	0	0	0
$Q_{31}$	$Q_{31}$	$Q_{33}$	0	0	0
0	0	0	$Q_{44}$	0	0
0	0	0	0	$Q_{44}$	0
0	0	0	0	0	$Q_{66}$

Shrout determined  $Q_{33}$  both by measuring  $P_s$  and the strain  $x_{33}$ , and by measuring the piezoelectric constant  $d_{33}$  in the single domain state.

In the former,

$$x_{33} = Q_{33} P_3^2 \quad \text{gave} \quad Q_{33} = 3.4 \times 10^{-2} \text{ m}^4/\text{c}^2$$

and the latter

$$d_{33} = 2\epsilon_0\epsilon_{33}Q_{33}P_s \quad \text{gave} \quad Q_{33} = 3.0 \times 10^{-2} \text{ m}^4/\text{c}^2$$

in reasonable accord.

Above  $T_c$ , Shrout measured  $d_{33}$  and  $d_{31}$  in DC field biased crystals to yield

$$Q_{33} = 1.65 \times 10^{-2} \text{ m}^4/\text{c}^2$$

and

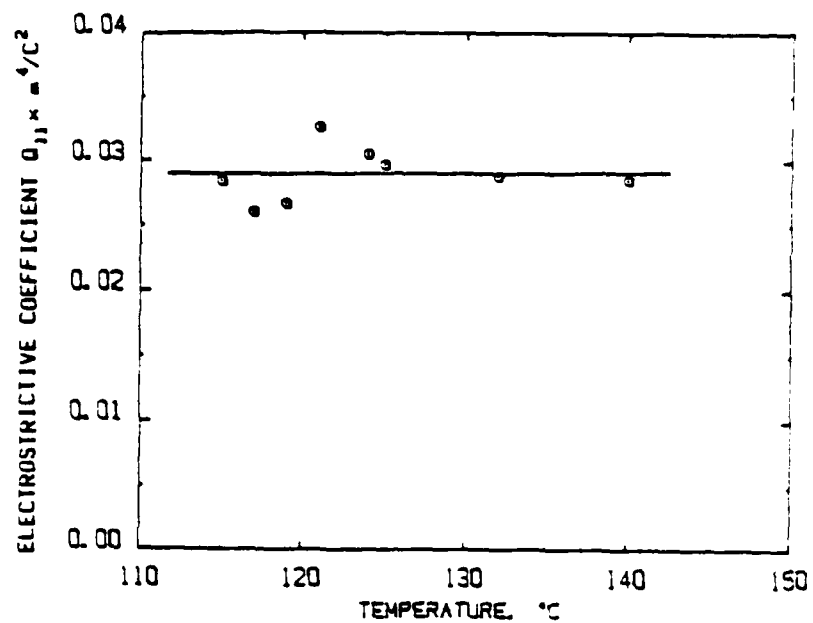
$$Q_{31} = 0.45 \times 10^{-2} \text{ m}^4/\text{c}^2.$$

At that time we could give no reasonable explanation for the discrepancy. In fact, near to  $T_c$  the measured data did not correspond to the expected form and a method due to Nomura<sup>(19)</sup> was used to correct for an apparent non-zero coupling  $k_{33}$  at zero bias.

In the present study C. Sundius measured  $Q_{11}$ ,  $Q_{33}^1$  and  $Q_{31}^1$  using the capacitance dilatometer to measure AC displacement due to the application of AC field at temperatures above  $T_c$ . Sawyer and Tower method was used to display the dielectric non-linearity and to determine the polarization value corresponding to the measured strain.

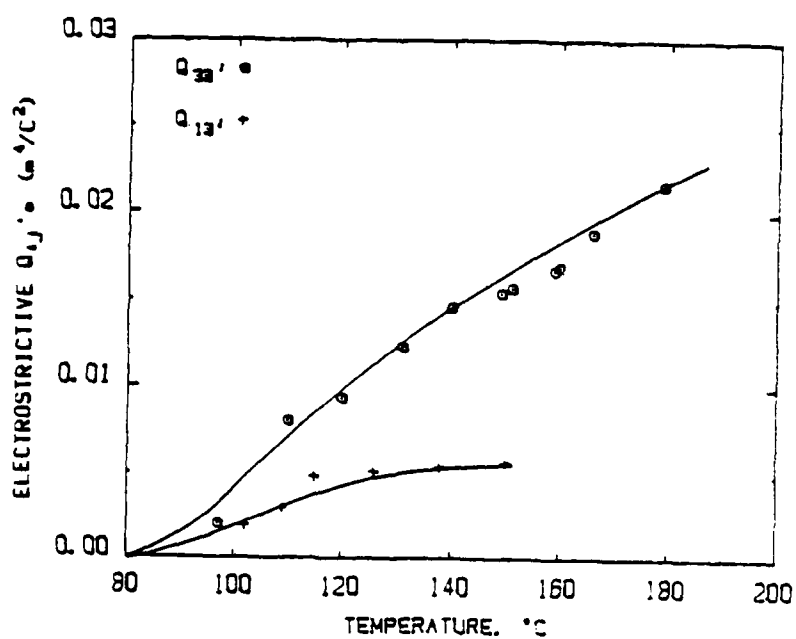
Results are summarized in Figures 8 and 9. Clearly  $Q_{33}$  and  $Q_{31}$  are markedly temperature dependent approaching zero at the Curie temperature  $T_c \approx 77^\circ\text{C}$ . The constant  $Q_{11}$ , however, appears to be completely temperature independent.

It is interesting to note that  $Q_{33}^1$  is changing quite markedly with temperature even at  $180^\circ\text{C}$  more than  $100^\circ\text{C}$  above  $T_c$ , and has still not attained the expected value  $Q_{33} \sim 3.0 \times 10^{-2} \text{ m}^4/\text{c}^2$ .  $Q_{31}$  appears to saturate much more quickly and even at  $150^\circ\text{C}$  is close to the value measured by Shrout in his



Electrostriction coefficient,  $Q_{11}$ , as a function of temperature for SBN 61/39.

Figure 8



Electrostrictive coefficients,  $Q_{33}$  and  $Q_{13}$ , as a function of temperature for SBN 61/39.

Figure 9



resonance experiments. A detailed account of this work has been given in the MS thesis of Carol Sundius 'Direct Measurement of the Temperature Dependence of Electrostriction Coefficients in strontium barium niobate. The abstract for this thesis is included in this report as Appendix 17.

We may note that in SBN the transition at 77°C is slightly diffuse even for the congruent melting 61:39 compositions, and some persistence of the polar phase above  $T_c$  is to be expected. For these bronzes, fluctuation effects in  $P_3$  should be particularly strong. It is also comforting to note that for  $P_1$  induced effects, fluctuations should be very small, and in fact we find  $Q_{11}$  temperature independent as expected. Additional work on low level electrostriction is presented in Appendix 18, and on the direct measurements in Appendix 19.

Evidently, all phenomena which depend on  $P_3^2$  should be anomalous near  $T_c$ . We hope to confirm these fluctuation effects by measurements of the thermal expansion and of the optical birefringence just above  $T_c$ .

4.2.3.5 Practical Electrostrictors. Over the past year effort has been concentrated upon the PLZT family of relaxor materials over the composition range from 7:65:35 to 9.5:65:35 PLZT.

Detailed studies of the polarizing and depolarizing behavior in the hot pressed transparent ceramics have been carried through to explore the nature of the 'depoling transition' in the 8:65:35 composition and the manner in which this is modified by change in the  $\text{La}_2\text{O}_3$  content. This work was presented at the European Meeting on Ferroelectricity and is included as Appendix 20.

In summary, it is clear that large remanent electric polarizations can be built up at low temperature across the whole composition range by cooling under DC bias. For all compositions studied, depoling occurs at temperature

well below the temperature of maximum dielectric permittivity and becomes progressively more gradual with increasing  $\text{La}_2\text{O}_3$  content. A model involving the ordering of superparaelectric micro-regions under field accounts well for all observed behavior.

Elastic strains accompanying polarization increase but become more hysteretic with decreasing lanthanum content. The 9.5:65:35 composition has anhysteretic transverse strains almost double those in the  $\text{Pb}(\text{Mg}_{1/3}\text{Nb}_{2/3})\text{O}_3$ : $\text{PbTiO}_3$  solid solutions at the 8 mole%  $\text{PbTiO}_3$  composition and should be of interest for micropositioner applications. Additional work in this area is reported in Appendices 21-23.

## 5. CONVENTIONAL PIEZOELECTRIC CERAMICS

### 5.1 Introduction

Over the current contract year, work has been continued to explore the property changes in pure and in doped PZT ceramics over the low temperature range down to 4°K. The emphasis has been to explore the 'freeze out' of the extrinsic domain wall and phase boundary contributions to dielectric, piezoelectric and elastic properties. The approach makes use of the thermodynamic phenomenology developed on earlier contract funds to calculate the base of single domain intrinsic properties and the manner in which they should vary with temperature and with zirconia:titania ratio.

Neutron diffraction and scattering experiments have been used to explore the single cell:multi cell rhombohedral phase change in the  $\text{PbZr}_{0.6}\text{Ti}_{0.4}\text{O}_3$  composition. The data suggest the possibility of a short range order in the Zr:Ti distribution or possibly a precursor of the tetragonal phase which becomes stable at morphotropy.

In two short studies, a method of continuous poling for long PZT rods or sheets has been explored, and a new technique for poling soft PZTs by cooling through  $T_c$  under quite weak fields has been explored.

## 5.2 Low Temperature Measurements

In studies initiated last year, it was observed that for a number of differently doped PZTs ranging from hard acceptor doped compositions to very soft donor doped formulations, the dielectric permittivity  $\epsilon_{33}$ , the piezoelectric  $d_{33}$  and  $d_{31}$  all appear to come to common values at 4K. pure PZTs, on the other hand, which have been chemically prepared with differing Zr:Ti ratios do not come to common values, and the profile of the intrinsic behavior is reflected in the low temperature response.

A more extensive series of measurements on doped compositions has confirmed fully the earlier study. Dielectric data for a wider range of frequencies shows very marked differences in the loss spectra for the different doping cations and we are in the process of sorting out the activation energies and distribution functions for these loss spectra.

The low temperature permittivity level is in excellent agreement with the value calculated from phenomenological theory using the Curie constant value of  $7.7 \times 10^5$  determined from thermal measurements. Extrapolating back to room temperature, however, it is clear that even in the very hard PZT almost 30% of the measured permittivity is extrinsic, and that in soft compositions the extrinsic component is quite dominant, Appendix 24.

For  $d_{33}$  and  $d_{31}$ , it is more difficult to decide a proper averaging in the ceramic from the intrinsic single domain values. Both for  $d_{33}$  and  $d_{31}$ , the calculated single domain values are larger than the observed values at 4K. This could reflect a smaller contribution from  $d_{15}$  to  $\bar{d}_{33}$  and  $\bar{d}_{31}$  or the influence of the degree of poling in these doped samples.

Work is now in progress to extend measurements to higher field levels to determine the temperature dependence of  $E_c$ , the coercive field, and to explore the kinetics of switching at these low temperatures. In parallel studies, we are extending and refining the phenomenological theory so as to be able to encompass the single cell:multi cell compositions towards the zirconia rich end of the phase diagram.

### 5.3 Diffraction Studies

#### 5.3.1 Neutron Diffraction of $\text{Pb}(\text{Zr}_{0.6}\text{Ti}_{0.4})\text{O}_3$

Neutron diffraction and diffuse scattering experiments have been carried out upon chemically prepared powders of  $\text{Pb}(\text{Zr}_{0.6}\text{Ti}_{0.4})\text{O}_3$ . Analysis of the pseudocubic 311 reflection indicates that the phase change from single to multi-cell forms is quite diffuse and takes place in the range from 2520 to 300°K. This is in reasonable extrapolation of the existing phase diagram, where the room temperature boundary is near the  $\text{PbZr}_{0.64}\text{Ti}_{0.36}\text{O}_3$  composition.

The diffuse scattering both at 295K and at 221K shows an interesting modulation consistent with a small shift of the oxygen ions in the octahedra about the  $\text{Ti}^{4+}$ , with some evidence of a tendency towards ordering of the Zr and Ti atoms.

Phenomenological calculations suggest that at the 60:40 composition, the Gibbs Free Energies of tetragonal and rhombohedral forms are quite close so that the possibility exists for local stabilization of nuclei of the tetragonal phase, by local stress fields or chemical inhomogeneities.

This work is discussed in more detail in Appendix 25.

#### 5.3.2 High Temperature X-ray Studies

It has been suggested by Takegawa<sup>(20)</sup> that x-ray line profile studies in the cubic phase above the Curie point  $T_c$  may be used as a sensitive indicator of the degree of homogeneity in the Zr:Ti ratio in a PZT. In fact, the

broadening is a sensitive indicator of microstrain in the powder and it is assumed that in the cubic structure above  $T_c$  this microstrain is caused by unmixing of the zirconium and titanium ions which are markedly different in atomic size.

To see if the technique could be applied as a relatively simple 'screening test' for PZT powders, powder samples were prepared from six different PZT transducer formulations supplied by the Navy Underwater Sound Reference Division in Orlando, Florida, and compared to a chemically prepared PZT powder made here in the Laboratory.

Measurements were made on a General Electric XRD6 using a specially designed hot stage. Profiles were obtained for (100), (110), (111), and (200) lines at  $400 \pm 0.5^\circ\text{C}$  using pure Si powder as an internal standard. A correction was made for instrument broadening, but no attempt was made to make the measurements absolute as only relative differences in broadening between the different samples were of interest.

Initial data suggest that the technique does show up systematic differences in homogeneity between samples from different sources. Unexpectedly, the chemically prepared samples which had only been heat treated to  $600^\circ\text{C}$  showed the largest broadening. Heat treatment of this sample to  $1,100^\circ\text{C}$  reduced the broadening markedly indicating that simple chemical co-precipitation is not of itself a guarantee of atomic mixing. This latter is in agreement with Kakegawa's work which indicates quite wide differences between different chemical preparation methods.

At the present stage, it is too early to recommend the method for general use, but it certainly merits additional study to attempt to correlate the heterogeneity with other characteristics of the piezoelectrics.

## 5.4 Poling Studies

### 5.4.1 Continuous Poling

A new technique has been developed for poling PZT fibers and ribbons along their length, and is the subject of Navy Patent application. The method gradually advances the sample past two flexible surface electrodes which are kept at a DC potential difference. With electrodes on both sides of a ribbon, thicknesses up to 1.4 mm have been poled in PZT 501A. Details of the method are given in Appendix 26 which also discusses the applications for pre-poled rods and ribbons in composite transducers.

### 5.4.2 Curie Point Poling of PZT 501A

The inherently high resistivity of donor doped soft PZTs can be exploited to enable poling at very low field levels by cooling through the Curie point  $T_c$  under DC bias. Fields between 5 and 8 kV/cm were found to give superior properties to those obtained by conventional poling at 25 kV/cm in a 140°C oil bath, when the field was applied above  $T_c$  and the sample cooled at  $\sim 10^\circ\text{C}/\text{minute}$  to a temperature well below  $T_c$ .

Permittivity  $\epsilon_3$ ,  $d_{33}$ , and  $k_p$  the planar coupling were all larger in the Curie point poled samples. More details of this study are given in Appendix.

## 6. PREPARATIVE STUDIES

### 6.1 Reaction Sequence in the Formation of Lead Zirconate:Lead Titanate

Studies showing the important influence of the  $\text{PbO}$  and  $\text{ZrO}_2$  raw materials upon the reaction sequences which lead to the formation of the  $\text{PbTiO}_3\text{:PbZrO}_3$  solid solution have now been completed and published. The very marked influence of the nature of the  $\text{ZrO}_2$  powder upon some of the intermediates in the calcining reaction sequence have been clearly documented. Details of this study are given in Appendix 28.

## 6.2 Molten Salt Synthesis

### 6.2.1 Preparation of Lead Metaniobate

The reaction of lead oxide and niobium oxide heated in molten KCl or NaCl has been shown to lead to partial substitution of the alkali ion to replace Pb ions in  $\text{PbNb}_2\text{O}_6$ . The incorporated alkali ions stabilize the tetragonal tungsten bronze structure, but reduce the ferroelectric Curie temperature. The reactivity of NaCl is greater than KCl, and can lead to the formation of a  $\text{NaNbO}_3$  phase with some incorporated lead. This work is discussed in Appendix 29.

Recently studies have been extended to  $\text{B}_2\text{O}_3$  fluxes. In this case, the tetragonal structure is not obtained, and the equilibrium rhombohedral phase is obtained as would be expected thermodynamically. Powders with highly acicular geometry in the ferroelectric tetragonal form obtained from the KCl flux are now being tested for incorporation in grain oriented ceramic:plastic composites.

### 6.2.2 Grain Oriented $\text{PbBi}_2\text{Nb}_2\text{O}_9$

The molten salt method has been used to synthesize platey crystallites of the bismuth oxide layer structure ferroelectric  $\text{PbBi}_2\text{Nb}_2\text{O}_9$  which have a very large shape anisotropy. Tape casting and simple uniaxial hot pressing have been used to fabricate ceramics with orientations of better than 90% and densities of 96% theoretical. Details of this work are given in Appendix 30.

## 6.3 Synthesis of $\text{PbTiO}_3\text{:BiFeO}_3$ Solid Solutions

$\text{PbTiO}_3$  and  $\text{BiFeO}_3$  are known to form complete solid solution and to crystallize in the cubic perovskite structure.  $\text{PbTiO}_3$  undergoes a phase change to a tetragonal ferroelectric form at  $470^\circ\text{C}$ , and this ferroelectric Curie temperature increases with increasing  $\text{BiFeO}_3$  in the solid solution. For

compositions in the region of 70 mole%  $\text{BiFeO}_3$ , a morphotropic phase boundary occurs between a tetragonal and a rhombohedral ferroelectric form. There appears to be a narrow region of co-existence but beyond 80 mole%  $\text{BiFeO}_3$  only the rhombohedral phase is stable.

In the present study, powders of different compositions in the range 0.5 to 0.8 mole%  $\text{BiFeO}_3$  have been fabricated from the mixed oxides. Comminution to an average particle size of  $5\text{ }\mu\text{m}$  was accomplished by a water quenching of the calcined cake. It appears that the very high tetragonal  $c/a$  ratio in the ferroelectric form leads to spontaneous rupture as the agglomerated powder is quenched through the Curie point.

Powders are now being incorporated into suitable elastomer matrix phases to form 0-3 connected piezoelectric composites.

#### 6.4 Relaxor Ferroelectrics

In conjunction with the Dielectric Center Studies, the effects of some 14 modifier cations incorporated into lead magnesium niobate have been assessed. Properties studied were the sintering characteristics, dielectric properties, electrostrictive  $Q_{12}$  and the diffuseness of the phase change at  $T_c$ . To maintain the perovskite structure, dopant levels were less than 10 mole% of the added oxide. In general, the maximum dielectric permittivity increased linearly with increasing Curie temperature. Linearity of dielectric response decreased with increasing permittivity. The electrostriction constant  $Q_{12}$  decreased with increasing diffuseness of transition, as measured by the frequency dispersion.

A detailed account of this study is given in Appendix 31.



## 6.5 Crystal Growth

### 6.5.1 Perovskite Halides

In connection with our program to measure electrostriction parameters of simple cubic crystals, it was necessary to grow crystals of the fluoride perovskites  $\text{KMgF}_3$ ,  $\text{KMnF}_3$ ,  $\text{KZnF}_3$  and  $\text{KCaF}_3$ . The technique chosen was the Stockbarger method. Starting chemicals were high purity fluoride  $\text{KF}$ ,  $\text{MgF}_2$ ,  $\text{ZnF}_2$ ,  $\text{MnF}_2$  and  $\text{CaF}_2$ . Stoichiometric proportions were reacted and pre-melted in a conical closed graphite crucible. The crucible was used in the Crystallox crystal growth system, and acted as the susceptor for R.F. heating. Cooling from the bottom of the crucible was accomplished by lowering out of the RF coil and thus uncoupling the susceptor, while rotating the crucible to even out lateral gradients.

Lowering rates  $\sim 3$  mm/hour were found to be optimum. The best samples produced so far have been for  $\text{KMgF}_3$  where we have generated single crystal boules in 1'' in diameter and over 1'' long.

### 6.5.2 $\text{Pb}_{1-x}\text{Ba}_x\text{Nb}_2\text{O}_6$

A major growth effort has been concerned with the attempt to grow single crystal of lead barium niobate at compositions very close to the  $\text{Pb}_{0.6}\text{Ba}_{0.4}\text{Nb}_2\text{O}_6$  composition of the morphotropic phase boundary. The MPB in this system is between a tetragonal 4 mm and an orthorhombic mm2 symmetry ferroelectric phase, but unlike the perovskite PZT system, the two modes of polarization are symmetry independent and the transition occurs because of an accidental degeneracy between the two Curie temperatures which vary in opposite manner with  $\text{BaNb}_2\text{O}_6$  addition to  $\text{PbNb}_2\text{O}_6$ .

The growth effort is shared with a Rockwell sponsored program which seeks to use the bronze close to the MPB for device application. In compositions on the tetragonal side,  $\epsilon_{11}$  increases as the composition comes closer to that of

the bounding phase, leading to very high values of  $d_{15}$  and  $r_{51}$  the piezoelectric and linear electro-optic effects. Since there are no ferroelastic twins in the uniaxial ferroelectric tetragonal state, the  $\text{Pb}_{0.6}\text{Ba}_{0.4}\text{Nb}_2\text{O}_6$  offers a most interesting practical attention to  $\text{BaTiO}_3$  for four wave mixing and optical phase conjugation.

In this program, the interest in the crystals is as a model system in which an MPB can be formed in a single crystal host so that the very sensitive optical methods can be employed to explore phase boundary motion, and the full single domain tensor properties can be measured and compared to predictions from phenomenological theory.

Progress to date is summarized in appendices 32 and 33.

### References

- (1) A. Safari. 'Perforated PZT:Polymer Composites with 3-1 and 3-2 Connectivity for Hydrophone Application,' Ph.D. Thesis in Solid State Science, The Pennsylvania State University (December, 1983).
- (2) M. Haun. 'Transverse Reinforced 1:3 and 1:3:0 PZT:Polymer Piezoelectric Composites with Glass Fibers,' M.S. Thesis in Solid State Science, The Pennsylvania State University (December, 1983).
- (3) N.M. Shorrocks, M.E. Brown, R.W. Whatmore, F.W. Ainger. *Ferroelectrics* 54:555 (1984).
- (4) R.Y. Ting, A.G. Halliyal, A. Bhalla. 'Polar Glass Ceramics for Sonar Transducers,' *Appl. Phys. Lett.* 44:852 (1984).
- (5) H. Banno, S. Saito. *Proc. 1st US:Japan Seminar on Electronic Ceramics, Rappongi, Tokyo* (1982).
- (6) T.R. Gururaja, W.A. Schulze, T.R. Shrout, A. Safari, L. Webster, L.E. Cross. *Ferroelectrics* 39:1245 (1981).
- (7) B.A. Auld, H.A. Kunkel, Y.A. Shui, Y. Wang. *Proc. IEEE Ultrasonics Symposium*, pg. 554 (1984).
- (8) B.A. Auld, Y.A. Shui, Y. Wang. *Journal de Physique* (in press).
- (9) K. Rittenmyer. 'Electrostriction in Cubic Halide Compounds,' Ph.D. Thesis in Solid State Science, The Pennsylvania State University (May, 1984).
- (10) A. Amin, L.E. Cross. *Ferroelectrics* 50:563 (1983).
- (11) X.L. Zhang, Z.X. Chen, L.E. Cross, W.A. Schulze. *J. Mat. Sci.* 18:968 (1983).
- (12) A.D. Bruce, R.A. Cowley. *J. Phys. C Solid State* 6:2422 (1973).
- (13) K. Uchino, L.E. Cross. *Ferroelectrics* 80:35 (1980).
- (14) P. Chen. *Int. J. Solids Structures* 16:1059 (1980).
- (15) H. Beige, G. Schmidt. *Exp. Technik. der Physik* 22:393 (1974).

- (16) E.J. Huibregtse, W.H. Bessey, M.E. Drougard. J. Appl. Phys. 30:899 (1959).
- (17) K. Roleder. J. Phys. E: Sci. Inst. 16:1157 (1983).
- (18) T. Shrout. 'A Phenomenological Theory for Predicting the Temperature Dependence of Elastic Compliance in Simple Proper Ferroelectric Tungsten Bronzes,' Ph.D. Thesis in Solid State Science, The Pennsylvania State University (May, 1981).
- (19) S. Nomura, K. Tonooka, J. Kuwata, L.E. Cross, R.E. Newnham. Proc. Second Mtg. on Ferroelectric Materials, Kyoto, Japan (1979).
- (20) K. Kakegawa. Solid State Comm. 24:769 (1977).

**APPENDIX 1**

The Pennsylvania State University  
The Graduate School  
Department of Materials Science and Engineering

Transverse Reinforcement of 1-3 and 1-3-0 PZT-Polymer  
Piezoelectric Composites with Glass Fibers

A Thesis in  
Ceramic Science


by  
Michael J. Haun

Submitted in Partial Fulfillment  
of the Requirements  
for the Degree of

Master of Science

December 1983

I grant The Pennsylvania State University the nonexclusive right to use this work for the University's own purposes and to make single copies of the work available to the public on a not-for-profit basis if copies are not otherwise available.

  
Michael J. Haun

## ABSTRACT

Piezoelectric PZT-polymer 1-3 and 1-3-0 composites were transversely reinforced with glass fibers to increase the hydrostatic piezoelectric charge and voltage coefficients ( $\bar{d}_h$  and  $\bar{g}_h$ ) for possible use in hydrophone applications. Modeling of these composites theoretically predicted large enhancements depending on the volume fractions of PZT rods, glass fibers, and polymer porosity, and on the Poisson's ratio and compliance of the polymer matrix. Experimentally fabricated composites also showed significant improvements in these coefficients with similar trends as theoretically predicted. These composites consisted of a foamed or non-foamed polymer matrix with PZT rods aligned parallel to the poling direction and glass fibers in the two transverse directions. The addition of glass fibers greatly decreased the transverse piezoelectric charge coefficient ( $\bar{d}_{31}$ ) by carrying most of the lateral stresses, while also reducing the adverse internal stresses that develop at the PZT/polymer interface. The longitudinal piezoelectric charge coefficient ( $\bar{d}_{33}$ ) is relatively unaffected, because the PZT rods carry most of the stress in the poling direction. This decoupling of the  $\bar{d}_{31}$  and  $\bar{d}_{33}$  coefficients enhances the hydrostatic piezoelectric charge coefficient ( $\bar{d}_h$ ). Due to the small percentage of PZT required, these composites have densities near that of water, and much lower dielectric constants than solid PZT, resulting in large increases in the hydrostatic piezoelectric voltage coefficient ( $\bar{g}_h$ ). By increasing the  $\bar{d}_h$  and  $\bar{g}_h$  coefficients the  $\bar{d}_h \bar{g}_h$  product, used as the figure of merit, is greatly enhanced.

**APPENDIX 2**



The Pennsylvania State University

The Graduate School

Perforated PZT-Polymer Composites with 3-1 and  
3-2 Connectivity for Hydrophone Applications

A Thesis in  
Solid State Science

by

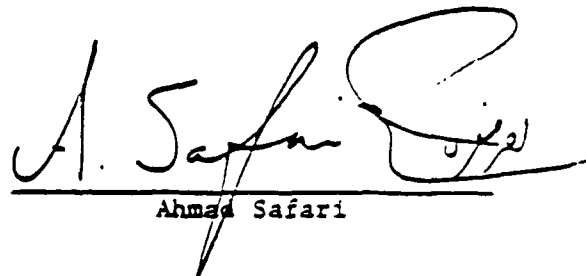
Ahmad Safari

Submitted in Partial Fulfillment  
of the Requirements  
for the Degree of

Doctor of Philosophy

December 1983

I grant The Pennsylvania State University the nonexclusive  
right to use this work for the University's own purposes and  
to make single copies of the work available to the public on  
a not-for-profit basis if copies are not otherwise available.



Ahmad Safari

## ABSTRACT

Lead zirconate-titanate (PZT) is widely used as a transducer material because of its high piezoelectric coefficients. However, for application in hydrophones, PZT is a poor material for several reasons. The hydrostatic piezoelectric coefficient,  $d_h (= d_{33} + 2d_{31})$ , is very low. The piezoelectric voltage coefficients,  $g_{33}$  and  $g_h$ , are low because of the high dielectric constant of PZT (1800). The acoustic matching of PZT with water is poor because of its high densities (7.9 g/cc). Moreover, it is a brittle, non-flexible ceramic.

In the last decade, several investigators have tried to fabricate composites of PZT and polymers to overcome the above problems of PZT. It has been shown that it is possible to improve upon the piezoelectric properties of homogeneous PZT by the composite approach. The concept that the connectivity of the individual phases control the the resulting properties has been demonstrated in a number of composites with different geometry and different connectivity of the individual phases. The piezoelectric properties of these composites are much more superior, compared to single-phase PZT. However, some of the earlier composites suffer from the disadvantages of difficulty in preparation or reduction in hydrostatic sensitivity with increasing pressure. Thus, there still exists a need to further improve the piezoelectric properties of these composites. Especially, it is

desirable to have the composites prepared without any problems in processing and fabrication and also show high figures of merit for hydrophone applications with little or no variation in static pressure sensitivity under hydrostatic loading.

In the present work, based on the theory of connectivity and the earlier work on composites with different connectivities, new composites with different connectivity patterns were fabricated, and their performance was evaluated for hydrophone applications. Most of the work was concentrated on composites with 3-1 and 3-2 connectivity. These composites were prepared by drilling either circular or square holes in prepoled PZT blocks, in a direction perpendicular to the poled axis and by filling the drilled holes with Spurr's epoxy. Initial theoretical modeling of the piezoelectric properties of these composites had shown a significant reduction in dielectric constants and a large enhancement in the piezoelectric  $\bar{d}_h$  and  $\bar{g}_h$  coefficients. The above model predicted large variations in both the dielectric and piezoelectric properties of composites on the geometry of composites (hole size, width and thickness). The model also predicted higher figures of merit for 3-2 composites.

Experimentally, the effects of several variables, such as poling of the composites during different stages of sample preparation, geometry and size of the composite and use of coupling agents, etc. on dielectric and piezoelectric properties of 3-1 composites, were investigated. On samples optimized for hydrophone performance, the  $\bar{g}_h$  and  $\bar{d}_h \bar{g}_h$  coefficients of composites were about 4 and 40 times greater for 3-1 composites and 25 and 150 times greater for 3-2 composites than those of solid PZT, respectively. For 3-1 composites, there was

practically no variation of  $\bar{\epsilon}_h$  with pressure up to 8.4 MPa. In the case of 3-2 composites, there was a slight variation of  $\bar{\epsilon}_h$  with pressure. Experimentally observed trends in the variation of dielectric and piezoelectric properties of both 3-1 and 3-2 composites were similar to those predicted by the model, and, as predicted by the model, 3-2 composites showed higher piezoelectric figures of merit than 3-1 composites.

As part of the present work, a simple procedure, suitable for mass production was developed to prepare composites of PZT spheres with a polymer. In this method, PZT spheres of different size could be prepared by grinding PZT cubes for several hours. Later, the PZT spheres were arranged in a monolayer and were covered with a suitable polymer to obtain composites with a 1-3 connectivity pattern. These composites had lower density and dielectric constants than solid PZT, and the values of  $\bar{d}_h$  and  $\bar{d}_h \bar{\epsilon}_h$  of these composites were comparable with the corresponding values of PZT. With this method, it is possible to prepare large areas of flexible composites with reproducible properties.

**APPENDIX 3**

## TRANSVERSELY REINFORCED 1-3 AND 1-3-0 PIEZOELECTRIC COMPOSITES

M.J. HAUN, P. MOSES, T.R. GURURAJA, W.A. SCHULZE AND R.E. NEWNHAM, Materials Research Laboratory, The Pennsylvania State University, University Park, PA 16802

**Abstract** Piezoelectric PZT-polymer 1-3 and 1-3-0 composites were transversely reinforced with glass fibers to increase the hydrostatic piezoelectric coefficients for possible use in hydrophone applications. Modeling of these composites theoretically showed that the  $d_{hgh}$  figure of merit is a function of the volume fractions of PZT rods, glass fibers, and polymer porosity, and of the Poisson's ratio and compliance of the polymer matrix. Experimental results showed significant enhancements of the  $d_{hgh}$  figure of merit with the addition of glass fibers. Comparisons of the theoretical predictions and the experimental results were made.

### INTRODUCTION

Lead zirconate titanate (PZT) ceramics have low hydrostatic piezoelectric charge and voltage coefficients,  $d_h$  and  $g_h$ , respectively. Even though the magnitudes of the  $d_{33}$  and  $d_{31}$  coefficients are large, the hydrostatic coefficient  $d_h (= d_{33} + 2d_{31})$  is low, because the  $d_{33}$  and  $d_{31}$  are opposite in sign. The hydrostatic coefficient  $g_h (= d_h/\epsilon_3)$  is also small, because the permittivity  $\epsilon_3$  is high for PZT. With the basic idea of decoupling the  $d_{33}$  and  $d_{31}$  coefficients and lowering the permittivity, PZT-polymer composites of different connectivity patterns have been fabricated with remarkable improvements in the  $d_h$  and  $g_h$  coefficients<sup>1</sup>.

One type of connectivity pattern that has been particularly successful is the 1-3 composite with PZT rods aligned in the poling direction ( $x_3$ ) held together by a polymer matrix. The stiffer PZT rods support most of an applied stress in the  $x_3$  direction, due to the parallel connection with the more compliant polymer phase. The  $d_{33}$  coefficient of the composite would ideally be equal to the  $d_{33}$  of single-phase PZT. In the  $x_1$  and  $x_2$  directions of the composite the PZT rods are connected in series with the polymer matrix. This leads to a reduction of the  $d_{31}$  coefficient compared to single-phase PZT. Thus the  $d_h$  coefficient for a 1-3 composite is increased. With the replacement of PZT with polymer, the permittivity of the composite is greatly reduced, resulting in a significantly enhanced  $g_h$  coefficient.

The Poisson's ratio of the polymer is a very important parameter in designing composites for hydrostatic applications. If the Poisson's ratio of the polymer is large, the polymer will be

M.J. HAUN, P. MOSES, T.R. GURURAJA, W.A. SCHULZE, R.E. NEWHAM

hydrostatically incompressible, and adverse internal stresses develop at the ceramic-polymer interface, which contribute to the  $d_{31}$  coefficient. Porosity can be introduced into the polymer phase to decrease these internal stresses. Glass fibers aligned in the  $x_1$  and  $x_2$  directions of the composite will also reduce the internal stresses, with the additional benefit of supporting the transverse stresses, decreasing the  $d_{31}$  coefficient without appreciable reduction of the  $d_{33}$  coefficient. The effect of glass fibers as transverse reinforcement in 1-3 and 1-3-0 composites was investigated. The product of the  $d_{31}$  and  $g_{31}$  coefficients was used as the figure of merit.

#### THEORETICAL MODELING

The theoretical modeling of piezoelectric PZT-polymer composites provides the understanding required for the selection of the properties of the materials used and the connectivity needed for the optimization of the desired figure of merit. In this section, the modeling of 1-3, 1-3-0, 1-2-3, and 1-2-3-0 piezoelectric composites will be described to demonstrate the improvements in properties that are theoretically possible through the use of composites compared to single-phase PZT<sup>2</sup>.

The following assumptions were made:

- 1) The fibers are homogeneous, linearly elastic, regularly and closely spaced in square arrays, and perfectly aligned.
- 2) The matrix is homogeneous, and linearly elastic.
- 3) Perfect bonding exists between constituent phases.
- 4) Constant stress exists across parallel connections.
- 5) Constant strain exists across series connections.
- 6) Planes of equal strain exist throughout individual fibers (no buckling of fibers occurs). Thus the fibers are supported by the regions of fiber cross over.
- 7) Polymer porosity is represented by an equivalent cubic volume.

The elastic properties of the PZT, polymer and glass fiber phases are accounted for, along with the internal stress effects due to the differences in the  $s_{ij}$  compliance coefficients of the phases. The addition of polymer porosity has also been accounted for through the modification of the elastic properties of the polymer phase.

The  $\bar{d}_{33}$  and  $\bar{d}_{31}$  coefficients were determined by modeling the stresses in the  $x_1$  and  $x_2$  directions of the composite separately. In each of these directions, the composite was divided into distinct parallel sections that were either single phase or a series connection of two or more phases. By determining the desired properties of the individual sections with series models, the sections were then combined with parallel models. The resulting equations relate the piezoelectric coefficients of the composite to the volume fractions and material constants of the constituent phase.

# TRANSVERSELY REINFORCED 1-3 AND 1-3-0 PIEZOELECTRIC COMPOSITES

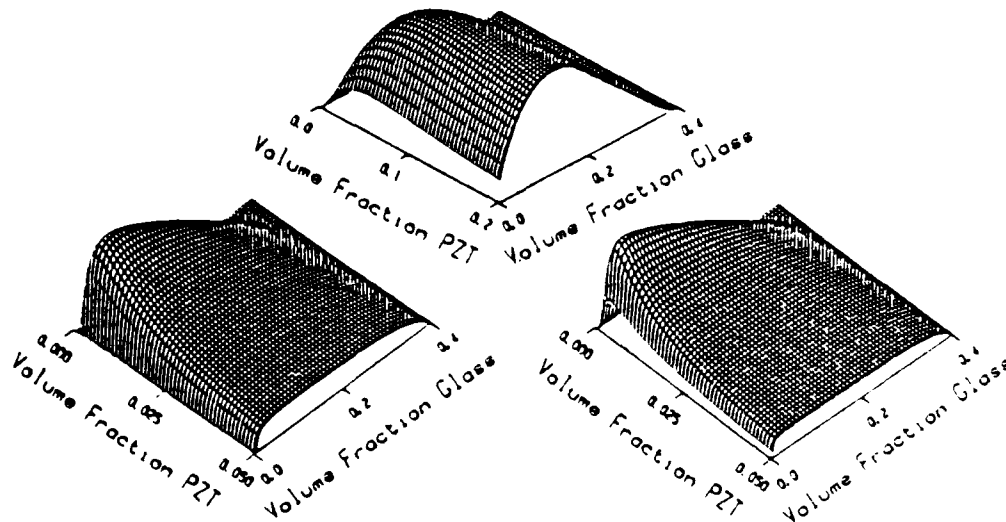
From the model, the dependencies of the  $d_{33}$  figure of merit were found with respect to the volume fractions of PZT rods, glass fibers, and polymer porosity, and the Poisson's ratio and compliance of the polymer matrix. Figure 1 shows three dimensional surfaces of the  $d_{33}$  figure of merit plotted against the volume of fractions of PZT rods and glass fibers for an unfoamed epoxy matrix, an unfoamed polyurethane matrix, and a twenty percent foamed polyurethane matrix, respectively. The following general observations were made:

- 1) The addition of glass fibers to all three polymer matrices significantly improves the  $d_{33}$  figure of merit.
- 2) Even though the compliance ( $s_{11}$ ) of polyurethane is about two orders of magnitude greater than that of epoxy, low figure of merit are seen when no glass fibers are present. This is due to the high Poisson's ratio of polyurethane, which creates large adverse internal stresses at the PZT-polymer interface that contribute to the  $d_{31}$  coefficient.

(a) Unfoamed Epoxy Matrix

$$\text{Max } d_{33} g_k = 11100 \times 10^{-15} \text{ m}^2/\text{N}$$

$$\text{PZT} = 10.8\% \quad \text{Glass} = 10.2\%$$



(b) Unfoamed Polyurethane Matrix

$$\text{Max } d_{33} g_k = 759000 \times 10^{-15} \text{ m}^2/\text{N}$$

$$\text{PZT} = 0.45\% \quad \text{Glass} = 4.7\%$$

(c) 20% Foamed Polyurethane Matrix

$$\text{Max } d_{33} g_k = 1105000 \times 10^{-15} \text{ m}^2/\text{N}$$

$$\text{PZT} = 0.35\% \quad \text{Glass} = 3.5\%$$

Figure 1. Three dimensional surfaces of the  $d_{33}$  figure of merit as a function of the volume fractions of PZT rods and glass fibers.



3) The addition of glass fibers and/or polymer porosity lowers the Poisson's ratio of the polymer, reducing the internal stresses, and thus increasing the figure of merit.

4) With increasing compliance of the polymer matrix (epoxy < polyurethane < foamed polyurethane), the maximum  $d_{33}$  figure of merit increases, and shifts to smaller volume fractions of PZT rods and glass fibers.

5) As the volume fraction of glass fibers approaches the maximum of 0.4 (the fibers are touching), the  $d_{33}$  figure of merit decreases, because the glass fibers significantly reduce the stress on the PZT rods in the  $x_3$  direction.

#### EXPERIMENTAL PROCEDURE

Fabrication of PZT-polymer composites with 1-3 and 1-3-0 connectivity has been reported earlier<sup>3,4</sup>. PZT rods were aligned parallel to each other using a brass rack, and suspended over film canister lids. The lids were filled with spurts epoxy and cured. The epoxy served as a base to hold the PZT rods in place, so that the brass racks could be removed. For the transverse reinforcement, E-glass fibers were aligned and supported by an epoxy base as described above. Two glass fiber arrays were interposed in the  $x_1$  and  $x_2$  directions through the PZT array. The arrangements provided the basic structure of a transversely reinforced 1-3 or a 1-2-3 composite. The PZT-glass fiber structures were placed in a container and vacuum impregnated in either spurts epoxy, Devcon polyurethane, or a foamed Devcon polyurethane matrix. After curing the polymer, samples were cut to a thickness of 4.5 mm along the  $x_3$  direction. To prevent the penetration of oil, the foamed polyurethane composites were provided with a thin layer of spurts epoxy in the  $x_1$  and  $x_2$  directions. Electrodes in the  $x_3$  direction were provided by silver epoxy.

The samples were poled in a 10°C oil bath with a field of 10 kV/cm applied for five minutes. After 24 hours, the capacitance and dissipation factor were measured at 1 kHz under atmospheric pressure, and also under hydrostatic pressure for use in  $d_{33}$  calculations at higher pressures. The hydrostatic piezoelectric coefficient,  $d_{33}$ , was measured in a sealed oil-filled chamber by applying pressure at the rate of 0.3 MPa/sec (50 psi/sec). The charge released by the sample was measured with an electrometer and plotted as a function of pressure on an x-y recorder. The composites were pressure-cycled at least five times with the calculated  $d_{33}$  values taken from the fifth cycle.

#### RESULTS AND DISCUSSION

Modeling of 1-3 and 1-2-3-0 composites showed that the addition of glass fibers as transverse reinforcement of normal 1-3 and 1-3-0 composites should improve the  $d_{33}$  figure of merit significantly. Composites of these types have been fabricated with five percent PZT rods and various volume fractions of glass fibers and polymer matrices. Figure 1 shows the experimental results of the

# TRANSVERSELY REINFORCED 1-3 AND 1-3-0 PIEZOELECTRIC COMPOSITES

$d_{33}$  figure of merit for measurements made at 0.6 MPa (100 psi) of epoxy, polyurethane, and encapsulated ten percent foamed polyurethane matrix composites as a function of the glass fiber percentage. Theoretical predictions are also shown on Figures 2(a) and 2(c).

Figure 2(a) shows that for epoxy composites, over a range of glass fiber percentages, the figure of merit increased from 2000 to nearly 3500, and then with greater percentages decreased to less than 1000. The differences in theoretical predictions and experimental results are probably due to the difficulties involved in fabricating these composites and the theoretical assumptions of equal strain across parallel connections and perfect bonding.

Figure 2(b) shows that for polyurethane composites almost an order of magnitude enhancement occurs from the addition of glass fibers. Most of this increase is probably due to the glass fibers reducing the internal stresses through the combined effects of the reduction of the polymer Poisson's ratio and the anisotropic stiffening of the polymer. A large difference exists between the

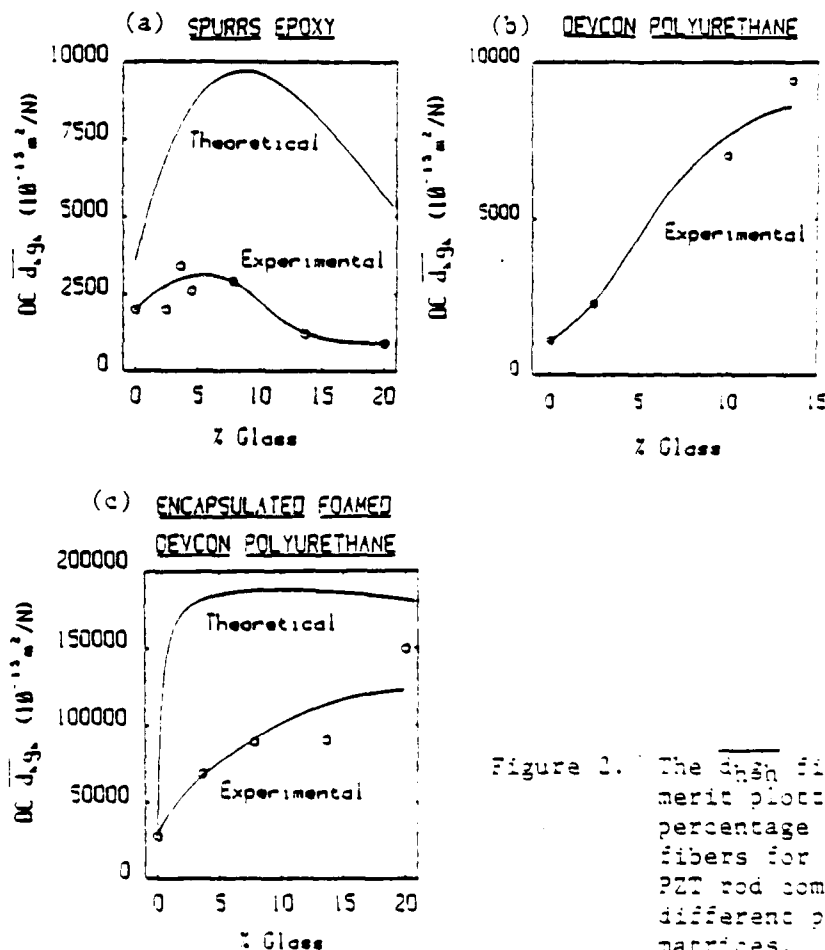


Figure 2. The  $d_{33}$  figure of merit plotted versus the percentage of glass fibers for five percent PZT rod composites with different polymer matrices.

M.J. HAUN, P. MOSES, T.R. GURURAJA, W.A. SCHULZE, R.E. NEWMHAM

theoretical and experimental results with the addition of glass fibers. Theoretically the  $\bar{G}_{Hgh}$  would increase from around 1000 at zero percent PZT to greater than 100,000 with only a small addition of glass fibers. Again this difference is due to the experimental processing difficulties and the theoretical assumptions. Polyurethane is very compliant, causing PZT rods to break and the bonding to be weak. For these reasons, the differences are larger than for the stiffer epoxy composites.

Figure 2(c) show that for encapsulated ten percent foamed polyurethane composites a very significant increase in the figure of merit occurs with the addition of glass fibers. The theoretical prediction is very good when no glass fibers are present, but an over-estimation develops when the glass fibers are added. During the fabrication of the polyurethane matrix composites, the glass fibers contributed to a larger breakage of PZT rods than when the glass fibers were not included. This along with the previously described reasons probably account for the differences in theoretical predictions and experimental results. The differences are much less for these composites compared to the unfoamed polyurethane composites probably due to the epoxy encapsulation used, which may have caused an additional transverse reinforcement.

#### CONCLUSIONS

- 1) Modeling of 1-2-3 and 1-2-3-0 composites has helped in the understanding and design of improved hydrophone devices.
- 2) The  $\bar{G}_{Hgh}$  figure of merit was shown theoretically to be a function of the volume fractions of PZT rods, glass fibers and polymer porosity, and of the Poisson's ratio and compliance of the polymer.
- 3) The assumption of constant strain across parallel connections and perfect bonding between the constituent phase along with the processing difficulties have caused the theoretical predictions to be greater than the experimental results, although similar trends were shown.
- 4) Transverse reinforcement of epoxy composites only slightly improved the  $\bar{G}_{Hgh}$  figure of merit.
- 5) Transverse reinforcement of polyurethane and encapsulated foamed polyurethane composites significantly improve the  $\bar{G}_{Hgh}$  figure of merit.
- 6) Encapsulation of foamed polyurethane composites reduces degradation and probably adds transverse reinforcement.

#### REFERENCES

1. R.E. Newnham, L.J. Bowen, K.A. Klinker, L.E. Cross, Mat. Engr. **2**, 93 (1980).
2. M.J. Haun, M.S. Thesis, The Pennsylvania State University, 1983.
3. K.A. Klinker, J.W. Biggers, R.E. Newnham, J. Am. Ceram. Soc. **64**(1), 5 (1981).
4. K.A. Klinker, W.A. Schulze, J.W. Biggers, J. Am. Ceram. Soc. **65**(2), C-108 (1982).

**APPENDIX 4**

## PERFORATED PZT-POLYMER COMPOSITES FOR PIEZOELECTRIC TRANSDUCER APPLICATIONS

A. SAFARI, R. E. NEWNHAM, L. E. CROSS† and W. A. SCHULZE

Materials Research Laboratory, The Pennsylvania State University, University Park,  
Pennsylvania 16802, USA

(Received April 5, 1981)

Composites of PZT and polymer with 3-1 and 3-2 connectivity patterns have been fabricated by drilling holes in sintered PZT blocks and filling the holes with epoxy. The influence of hole size and volume fraction PZT on the hydrostatic properties of the composite was evaluated. By decoupling the piezoelectric  $d_{31}$  and  $d_{32}$  coefficients in the composite, the hydrostatic coefficients are greatly enhanced. On samples optimized for hydrophone performance, the dielectric constants of 3-1 and 3-2 composites are 600 and 300 respectively. The piezoelectric coefficients  $\bar{d}_3$ ,  $\bar{g}_3$ , and  $\bar{d}_3\bar{g}_3$  for 3-1 composites are 230 (pC/N<sup>-1</sup>),  $34 \times 10^{-11}$  Vm/N<sup>-1</sup>, and 7800 ( $10^{-13}$  m<sup>2</sup>N<sup>-1</sup>) respectively, and the corresponding values for 3-2 composites are 172 (pC/N<sup>-1</sup>), 123 ( $10^{-11}$  Vm/N<sup>-1</sup>), and 45000 ( $10^{-13}$  m<sup>2</sup>N<sup>-1</sup>).

### 1. INTRODUCTION

In recent years several types of PZT-polymer composites have been fabricated to improve the piezoelectric properties of poled PZT (lead zirconate titanate) ceramics. Different types of macro-symmetry and interphase connectivity were utilized in the design of the PZT-polymer composites listed in Table I.<sup>1-6</sup> Here connectivity 1-3 means that the PZT phase is self-connected in one direction, and the polymer phase is self-connected in all three directions. In all composites, the dielectric constant  $\bar{K}_{11}$  of solid PZT is lowered by the introduction of a polymer phase, and in all cases the hydrostatic piezoelectric charge coefficient  $\bar{d}_3$  is also enhanced. The hydrostatic piezoelectric voltage coefficient  $\bar{g}_3$  and the  $\bar{d}_3\bar{g}_3$  product used as a figure of merit for hydrophone application are therefore considerably enhanced in all the composite designs.

Klicker *et al.*<sup>4</sup> have fabricated 1-3 composites of PZT rods embedded in an epoxy matrix. As shown in Table I, these composites have better piezoelectric properties than solid PZT. The hydrostatic coefficients  $\bar{d}_3$  and  $\bar{g}_3$  are a function of the dimension of PZT rods, the spacing between the PZT rods, and the thickness of the composite. Based on the previous work with PZT-polymer

composites and on simple series and parallel models,<sup>1</sup> it is clear that the difference in the elastic compliances of the PZT and epoxy has a favorable influence on piezoelectric properties by altering the stress pattern inside the composites.

Rittenmyer *et al.*<sup>1</sup> have fabricated 3-3 composites of PZT and polymer (polymethyl methacrylate) with PZT powder in an organic binder and firing the mixture to give a ceramic skeleton. After cooling, the ceramic skeletons were back-filled with polymer (Burps composites). As shown in Table I, these composites have better piezoelectric and mechanical properties compared to 1-3 composites of PZT rods with epoxy. In addition, the Burps composites are much easier to prepare.

The present study focuses on composites with 3-1 and 3-2 connectivity patterns, in which the PZT phase is self-connected in three dimensions and the polymer phase is self-connected in either one or two dimensions. Samples were prepared by drilling holes in sintered PZT blocks either in one direction (3-1 connectivity) or in two directions (3-2 connectivity) and backfilling the perforated PZT blocks with a suitable polymer. Enhancement of  $\bar{d}_3$  was anticipated in these composites because of the modified stress distribution within the composite.

### 2. SAMPLE PREPARATION

PZT-polymer composites were prepared by drilling holes in sintered PZT blocks and filling the

† Also affiliated with the Department of Electrical Engineering.

TABLE I  
Piezoelectric Properties of PZT-Polymer Composites

	$\bar{K}_{11}$	$\bar{d}_3$ (PCN <sup>-1</sup> )	$\bar{d}_3$ (10 <sup>-11</sup> VmN <sup>-1</sup> )	$\bar{d}_3\bar{g}_3$ (10 <sup>-19</sup> m <sup>3</sup> N <sup>-1</sup> )	Reference
PZT	1600	50	4	200	Present work
PZT particles in silicone rubber matrix (0-3 connectivity)	100	28.3	32	900	4
PZT replamine in a silicone rubber matrix (3-3 connectivity)	50	35.8	80	2800	2
PZT rods in an epoxy matrix (1-3 connectivity)	200	77.6	40.4	3138	5
PZT rods in a polyurethane matrix (1-3 connectivity)	83	176.2	239	42100	5
Burps composite (epoxy matrix) (3-3 connectivity)	500	120	27	3200	3
Burps composite (silicone rubber matrix) (3-3 connectivity)	300	260	100	26000	3

perforated block with a polymer. To prepare the ceramic, 95 wt% of PZT 501A† was mixed with 5 wt% of 15% PVA solution. After mixing and drying the powder, square pellets measuring 2 cm on edge and 4 to 8 mm thick, were pressed at 20,000 psi (140 MPa). The pellets were placed on a platinum sheet and the binder was burned out at 550°C for one hour. Sintering was carried out in a sealed alumina crucible using a silicon carbide resistance furnace at a heating rate of 200°C per hour, with a soak period of one hour at 1285°C. A PbO-rich atmosphere was maintained with sacrificial ceramic pellets of composition 97 mole% PZT and 3 mole% PbO inside the crucible.<sup>9</sup> After firing, the samples were polished and cut into smaller pieces of various dimensions. Air-dried silver paste electrodes‡ were applied to the pellets. Poling was done in a stirred oil bath at 140°C at a field of 25 KV/cm for three minutes. After poling, three or four holes were drilled perpendicular to the poling direction using an ultrasonic cutter.§ Samples were prepared with different hole sizes and hole separation  $X$  (Figure 3a). The drilled samples were then placed in a small plastic tube and a commercial polymer (vinylcyclohexene dioxide-epoxy||) was poured into the tube. The epoxy was cured

at 70°C for eight hours. Finally, the composites were polished on silicon carbide paper to expose the PZT and to ensure that the faces of the disk were smooth and parallel. Electrodes of air-dried silver paste were applied and the composites were aged for at least 24 hours prior to any measurement. Some of the 3-1 and 3-2 composites are shown in Figure 1.

### 3. MEASUREMENTS

The dielectric constants and loss factors of all the samples were measured at a frequency of 1 KHz using an automated capacitance bridge.¶ The piezoelectric coefficient  $\bar{d}_{31}$  along the poling direction was measured using a  $d_{31}$  meter.\*\* The hydrostatic piezoelectric  $\bar{d}_4$  was measured by a pseudo-static method.<sup>1</sup> Samples were immersed in an oil-filled cylinder, and pressure was applied at a rate of 3.5 MPa/sec. The resulting charge was collected with a Keithley electrometer‡‡ operated in a feedback charge integration mode. The piezoelectric voltage coefficients  $\bar{g}_{31} = d_{31}/\epsilon_0\bar{K}_{11}$  and  $\bar{g}_4 = d_4/\epsilon_0\bar{K}_{11}$  were calculated from the measured values of  $d_{31}$ ,  $d_4$  and  $\bar{K}_{11}$ .

† Ultrasonic Powders, Inc., South Plainfield, NJ (PZT 501A).

‡ Materials for Electronics, Inc., Jamaica, NY, Demetron 200.

§ Sheffield Ultrasonic Machine Tool, Dayton OH.

|| Spurr's low viscosity embedding media, No. 5135, Polysciences Inc., Warrington, PA, 1976.

¶ Hewlett Packard (Model 4270A) Automated Capacitance Bridge, Hewlett Packard, 1-59-1 Yoyogi, Tokyo, Japan. §

\*\* Bertincourt (Model 333)  $d_{31}$  meter, Channel Products, Inc., 16722 Park Circle Drive, Chagrin Falls, OH, 44020.

‡‡ Keithley (Model 516) Digital Electrometer, Keithley Instruments, Inc., Cleveland, OH.

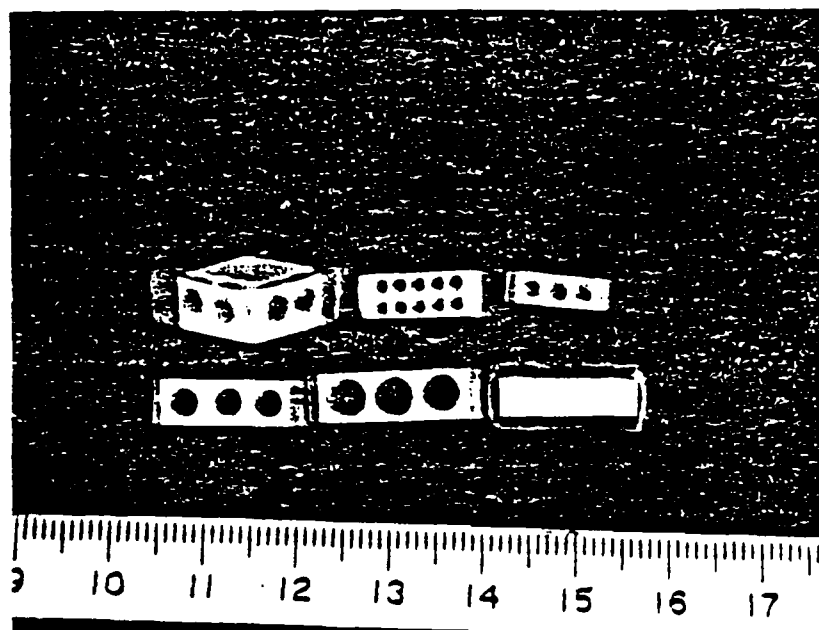


FIGURE 1.

#### 4. RESULTS AND DISCUSSION

Unless otherwise stated, the results refer to composites with 3-1 connectivity. The dielectric constants for 3-1 composites are plotted in Figures 2 and 3 as a function of  $X$  (the center-to-center distance for adjacent holes) for two different hole sizes. The dielectric constant increases linearly with  $X$  at lower values of  $X$ , but reaches a saturation value for higher values. Composites with smaller thicknesses have lower dielectric constants. Also, it is observed that for the same  $D/t$  (diameter to thickness ratio), composites with smaller diameter holes have higher dielectric constants than composites with larger holes (see Figures 2 and 3). Dielectric constants of 3-2 composites were much lower than the 3-1 composites for samples with identical hole sizes (Table II). Calculated values of dielectric constants are also plotted in Figures 2 and 3 for comparison.

The values of  $d_{31}$  were used as a measure of the degree of poling. Measured values of  $d_{31}$  for 3-1 composites are plotted as a function of  $X$  in Figure 4. It is observed that  $d_{31}$  increases linearly with  $X$  at lower values of  $X$ , but approaches a saturation value at higher values of  $X$ . Each of the data points represents the average of at least twelve

value measurements at different places on the electroded surface of the composites. The measured values of  $d_{31}$  in the regions over the holes were about 10% lower than the  $d_{31}$  values in solid regions (Figure 8a). It is significant that the  $d_{31}$  values for most of the composites exceed 300 pC/N, which is close to the  $d_{31}$  coefficients of solid PZT (400 pC/N). It is found that in all composites  $d_{31}$  decreases slightly with thickness. Also, composites with smaller hole sizes had larger  $d_{31}$  coefficients than composites with larger hole sizes. In all 3-2 composites the measured  $d_{31}$  values were also higher than 300 pC/N (Table I).

In Figure 5 the hydrostatic piezoelectric coefficient ( $\bar{d}_h$ ) of 3-1 composites is plotted as a function of  $X$  for different thicknesses. A broad maximum is observed for  $X$  values between 4 and 4.5 mm for composites containing 60% to 70% PZT by volume. Figure 6 shows  $\bar{d}_h$  plotted as a function of thickness for composites with different  $X$ . Again it is found that  $\bar{d}_h$  increases with thickness, up to certain thickness, and then decreases. Figure 7 shows the effect of poling on the values of  $\bar{d}_h$ , when poling is carried out at several different stages in the process:

1. Poling PZT block before drilling the holes.





TABLE II

	Hole Size (mm)	Composite Thickness (mm)	X (mm)	$\bar{K}_{11}$	$\bar{d}_{11}$ (PCN <sup>-1</sup> )	$\bar{g}_{11}$ (10 <sup>-3</sup> VmN <sup>-1</sup> )	$\bar{d}_h$ (PCN <sup>-1</sup> )	$\bar{g}_h$ (10 <sup>-3</sup> VmN <sup>-1</sup> )	$\bar{d}_h \bar{g}_h$ (10 <sup>-13</sup> M <sup>2</sup> N <sup>-1</sup> )
Perforated PZT/epoxy (3-1 connectivity)	3.2	6.5	4.25	810	340	47	210	29	6000
Perforated PZT/epoxy (3-1 connectivity)	3.2	6	4.25	760	350	52	230	34	7300
Perforated PZT/epoxy (3-1 connectivity)	3.2	5.5	4.25	740	330	50	200	30	6000
Perforated PZT/epoxy (3-1 connectivity)	3.2	4.5	4.25	680	320	53	190	31	5900
Perforated PZT/epoxy (3-1 connectivity)	4.2	6.8	4.75	470	290	70	190	46	8600
Perforated PZT/epoxy (3-1 connectivity)	4.2	6.5	4.75	450	290	73	222	56	12300
Perforated PZT/epoxy (3-1 connectivity)	4.2	6	4.75	425	280	74	170	45	7600
Perforated PZT/epoxy (3-1 connectivity)	4.2	5.5	4.75	410	275	76	120	33	3950
Perforated PZT/epoxy (3-2 connectivity)	3.2	6.7	4.5	360	290	90	238	74	17600
Perforated PZT/epoxy (3-2 connectivity)	3.2	6.2	4.5	330	290	99	294	100	29000
Perforated PZT/epoxy (3-2 connectivity)	3.2	6	4.5	320	300	105	322	113	36300
Perforated PZT/epoxy (3-2 connectivity)	3.2	5.8	4.5	290	290	114	329	128	42000
Perforated hollow PZT sealed with polymer (3-2 connectivity)	3.2	6.2	4.5	340	340	112	372	123	45700

2. Poling the perforated PZT before filling it with epoxy.

3. Poling after embedding the perforated PZT block with epoxy.

From these experiments it was concluded that to get higher values of  $d_h$  it is necessary to prepole the PZT blocks before drilling.

It should be emphasized that for all composites, the  $d_h$  coefficients are at least twice that of solid PZT (50 pC/N). Hydrostatic coefficients for the 3-2 composites are much larger than those of 3-1 composites. An even higher value of  $d_h$  was observed when measurements were made on perforated blocks of PZT in which the open sides were enclosed with a thin polymer sheet, thereby keeping the inside region completely empty. When measured in this way a  $d_h$  value of nine times greater than that of solid PZT was observed (Table II).

Some typical values of  $\bar{K}_{11}$ ,  $\bar{d}_{11}$ , and  $\bar{d}_h$  are given in Table II. It is important to note that  $d_h$  depends markedly on the thickness of the PZT region above and below the holes (see Figure 3a). There

is a critical thickness for which  $\bar{d}_h$  becomes a maximum (Table II).

Piezoelectric voltage coefficients  $\bar{g}_{11}$  and  $\bar{g}_h$  are also substantially larger than those of solid PZT. As shown in Table II, the piezoelectric voltage coefficients  $\bar{g}_{11}$  and the hydrostatic voltage coefficients  $\bar{g}_h$  are very large for 3-2 composites. The  $d_h \bar{g}_h$  product used as a figure of merit for hydrostatic applications is more than 200 times the corresponding value for solid PZT.

## 5. THEORETICAL MODEL

The physical properties of 3-1 composites can be approximated with the model illustrated in Figure 3. For simplicity, consider a square of length  $l$  whose area is equal to that of a circle with radius  $r$ . Then  $l = r\sqrt{\pi}$ .

We can visualize the 3-1 composite as made up of two parts A and B connected in parallel as shown in Figure 3b. Part B is composed of two phases connected in series, PZT and polymer. The

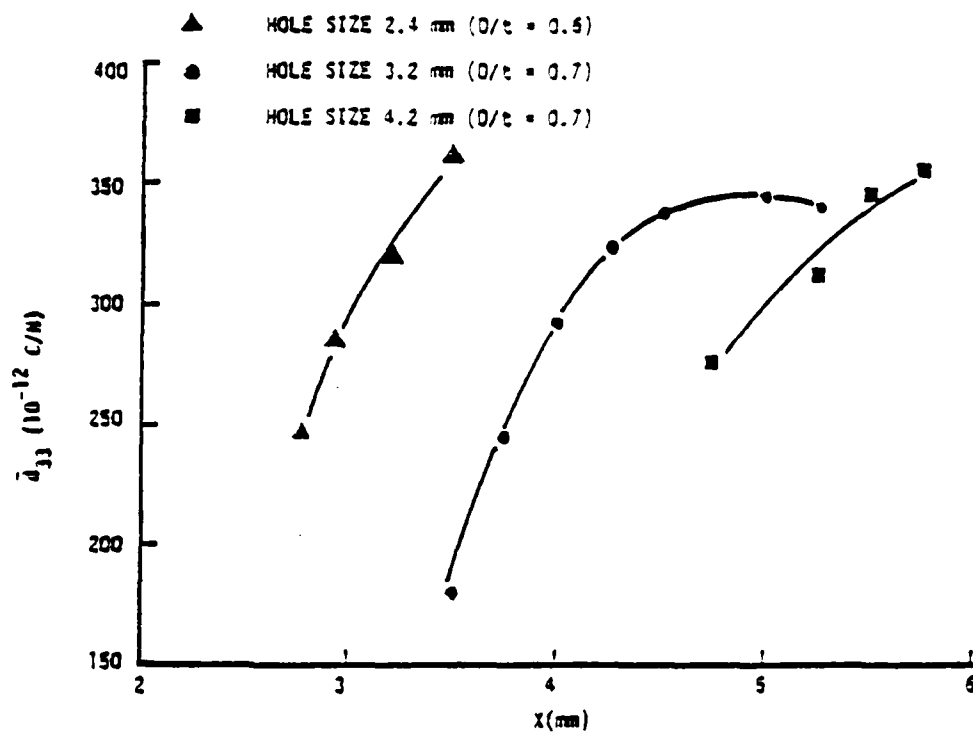


FIGURE 4.

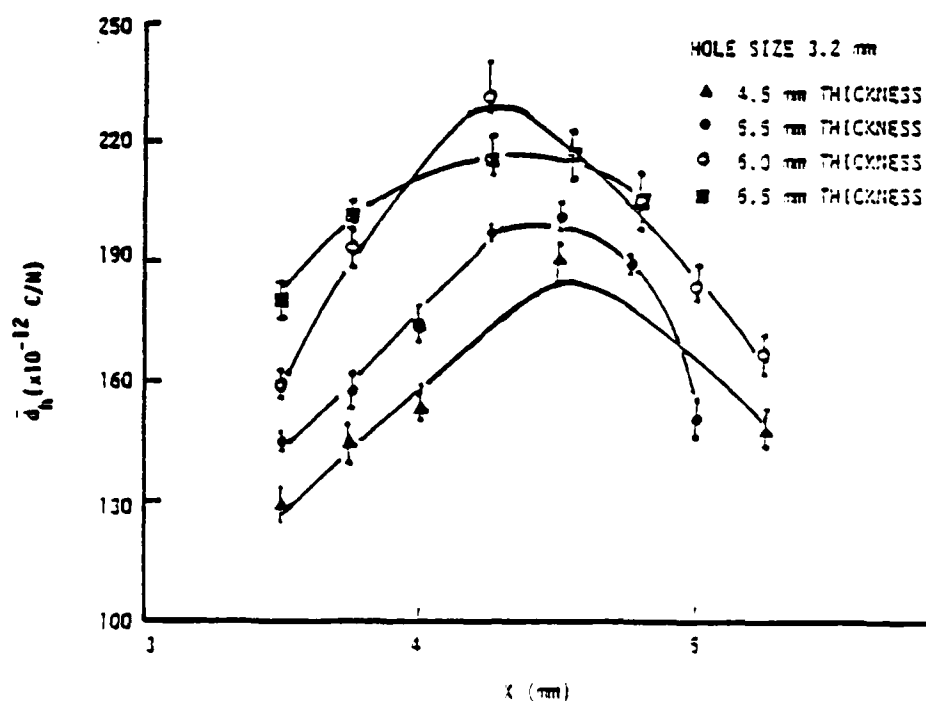


FIGURE 5.

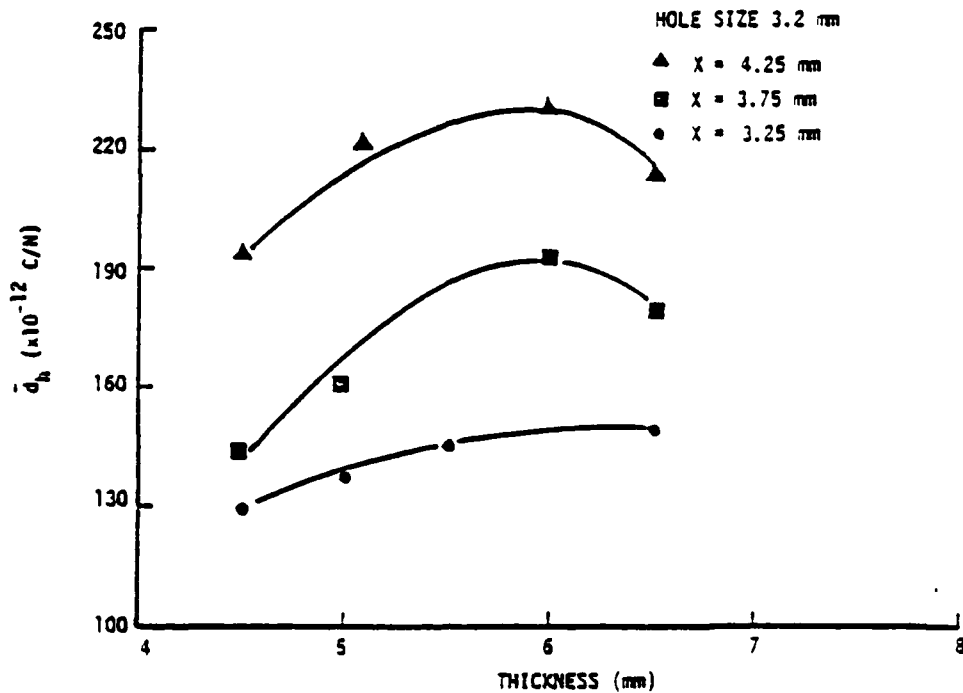


FIGURE 6.

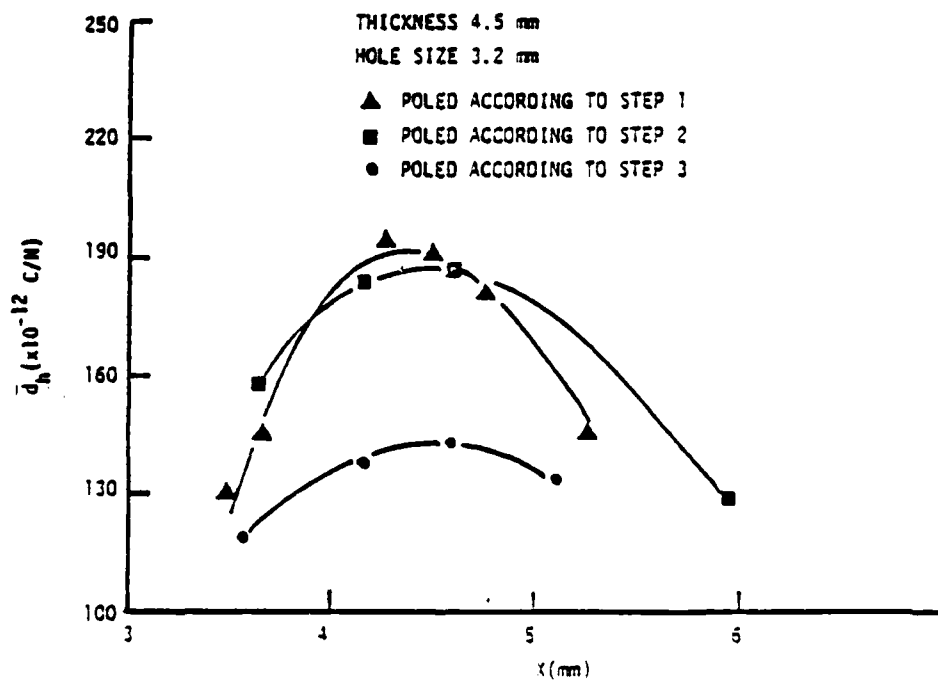


FIGURE 7

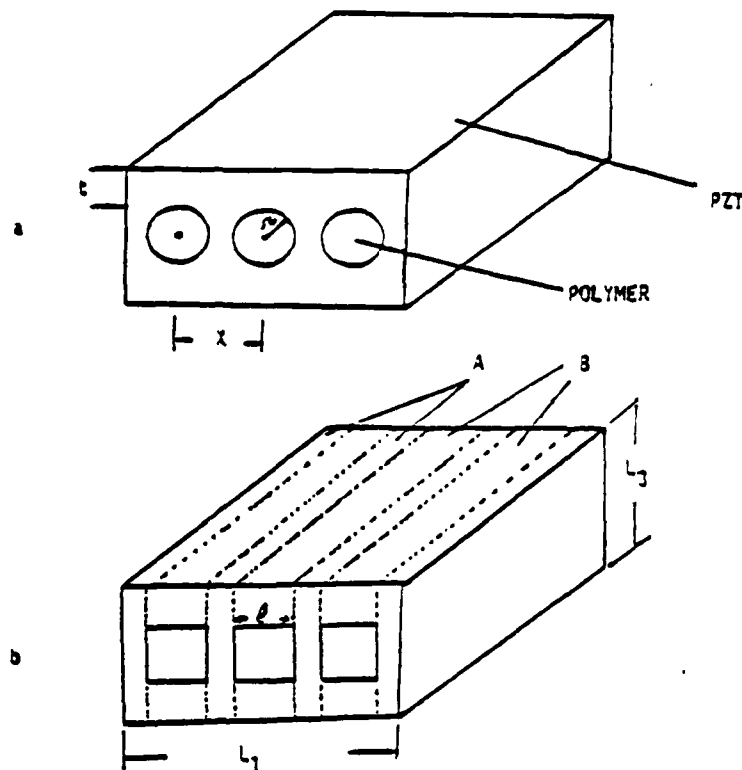


FIGURE 1.

following quantities can be defined with respect to the dimensions of the composites.

$${}^A V \text{ (volume fraction of PZT of part A)} = (L_1 - nL)/L_1$$

$${}^B V \text{ (volume fraction of part B)} = nL/L_1$$

$${}^{1B} V \text{ (volume fraction of PZT in part B)} = (L_1 - L)/L_1$$

$${}^{2B} V \text{ (volume fraction of polymer in part B)} = L/L_1$$

where  $L_1$  and  $L$  are length and thickness of composite and  $n$  is the number of holes.

### 5.1 Dielectric Constant

The component of the dielectric constant of interest is  $\bar{K}_{11}$ , since the electrode surfaces are perpendicular to the poling direction. In the notation used here,  $\bar{K}_{11}$  is the dielectric constant of the composite,  ${}^A \bar{K}_{11}$  the dielectric constant of PZT,  ${}^B \bar{K}_{11}$  that

of the polymer, and  ${}^{1B} \bar{K}_{11}$  is the dielectric constant of part B. Since part A and part B are in parallel connection,

$$\bar{K}_{11} = {}^A V {}^A \bar{K}_{11} + {}^B V {}^B \bar{K}_{11}$$

Because PZT and polymer in part B are in series connection we can apply series model:

$${}^{1B} \bar{K}_{11} = {}^{1B} V {}^A \bar{K}_{11} + {}^{2B} V {}^{1B} \bar{K}_{11}$$

Using these relations we can calculate  $\bar{K}_{11}$  of composites. Since  ${}^A \bar{K}_{11} = 1600$  and  ${}^{1B} \bar{K}_{11} = 5$ , most of the contribution to  $\bar{K}_{11}$  comes from part A, which is PZT. Calculated values are plotted in Figures 2 and 3. In general, the measured dielectric constants are somewhat higher than the predicted values. This may be due to the approximations involved in the above calculations. The contribution to the dielectric constant from part B may be much higher than that assumed above because of the bending of the flux lines around the holes containing the polymer.

### 5.2 Piezoelectric Coefficients

The longitudinal coefficient  $\bar{d}_{11}$  relates the polarization component  $P_1$  to stress component  $\sigma_1$  by the following relation:  $P_1 = d_{11}\sigma_1$ . As stated earlier, the  $d_{11}$  values of 3-1 composites are slightly smaller than that of solid PZT. In a composite most of the stresses are borne by the ceramic, and if the stress transfer to the vertical columns (section A, Figure 8b) is complete, the  $\bar{d}_{11}$  of the composite should be equal to the value of  $d_{11}$  for PZT. But because of the curved shapes around the perforations, the stress distribution in the composite is not as simple as the model predicts. Horizontal components of stress are produced which lower the  $d_{11}$  coefficient.

The hydrostatic coefficient of the composite is given by the relation  $\bar{d}_h = d_{11} + 2d_{31}$ . In a solid PZT ceramic, the value of  $d_h$  is low due to the fact that  $d_{31} = -2d_{11}$ . In the 3-1 composites the arc-like geometry of the composite results in mechanically stiffened electrodes which transfer the horizontal stress pattern, significantly lowering  $d_{31}$ , and enhancing  $d_h$ . The fact that in some of the 3-1 and 3-2 composites  $\bar{d}_h = d_{11}$  clearly indicates that  $d_{31}$  is almost zero in some cases.

### SUMMARY

A simple technique for fabricating PZT polymer composites with 3-1 and 3-2 connectivity patterns has been proposed. These composites exhibit better piezoelectric properties than the previously

studied PZT polymer composites with different types of connectivity patterns. For 3-2 composites the  $\bar{K}_{11}$ ,  $\bar{d}_h$ ,  $\bar{g}_h$ , and  $\bar{d}_h\bar{g}_h$  values are 300,  $370 \times 10^{-12}$  C/N,  $123 \times 10^{-3}$  Vm/N and  $45,000 \times 10^{-15}$  m<sup>2</sup>/N respectively.

### ACKNOWLEDGEMENT

This work was sponsored by the Office of Naval Research through Contract No. N00014-78-C-0291. We also wish to thank Mr. Arvind Halliyal and our other colleagues at the Materials Research Laboratory.

### REFERENCES

1. R. E. Newnham, D. P. Skinner and L. E. Cross, *Mat. Res. Bull.*, **18**, 525 (1978).
2. D. P. Skinner, R. E. Newnham and L. E. Cross, *Mat. Res. Bull.*, **13**, 599 (1978).
3. K. Rittenmyer, T. Shrout, W. A. Schulze and R. E. Newnham, *Ferroelectrics* (accepted).
4. W. B. Harrison, Proc. Workshop on Sonar Transducer Materials, Naval Research Laboratory (Feb. 1976).
5. K. A. Klicker, Ph.D. Thesis, Solid State Science, The Pennsylvania State University (1980).
6. T. R. Shrout, L. J. Bowen and W. A. Schulze, *Mat. Res. Bull.*, **15**, 1371 (1980).
7. R. E. Newnham, L. J. Bowen, K. A. Klicker and L. E. Cross, *Int. J. Mat. in Eng.*, **2**, 93 (1980).
8. K. A. Klicker, J. V. Biggers and R. E. Newnham, *J. Amer. Ceram. Soc.*, **64**, 5 (1981).
9. K. A. Klicker, Control of PbO Partial Pressure During the Sintering of PZT Ceramic, M. S. Thesis, The Pennsylvania State University (1979).
10. J. F. Nye, *Physical Properties of Crystal*, Oxford University Press, London (1957).

**APPENDIX 5**

## PIEZOELECTRIC 3-3 COMPOSITES

K. RITTENMYER, T. SHROUT, W. A. SCHULZE and R. E. NEWNHAM

*Materials Research Laboratory, The Pennsylvania State University,  
University Park, Pennsylvania 16802, USA*

(Received February 4, 1981)

Piezoelectric composites of PZT and polymers were prepared by mixing tiny plastic spheres with PZT powder in an organic binder and firing the mixture to give a ceramic skeleton. After crowing, the skeleton was back-filled with polymer and potted. Dielectric and piezoelectric properties were measured on samples ranging from 30 to 70 volume % PZT, and compared with a rectangular skeleton model for 3-3 composites. Composites containing 50% PZT-50% silicone rubber appear especially useful for hydrophone applications with  $d_{33}$  products a hundred times larger than PZT.

### INTRODUCTION

In a 3-3 composite,<sup>1</sup> each of the constituent phases is continuously self-connected in three dimensions to give two interlocking skeletons in intimate contact with one another. This type of structure is exhibited by certain polymer foams, by some phase-separated metals and glasses, by three-dimensional weaves, and by natural substances such as wood and coral. The piezoelectric and pyroelectric properties of 3-3 composites have been investigated recently with some rather remarkable results.<sup>2-4</sup> For certain coefficients, dramatic improvements can be made over the best single-phase piezoelectrics.

Piezoelectric ceramic-polymer composites with 3-3 connectivity were first made by Skinner<sup>5</sup> using a lost-wax method with coral as a starting material. Among the advantages of these composites are high hydrostatic sensitivity, low dielectric constant, low density for improved acoustic impedance matching with water, high compliance to provide damping, and the mechanical flexibility needed to develop conformable transducers. ShROUT<sup>3</sup> has described a simpler method for fabricating a three-dimensionally interconnected lead zirconate-titanate (PZT) and polymer composite with properties similar to the coral-based composites. The simplified preparation method involves mixing plastic spheres and PZT powder in an organic binder. When carefully sintered, a porous PZT skeleton is formed, and later back-filled with polymer to form a 3-3 composite. This technique

is commonly referred to as the BURPS process, an acronym for burned-out plastic spheres. Since the process involves the generation and emission of gaseous hydrocarbons, the name BURPS is highly appropriate. The composites prepared by ShROUT<sup>3</sup> contained a PZT/polymer volume ratio of 30/70. In this study, we report the electromechanical properties of 3-3 composites having a wide range of PZT/polymer ratios, and compare the results with other piezoelectric materials, including some recent Japanese work<sup>4,6</sup> on similar composites. A three-dimensional skeleton model is proposed to explain the results.

### EXPERIMENTAL PROCEDURE

#### *Sample preparation*

The 3-3 composites were made from commercially available PZT powder\* mixed in a ball mill with tiny spheres of polymethyl methacrylate (PMMA) in PZT/PMMA volume ratios of 30/70, 40/60, 50/50, 60/40, and 70/30. The PMMA spheres ranged from 50 to 150 microns in diameter, and the PZT particles were about 1-4 microns in diameter. Four to eight weight percent of polyvinyl alcohol was added to the mixture as a bonding agent, and one inch diameter pellets were pressed

\* Ultrasonic Powder PZT-501A, Ultrasonics Powders, Inc.,  
2283 S. Clinton Ave., South Plainfield, NJ 07080  
† Pyroscience, Inc., Warrington, PA 15760

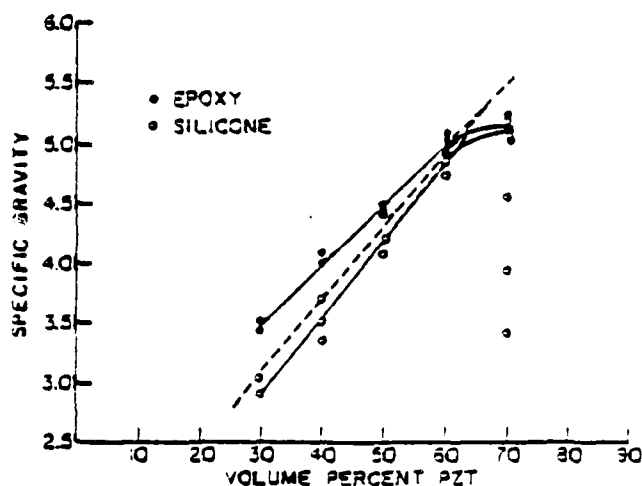


FIGURE 1. Specific gravity of 3-3 composites plotted as a function of volume fraction PZT in the starting mix. Composites filled with epoxy are denoted by solid circles, those with silicone rubber by open circles. The dashed line is the ideal density computed from the initial volume percent PZT.

at 10,000 psi. The pellets were heated over a 48-hour period to 450°C in order to volatilize the PMMA spheres; a slow heating rate is necessary to prevent excessive cracking. The samples were then placed on a platinum sheet in high purity aluminum crucibles and sintered in a silicon carbide resistance furnace at a heating rate of 200°C per hour, with a soak period of 30 minutes at 1340°C. A lead-rich atmosphere was maintained during sintering by placing powdered lead zirconate near the PZT samples. After firing, the samples were impregnated with either a stiff vinylcyclohexene dioxide epoxy<sup>1</sup> or a high-purity soft silicone elastomer.<sup>2</sup> Finally, the samples were polished on silicon carbide paper to ensure that the faces of the disk were parallel and smooth. Electrodes of air-dry silver were applied and the samples poled for two minutes in a stirred oil bath at 30°C with fields of 20–25 kv/cm. The composites were aged for at least twenty-four hours before measurements were taken.

#### Characterization

The density of the composites was computed from the mass and the measured volume of each disk. This procedure was performed prior to electroding

to avoid including the silver in the measurement. In Figure 1, the measured densities are plotted as a function of the nominal volume percent PZT. The relationship is essentially linear for both types of composites. As expected, the epoxy samples are slightly denser than the silicone rubber samples because epoxy wets the surface of PZT extremely well and densifies the samples. Incomplete back-filling in high volume percent PZT samples causes a noticeable scatter in the values. These density variations affect all subsequent measurements.

Figures 2a and 2b show micrographs at two different magnifications of a polished surface of a composite made from 50/50 volume ratio. The samples are poled in the vertical direction, as indicated in Figure 2a. At lower magnification (Figure 2b, 55X) the material appears reasonably homogeneous. Figure 2c shows a 30/70 PZT polymer composite in which the PZT is only slightly interconnected. A certain amount of interconnectivity is, of course necessary for electric poling, but to minimize the density and dielectric permittivity, the PZT content should be as low as possible.

In all the sections examined the PZT regions range from a few microns to about 100  $\mu$ m. The same is true of the polymer regions. The microstructure shows visible cracks in the PZT regions perpendicular to the poling direction. This has an important effect on the dielectric permittivity of the sample, as discussed later. Since microscop-

<sup>1</sup>Source: Low-Viscosity Embedding Media, No. 5135, Polysciences, Inc., Warrington, PA 18976.

<sup>2</sup>Dow Corning MQX-442110, Dow Corning Medical Products, Midland, MI 48661.

FIGURE 2a  
50/50 PZT  
polym.

FIGURE 2b  
50/50 PZT  
polym.

FIGURE 2c  
30/70 PZT  
polym.



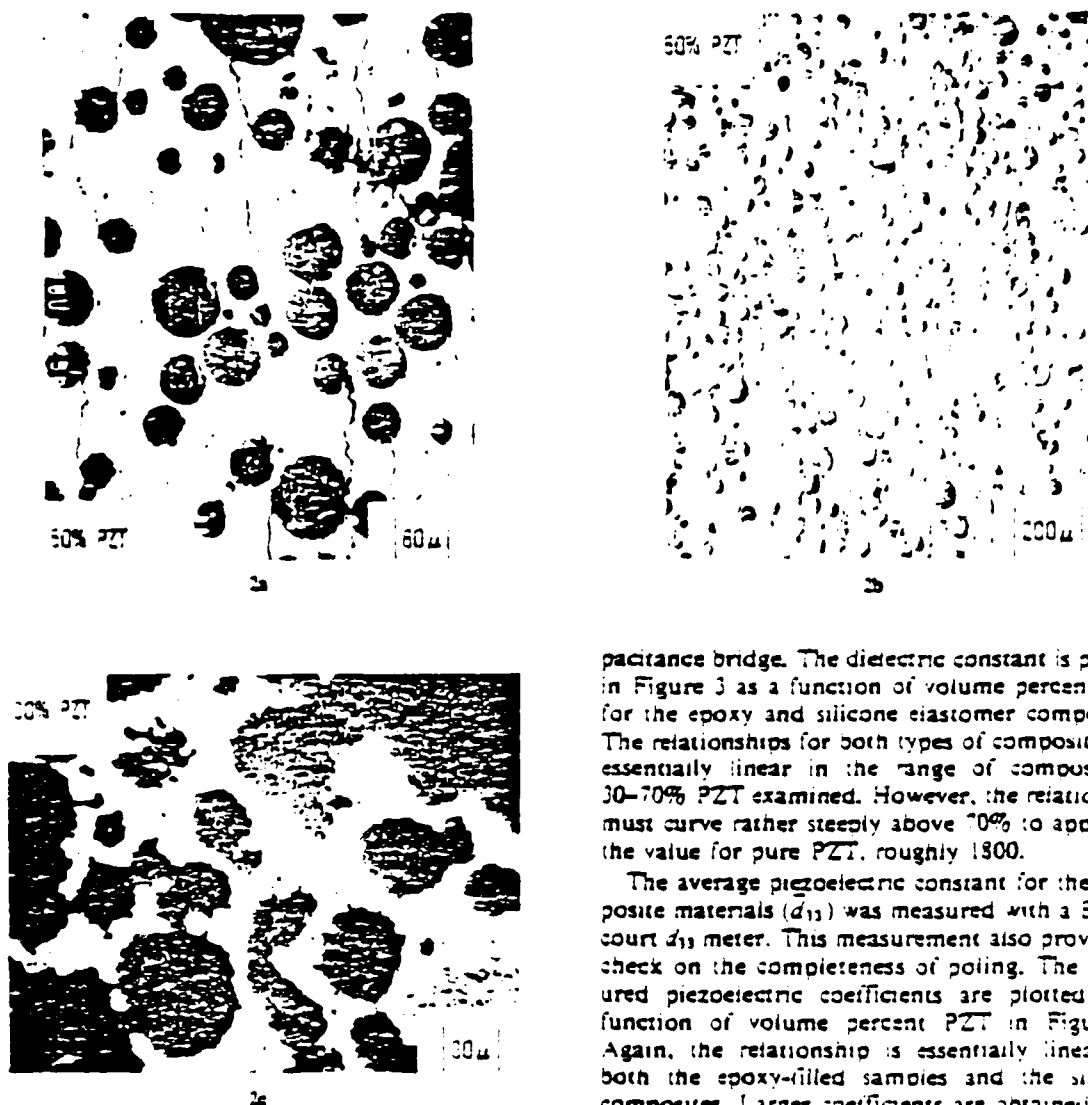


FIGURE 2. SEM micrographs of P-3 composites (a and b) filled with 50% polymer and (c) with 10% polymer. Note the horizontal fracture lines in (a) introduced during poing.

ture of these samples is on a finer scale than many other composites, more homogeneous electromechanical properties can be expected, which is advantageous for high frequency applications.

#### Measurements

The dielectric permittivity and loss were measured at a frequency of 1 kHz using an automated ca-

pacitance bridge. The dielectric constant is plotted in Figure 3 as a function of volume percent PZT for the epoxy and silicone elastomer composites. The relationships for both types of composites are essentially linear in the range of compositions 30-70% PZT examined. However, the relationship must curve rather steeply above 70% to approach the value for pure PZT, roughly 1800.

The average piezoelectric constant for the composite materials ( $d_{31}$ ) was measured with a Bertin-court  $d_{31}$  meter. This measurement also provides a check on the completeness of poing. The measured piezoelectric coefficients are plotted as a function of volume percent PZT in Figure 4. Again, the relationship is essentially linear for both the epoxy-filled samples and the silicone composites. Larger coefficients are obtained from the silicone specimens, perhaps because of their high elastic compliance which promotes stress transfer to the PZT. The  $d_{31}$  coefficient of solid PZT 501A is approximately 400 pC/N. Hydrostatic piezoelectric coefficients ( $d_{11}$ ) were measured by a pseudostatic method. Pressure was applied in an oil-filled cylinder at a rate of 500 psi/sec, and the resulting charge was collected with a Keithley Electrometer operated in a feedback charge-integration mode. Figure 5 shows  $d_{11}$  plotted as a function of volume percent PZT. A broad maximum is observed in the 50-70% PZT composition range. Hydrostatic coefficients for the silicone

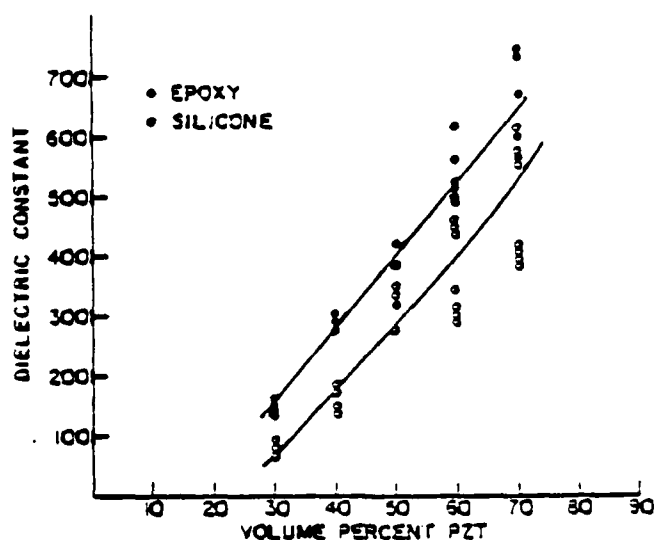
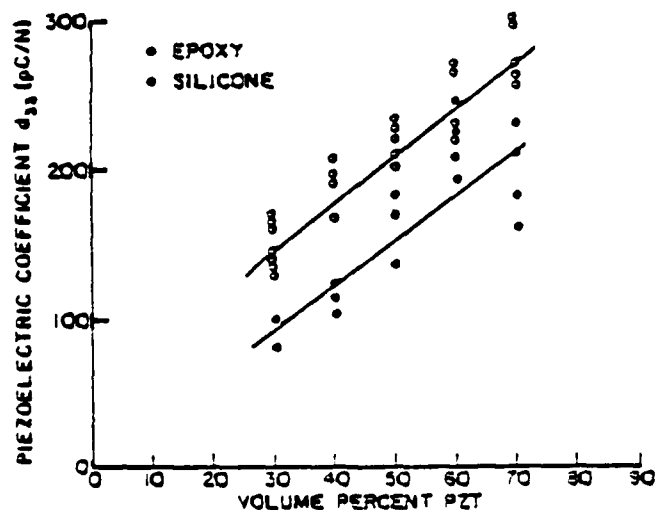


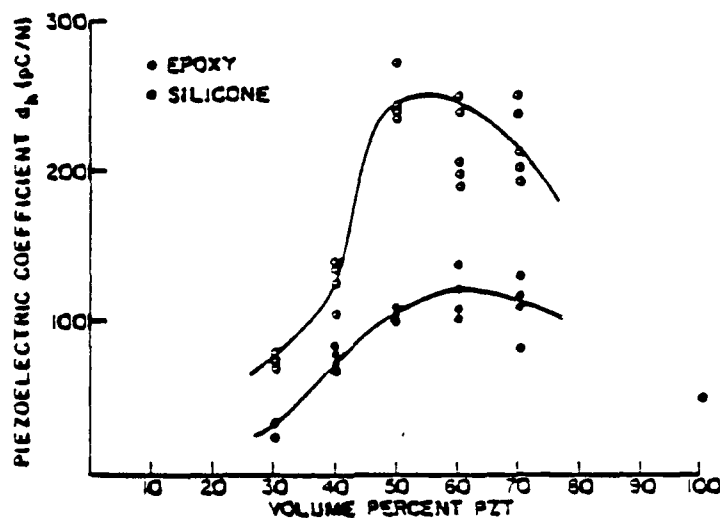
FIGURE 3 Dielectric constant of PZT-polymer composites plotted as a function of volume percent PZT.

FIGURE 4 Longitudinal piezoelectric coefficient  $\bar{d}_{33}$  for PZT-polymer composites with 3-3 connectivity.

composites are about twice as large as epoxy composites of the same volume fraction PZT and up to five times larger than the  $d_{33}$  value of PZT ( $\sim 50$  pC/N).

The piezoelectric voltage coefficients  $\bar{g}_{33}$  and  $\bar{g}_{31}$  are also substantially larger than those of solid PZT because the composites have much lower dielectric constants. A composite containing 30% PZT and 70% silicone elastomer has a  $\bar{g}_{33}$

( $=\bar{d}_{33}/\bar{K}_{330}$ ) coefficient of about  $200 \times 10^{-11}$  Vm/N compared to  $25 \times 10^{-11}$  for the solid ceramic. For hydrostatic conditions,  $\bar{g}_{31}(=\bar{d}_{31}/\bar{K}_{330})$  is about  $100 \times 10^{-11}$  for many of the silicone rubber composites, while that of solid PZT is only  $3 \times 10^{-11}$ . Epoxy composites have somewhat smaller voltage coefficients than those made with silicone elastomer. The hydrostatic figure of merit ( $d_{33}\bar{g}_{31}$ ) for hydrophone applications is

FIGURE 5 Hydrostatic piezoelectric coefficient  $d_{33}$  for PZT-polymer composites.

largest for PZT-silicone rubber composites containing 50% PZT. For these samples  $d_{33}$  exceeds  $2 \times 10^{-11}$  C/Vm/N<sup>1</sup>, more than a hundred times larger than solid PZT ceramics.

The results compare favorably with measurements on similar materials. Using the same technique described in this paper, Shrout<sup>1</sup> previously prepared a number of PZT-polymer composites containing 30 volume percent PZT. The PZT-silicone rubber samples had dielectric constants between 40 and 200,  $d_{33}$  values in the range  $30-240 \times 10^{-12}$  C/Vm/N, and  $\bar{g}_{33}$  values of  $50-70 \times 10^{-3}$  Vm/N. Piezoelectric coefficients for PZT-epoxy composites were somewhat smaller:  $d_{33}$   $60-110 \times 10^{-12}$  and  $\bar{g}_{33}$  about  $40 \times 10^{-3}$ . Porous interconnected PZT-silicone rubber samples prepared by Nagata and co-workers<sup>4</sup> gave  $\bar{g}_{33} = 130 \times 10^{-3}$  Vm/N. These composites contained 48 volume % PZT. The ladder-type composites reported by Miyashita and co-workers<sup>5</sup> gave slightly lower values of  $90 \times 10^{-3}$  for  $\bar{g}_{33}$ .

### THEORETICAL MODEL

The physical properties of 3-3 composites can be described with the cubic array illustrated in Figure 6. The model consists of intersecting rectangular columns of PZT arranged in three perpendicular directions and embedded in a polymer matrix. For simplicity, it is assumed that one set of columns is parallel to the poling direction ( $X_1$ ).

and that this set of columns are fully poled, while those in the perpendicular directions along  $X_2$  and  $X_3$  are unpoled.

Bertincourt<sup>7</sup> used a similar model to explain the piezoelectric properties of PZT sponge, a porous ceramic made by Clevite Corporation about twenty years ago. The sponge was 3-3 structure made from a slurry of PZT, water, and soapsuds, but it was difficult to back-fill, and therefore composites were not prepared.

In one "unit cell" of the cubic array, there are four kinds of PZT blocks: (i) rectangular blocks parallel to  $X_1$ , (ii) rectangular blocks parallel to  $X_2$ , (iii) rectangular blocks parallel to  $X_3$ , and (iv) cubic blocks at the intersections. The cubic lattice contains equal number of the four types. If the

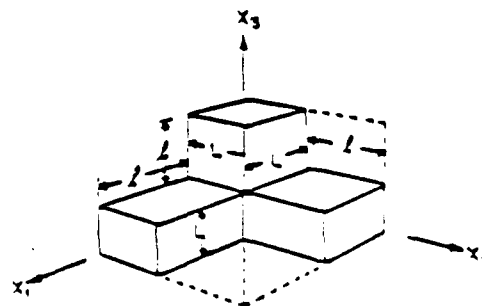


FIGURE 6 The repeat unit of a cubic skeleton used to model the dielectric and piezoelectric properties of 3-3 composites.

length of the rectangular blocks is  $l$ , and the width  $L$ , then the volume of the rectangular blocks is  $L^2l$  and that of the cubic blocks  $L^3$ . In one unit cell of the cubic array, the volume of PZT is  $L^3 + 3L^2l$ , and the volume fraction PZT is

$$v = \frac{L^3 + 3L^2l}{(L + l)^3} \quad (1)$$

The remainder of the volume is filled with polymer.

#### Dielectric constants

The dielectric constant of interest is  $\bar{K}_{33}$  since the electrode surfaces are perpendicular to  $X_3$ . In the notation used here,  $\bar{K}_{33}$  is the dielectric constant of the composite,  ${}^1\bar{K}_{33}$  is the dielectric constant of PZT, and  ${}^2\bar{K}_{33}$  is that of the polymer. Since  ${}^1\bar{K}_{33} \gg {}^2\bar{K}_{33}$ , the dielectric properties of PZT tend to dominate the calculations. The rectangular blocks parallel to  $X_3$ , together with the cubic blocks, contribute most to  $\bar{K}_{33}$ . The blocks parallel to  $X_1$  and  $X_2$  are connected in series with polymer and therefore contribute relatively little.

For a unit cube ( $L + l = 1$ ), the dielectric constant is approximately

$$\bar{K}_{33} = {}^1\bar{K}_{33} L^2 \quad (2)$$

where  $L$  is the width of the rectangular blocks (Figure 6), expressed in cell fractions. This assumes that the permittivity of PZT ( ${}^1K \sim 1800$ ) is far larger than that of the polymer ( ${}^2K \sim 10$ ). Using the relationship between  $L$ ,  $l$ , and  $v$  given in Eq. (1), the dielectric constant of the composite can be written as a function of the volume fraction PZT ( $v$ ). This is plotted in Figure 7. The measured dielectric constants are lower than the predicted values. This may be due to deficiencies in the theoretical model, but the cracks caused by poling (see Figure 2a) undoubtedly contribute to the discrepancy. Since the cracks are oriented perpendicular to the poling direction, the material is essentially divided up into capacitive elements with air and PZT connected in series. Under these conditions, the permittivity drops rapidly with only a slight amount of fracture. Silicone rubber provides less mechanical support for the ceramic than does epoxy. This may explain why more cracking was observed in the silicone rubber com-

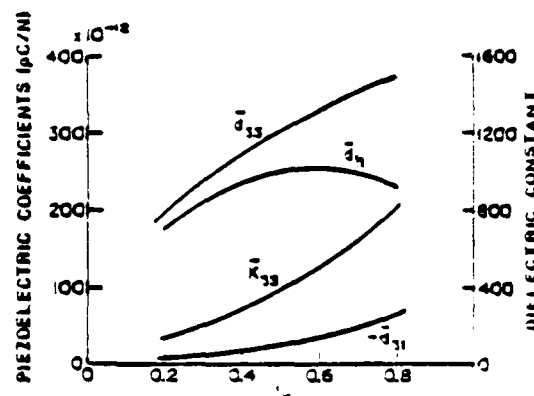


FIGURE 7. Piezoelectric and dielectric coefficients calculated from the cubic array model.

posites, and why they have lower dielectric constants.

The dielectric constant of a 3-3 composite decreases rapidly with increasing polymer content. For simple parallel connection, a linear relation between the dielectric constant and the volume fraction PZT is expected. For a cubic lattice model, the decrease is faster than linear, which is advantageous for the piezoelectric voltage coefficient. The reason for the rapid decrease is that much of the PZT is in series with polymer.

#### Piezoelectric coefficients

The longitudinal coefficient  $\bar{d}_{33}$  relates the polarization component  $P_3$  to stress component  $\sigma_3$ . For a composite, the magnitude of  $\bar{d}_{33}$  depends strongly on what fraction of the stress is borne by the piezoelectric element. Ideally, the stiff piezoelectric ceramic bears all the stress and the polymer none. For a perfect parallel connection

$$\bar{d}_{33} = \frac{v {}^1d_{33} {}^2s_{33} + v {}^2d_{33} {}^1s_{33}}{v {}^2s_{33} + v {}^1s_{33}} \quad (3)$$

where  $v$  and  $v$  are the respective volume fractions of PZT and polymer. Longitudinal compliances are denoted by  ${}^1s_{33}$  and  ${}^2s_{33}$ , and the piezoelectric effect of the polymer is assumed to be zero  ${}^2d_{33} = 0$ .

Composites with 3-3 connectivity are partially in parallel and partially in series, and therefore Eq. (3) will not be accurate. Referring to Figure 6, the portion of PZT in parallel with the polymer

matrix consists of the cubic blocks together with the rectangular columns parallel to  $X_1$ . This part of the PZT skeleton is assumed to be fully poled, and therefore piezoelectrically active. The rectangular blocks parallel to  $X_1$  and  $X_2$  are in series with polymer, and since they are unpoled, contribute nothing to the piezoelectric effect. Thus much of the PZT (approximately two-thirds for small fractions) is inactive, and the composite behaves as if it contains a much smaller volume fraction PZT. The formula for  $d_{33}$  can be rewritten as

$$\bar{d}_{33} = \frac{{}^1v^a {}^1d_{33} {}^2s_{33}^a}{{}^1v^a {}^2s_{33}^a + {}^2v^a {}^1s_{33}} \quad (4)$$

where  ${}^1v^a$  is the volume fraction of active PZT and  ${}^2v^a$  is the volume fraction of polymer loaded with inactive PZT.  ${}^2s_{33}^a$  is the modified compliance of the polymer. The volume fraction of active PZT is

$${}^1v^a = \frac{L^3 + L^2l}{(L + l)^3} \quad (5)$$

where  $L$  and  $l$  are the dimensions referred to Figure 6. The loaded polymer volume fraction  ${}^2v^a = 1 - {}^1v^a$ . Elastic compliance coefficient  ${}^2s_{33}^a$  is less than  ${}^1s_{33}$ , but is substantially larger than  ${}^1s_{33}$ , the compliance of pure PZT. In Figure 7, the value of  $\bar{d}_{33}$  is plotted as a function of  ${}^1v$ , the total volume fraction of PZT, assuming a value of 0.1 for  ${}^1s_{33}/{}^2s_{33}^a$ . If this ratio is very much smaller,  $\bar{d}_{33}$  is independent of  ${}^1v$ , reverting to the ideal parallel connection model.

Piezoelectric coefficient  $\bar{d}_{31}$  is more straightforward. Two parts of the PZT network are piezoelectric, the rectangular columns parallel to  $X_1$  and the cubic blocks at the intersecting columns. Since stress component  $\sigma_1$  is carried by the lateral rectangular columns, the stress is transmitted to the cubic blocks but not to the vertical columns.

Therefore only the cubic blocks contribute to  $\bar{d}_{31}$ :

$$\bar{d}_{31} = L^3 {}^1d_{31} / (L + l)^3.$$

In Figure 7,  $\bar{d}_{31}$  is plotted as a function of total volume fraction PZT. When  ${}^1v$  is large, the composite consists mainly of cubic intersections, and  $\bar{d}_{31}$  is large. When  ${}^1v$  is very small, the intersection cubes nearly disappear, and so does  $\bar{d}_{31}$ . The rapid decrease of  $\bar{d}_{31}$  with  ${}^1v$  is a strong contributing factor to the hydrostatic sensitivity.

The hydrostatic piezoelectric coefficient  $\bar{d}_h$  is obtained from  $\bar{d}_{33} + 2\bar{d}_{31}$  and is plotted as a function of  ${}^1v$  in Figure 7. Note that  $\bar{d}_h$  goes through a broad maximum near the 50% composition, similar to the experimental values (Figure 5). In general the model gives good agreement with the experimental results.

#### ACKNOWLEDGEMENTS

We wish to thank our colleagues at the Materials Research Laboratory for their advice and encouragement. This work was supported by the Office of Naval Research through Contract No. N00014-78-C-0291.

#### REFERENCES

1. R. E. Newnham, D. P. Skinner and L. E. Cross, *Mat. Res. Bull.*, **13**, 525 (1978).
2. D. P. Skinner, R. E. Newnham and L. E. Cross, *Mat. Res. Bull.*, **13**, 599 (1978).
3. T. R. Shrout, W. A. Schulze and J. V. Biggers, *Mat. Res. Bull.*, **14**, 1553 (1979).
4. K. Nagata, H. Igarashi, K. Okazaki and R. C. Bradt, *Jap. J. Appl. Phys.*, **19**, L17 (1980).
5. M. Miyashita, K. Takano and T. Toda, *Ferroelectrics*, **28**, 397 (1980).
6. R. E. Newnham, D. P. Skinner, K. A. Klinker, A. S. Bhalla, B. Hardiman and T. R. Gururaja, *Ferroelectrics*, **27**, 49-55 (1980).
7. D. Berlincourt, "Properties of Sponge Ceramic," Clevite Corporation Internal Report, December 1960.

**APPENDIX 6**

Polymer-Piezoelectric Ceramic Composites  
R. E. Newnham and J. P. Runt  
Materials Research Laboratory  
The Pennsylvania State University  
University Park, PA 16802

*Revised 12/80  
J. P. Runt*

1. Introduction and Background

Several crystal classes whose internal symmetry results in a permanent electric polarization display the property of piezoelectricity. These materials produce an electrical response due to the application of mechanical stress. The magnitude of the charge is linearly proportional to the stress through the piezoelectric coefficient ( $d$ ) and the sign of the charge can be changed by reversing the direction of the stress. The polarization ( $P_i$ ) developed under this direct piezoelectric effect is:

$$P_i = d_{ij} \sigma_j \quad (1)$$

where  $\sigma$  is the applied stress and  $i$  and  $j$  refer to orthogonal directions within the sample. In addition to the direct effect, piezoelectric materials can also convert electrical energy into a mechanical response. This converse piezoelectric effect is given by:

$$S_i = d_{ji} E_j \quad (2)$$

where  $S$  is the mechanical strain produced by the applied electric field ( $E$ ).

Piezoelectric materials have found application in a large number of areas including radio transmitters, hydrophones, resonators and phonographic pickups. At one time, natural crystals (such as quartz) were used as the piezoelectric element. Today, however, many piezoelectric materials are prepared from polycrystalline ceramics such as lead zirconate titanate (PZT) and barium titanate. Application of high electric fields (poling) at temperatures just below the Curie temperature are required to introduce a polar axis in these materials. As can be seen in Table 1, the poled ceramics have quite large  $d$ -coefficients which are

desirable in piezoelectric driver applications such as ultrasonic cleaners and sonar. For hydrophones and phonograph pickups a useful figure of merit is the piezoelectric voltage coefficient ( $g$ ) which is defined as:

$$g_{ij} = \frac{d_{ij}}{\epsilon_i} \quad (3)$$

where  $\epsilon$  is the dielectric permittivity of the material. The  $g$ 's of the ceramics listed in Table 1 are somewhat less outstanding than their  $d$ -coefficients due to their large dielectric permittivities.

In the last decade considerable effort has been devoted to developing piezoelectric polymers (1,2). The polymer that has received by far the most attention is poly(vinylidene fluoride) ( $PVF_2$ ).  $PVF_2$  is a semi-crystalline polymer (typically about 50% crystallinity) with a glass transition temperature of near  $-40^\circ\text{C}$ . Currently, four forms of crystalline  $PVF_2$  are known (1). These are generally referred to as forms I, II, III and II<sub>p</sub> or  $\beta$ ,  $\alpha$ ,  $\gamma$  and  $\alpha_p$ , respectively. The form of most importance from a piezoelectric standpoint is form I (2) since in this phase the dipoles of the monomer units are parallel resulting in a substantial dipole moment. Commercial  $PVF_2$  usually consists of antipolar form II crystals and must therefore be taken through a series of processing steps in order to render the material piezoelectrically-active. A typical approach involves stretching commercial  $PVF_2$  film at 50 to 65°C to about four times its original length. The film is then electroded and poled at a field of approximately  $5 \times 10^5$  V/cm at 100°C for an hour. The films are subsequently cooled to room temperature under the applied field to prevent depoling.

$PVF_2$  has a dielectric constant of about 15 which is relatively large for organic materials but is some two orders of magnitude less than PZT ceramics. The longitudinal piezoelectric strain coefficient ( $d_{33}$ ) of poled  $PVF_2$  is quite high for polymers - on the order of 20 to 30  $\frac{\text{pc}}{\text{N}}$ , but this is signi-



ificantly lower than the  $d_{33}$  values for PZT ceramics which range from about 100 to 600  $\frac{\text{pC}}{\text{N}}$ . Despite the relatively small  $d_{33}$ , the permittivity of  $\text{PVF}_2$  is sufficiently low that a large voltage coefficient ( $g_{33}$ ) is obtained.

The relative compliance and flexibility of  $\text{PVF}_2$  is high and its density is low compared to conventional piezoelectric ceramics, and these properties impart some decided advantages to  $\text{PVF}_2$  when used as a piezoelectric sensor. A low density piezoelectric has better acoustic coupling to water and can be more easily adjusted to neutral buoyancy than the high density PZT ceramics now used for hydrophones. Compliant polymers also have better shock resistance than conventional ceramic transducers and the large compliance also means high damping, which is often desirable in a passive device. In addition, a flexible material could be deformed to any desired profile.

Overall, this combination of properties appears quite attractive and, in fact,  $\text{PVF}_2$  has gained the attention of a number of investigators whose efforts have been directed toward developing devices based on piezoelectricity in  $\text{PVF}_2$  (3,4). There are, however, problems associated with the use of  $\text{PVF}_2$ . The low piezoelectric strain coefficient reduces its importance as an active device, and although its high voltage sensitivity means it may be good as a passive device, a problem arises here, too. When used as a hydrophone, the material must be fixed to a curved surface which can flex in response to pressure changes. The difficulty lies in designing a sealed flexible mount for the polymer which will function when exposed to the high pressures which exist deep in the ocean and still retain sensitivity when near the surface. So we see, then, that the figure of merit  $g_{ij}$  is not the sole criterion, but that other aspects of the problem must be examined as well.

Another approach to the development of high sensitivity, rugged and relatively flexible piezoelectric materials is to combine the large piezoelectric effects found in poled piezoelectric ceramics with the desired mechanical properties of polymers. The main problem in these composites is to effect the combination in such a way as to exploit the desirable features of both components and thereby maximize the figure of merit. In the last several years, considerable progress has been made in the development of piezoelectric composites made with polymers and piezoelectric ceramics. Some of the results and a few design principles are reviewed in the next sections.

## II. Piezoelectric Composites

### 1. Connectivity

Connectivity is a key feature in property development in multiphase solids since physical properties can change by many orders of magnitude depending on the manner in which connections are made. Imagine, for instance, an electric wire in which the metallic conductor and its polymeric insulation are connected in series rather than in parallel!

Each phase in a composite may be self-connected in zero, one, two, or three dimensions. It is natural to confine attention to three perpendicular axes because piezoelectricity and other property tensors are referred to such systems (5). If we limit the discussion to diphasic composites, there are ten possible connectivity patterns as shown in Figure 1. These are designated as 0-0, 1-0, 2-0, 3-0, 1-1, 2-1, 3-1, 2-2, 3-2, and 3-3. A 2-1 connectivity pattern, for example, has one phase self-connected in two-dimensional layers, the other self-connected in one-dimensional chains or fibers. The connectivity patterns are not geometrically unique. In the case of a 2-1 pattern the fibers of the second phase might be perpendicular to the layers of the first phase, as in Figure 1, or they might be parallel to the layers. In the notation that we will use in following sections the self-connectivity of the piezoelectric phase will be given first and the inactive phase second. Thus a 1-3 composite consists of piezoelectric ceramic fibers

embedded in a non-piezoelectric polymer matrix and a 3-1 composite is a solid piece of piezoelectric ceramic with parallel holes filled with an inactive polymer.

## 2. Piezoelectric ceramic particles dispersed in polymers

Some of the earliest attempts at preparing piezoelectric ceramic/polymer composites consisted of dispersing piezoelectric ceramic particles in a polymer matrix (0-3 composites). Flexible 0-3 composites made at Gould were fabricated using 5 to 10  $\mu\text{m}$  particles bound in a polyurethane matrix (6). A similar material was developed by Harrison using 120  $\mu\text{m}$  particles in a silicone rubber matrix (7). The longitudinal  $d$  values obtained in both cases were comparable to piezoelectric  $\text{PVF}_2$  but the voltage sensitivities were lower because of the higher permittivities in the composites. The difficulty with this type of composite where the piezoelectric particles are smaller in diameter than the thickness of the polymer sheet (Figure 2a) is that low permittivity polymer layers separate the piezoelectric particles, preventing saturation poling after the composite is formed. Even after some poling has been achieved, the interleaved compliant polymer attenuates the piezoelectric response of the composite.

Composites have been prepared at Honeywell which contain much larger particles (up to 2.4 mm in diameter)(7). A material of this type is shown schematically in Figure 2b. Here the particle size approaches the thickness of the composite and these materials therefore have at least partial 1-3 connectivity. Since the piezoelectric particles extend from electrode to electrode, near saturation poling can be achieved. The large rigid piezoelectric particles can transmit an applied stress well leading to high  $d$  values if  $d$  is measured across the particles. Permittivities in these materials are low compared to homogeneous PZT, resulting in a relatively high  $g$  coefficient. The problem here is that properties of the composite are extremely position sensitive.

To make an effective composite transducer, it can be seen that one cannot merely mix two materials together - some other consideration is necessary. Designing a composite entails not only choosing component phases with the right properties but also coupling the materials in the optimal manner. The connectivity of each phase is of major importance since this controls the electric flux pattern and the mechanical stress distribution.

The Japanese have been especially active in the development of piezo-electric ceramic particle-filled polymers (8-10). In fact, NTK has commercialized two such products: 'Piezo-Film' and 'Piezo-Rubber', composites of PZT particles with an unspecified thermoplastic resin and elastomer matrix, respectively. These materials look promising in a number of applications including audio headphones, microphones and pressure gauges.

Finally, it is interesting to note the similarity in structure between the true 0-3 ceramic/polymer composites and  $PVF_2 : PVF_2$  can be thought of as a composite consisting of piezoelectric crystals in an amorphous matrix. The 0-3 composites have in fact been used as models for the piezoelectric effect in  $PVF_2$  (11).

### 3. Parallel and Series Connections in Composites

To illustrate the major modifications in ensemble properties which can be effected even in simple linear systems, one-dimensional solutions are summarized for the piezoelectric properties of heterogeneous two-phase structures (12,13).

Consider first the piezoelectric properties of lamellar diphasic composites. The longitudinal piezoelectric coefficient  $d_{33}$  has been derived for a diphasic piezoelectric with the constituent phases arranged in alternating layers normal to the  $X_3$  direction (Figure 3a). Designating

phase 1 with a superscript 1, and phase 2 with superscript 2, phase 1 has volume fraction  $^1v$ , piezoelectric coefficient  $^1d_{33}$  and permittivity  $^1\epsilon_{33}$ , and phase 2 has  $^2v$ ,  $^2d_{33}$ , and  $^2\epsilon_{33}$ , respectively. Solving for the piezoelectric coefficient of the composite gives:

$$\bar{d}_{33} = \frac{^1v^1d_{33}^2\epsilon_{33} + ^2v^2d_{33}^1\epsilon_{33}}{^1v^2\epsilon_{33} + ^2v^1\epsilon_{33}} \quad (4)$$

Using the relation  $g_{33} = d_{33}/\epsilon_{33}$  yields the composite piezoelectric voltage coefficient:

$$\bar{g}_{33} = ^1v^1g_{33} + ^2v^2g_{33} \quad (5)$$

It is interesting to note that for a series connection even a very thin low-permittivity layer rapidly lowers the d-coefficient but has little effect on the corresponding g-coefficient.

If the two phases lie in layers oriented perpendicular to the electrodes (Figure 3b), again for the one-dimensional case and neglecting transverse coupling, the composite piezoelectric coefficient is

$$\bar{d}_{33} = \frac{^1v^1d_{33}^2s_{33} + ^2v^2d_{33}^1s_{33}}{^1v^2s_{33} + ^2v^1s_{33}} \quad (6)$$

where  $^1s_{33}$  and  $^2s_{33}$  are the elastic compliances for stresses normal to the electrodes. A similar expression can be written for  $\bar{g}_{33}$ .

A composite of interest here is that of an elastically compliant nonpiezoelectric polymer in parallel with a stiff piezoelectric ceramic. In this case  $^1d_{33} \gg ^2d_{33}$ ,  $^1s_{33} \ll ^2s_{33}$ . If we assume  $^1v = ^2v = 1/2$  then  $\bar{d}_{33} = ^1d_{33}$ , i.e. the piezoelectric d-coefficient of the composite is the same as the pure piezoelectric alone. If  $^1\epsilon_{33} \gg ^2\epsilon_{33}$ ,  $\bar{g}_{33} = \frac{^1d_{33}}{^1\epsilon_{33}} = \frac{^1s_{33}}{^1v}$ , and for small volume fractions of the piezoelectric phase

the  $g$ -coefficient is correspondingly amplified. It is this case which accounts for the highly successful performance of the transducer structures described in later sections. The structure also has considerable hydrostatic sensitivity.

#### 4. Hydrostatic Sensitivity

A problem arises when one attempts to use solid PZT as a hydrostatic sensor because  $d_{33}$  is approximately equal to  $-2d_{31}$ , resulting in a low piezoelectric response to hydrostatic pressure change. Since sizeable  $\bar{g}_{33}$  coefficients can be obtained for composites with parallel connection, it is interesting to inquire into the hydrostatic sensitivity of this type of connectivity.

To evaluate the effective hydrostatic sensitivity for parallel connection, it is necessary to evaluate the transverse piezoelectric coefficient  $\bar{d}_{31}$  since  $P_3 = -p(\bar{d}_{33} + 2\bar{d}_{31})$  where  $p$  is the applied hydrostatic pressure. Since the piezoelectric rods are approximately connected in series in the lateral directions it can be shown that  $\bar{d}_{31} = \frac{1_v}{1_v + 2} d_{31} + \frac{2_v}{1_v + 2} d_{31}$ . This leads to a hydrostatic piezoelectric coefficient:

$$\bar{d}_h = \bar{d}_{33} + 2\bar{d}_{31} = \frac{\frac{1_v}{1_v + 2} d_{33} + \frac{2_v}{1_v + 2} d_{33}}{\frac{1_v}{1_v + 2} + \frac{2_v}{1_v + 2}} + 2(\frac{1_v}{1_v + 2} d_{31} + \frac{2_v}{1_v + 2} d_{31}) \quad (7)$$

Suppose for the composite we choose equal volumes of piezoelectric PZT (phase 1) and a compliant elastomer (phase 2) such that  $\frac{1_v}{1_v + 2} = \frac{2_v}{1_v + 2} = \frac{1}{3}$ ,  $\frac{1_v}{1_v + 2} s_{33} \ll \frac{2_v}{1_v + 2} s_{33}$ ,  $\frac{1_v}{1_v + 2} d_{33} \gg \frac{2_v}{1_v + 2} d_{33}$ , and  $\frac{1_v}{1_v + 2} d_{33} = -2 \frac{1_v}{1_v + 2} d_{31}$ . For the composite,  $\bar{d}_{31} = \frac{1}{3} d_{31}$  and  $\bar{d}_{33} = \frac{1}{3} d_{33}$ , giving  $\bar{d}_h = \frac{1}{3} d_{33}$ .

This is a considerable improvement over single phase performance.

AD-A145 115

PIEZOELECTRIC AND ELECTROSTRICTIVE MATERIALS FOR  
TRANSDUCER APPLICATIONS(U) PENNSYLVANIA STATE UNIV  
UNIVERSITY PARK MATERIALS RESEARCH LAB

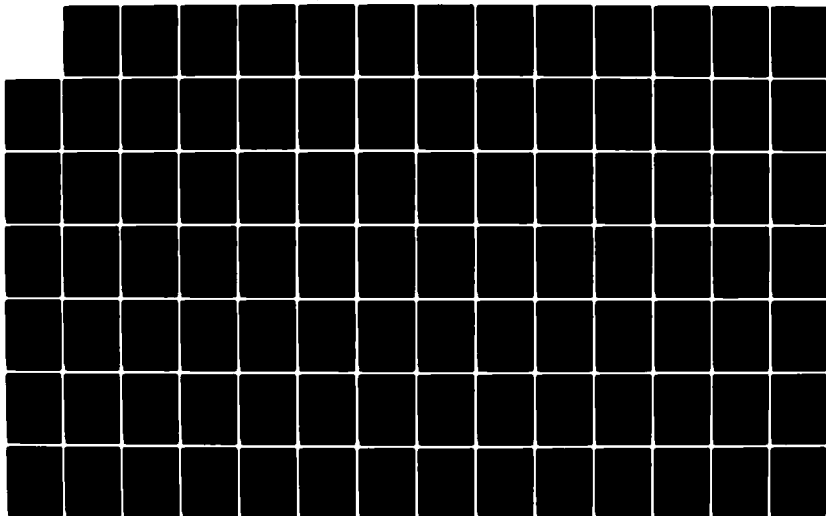
24

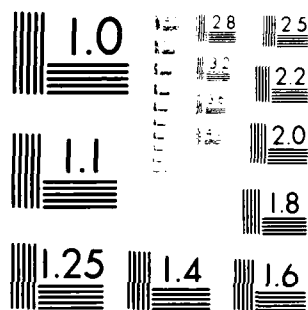
UNCLASSIFIED

L E (RHS) F I AL. MAY 84 N00014 82-K-0339

F / G 20/3

NL





MICROCOPY RESOLUTION TEST CHART  
NATIONAL BUREAU OF STANDARDS-1963-A



Since the hydrophones used under hydrostatic conditions are normally voltage generators, the further favorable enhancement of the voltage coefficient  $\bar{g}_h$  can also be exploited:  $\bar{g}_h = \bar{d}_h / \bar{\epsilon}_{33}$ . Lowering the permittivity  $\bar{\epsilon}_{33}$  increases the sensitivity to small pressure changes by raising  $\bar{g}_h$ .

##### 5. Piezoelectric Composites with 1-3 Connectivity

Considering the parallel connectivity described previously, the ideal three dimensional case is one of PZT rods embedded in a continuous polymer phase, that is, 1-3 connectivity. According to equal strain composite theory,  $\bar{d}_{33}$  should not be a function of the volume fraction of PZT in the composite. This assumes an idealized situation in which the polymer phase is far more compliant than PZT, causing all the stress on the polymer to be transferred to the PZT rods. That is, as the volume fraction PZT decreases, the stress on the rods increases proportionally, so that the charge per unit area of the composite is constant. For pressure sensors, it is not necessary that  $\bar{d}_{33}$  be large in order to enhance the  $\bar{d}_h$  coefficient of the composite. If, as the volume fraction of PZT is decreased,  $|\bar{d}_{31}|$  decreases more rapidly than  $\bar{d}_{33}$ , then  $\bar{d}_h$  will be increased. Likewise, if  $\bar{\epsilon}_{33}$  decreases more rapidly than  $\bar{d}_h$ , as the volume fraction PZT decreases, then  $\bar{g}_h$  will be enhanced.

Klicker, et. al. (14) prepared 1-3 composites consisting of PZT rods aligned parallel to the poling axis and embedded in a matrix of epoxy or polyurethane (Figure 4 ). The rods were in contact with the surface electrodes and this allowed for good poling of the ceramic. The size of the rods and the total amount of PZT in the composites can be easily manipulated with this design. Figures 5 and 6 illustrate the piezoelectric

properties obtainable from 1-3 PZT/epoxy composites. Figure 5 shows that for PZT volume fractions down to 40%, the  $\bar{d}_{33}$  coefficients are comparable to the  $d_{33}$  of solid PZT, about 400 pC/N. Below 40% PZT, the  $\bar{d}_{33}$  values decrease but even at 10% are still greater than one half the value for pure PZT. Figure 6 shows the dependence of  $\bar{g}_{33}$  on PZT volume fraction for composites of 4mm thickness. As anticipated, all the composites have larger  $g_{33}$  coefficients than pure PZT and  $\bar{g}_{33}$  is greatly affected by volume fraction. Note that a composite with 2.5% PZT has a piezoelectric voltage coefficient some nine times that of pure PZT. The epoxy/PZT composites also have substantial hydrostatic piezoelectric coefficients and quite large hydrostatic voltage coefficients. The density of the composite can be adjusted between the density of PZT (7.9 gm/cc) and that of the epoxy (about 1 gm/cc). It is important to note that the greatest values of  $\bar{d}_n$ ,  $\bar{g}_n$ , and  $\bar{g}_{33}$  are all found in the composites with low volume fractions of PZT. Therefore the desired properties of low density and large piezoelectric coefficients are obtained with the same composites.

1-3 composites prepared with PZT and other polymer glasses (polystyrene and poly(methyl methacrylate)(PMMA)) and several semi-crystalline polymers (e.g. nylon 11, poly(butylene terephthalate) and different Hytrels) have piezoelectric properties which are quite similar to the epoxy composites (15,16). In addition, foamed polyurethane PZT composites have exceptional piezoelectric properties but are very pressure dependent due to collapse

of the void structure as pressure is increased(17). The hydrostatic piezoelectric properties of several 1-3 composites are listed in Table 2 .

Somewhat different 1-3 composites were prepared by Safari, et. al ( 18). Recall that early work on PZT-polymer composites undertaken by Harrison and co-workers (7) utilized coarse granules of sintered PZT rather than PZT rods. A schematic drawing of this PZT-loaded silicone rubber film is shown in Figure 2b. The piezoelectric properties were optimized by adjusting the size of the granules and the volume fraction of PZT. Typical values were given in Table 2.

PZT granules of irregular shape assume a variety of orientations with respect to the parallel surface of the composite and thus grinding does not expose every granule to the electroded surface. For poling of the PZT elements to occur, these elements must be in electrical contact with both electroded surfaces. Therefore, composites fabricated from irregular granules are not particularly efficient. The inactive PZT fragments not only detract from the piezoelectric response of the composite but also increase the density and decrease the flexibility unnecessarily.

The Safari, et. al. composites were fabricated using PZT spheres instead of irregular granules. Spheres offer several potential advantages over irregularly shaped particles. Composites are easily fabricated by pouring the spheres into a pan to form a monolayer, and then covering them with the polymer phase. A light sanding exposes the PZT, allowing

contact to both electrodes. The dielectric constant of these composites were 300 to 400 and  $\bar{\epsilon}_{33}$  was 45 to 55 x  $10^{-3}$  Vm/N. The high frequency properties of these composites were measured in both the thickness and radial mode of resonance. The frequency constants and coupling coefficients of the composites for the thickness mode of resonance are comparable with the values for PZT. Possible applications of the composites as band-pass filters have been developed.

#### 6. Piezoelectric Composites with 3-3 Connectivity

In a 3-3 composite each of the constituent phases is continuously self-connected in three dimensions to give two interlocking skeletons in intimate contact with one another. This type of structure is exhibited by certain polymer foams, by some phase-separated metals and glasses, by three-dimensional weaves, and by natural substances such as wood and coral. The piezoelectric properties of 3-3 composites have been investigated with some rather remarkable results. For certain coefficients, dramatic improvements can be made over the best single-phase piezoelectrics.

Piezoelectric ceramic-polymer composites with 3-3 connectivity were first made by Skinner, et al. (13) using a lost-wax method with coral as a starting material. Among the advantages of these composites are high hydrostatic sensitivity, low dielectric constant, low density for improved acoustic impedance matching with water, high compliance to provide damping, and the mechanical flexibility needed to develop conformable transducers. Shrout, et al. (19) have developed a simpler method for fabricating a three-dimensionally interconnected PZT/polymer composite with properties similar to the coral-based composites. The simplified preparation method involves mixing PMMA spheres and PZT powder in an organic binder. When carefully

sintered, a porous PZT skeleton is formed, and later back-filled with polymer to form a 3-3 composite. This technique is commonly referred to as the BURPS process, an acronym for burned-out plastic spheres. Since the process involves the generation and emission of gaseous hydrocarbons, the name BURPS is highly appropriate. The composites prepared by Shrout, et al. contained a PZT/polymer volume ratio of 30/70.

More recently, the electromechanical properties of 3-3 composites having a wide range of PZT/polymer ratios were measured (20), and compared to the results with other piezoelectric materials, including some earlier Japanese work on similar composites (21,22). Dielectric and piezoelectric properties were measured on samples ranging from 30 to 70 volume % PZT, and compared with a rectangular skeleton model for 3-3 composites. Composites containing 50% PZT-50% silicone rubber appear especially useful for hydrophone applications with  $\bar{d}_h \bar{g}_h$  products a hundred times larger than PZT.

#### 7. Perforated PZT/Polymer Composites

Composites of PZT and polymer with 3-1 and 3-2 connectivity patterns have been fabricated by drilling holes in sintered PZT blocks and filling the holes with epoxy (23). The influence of hole size and volume fraction PZT on the hydrostatic properties of the composite was evaluated. By decoupling the piezoelectric  $d_{33}$  and  $d_{31}$  coefficients in the composite, the hydrostatic coefficients are greatly enhanced. On samples optimized for hydrophone performance, the dielectric constants of 3-1 and 3-2 composites are 600 and 300 respectively. For two typical composites, the piezoelectric coefficients  $\bar{d}_h$ ,  $\bar{g}_h$ , and  $\bar{g}_h \bar{d}_h$  for 3-1 composites are 230 ( $\text{pC N}^{-1}$ ),  $34 (10^{-3} \text{ V m N}^{-1})$ , and  $7800 (10^{-15} \text{ m}^2 \text{ N}^{-1})$  respectively, and the corresponding values for 3-2 composites are 372 ( $\text{pC N}^{-1}$ ), 123 ( $10^{-3} \text{ V m N}^{-1}$ ), and  $45000 (10^{-15} \text{ m}^2 \text{ N}^{-1})$ .

These composites are extremely rugged and show no pressure dependence. Similar composites can be prepared by extruding the ceramic rather than drilling.(24). Composites with 3-1 connectivity were fabricated by impregnating an extruded, sintered honeycomb configuration of PZT with epoxy. The composites had lower density and lower dielectric constant than that of solid PZT. The maximum piezoelectric  $\bar{d}_{33}$  coefficient of the composites was 350 pC/N, and the maximum  $\bar{d}_h$  was 220 pC/N.  $\bar{g}_h$  and  $\bar{d}_h \bar{g}_h$  of the composites were an order of magnitude higher than that of solid PZT.

#### SUMMARY AND CONCLUSION

Composite piezoelectric elements form an interesting family of materials which highlight the major advantages composite structures afford in improving coupled properties in solids for transduction applications. By careful consideration of the crystal symmetry, macrosymmetry, and possible modes of phase interconnection (connectivity) which can be realized by modern processing technologies, it is possible to design new composite transducers with property combinations tailored for specific device requirements.

We believe that the composite materials offer a new versatility in property combinations, and it will be most interesting to observe how this is taken up and exploited in subsequent generations of piezoelectric devices.

### References

1. G. M. Sessler, J. Acoust. Soc. Am. 70, 1596 (1981).
2. R. G. Kepler, Ann. Rev. Phys. Chem. 29, 497 (1978).
3. S. Edelman, Proceedings of the Workshop on Sonar Transducer Materials, Naval Research Laboratory (Feb. 1976).
4. Y. Wada and R. Kayakawa, Japan, J. Appl. Phys. 15 2041 (1976).
5. J. F. Nye, Physical Properties of Crystals, Oxford University Press, London (1957).
6. L. A. Pauer, I.E.E.E. Int'l. Conv. Rec., 1973 p 1 (1973).
7. W. B. Harrison, Proceedings of the Workshop on Sonar Transducer Materials, Naval Research Laboratory (Feb. 1976).
8. T. Furukawa, K. Ishida and E. Fukada, J. Appl. Phys. 50, 4904 (1979).
9. T. Yamada, T. Ueba and T. Kitayama, J. Appl. Phys. 53, 4328 (1982).
10. H. Banno and S. Saito, Japan-U.S. Study Seminar on Dielectric and Piezo-electric Ceramics, Paper M-4 (1982).
11. T. Furukawa, K. Kujino and E. Fukada Jap. J. Appl. Phys. 15, 2119 (1976).
12. R. E. Newnham, D. P. Skinner and L. E. Cross. Mat. Res. Bull. 13 525 (1978).
13. D. P. Skinner, R. E. Newnham, and L. E. Cross, Mat. Res. Bull. 13 599 (1978).
14. K. A. Klicker, J. V. Biggers and R. E. Newnham, J. Am. Cer. Soc. 64, 5 (1982).
15. J. Runt, and E. C. Galgoci, J. Appl. Polym. Sci. Submitted.
16. J. Runt and E. C. Galgoci, Mat. Res. Bull. Submitted.
17. K. A. Klicker, Ph.D. Thesis, The Pennsylvania State University (1980).
18. A. Safari, A. Halliyal, L. J. Bowen and R. E. Newnham, J. Am. Cer. Soc. 65, 207 (1982).
19. T. R. Shrout, W. A. Schulze and J. V. Biggers, Mat. Res. Bull. 14, 1553 (1979).
20. K. Rittenmyer, T. R. Shrout and R. E. Newnham, Ferroelectrics 41, 139 (1982).
21. K. Nagata, H. Igarashi, K. Okazaki, and R. C. Bradt, Japan J. Appl. Phys. 19, L37 (1980).
22. M. Miyashita, K. Takano, and T. Toda, Ferroelectrics 28, 397 (1980).
23. A. Safari, R. E. Newnham, L. E. Cross, and W. A. Schulze, Ferroelectrics 41, 197 (1982).
24. A. Safari, A. Halliyal, R. E. Newnham, and I. M. Lachman, Mat. Res. Bull. 17, 301 (1982).

Table 1

## Properties of Piezoelectric Materials

Piezoelectric Material	Property							
	Relative Permittivity		Elastic Compliance		Piezoelectric Coefficient		Piezoelectric Voltage Coefficient	
	$\epsilon_1$	$\epsilon_3$	$S_{11}$ $\text{pm}^2\text{N}^{-1}$	$S_{33}$ $\text{pm}^2\text{N}^{-1}$	$d_{31}$ $\text{pC}\text{N}^{-1}$	$d_{33}$ $\text{pC}\text{N}^{-1}$	$g_{31}$ $\times 10^{-3}\text{VmN}^{-1}$	$g_{33}$ $\times 10^{-3}\text{VmN}^{-1}$
$\alpha$ Quartz Single Crystal	4.5	4.6	12.8	9.6	23( $d_{11}$ )		57.0( $g_{11}$ )	
BaTiO <sub>3</sub> Single Crystal	2920	168	8.05	15.7	-34.5	85.6	-23.0	57.6
BaTiO <sub>3</sub> Ceramic	1620	1900	8.55	8.93	-79.0	191.0	-4.7	11.4
PST 0.48 $\mu\text{m}$ 0.52 $\mu\text{m}$ Ceramic	1180	730	13.8	17.1	-93.5	223.0	-14.5	34.5
PVF <sub>2</sub>		15	330		17.9 to 37	-20 to -30	95	-140



Table 2

Hydrostatic Mode Materials

	Dielectric Constant ( $\epsilon_{33}$ )	$d_h$ (pC/N)	$s_h$ $10^{-3} \text{Vm}/\text{N}$	$d_h s_h$ $10^{-15} \text{m}^2/\text{N}$
PZT	1600	50	4	200
$\text{PbNb}_2\text{O}_6$ (ceramic)	225	65	35	2300
$\text{PVF}_2$	12	11	100	1100
Selected Composites				
0-3 PZT/ silicone rubber	100	28	32	900
1-3 PZT/epoxy	70	30	50	1500
1-3 PZT/foamed polyurethane	75	85	135	10000
3-3 PZT/silicone rubber	450	180	45	8100
3-2 PZT/epoxy	410	200	55	11000

### Figure Captions

- Fig. 1 Ten connectivity patterns for a diphasic solid. Each phase has zero-, one-, two- or three-dimensional connectivity to itself. In the 3-1 composite, for instance, the shaded phase is three-dimensionally connected and the unshaded phase is one-dimensionally connected. Arrows are used to indicate the connected directions. Two views of the 3-3 and 3-2 patterns are given because the two interpenetrating networks are difficult to visualize on paper. The views are related by 90° counterclockwise rotation about Z.
- Fig. 2 Two types of piezoelectric ceramic/polymer composites: (a) represents small piezoelectric particles suspended in a polymer film; (b) represents bound piezoelectric particles of a size comparable to the thickness of the polymer sheet.
- Fig. 3 The series (a) and parallel (b) models used in estimating the piezoelectric effects of diphasic solids.
- Fig. 4 Fabrication of 1-3 composites with PZT rods and an epoxy.
- Fig. 5  $\bar{d}_{33}$  vs volume % PZT for 1-3 PZT/epoxy composites.
- Fig. 6  $\bar{g}_{33}$  as a function of volume % PZT for 1-3 PZT/epoxy composites.

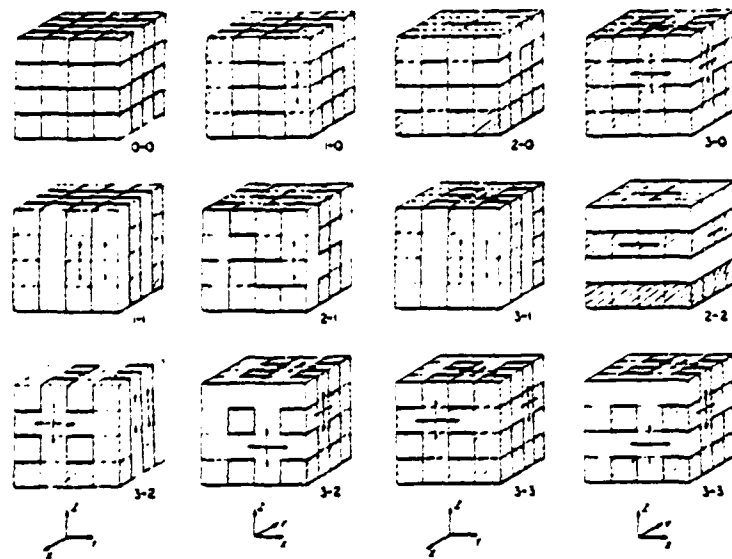


Fig 1

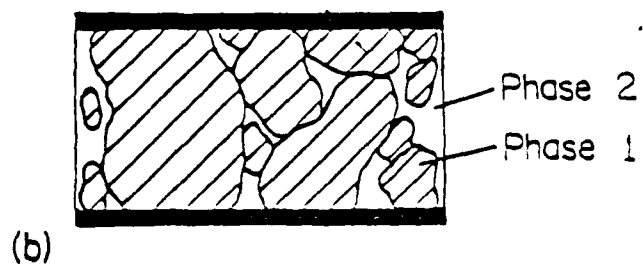
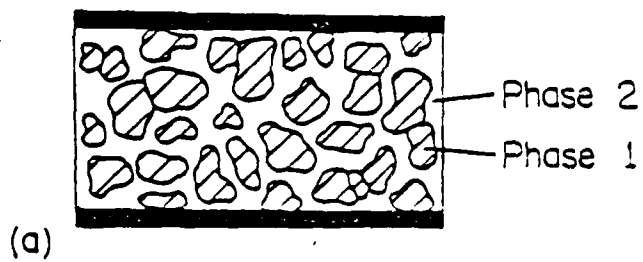
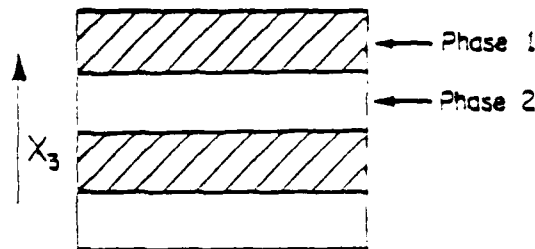
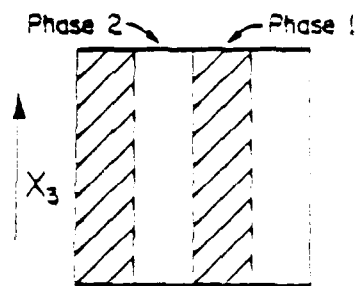


Fig 2



(a)



(b)

Fig 3

PHOTO OF 1-3 COMPOSITES  
 - GOOD REPRODUCTION NOT  
 AVAILABLE AT THIS TIME

Fig 4

Fig. 5

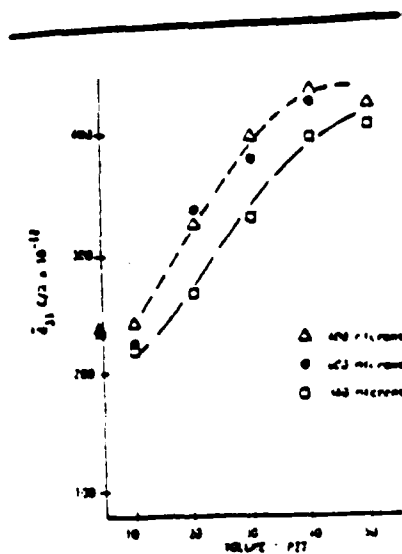
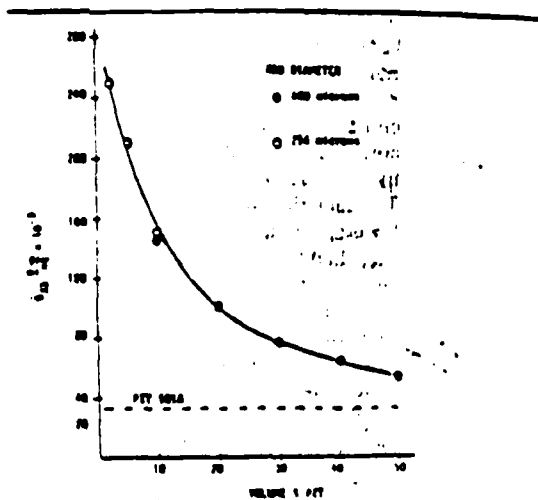


Fig. 6



**APPENDIX 7**

*11.11.1981*  
*Accepted*  
Piezoelectric Composites of PZT and Some Semi-Crystalline Polymers

J. Runt\* and E. C. Galgoci

Polymer Science Program

Department of Materials Science and Engineering

The Pennsylvania State University

University Park, PA 16802

\* To whom correspondence should be sent

## I. Introduction and Background

By careful choice of design, multiphase materials may be produced which possess ultimate properties which are superior to the sum of those of the individual components.<sup>(1)</sup> With this idea in mind, novel piezoelectric transducers have been produced and tested for applications such as hydrophones and medical ultrasound.<sup>(2)</sup> One of the most successful designs to date consists of slender, extruded fibers of lead zirconate titanate (PZT) aligned normal to two electroded surfaces and surrounded by a polymer matrix (3,4,5). These composites are referred to as 1-3 composites in the nomenclature adopted by Newnham, et al. (6), where the numbers refer to the total orthogonal directions (in an orthogonal axis system) in which each phase is self-connected. Since the PZT rods are continuous from one electrode surface to the other, saturation poling can be accomplished; thereby ensuring the maximum piezoelectric sensitivity.

The hydrostatic piezoelectric response can be defined by the piezoelectric strain ( $d_h$ ) and voltage ( $g_h$ ) coefficients.  $d_h$  is a measure of the polarization produced as a result of applying a hydrostatic stress and is given by:

$$d_h = d_{33} + 2d_{31} \quad (1)$$

where the subscripts refer to directions in an orthogonal axis system according to the common reduced notation. The 3-direction is defined as the direction parallel to the PZT fiber axis. Charge which develops on the electrode surface as a result of stresses parallel and perpendicular to the poling axis is governed by  $d_{33}$  and  $d_{31}$ , respectively. The voltage coefficient is related to  $d_h$  by:

$$g_h = \frac{d_h}{K_{33}\epsilon_0} \quad (2)$$

where  $K_{33}$  is the dielectric constant in the poling direction and  $\epsilon_0$  is the



permittivity of free space. Since, for PZT,  $d_{33}$  is opposite in sign to and slightly twice the value of  $d_{31}$ , and  $K_{33}$  is large, both  $d_h$  and  $g_h$  are relatively low.

For piezoelectric 1-3 composites a simple parallel-series model developed by Skinner, et al.<sup>(7)</sup> predicts that the  $d_{33}$  ( $\bar{d}_{33}$ ) of a composite containing a very compliant matrix is equal to the  $d_{33}$  of PZT. The composite  $d_{31}$  ( $\bar{d}_{31}$ ) is given by:

$$\bar{d}_{31} = {}^1_v {}^1_d d_{31} \quad (3)$$

where  $v$  is the volume fraction and the superscript 1 refers to the PZT phase. The composite hydrostatic piezoelectric coefficient ( $\bar{d}_h$ ) can then be expressed as:

$$\bar{d}_h = {}^1_d d_{33} + {}^1_v {}^1_d d_{31} \quad (4)$$

Also, the composite voltage coefficient, which is important for hydrophones, is given by:

$$\bar{g}_h = \frac{\bar{d}_h}{{}^1_v \bar{K}_{33} \epsilon_0} \quad (5)$$

Therefore, the simple model predicts large increases in  $\bar{d}_h$  and  $\bar{g}_h$  over PZT as the amount of PZT in the composite is decreased.

However, recent experimental work<sup>(4,5,8)</sup> has shown that the quantitative predictions of the Skinner, et al. scheme are not realized if flexible electrodes are used for 1-3 composites. Several explanations have been proposed to account for these discrepancies. These include: the effective matrix region of influence<sup>(8)</sup>, internal stresses arising from differences in the Poisson's strain between the ceramic and polymer<sup>(9)</sup>, and relic processing stresses<sup>(5)</sup>. In the

case of glassy thermoplastic polymer matrices, annealing the composites at temperatures near the glass transition temperature ( $T_g$ ) of the matrix was found to improve their piezoelectric response <sup>(5)</sup>. This is presumably due to relief of some of the residual processing stresses.

All 1-3 composites studied to date have used amorphous polymers as the matrix phase. Semi-crystalline polymer matrices have never been employed in these types of piezoelectric composites. Low  $T_g$ , semi-crystalline polymers such as polyethylene and the Hytrel poly(ester/ether) block copolymers have mechanical properties which are intermediate between glassy and elastomeric materials. Also, it is possible to conveniently alter the degree of crystallinity of these materials by thermal annealing at temperatures approaching the melting point or, in the case of the Hytrels, by varying the crystallizable-segment content. This allows one to investigate the effect of matrix compliance on composite performance. This paper reports some of our initial studies on 1-3 PZT/semi-crystalline polymer composites.

## II. Experimental

### A. Composite Fabrication

The PZT rods used in this study were prepared by a technique described previously <sup>(3)</sup>. All composites contained rods which were 12-mil (305  $\mu$ m) in diameter and were prepared from PZT 501A powder (obtained from Ultrasonic Powders, Inc.). The sintered PZT fibers were aligned in racks which consisted of two parallel plates of aluminum foil separated by  $\sim 2$  cm. Each plate had an array of perforations through which the rods were inserted so as to be held in place during polymer processing. This was done to insure the proper volume fraction (4%) of PZT for all composites.

#### (a) PZT/Poly(butylene terephthalate) Composites

Poly(butylene terephthalate) (PBT) is a semi-crystalline polymer with a melting point ( $T_m$ ) of  $\sim 220^\circ\text{C}$  and a  $T_g$  of  $70^\circ\text{C}$ . Therefore, PBT is a glassy semi-crystalline material and possesses mechanical properties characteristic of rigid

polymers (e.g. Young's modulus ( $E$ )  $\approx 10^9 \text{ N/m}^2$ ). PBT is polymerized by condensation methods and has a relatively low molecular weight (ca. 20,000-30,000 gm/mole). Its melt viscosity is therefore also comparatively low, making small scale melt composite processing feasible without the use of high pressures.

PZT/PBT composites were prepared by placing filled racks of PZT rods and dried PBT pellets (obtained from Scientific Polymer Products, Inc.) into glass molds which were then purged with nitrogen and immersed in a  $250^\circ\text{C}$  oil bath until the pellets melted and no voids were present in the melt. The system was allowed to cool to room temperature over a 5 hour period.

#### (b) PZT/Nylon 11 Composites

Like PBT, nylon 11 is a glassy, semi-crystalline polymer ( $T_m \approx 185^\circ\text{C}$ ,  $T_g \approx 45^\circ\text{C}$ ,  $E \approx 10^9 \text{ N/m}^2$ ) and has a relatively low melt viscosity. However, in order to avoid the problem of polymer degradation at high temperatures, we decided to prepare these composites by insitu polymerization of the monomer.

Racks of PZT in glass molds were surrounded by 11-aminoundecanoic acid ( $T_m \approx 190^\circ\text{C}$ ) and the molds (under a continuous nitrogen purge) were placed in a  $220^\circ\text{C}$  silicone oil bath. Water vapor which formed during the polymerization was forced through an exit tube by the gas pressure. The polymerization was terminated by cooling for one hour after water formation ceased.

#### (c) PZT/Hytrel Composites

The Hytrels (E. I. duPont de Nemours and Co., Inc.) are a series of thermoplastic elastomers composed of polyester "hard" segments which are crystallizable and non-crystallizable, low  $T_g$  polyether "soft" segments. By varying the concentration of polyester units, the degree of crystallinity and, hence, the modulus of the resultant copolymer can be adjusted. Some characteristics of the three Hytrels used in this study are shown in Table 1<sup>(10)</sup>. Note that all the

Hytrels have moduli which are significantly lower than both PBT and nylon 11.

Composites were prepared in the same manner as the PZT/PBT materials except that the oil bath was heated to 220°C and cooling to room temperature was done over a 48 hour period.

After solid composites were fabricated, the molds were broken and the composites were sectioned perpendicular to the rod axis using an electric diamond saw or a hacksaw. The as-cut slugs were then sanded with 60 grit garnet paper followed by polishing using 200 grit garnet paper. All composites were 4mm thick in the fiber direction.

Air-dry silver electrodes were applied to the two faces perpendicular to the rods and the composites were poled at 75°C in an oil bath with a field of 22kV/cm for 5 min. After the composites were removed from the bath, they were allowed to cool in air under a field of 7.5 kV/cm for 10 minutes to prevent depoling during cooling. The poled composites were aged for at least 24 hours prior to piezoelectric and dielectric measurements.

### B. Measurement of Dielectric and Piezoelectric Properties

Dielectric measurements were performed with a Hewlett Packard 4270A Automatic Capacitance Bridge at 1kHz and 1 volt.  $\bar{d}_{33}$  was measured using a Berlincourt Piezo  $\bar{d}_{33}$ -Meter with rounded rams. The ratio of the diameter of the rams to the center-to-center distance of the PZT rods was 0.74. The  $\bar{d}_{33}$  was taken as the average of 20 random measurements (10 on each electroded surface of the composite) at a ram pressure of approximately 55 psi. The hydrostatic piezoelectric coefficients ( $\bar{d}_h$  and  $\bar{g}_h$ ) were measured by a dynamic <sup>(11)</sup> method. The apparatus consisted of an oil-filled chamber in which the samples and a PZT standard of known  $d_h$  and  $g_h$  were immersed. The pressure inside the vessel was raised to 100

psi and alternating sinusoidal pressure cycles (amplitude = 0.1 psi) were imposed using an AC stress generator driven by a function generator adjusted to the proper frequency. The sample (or standard) voltage was recorded on an oscilloscope display.

### III. Results and Discussion

Comparison of composite dielectric and piezoelectric properties with conventional single phase materials can be found in Table 2. As expected, the composite dielectric constants are low compared to that of PZT but, except for the PZT/Hytrel 4056 composite,  $\bar{K}_{33}$  values are greater than that predicted by the rule of mixtures (theoretical  $\bar{K}_{33} = 64$ ). Since applied compressive stress is known to increase the dielectric constant of PZT <sup>(12)</sup>, radial compression between the rods and the matrix may be responsible for these results <sup>(5)</sup>. Radial stresses may have originated from thermal expansion mismatches, mechanical processing conditions, or polymer crystallization shrinkage.

For a more compliant polymer, stress transfer from the matrix to the PZT rods should be more efficient than for a stiffer matrix. Thus,  $\bar{d}_{33}$  would be expected to increase as matrix compliance increases and this is seen to be the general trend for the polymers examined in this study with the PZT/Hytrel 4056 and PZT/Hytrel 1000 composites exhibiting  $\bar{d}_{33}$ 's which are larger than some of the higher modulus composites.

A somewhat surprising result is that  $\bar{d}_{31}$  increases as polymer modulus increases. Since  $\bar{d}_{33}$  increases as the matrix stiffness decreases,  $|\bar{d}_{31}|$  must increase accordingly. In general, as the compliance of a polymer increases, its Poisson's ratio ( $\nu$ ) increases and the enhancement of  $|\bar{d}_{31}|$  is thought to arise from stresses due to differences in Poisson's contraction between the phases <sup>(9)</sup>. Although one cannot alter the characteristic modulus and  $\nu$  independently in solid polymers, one can lower both simultaneously through matrix foaming. Such compliant, foamed composites would be expected to have outstanding hydrostatic figures of merit. This has, in fact, been shown to be the case by Klicker, et al. for PZT/foamed polyurethane composites <sup>(13)</sup>.

The hydrostatic piezoelectric coefficients ( $\bar{d}_h$ ) for the PBT, nylon 11 and Hytrel 995 composites are smaller than those of PZT but similar to those observed previously for 1-3 composites with rigid matrices (5,11).  $\bar{d}_h$  for the Hytrel 4056 and 1000 composites are comparable to that of PVDF but considerably smaller than the other composites presumably due to Poisson's ratio stresses. The voltage coefficients of all composites are greater than that of PZT because the permittivities of the composites are much lower than the values for PZT alone.  $\bar{g}_h$  for the composites with relatively stiff matrices (PBT, nylon 11 and Hytrel 995) are about an order of magnitude larger than PZT but, because of their low  $\bar{d}_h$ , the Hytrel 4056 and 1000 composites exhibit significantly lower values. This results in  $\bar{g}_h \bar{d}_h$  for the composites with stiff matrices being about five times larger than that of PZT and comparable to that of PVDF while the figures of merit of the more compliant matrix composites are somewhat less than PZT. Finally, no frequency dependence of  $\bar{d}_h$  was observed for any composite from 30 to 160 Hz (Figure 1).

#### IV. Conclusions

The piezoelectric figures of merit for composites with stiff polymer matrices are about five times larger than PZT and comparable to PVDF. The primary reason for the enhancement of  $\bar{d}_h \bar{g}_h$  over PZT is that the composites have much lower  $\bar{K}_{33}$  values than PZT. An unexpected result was the decrease in  $\bar{d}_h$  as matrix modulus decreased. Since  $\bar{d}_{33}$  was found to increase as the matrix modulus decreases,  $|\bar{d}_{31}|$  must be increasing as the polymer stiffness decreases. The enhanced component of  $|\bar{d}_{31}|$  presumably results from differences in Poisson's contraction between the phases and ultimately results in relatively low figures of merit for composites with compliant polymer matrices.

#### Acknowledgements

The authors would like to thank the Office of Naval Research for partial support of this work through contract N00014-82-K-0339.

REFERENCES

1. R. E. Newnham, D. P. Skinner, and L. E. Cross, *Mat. Res. Bull.*, 13 , 525 (1978).
2. R. E. Newnham, L. J. Bowen, K. A. Klicker, and L. E. Cross, *Mater. Eng.*, 2 , 93 (1980).
3. K. A. Klicker, J. V. Biggers, and R. E. Newnham, *J. Amer. Ceram. Soc.*, 64 , 5(1981).
4. S. Y. Lynn, R. E. Newnham, K. A. Klicker, K. Rittenmeyer, A. Safari, and W. A. Schulze, *Ferroelectrics*, 38 , 955 (1981).
5. J. Runt and E. C. Galgoci, *J. Appl. Polym. Sci.* Accepted for publication.
6. R. E. Newnham, D. P. Skinner, and L. E. Cross, *Mat. Res. Bull.*, 13 , 525 (1978).
7. D. P. Skinner, R. E. Newnham, and L. E. Cross, *Mat. Res. Bull.*, 13 , 599 (1978).
8. K. A. Klicker, Ph.D. Dissertation, The Pennsylvania State University, (1980).
9. M. Haun, M.S. Thesis, The Pennsylvania State University, 1983.
10. R. J. Cella, "Polyesters, Elastomeric", Encyclopedia of Polymer Science and Technology , supplement Volume II, pgs. 485-510, 1977, John Wiley and Sons, Inc.
11. S. Y. Lynn, M.S. Thesis, The Pennsylvania State University, 1981.
12. B. Jaffe, W. R. Cook, and H. Jaffe, Piezoelectric Ceramics , London, Academic Press (1971).
13. K. A. Klicker, W. A. Schulze and J. V. Biggers, *Comm. Amer. Ceram. Soc.* 65 , 208 (1982).

Table 1. Properties of Hytrel Copolymers (10)

Hytrel	Wt. % Polyester segments	T <sub>m</sub> (°C)	T <sub>g</sub> (°C)	Density (gm/cc)	Modulus (10 <sup>3</sup> N/m <sup>2</sup> )
4056	~30	150	-80	1.17	0.34
1000	49	186	-65	1.19	1.48
995	81	218	-5	1.23	4.00



Table 2

Piezoelectric Properties of 1-3 Composites and Single Phase Materials

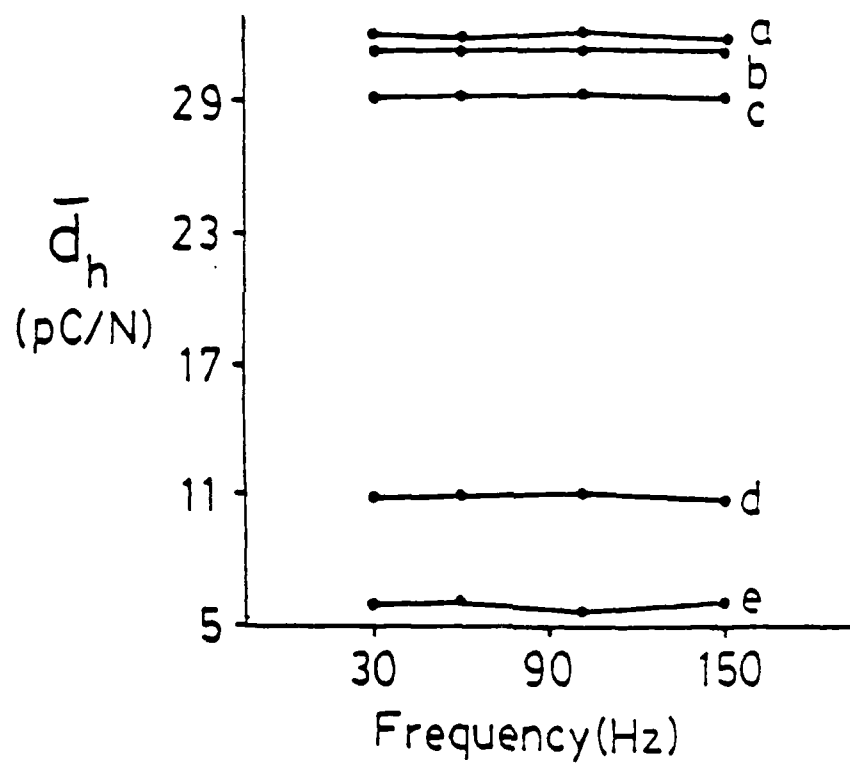
Material	Density <sup>*</sup> (g/cc)	$\bar{K}_{33}$	$\bar{d}_{33}$ <sup>**</sup> ( $10^{-12}$ C/N)	$\bar{d}_h$ <sup>***</sup> ( $10^{-12}$ C/N)	$\bar{g}_h$ <sup>***</sup> ( $10^{-3}$ V-m/N)	$\bar{d}_h \bar{g}_h$ <sup>***</sup> ( $10^{-15}$ m/N)
PZT/PBT	1.35	97	$110 \pm 20$	29	34	.990
PZT/nylon 11	1.31	105	128	32	34	1090
PZT/Hytrel 4056	1.44	62	$174 \pm 43$	6	10	60
PZT/Hytrel 1000	1.46	94	$215 \pm 50$	11	13	140
PZT/Hytrel 995	1.49	94	$141 \pm 25$	32	38	1220
PZT	7.9	1600	400	50	4	200
PVDF	1.4	12	24	11	104	1140

<sup>\*</sup> Calculated for composites<sup>\*\*</sup> Errors are  $\pm$  standard deviation.<sup>\*\*\*</sup> Estimated errors are:  $\bar{d}_h \pm 12\%$ ,  $\bar{g}_h \pm 16\%$ , and  $\bar{d}_h \bar{g}_h \pm 20\%$ .

Figure Caption

Figure 1:  $\bar{d}_n$  of composites as a function of test frequency.

- a. PZT/Nylon 11
- b. PZT/Hytrel 995
- c. PZT/PBT
- d. PZT/Hytrel 1000
- e. PZT/Hytrel 4056



**APPENDIX 8**

*C. J. Runt, E. C. Galgoc*

Polymer/Piezoelectric Ceramic Composites:  
Polystyrene and Poly(methyl methacrylate) with PZT

J. Runt\* and E. C. Galgoci

Polymer Science Program  
Department of Materials Science and Engineering  
The Pennsylvania State University  
University Park, Pa 16802

\* To whom correspondence should be sent.

## L Introduction

Piezoelectric composites have been the center of much recent study<sup>(1)</sup> because of their possible advantages over single phase piezoelectrics (e.g., poly(vinylidene fluoride)(PVDF) and lead zirconate-titanate (PZT)) for hydrophone applications. The phase connectivity<sup>(2)</sup> is a particularly important parameter which ultimately determines the properties of a composite solid. For piezoelectric composites made from PZT and polymers designs which allow the ceramic to be poled to saturation produce relatively large piezoelectric coefficients even for low PZT concentrations.

One such motif studied by Klinker et al.<sup>(3)</sup> consisted of slender PZT rods aligned perpendicular to the electrode surface and surrounded by a thermosetting polymer (epoxy). These diphasic materials are designated 1-3 composites in the notation adopted by Newnham, et al.<sup>(2)</sup> The numbers refer to the total orthogonal directions in which each phase is continuous throughout the object. In this case the active phase (PZT) extends continuously in one direction, while the polymer matrix spans the composite in all three orthogonal directions. Klinker et al.'s PZT/epoxy composites have hydrostatic "figures of merit" about an order of magnitude larger than homogeneous PZT.<sup>(3)</sup> In addition, these materials have low densities ( $\rho < 1.8 \text{ g/cm}^3$ ), which provide for better acoustic coupling to water than PZT ( $\rho = 7.8 \text{ g/cm}^3$ ), and are flexible relative to PZT ceramics.

Even though the major improvements in properties for these composites over PZT ceramics can be traced to the polymeric phase, few polymer systems have been studied as possible matrix materials. Furthermore, only thermosetting polymers (e.g., epoxies and polyurethanes) have been employed previously in 1-3 composites. Because the mechanical and physical properties of polymers can vary widely, and because theory<sup>(4)</sup> suggests that matrix mechanical properties should strongly affect composite piezoelectric response, we have fabricated composites with a variety of thermoplastic polymers. This paper describes our initial studies on polystyrene (PS)/PZT and poly(methyl methacrylate) (PMMA)/PZT 1-3 composites.

## II. Background-Theory

Piezoelectric materials experience a polarization (P) due to an applied stress ( $\sigma$ ). The piezoelectric coefficient (d) is a measure of the polarization produced per unit stress. Under hydrostatic conditions, the piezoelectric coefficient is given by:

$$d_h = d_{33} + 2d_{31} \quad (1)$$

where the subscripts are the reduced notation for designated directions in an orthogonal axis system. The  $d_{33}$  and  $d_{31}$  coefficients refer to polarizations which develop along the poling axis (i.e., the 3 direction) due to applied stresses parallel and transverse to the poling direction, respectively. For PZT,  $d_{33}$  is opposite in sign to and approximately one-half of  $d_{31}$ ; therefore,  $d_h$  is small. The hydrostatic voltage coefficient ( $g_h$ ) is related to  $d_h$  by:

$$g_h = \frac{d_h}{\epsilon_{33}} \quad (2)$$

where  $\epsilon_{33}$  is the dielectric permittivity. Since  $d_h$  is low and the permittivity is high for PZT, the voltage coefficient, which is important for hydrophone applications, is very low. For a hydrostatic transducer material the  $d_h g_h$  product is considered to be an all-encompassing "figure of merit".

A simple theory to describe the piezoelectric coefficients of composites with 1-3 connectivity has been described by Skinner, et al. <sup>(4)</sup> The theoretical piezoelectric and dielectric coefficients are given by:

$$\bar{d}_{33} = \frac{1_v 1_{d_{33}} 1_{J_{33}} + 2_v 2_{d_{33}} 1_{J_{33}}}{1_v 2_{J_{33}} + 2_v 1_{J_{33}}} \quad (3)$$

$$\bar{d}_{31} = 1_v 1_{d_{31}} - 2_v 2_{d_{31}} \quad (4)$$

$$\bar{\epsilon}_{33} = 1_v 1_{\epsilon_{33}} - 2_v 2_{\epsilon_{33}} \quad (5)$$

where  $v$  and  $J$  are the volume fraction and elastic compliance, respectively. The superscripts refer to phase 1 (PZT) or phase 2 (polymer), and the bar represents the average composite coefficient.

Equations 3 through 5 can be reduced by considering that most polymers are non-piezoelectric (i.e.,  ${}^2d_{33} = {}^2d_{31} = 0$ ), and possess relatively low dielectric permittivities ( ${}^1\epsilon_{33} \gg {}^2\epsilon_{33}$ ). Therefore, equations 3-5 become:

$$\bar{d}_{33} = \frac{{}^1v {}^1d_{33} {}^2J_{33}}{{}^1v {}^2J_{33} + {}^2v {}^1J_{33}} \quad (6)$$

$$\bar{d}_{31} = {}^1v {}^1d_{31} \quad (7)$$

$$\bar{\epsilon}_{33} = {}^1v {}^1\epsilon_{33} \quad (8)$$

Since most polymers are much more compliant than PZT (i.e.,  ${}^2J_{33} \gg {}^1J_{33}$ ), equation 6 further reduces to:

$$\bar{d}_{33} = {}^1d_{33} \quad (9)$$

In this case, all of the force in the fiber direction is borne by the ceramic rod elements. However, if  ${}^1v \ll {}^2v$ , this approximation to equation 6 is invalid.

By combining equations 1, 6, and 7, the hydrostatic piezoelectric coefficient is obtained:

$$\bar{d}_h = \frac{{}^1v {}^1d_{33} {}^2J_{33}}{{}^1v {}^2J_{33} + {}^2v {}^1J_{33}} - {}^2v {}^1d_{31} \quad (10)$$

Figure 1 shows how  $\bar{d}_h$  varies as a function of  ${}^1v$  according to equations 2, 3 and 10 for several values of matrix compliance. For low concentrations of PZT,  $\bar{d}_h$  is predicted to vary significantly as the matrix compliance changes.

Several modifications to Skinner, et. al.'s model have been suggested (5,6). Klinker (6) has shown that  $\bar{d}_{33}$  is not necessarily equal to the  $d_{33}$



of PZT, but is a function of PZT rod diameter and volume fraction, composite thickness, and matrix compliance. Additionally, the internal forces arising from a difference in constriction between the phases through Poisson's ratio produce an enhancement of  $|d_{31}|$  over that predicted by equations 4 or 7<sup>(5)</sup>. These considerations lead to the conclusion that  $\bar{d}_n$  predictions based on the Skinner et al. approach are overestimates for 1-3 PZT/polymer composites.

Another important internal stress is that which is due to a mismatch in thermal expansion (or contraction) between the constituent phases <sup>(7,9)</sup>. Polymers have coefficients of thermal expansion which are at least an order of magnitude larger than PZT ceramics. Therefore, large compressive stresses can develop at the interface of the resin and the PZT rods. These stresses may alter the piezoelectric and dielectric response of composite piezoelectrics. Furthermore, stresses related to curing or polymerization may also be of consequence.

### III. Experimental

The preparation of the PZT rods used in this study has been described elsewhere <sup>(3)</sup>. All rods were 12-mil (305 $\mu$ m) in diameter and were prepared from PZT 501A (Ultrasonic Powders, Inc. South Plainfield, NJ). The sintered rods were aligned in racks which consisted of two parallel plates of aluminum foil separated by 12cm. Each plate had an array of perforations through which the rods were inserted to be held in place during polymerization of the matrix in order to insure the proper volume fraction (4%) of PZT for all composites.

In-situ polymerization of liquid monomers was the most convenient method to prepare composites because of the fragile nature of the PZT rods. The liquid monomers (styrene and methyl methacrylate) were purified by vacuum distillation prior to use. Polymerization was initiated by 0.5 weight percent benzoyl peroxide. Prepolymer syrups (polymer in monomer) were prepared by heating the monomer-initiator systems at 30°C for 15 minutes and then cooling the mixture to room temperature. By using a prepolymer, the resulting composites were found to be essentially void free.

Composites were then fabricated by placing filled racks of PZT rods into glass molds and pouring a given prepolymer into the mold until the rods were submerged in the liquid and covered over by ~1cm. The molds were then placed in an oven maintained at 50°C until the polymer solidified. Additional heating to 90°C for one hour completed the polymerizations. After the molds were removed from the oven and allowed to cool, the glass mold was broken and the composites were sectioned perpendicular to the rod axis using an electric diamond saw or a hacksaw. The as-cut slugs were then sanded with 60 grit garnet paper followed by polishing using 200 grit garnet paper. All composites were 4mm thick in the fiber direction. The glass transition temperatures ( $T_g$ ) of the matrices were determined with a Perkin Elmer DSC 2 equipped with a Thermal Analysis Data Station. The  $T_g$  of both the PS and PMMA was found to be approximately 100°C.

Air-dry silver electrodes were applied to the two faces perpendicular to the rods and the composites were poled at 75°C in an oil bath with a field of 22kV/cm for 5 min. After the composites were removed from the bath, they were allowed to cool in air under a field of 7.5 kV/cm for 10 minutes to prevent de-poling during cooling. The poled composites were aged for at least 24 hours prior to piezoelectric and dielectric measurements.

Dielectric measurements were performed with a Hewlett Packard 4270A Automatic Capacitance Bridge at 1kHz and 1 volt.  $\bar{d}_{33}$  was measured using a Berlincourt Piezo  $\bar{d}_{33}$ -Meter with rounded rams. The ratio of the diameter of the rams to the center-to-center distance of the PZT rods was 0.74. The  $\bar{d}_{33}$  was taken as the average of 20 random measurements (10 on each electroded surface of the composite) at a ram pressure of approximately 55 psi. The hydrostatic piezoelectric coefficients ( $\bar{d}_h$  and  $\bar{g}_h$ ) were measured by a dynamic <sup>(9)</sup> method. The apparatus consisted of an oil-filled chamber in which the samples and a PZT standard of known  $\bar{d}_h$  and  $\bar{g}_h$  were immersed. The pressure inside the vessel was raised to 100 psi and alternating sinusoidal pressure cycles (amplitude  $\pm 0.1$  psi) were imposed using an AC stress generator driven by a function generator adjusted to the proper

frequency. The sample (or standard) voltage was recorded on an oscilloscope display.

After the composites were tested, they were annealed at 95°C for 15 hours under vacuum followed by slow cooling to room temperature. The annealed composites were repoled in order to ensure saturation poling of the PZT rods and then retested as described above.

#### IV. Results and Discussion

The dielectric and piezoelectric properties of the PZT/PS and PZT/PMMA composites are summarized in Table 1. As expected, the composite dielectric constants ( $\bar{\epsilon}_{33}$ ) were considerably less than that of PZT ( $\epsilon_{33} \approx 1600$ ). The value of  $\bar{\epsilon}_{33}$  predicted by the simple parallel model for a 4% PZT/polymer, 1-3 composite is 64. The PZT/PS composites approached the theoretical value; however, the PZT/PMMA materials far exceeded the prediction. One possible explanation for this discrepancy may involve cracking or crazing of the PS matrix. Examination of Unannealed PZT/PS composites under a light microscope revealed crazes (or cracks) emanating radially away from each rod into the PS matrix at the electrode surface. No such cracks were observed in PZT/PMMA samples. Since applied compressive stress is known to increase the dielectric constant of PZT <sup>(10)</sup> one would expect  $\bar{\epsilon}_{33}$  of the PZT/PS composites to be less than  $\bar{\epsilon}_{33}$  of the PZT/PMMA materials if the cracks acted to relieve interfacial compressive stresses.

The presence of internal stresses in these composites is further supported by the decrease in the dielectric constant after they were annealed. If the annealing process acts to relieve some radial compression between the rods and the matrix, then the dielectric constant would be expected to be lower than the  $\bar{\epsilon}_{33}$  before annealing. Presumably, the radial stresses resulted from thermal expansion mismatches, mechanical processing (cutting and polishing), or polymerization

shrinkage.

The simple Skinner, et al. model predicts that the  $\bar{d}_{33}$  for composites with matrices of the same stiffness should be the same. Since PS and PMMA have roughly the same elastic modulus ( $\sim 3 \times 10^9 \text{ N/m}^2$ ) it is not surprising that  $\bar{d}_{33}$  is similar for both composite materials. However, the predicted  $\bar{d}_{33}$  values are three times greater than those observed. Clearly, transfer of applied stress from matrix to rods is more complex than allowed for by the simple parallel model. If the effective matrix region of influence on the rods is less than the total matrix area, then the amount of stress experienced by the rods would be less than predicted by the Skinner, et al. model (6). This would act to decrease  $\bar{d}_{33}$  relative to the predicted value.

The standard deviations of  $\bar{d}_{33}$  values obtained from a  $\bar{d}_{33}$ -meter using rounded probes gives an indication of the relative piezoelectric homogeneity of the composites. For the composites tested here the standard deviations of the  $\bar{d}_{33}$  measurements were similar. Again, considering that the matrices used in this work have similar mechanical properties, this result is not unexpected.

The hydrostatic piezoelectric coefficients ( $\bar{d}_h$ ) reported in Table 1 are smaller than those of PZT but similar to that observed by Lynn<sup>(9)</sup> for the PZT/epoxy system. The voltage coefficients are roughly an order of magnitude larger than PZT because the permittivities of the composites are much lower than the values for PZT alone. This results in  $\bar{d}_h/\bar{\epsilon}_h$  being significantly larger than that of PZT and comparable to that of PVDF. Also, no frequency dependence of  $\bar{d}_h$  was observed from 30 to 160 Hz (Figure 2). Annealing was found to improve the piezoelectric coefficients (especially  $\bar{g}_h$ ) due to a significant decrease in  $\bar{\epsilon}_{33}$ .

Composite densities are roughly  $1.4 \text{ g/cm}^3$  (calculated), which is considerably lower than the  $7.3 \text{ g/cm}^3$  of PZT. Low density materials provide better acoustic coupling to an aqueous environment than ones of high density. Therefore, these types of composites may be useful as shallow-water hydrophones or for medical ultrasound applications.

#### IV. Conclusions

Composites of uniaxially oriented, continuous PZT rods embedded in polystyrene or poly(methyl methacrylate) matrices possess hydrostatic piezoelectric coefficients somewhat lower than that of homogeneous PZT. However, hydrostatic voltage coefficients for these materials are approximately an order of magnitude larger than the ceramic element. Enhancement of  $\bar{g}_H$  is primarily due to the reduction of  $\bar{K}_{33}$  over PZT. Further enhancement of the piezoelectric response can be accomplished by annealing which further reduces  $\bar{K}_{33}$ . The  $\bar{d}_{33}$  values and the standard deviation of the  $\bar{d}_{33}$  measurements are similar for both types of composites. Predictions of the composite piezoelectric coefficients based on the Skinner, et. al. model are qualitatively correct but quantitatively overestimated.

#### Acknowledgements

The authors would like to thank the Office of Naval Research for partial support of this work through contract N00014-82-K-0339. We would also like to thank Drs. R. E. Newnham and L. E. Cross for stimulating our interest in this subject.

### References

1. R. E. Newnham, L. J. Bowen, K. A. Klicker, and L. E. Cross, *Mat. Eng.*, 2 , 93 (1980).
2. R. E. Newnham, D. P. Skinner, and L. E. Cross, *Mat. Res. Bull.*, 13 , 525 (1978).
3. K. A. Klicker, J. V. Biggers, and R. E. Newnham, *J. Am. Ceram. Soc.*, 64 , 5(1981).
4. D. P. Skinner, R. E. Newnham, and L. E. Cross, *Mat. Res. Bull.*, 13 , 599 (1978).
5. M. Haun, M.S. Thesis, The Pennsylvania State University, 1983.
6. K. A. Klicker, Ph.D. Thesis, The Pennsylvania State University, 1980.
7. J. Selsing, *J. Amer. Ceram. Soc.*, 44 , 419 (1961).
8. W. H. Haslett and F. J. McGarry, *Modern Plastics*, 40 , 135 (1962).
9. S. Y. Lynn, M.S. Thesis, The Pennsylvania State University, 1981.
10. B. Jaffe, W. R. Cook, and H. Jaffe, Piezoelectric Ceramics , London, Academic Press (1971).

### Figure Captions

Figure 1. Theoretical plot of  $\log (\overline{d_h g_h})$  as a function of volume fraction of PZT ( $v$ ). Curve I corresponds to  $^2J_{33} = 10^{-7} \text{ m}^2/\text{N}$ ; for curve II,  $^2J_{33} = 10^{-9} \text{ m}^2/\text{N}$ ; and for curve III,  $^2J_{33} = 10^{-10} \text{ m}^2/\text{N}$ . The broken line represents the  $d_h g_h$  for homogeneous PZT.

Figure 2. Piezoelectric response of PZT/PS and PZT/PMMA composites as a function of frequency.

(a) Unannealed.

(b) Annealed.

Table 1

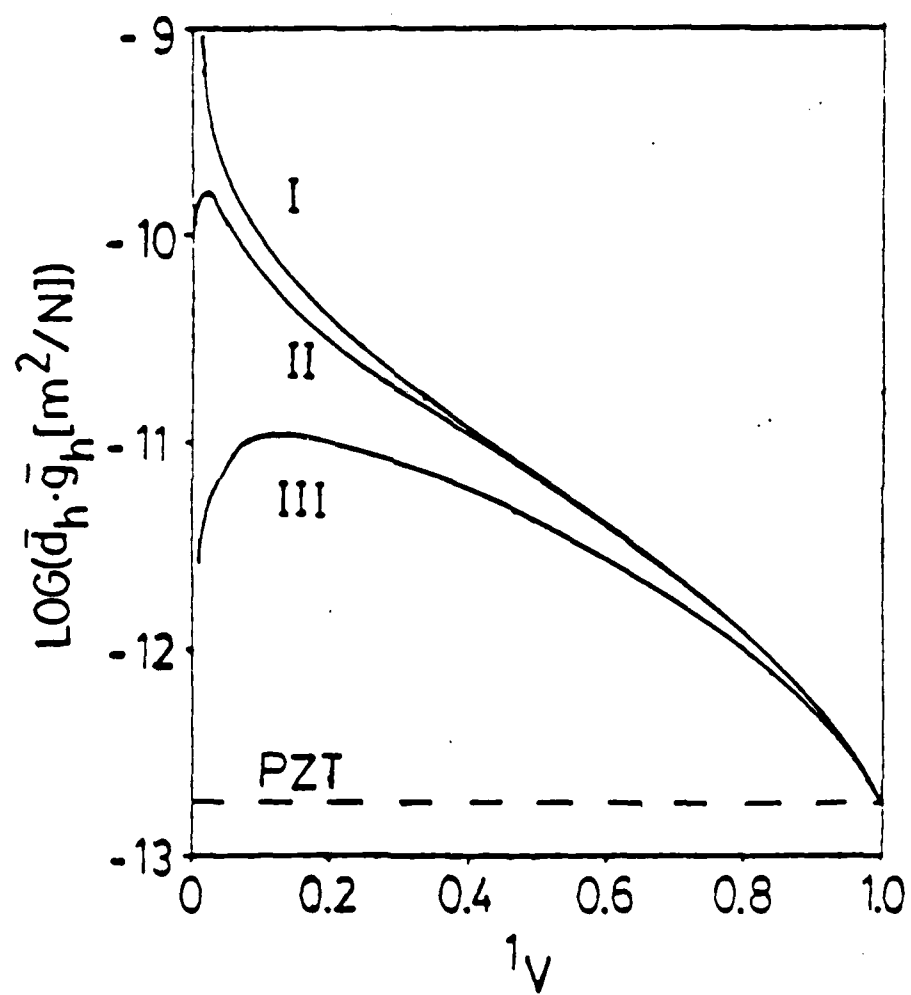
Piezoelectric Properties of 1-3 Composites and Single Phase Materials.

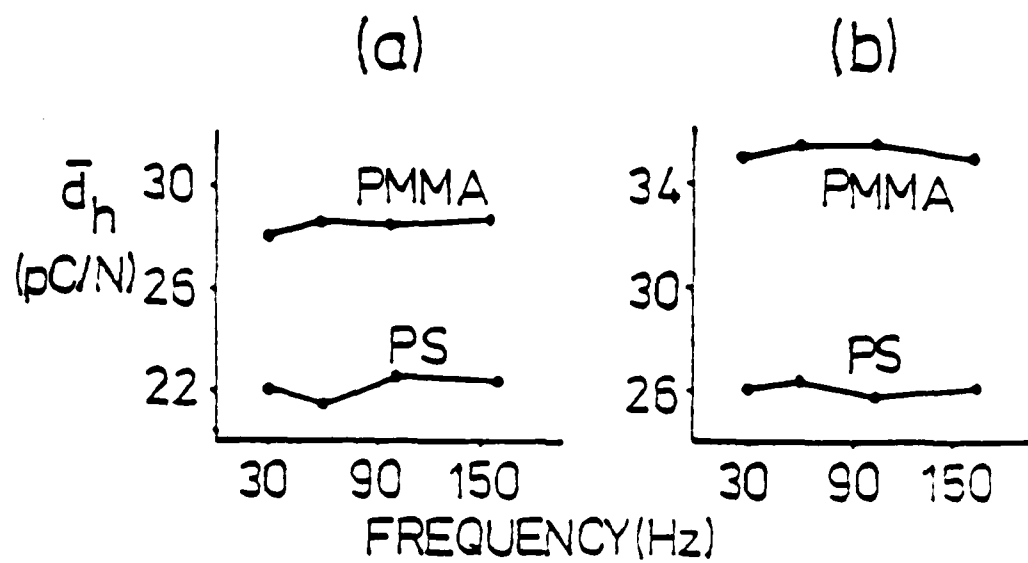
Material	Density (g/cm <sup>3</sup> )	$\bar{k}_{33}$	$\bar{d}_{33}^*$ (10 <sup>-12</sup> C/N)	$\bar{d}_h^{**}$ (10 <sup>-12</sup> C/N)	$\bar{g}_h^{**}$ (10 <sup>-3</sup> V-m/N)	$\bar{d}_h \bar{g}_h^{**}$ (10 <sup>-15</sup> m <sup>2</sup> /N)
PZT/PS	1.32	70	110 ± 16	22	36	790
PZT/PS (Annealed)	1.32	54	130 ± 18	26	54	1400
PZT/PMMA	1.46	131	110 ± 18	28	25	700
PZT/PMMA (Annealed)	1.46	100	125 ± 21	35	39	1370
PZT	7.9	1600	400	50	4	200
PVDF	1.8	12	30	11	104	1140
PZT/Epoxy (Ref. 9)	1.4	97	-	32	51	1630

\* Errors are ± one standard deviation.

\*\* Estimated errors are:  $\bar{d}_h$  ± 12%,  $\bar{g}_h$  ± 16%, and  $\bar{d}_h \bar{g}_h$  ± 20%.







**APPENDIX 9**

## RESONANT MODES OF VIBRATION IN PIEZOELECTRIC PZT-POLYMER COMPOSITES WITH TWO DIMENSIONAL PERIODICITY

T.R. GURURAJA, W.A. SCHULZE AND L.E. CROSS  
Materials Research Laboratory, The Pennsylvania State  
University, University Park, PA 16802

B.A. AULD, Y.A. SHUI AND Y. WANG  
Department of Applied Physics, Stanford University, Stanford,  
CA 94305

Abstract—High frequency resonance characteristics of piezoelectric PZT rod-polymer composites with 1-3 connectivity have been investigated. Electrical admittance plots and laser probe dilatometry of the dynamic displacement on the composite as a function of frequency are used to interpret the vibration pattern of resonant modes.

### INTRODUCTION

Piezoelectric PZT-polymer composites of different connectivity pattern have been investigated to evaluate their adaptability as ultrasonic transducers for medical applications in the low megahertz frequency range<sup>1</sup>. Among all the different composites, those with PZT-501A fibers embedded in Spurr's epoxy (Polysciences, Warrington, PA) matrix with regular periodicity (1-3 connectivity) appeared to be very promising for this application. The present paper is a brief report on the high frequency dynamic behavior of these composites in resonant configuration aimed at understanding their physics and possibly extending their usefulness in devices other than hydrophones.

Samples for the present study consisted of fired PZT-501A fibers (diameter = 0.45 mm) arranged in square lattice and impregnated in Spurr's epoxy matrix. Disc shaped composites (diameter = 1.9 cms) with 5, 10, 20, and 30 volume percent PZT were cut and ground to proper thickness and poled at 20 kV/cm.

### THEORY

Resonance modes which can be expected in a cylindrically shaped composite are: fundamental radial and thickness modes and their overtones, and possible resonant lateral modes due to the regular periodicity of the PZT fibers in the composite.

Radial mode resonance is mainly determined by the effective modulus  $C_T$  normal to the fiber axis and the average density of the composite. The effective modulus  $C_T$  was calculated by the Reuss constant stress model<sup>2</sup>. Similarly the thickness mode resonance is defined by the effective modulus  $C_L$  along the fiber axis and

the average density of the composite. The effective modulus  $C_L$  was estimated by the Voigt constant strain model<sup>2</sup>. For the effective modulus calculations, elastic stiffness of the fiber perpendicular to the length was chosen to be  $C_{11}^E = 12.1 \times 10^{10}$  N/m<sup>2</sup> and along the fiber axis Young's modulus  $E = 1/S_{33}^D = 10.5 \times 10^{10}$  N/m<sup>2</sup> was chosen. For the epoxy, the modulus was determined to be  $4.7 \times 10^{10}$  N/m<sup>2</sup>.

At wavelengths comparable to the unit cell dimensions of the array, the analysis is more complicated. A Brillouin theory of elastic wave propagation in a two dimensionally periodic lattice corresponding to composites with 1-3 connectivity has been developed<sup>3</sup>. For laterally propagating shear waves with polarization along the fibers, the lowest stop band frequencies have been calculated.

#### EXPERIMENTAL EVALUATION OF RESONANCE MODES

Absolute value of electrical admittance was measured on samples as a function of frequency in the ambients of air and water using a spectrum analyzer (HP-3585A). Here samples of different thickness and volume fraction were examined to identify the different resonances observed in the 0-2 MHz frequency range. The three major resonances of interest are designated as  $f_1$ ,  $f_{t1}$ , and  $f_{t2}$  as categorized in Table 1. To analyze the nature of vibration at these frequencies, detailed laser probe measurement of actual mechanical displacement on the composite was performed by laser heterodyne technique<sup>4</sup>. Frequency scans of the ultrasonic displacement at several points on the composite were combined with automated position scans across the diameter of the composite at frequencies  $f_1$ ,  $f_{t1}$  and  $f_{t2}$  to study the vibration pattern.

The resonance frequency  $f_1$  was inversely proportional to thickness of the sample. The vibration on PZT fiber was in phase with that of the epoxy. For samples resonating at low frequencies ( $\sim 300$  KHz), the amplitude on the rod was only a little bit smaller than that on the epoxy. The resonance was heavily damped when the

Table 1. Resonant Modes in PZT Rod-Polymer Composites.

Volume % PZT	Porosity (%)	Thickness (mm)	Resonance Frequencies in KHz			$f_1 = 1/2d$ of sec	$f_{t1} = 1/2d_{t1}$ of sec	$f_{t2} = 1/2d_{t2}$ of sec
			$f_1$	$f_{t1}$	$f_{t2}$			
1	1.76	4.00	125	488	491	1240	453	459
		4.00	162	449	—	1237	790	—
		1.20	122	487	730	1269	749	908
10	1.27	1.66	410	642	1006	1492	640	902
		1.12	162	644	—	1249	717	—
		1.24	140	594	—	1371	804	—
10	0.20	1.00	433	620	—	1287	747	—
		1.25	140	618	—	1274	749	—
		4.00	190	480	—	1261	792	—
10	0.73	1.12	170	621	—	1290	742	—
		1.06	169	1225	—	1289	821	—
		1.12	176	1188	—	1214	867	—

# RESONANT MODES OF VIBRATION IN PIEZOELECTRIC PZT-POLYMER COMPOSITES

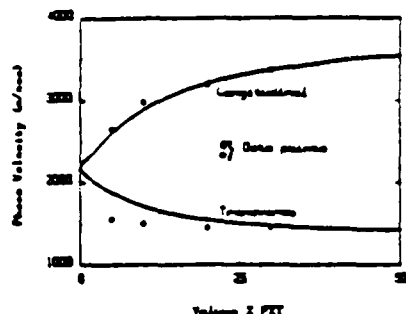


Figure 1. Phase velocities for PZT-fiber-polymer composites.

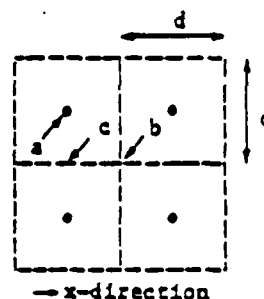


Figure 2. Unit cells in the composite.

resonator was immersed in water. Such a behavior suggests that this is the longitudinal thickness mode. Longitudinal velocities of sound along the fiber axis calculated using the resonance frequency agree very well with the theoretically estimated values for the composites of different volume fraction (Figure 1).

Resonances at  $f_{t1}$  and  $f_{t2}$  are quite similar in nature. For a certain volume fraction the resonances always occur at specified frequencies immaterial of the thickness. This observation indicates that the two resonances are due to transverse periodicity in the lattice.

The vibration pattern at  $f_{t1}$  can be explained by referring to Figure 2 which has four unit cells. At this frequency all the rods vibrate in phase. The vibration amplitude  $A$  at points  $a$ ,  $b$ , and  $c$  in Figure 2 follows the relation  $A_a \approx A_b \gg A_c$ . The phase difference between points  $a$  and  $b$  was found to be  $180^\circ$ . The observed behavior can be explained by the superposition of two standing shear wave patterns of wavelength equal to the lattice periodicity ( $d$ ) existing along both  $x$  and  $y$  axes. This resonance corresponds to one of the stop bands predicted by the theory. Velocity of transverse shear waves,  $V_s = df_{t1}$ , is tabulated in Table 1.

At frequency  $f_{t2}$ , the amplitude  $A$  at points  $a$ ,  $b$ , and  $c$  follows the relation  $A_b > A_c > A_a$ . Points  $a$  and  $b$  vibrate in phase and there is  $180^\circ$  phase difference between the vibrations at points  $b$  and  $c$ . Superposition of standing shear waves along the two diagonals explain the observed vibration pattern. This lateral shear resonance along the diagonal fits a predicted stop band. Again the transverse shear velocity is calculated by the equation  $V_s = df_{t2}/\sqrt{2}$ . The calculated shear velocity is about 25% lower than the measured velocity in epoxy by the transmission technique (1050-1100 m/sec). This is quite possibly due to the mass loading by PZT fibers.

The thickness coupling coefficient  $k_t$  and  $Q$  of the composites are given in Table 2. The data is mainly divided into two groups. Thin samples with thickness around 0.6 mm resonating around 2.25

MHz and thick samples with thickness above 2 mm with resonance frequency around 500 KHz. In thin samples, the resonance frequency is much higher than that of the strong lateral modes. Therefore, the PZT fibers can be pictured as vibrating independently resulting in  $k_p$  close to that of PZT. The low  $Q$  indicates that the PZT rods are partially damped by the surrounding polymer. For thick composites, the resonance is close to the lateral modes and the vibration of PZT fibers is laterally coupled through the epoxy as evidenced by the uniform mechanical displacement across the sample and is indicated by low  $k_p$ . The high  $Q$  for thick composites is a result of very low attenuation losses in the epoxy at around 0.5 MHz.

The radial mode coupling coefficient  $k_p$  was 22% for 5% PZT composites and increased to 27% for 30% PZT composites. The transverse longitudinal velocity  $V_T$  calculated using the resonance frequency and the diameter of the composite is compared with the theory in Figure 1. The large discrepancy between the calculated and measured velocities of transverse longitudinal wave is probably due to the finite diameter of the PZT fibers. Elastic stiffening by the PZT fibers is provided only at discrete points in the composite, and the approximations in the Reuss model are therefore not completely valid.

#### SUMMARY

PZT rod-polymer composites with 1-3 connectivity have, in addition to thickness and radial modes, complex lateral vibrational modes due to the periodicity of the lattice. The correspondence between the theory and experiment for the lateral modes is remarkably close. The thickness mode resonance in relatively thick composites follows the Voigt constant strain mode'.

#### REFERENCES

1. T.R. Gururaja, W.A. Schulze, T.R. Shrout, A. Safari, L. Webster and L.E. Cross, *Ferroelectrics* **39**, 1245 (1981).
2. S. Lees and C.L. Davidson, *IEEE Trans. on Sonics and Ultrasonics*, SU-24, 222 (1977).
3. B.A. Auld, Y.A. Shui and Y. Wang, International Conference on the Dynamics of Interfaces, France (Sept. 1983) (to be published in the *Journal de Physique*).
4. B.A. Auld and H.A. Kunkel, *Ferroelectrics*, **33**, 971, (1981).

Table 2. Thickness Mode Resonance.

Volume % PZT	Thickness t mm	$k_p$	Q
5	Thin	37.1	5.2
	Thick	27.3	31.6
10	Thin	68.2	7.0
	Thick	40.0	13.7
20	Thin	68.9	9.9
	Thick	33.1	18.1
30	Thin	—	—
	Thick	61.1	26.8

**APPENDIX 10**



## THE INCORPORATION OF RIGID COMPOSITES INTO A CONFORMAL HYDROPHONE

W. SCHULZE, G. DAYTON, D. LAUBSCHER, L. WEBSTER, E. BIBEAU,  
R. MILLER, B.J. KEARNS, S.R. BRENNEMAN, D. CROSS, M. HAUN,  
A. NARTHASILPA, B. JONES, A. SAFARI, T. SHROUT, S.-Y. LYNN,  
R. WILSON AND J. BIGGERS

Materials Research Laboratory, The Pennsylvania State  
University, University Park, PA 16802

Abstract During the past five years, numerous composite configurations have been analysed for hydrostatic transducer application. Although some of these composite configurations have been flexible, a configuration with good sensitivity and mechanical durability has not been produced. The need for a sheet or mat, large area transducer that will conform to the hull of a ship has led to the incorporation of small rigid composite elements into a macrocomposite. The goals set for the conformal transducer were sensitivity greater than -200 dB re 1 V/ $\mu$ Pa, operation to at least 7 MPa, maximum frequency of 100 Hz, conforming to a 0.10 m radius and a hydrophone section of at least 0.01 m<sup>2</sup>.

In the study three types of rigid composites are used to determine the effect of compliant hinge material and flexible electrodes on the hydrostatic sensitivity. Typical response of a 1-3 rod composite in flexible form is a sensitivity of -193 dB re 1 V/ $\mu$ Pa, with a capacitance of 1-1.5  $\mu$ F per m<sup>2</sup> and only 2 dB degradation when operating at 7 MPa.

### INTRODUCTION

During the past five years the Ferroics Group at the Materials Research Laboratory of The Pennsylvania State University has theoretically and practically explored the use of polymer ceramic composites as hydrostatic pressure sensors<sup>1</sup>. Advances in the design of these composites have made them interesting candidates to replace traditional tube and sphere based hydrophones for applications that cover large areas and require conformability. A piezoelectric composite approaches the problem of the low hydrostatic sensitivity in PZT (lead zirconate titanate) in a manner similar to that used in existing hydrophones. Both devices increase hydrostatic sensitivity by decoupling the longitudinal and transverse stresses.

Although PZT has large piezoelectric charge coefficients  $d_{33}$  and  $d_{31}$  (3 is the poling direction), the hydrostatic charge coefficient ( $d_h$ ), which is the sum of  $d_{33}-2d_{31}$  is low. This is because  $d_{33}$  is opposite in sign to  $d_{31}$  and equal to slightly more than

twice its magnitude. In a properly designed composite, it should be possible to decouple the  $d_{33}$  component from  $d_{31}$ , enhancing  $d_{31}$  while still maintaining a strong monolithic device. Work with composite hydrophones material has demonstrated the additional advantages of low density, low permittivity, the possibility of increased resistance to mechanical shock and also the possibility of fabrication in flexible form.

#### DESCRIPTION OF HYDROPHONE

Our goal was to prepare trial hydrophones that were conformable and had a moderate area of 100 cm<sup>2</sup>. Evaluation of the various one, two or three dimensionally connected PZT networks has indicated that most truly flexible materials are not physically stable with pressure cycling and have properties that continually change with flexural cycling. For this reason the flexible composite transducers were limited to solid materials that are hinged to make a flexible sheet or a composite-composite. These hydrophones were prepared from three of the most promising composite techniques: (a) a three dimensionally connected PZT-epoxy composite known as BURPS<sup>2</sup>; (b) a one dimensionally connected PZT rod assembly (1-3-0) held together by epoxy loaded with glass spheres<sup>3</sup>; (c) a shape (3-1) that is basically a PZT cube with a cylindrical hole perpendicular to the poling direction<sup>4</sup>.

Each test hydrophone was 1/16 the normal active area or 2.5x 2.5 cm and has a thickness of about 0.3 cm. The device is flexible enough to bend around a 4 cm radius. Figure 1 shows a cross-section of this design. The active-elements comprise approximately 40% of the hydrophones total area and are held together by insulating polyurethane which gives the device its flexibility. Polyurethane and other viscoelastic polymers have a poisson's ratio of 0.5 and therefore are hydrostatically stiff. This was shown to be a problem when using polyurethane as the matrix in 1-3 composites, and was also found to be a problem when used with these very large cross-section blocks. To alter the poisson's ratio, the polyurethane was filled with glass balloons, polymethyl methacrylate spheres or gas bubbles.

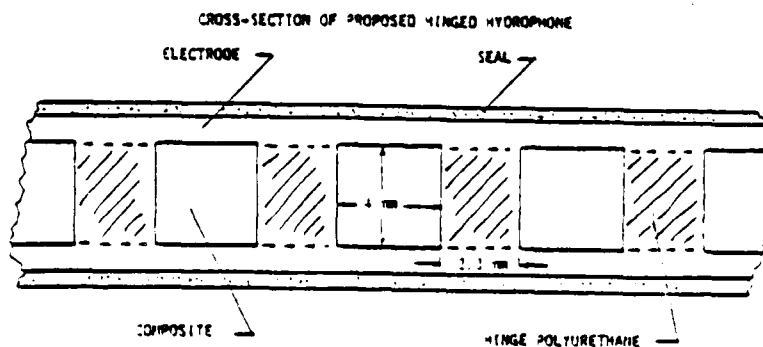


Figure 1. Cross-section of flexible transducer.

## THE INCORPORATION OF RIGID COMPOSITES INTO A CONFORMAL...

The electrode of a flexible composite must endure numerous bends and still maintain a low resistance. In-house experiments with various conductor loaded organics have led to the selection of a dual electrode system. First each rigid element (4x4 mm) of the hydrophone is electroded with highly conducting silver frit or silver epoxy to give a very low resistance across the surface. These electrodes are then tied together by a layer of carbon loaded polyurethane. The carbon loaded polyurethane bonds very well to the polyurethane connecting material and has sufficient conductivity ( $5 \times 10^{-2} \Omega\text{-cm}^{-1}$ ) to allow a frequency response to about 100 KHz depending on the capacitance of the elements involved.

The outermost layer is for the purpose of electrical insulation and chemical protection from the environment. This layer has remained the same in all the designs and is the most flexible of the polyurethane series used.

The merits of the three sensing materials were judged to be a combination of sensitivity, durability, and ease of fabrication. A fourth criterion, flexibility, is held constant in this study. The levels of the device response as given in Table 1 depends on the connectivity of the composite and on the properties of the components. The materials used in the following composites are not proposed as a maximized combination but only as the best components selected from a relatively limited number available at our facilities.

The PZT used in all composites will be type 501A produced by Ultrasonic Powders, Inc. Depending on the internal pressures generated, a different type of material may increase sensitivity or stability but this PZT should be a good compromise for the initial samples produced in this study. Even though the green processing and fired shapes are markedly different, experience has shown the properties of the PZT to remain relatively constant.

Table 1. Properties of composite materials.

Composite type	COMPOSITES					
	Materials Properties					
	$\kappa$	$\rho$ gr/cm <sup>3</sup>	$d_h$ (30 Hz) C/V $\times 10^{-12}$	$g_h$ V $\cdot$ m/V $\times 10^{-3}$	$g_h^2 d_h$ $\pi^2$ /V $\times 10^{-15}$	$d_{33}$ pC/V
3URPS	400	4.3	45	13	3400	150
1-3-0	100	1.3	55	52	3400	220
3-1 macro-composite	350	5.0	90	23	4400	190

## DISCUSSION OF SPECIFIC COMPOSITES

### 3-1 Macrocomposite

This composite is one of the more recent designs arising from the consideration for mass production (extrusion) and the realization that a totally rigid electrode area transfers the maximum force to the active element while providing a stiffening against the transverse ( $d_{31}$ ) stresses. The original paper and this study utilize parts produced by ultrasonic drilling, but this should be replaced by extruding a slug of PZT with a cylindrical hole. The tube may then be cut to desired length. A permittivity of 950 and a density of 5 make devices using this material the heaviest and the lowest in electrical impedance of the three composites proposed.

### 1-3-0

This design is the most difficult to fabricate but also is the system with the most versatility. It is this system that has been constructed as a naturally flexible material although more study is needed to develop a non-dispersive flexible polymer that is not hydrostatically incompressible. The 1-3 composite in this study is a compromise between a high  $g_h$  for maximum sensitivity (-193 dB re 1 V/ $\mu$ Pa) and an arbitrary minimum capacitance (K-100) of 1000 pf. There is also a slight frequency and pressure dependency of about 1 dB for 0 to 1000 psi and 20 to 200 Hz.

### BURPS

The BURPS technology is perhaps the simplest to fabricate. The solid material is produced by conventional powder/slug fabrication. Once the pores of the three dimensional PZT network are filled with a polymer, the material probably also becomes the most rugged of the candidates. It can then be cut and shaped with normal machining techniques. Electroding is done with conducting epoxy and the material is poled to saturation at 120°C.

The sensitivity of the BURPS composite is the lowest (-203 dB re 1 V/ $\mu$ Pa) of the three but has little pressure sensitivity even to 1000 psi. The permittivity of 400 is sufficient to give 3.5 nF capacitance per 10x10 tile.

## RESULTS AND DISCUSSION

As was found when exploring the response of 1-3 composites, the matrix (hinge) can strongly influence the response of the PCT (in this case the composite). The #30 flaxane is more compliant than the #60 flaxane and is believed to be hydrostatically stiffer (poisson's ratio near 0.5). As can be seen in Table 1, the #30 flaxane always reduced the response of the composites and in the case where the polyurethane (PV) filled the center of the 1-3, the  $g_h$  was reduced to almost that of solid PZT. It appears that the hydrostatically stiff hinge material stiffens the device and removes stress from the composite.

# THE INCORPORATION OF RIGID COMPOSITES INTO A CONFORMAL...

Table 2. Properties of trial sheet hydrophones.

HINGE MATERIAL	$\epsilon_0/\mu^2$	SENSITIVITY	CHARGE	$\gamma$	$\gamma_c$	$\frac{d_h}{d_h^2}$	EXPECTED $\gamma$
	$\mu^2/\mu^2$	dB/Pa	at 1000 psi	dB/Pa	C/R	$\mu^2/\mu^2$	dB/Pa
3-1							
#30 (PU 18 CENTRE)	538	-212	-	6	19	110	-
#30		-206	-1	13	43	560	25
#60		-201	-2	22	75	1650	
#30 FOAMED		-200	-3	25	85	2120	
#30 + 40 1/2 MB		-201	-3	23	67	540	
#30 + 55 1/2 MB		-195	-6	15	40	1200	
#30 + 35 1/2 MB		-201	-2	22	75	650	
#30 + 40 1/2 MB		-202	-4	21	71	490	
1-3-0							
#60 18 MB 1000	20	-198	-1	30	4	480	62
#60 12 MB 1000		-197	3	27	9	700	
#30 + 40 1/2 MB		-192	1	60	15	2100	

Hydrostatically soft fillers were utilized to reduce the bulk modulus of the #30 flexane to produce a flexible hinge that would not limit the hydrostatic response of the composite elements. The three types of fillers were a) gas bubbles; b) polymethyl methacrylate (PMMA) spheres and glass balloons (MB). A second difficulty became evident when using the bubbles. If the hinge is very soft, the stiff carbon fiber electrode acts as a force gathering element and the composite appears to have a response larger than normal at low pressure. This effect drops out at high hydrostatic pressure and the device has the response of a solid hinge configuration. At 1000 psi most devices have the same response at about -203 dB.

The two solid fillers were spherical particles in the order of 100  $\mu$ m diameter and gave similar sensitivity levels. The PMMA spheres were easier to mix with the PU than the microballoon MB and gave more pressure stable results. Some of the high values recorded on MB filled PU is attributed to the incorporation of small air bubbles during mixing.

The 1-3-0 elements suffer from the same clamping effect as the 3-1 composite. As expected, the 1-3-0 give a higher  $g_h$  sensitivity than the 3-1 but lower  $d_h$  because of the reduced permittivity.

The  $d_h$  and  $g_h d_h$  product of all the devices is lowered considerably from the actual value of the composite because of the increased device area needed for the hinging material. The current design uses a 2.3 mm wide hinge and has more than adequate flexibility. A reduction of the hinge width to 1 mm would increase  $d_h$  and  $g_h d_h$  by 58%.

Although it was not possible to make sensitivity measurements to 100 kHz, resonance measurements were made on the individual elements and the devices. The 1-3-0 material had a thickness resonance at 200 kHz which was almost totally damped out in device form. The 3-1 material had an unidentified resonance at 1-0 kHz, but did not exhibit significant noncapacitance impedance until about 250 kHz.

SUMMARY

- 1) Rigid composite hydrophone material can be incorporated into a conformal sheet hydrophone with sensitivity greater than -200 dB and capacitance greater than 300 nF/m<sup>2</sup>.
- 2) Reduction in flexibility by decreased hinge thickness can significantly increase sheet capacitance or  $g_{hdh}$  product.
- 3) Care must be given to the hinge material to achieve a flexible but still hydrostatically compressible material.

ACKNOWLEDGEMENT

The authors wish to acknowledge the sponsorship of the Office of Naval Research through contract N00014-82-0231.

REFERENCES

1. R.E. Newnham, L.J. Bowen, K.A. Klinker and L.E. Cross, Materials in Engineering **2**, 93-106 (1980).
2. K. Rittenmyer, T. Shrout, W.A. Schulze and R.E. Newnham, Ferroelectrics **41**, 189-195 (1982).
3. K.A. Klinker, J.V. Biggers and R.E. Newnham, J. Amer. Ceram. Soc. **64**(1), 5-9 (1981).
4. A. Safari, R.E. Newnham, L.E. Cross and W.A. Schulze, Ferroelectrics **41**, 197-205 (1982).

**APPENDIX 11**

## GRAIN ORIENTED GLASS-CERAMICS: NEW MATERIALS FOR HYDROPHONE APPLICATIONS

A. HALLIYAL, A. SAFARI, A.S. BHALLA AND R.E. NEWNHAM  
Materials Research Laboratory, The Pennsylvania State  
University, University Park, PA 16802

**Abstract** Grain oriented glass-ceramics of fresnoite ( $\text{Ba}_2\text{TiSi}_2\text{O}_8$ ) and its modifications  $\text{Sr}_2\text{TiSi}_2\text{O}_8$  and  $\text{Ba}_2\text{TiGe}_2\text{O}_8$  have been prepared by recrystallizing glasses in a temperature gradient. Piezoelectric voltage coefficients  $g_{33}$  and hydrostatic voltage coefficient  $g_H$  of these glass-ceramics are comparable to those of  $\text{PVF}_2$  and an order of magnitude higher than the corresponding values of PZT. These glass-ceramics seem to be attractive candidate materials for hydrophones and several piezoelectric devices. Hydrostatic piezoelectric properties of  $\text{Ba}_2\text{TiSi}_2\text{O}_8$  and  $\text{Ba}_2\text{TiGe}_2\text{O}_8$  single crystals are also reported.

### INTRODUCTION

It has been shown in our earlier studies<sup>1-5</sup> that the technique of recrystallizing glasses in a temperature gradient can be utilized to produce grain oriented glass-ceramics with useful pyroelectric and piezoelectric properties. From this technique, which is suitable for preparing inexpensive large area pyroelectric detectors and piezoelectric resonators, glass-ceramics with both crystallographic and polar orientation are obtained. Several glass forming systems like  $\text{Li}_2\text{O}-\text{SiO}_2$ ,  $\text{Li}_2\text{O}-\text{SiO}_2-\text{BaO}_3$ ,  $\text{BaO}-\text{SiO}_2-\text{TiO}_2$ ,  $\text{SrO}-\text{SiO}_2-\text{TiO}_2$  and  $\text{BaO}-\text{GeO}_2-\text{TiO}_2$  were examined to obtain glass-ceramics with optimum properties. The crystalline phases recrystallized from the above systems were  $\text{Li}_2\text{Si}_2\text{O}_5$ ,  $\text{Li}_2\text{B}_4\text{O}_7$ ,  $\text{Ba}_2\text{TiSi}_2\text{O}_8$ ,  $\text{Sr}_2\text{TiSi}_2\text{O}_8$  or  $\text{Ba}_2\text{Ge}_2\text{TiO}_8$ . All these crystalline phases are nonferroelectric and belong to one of the ten polar point groups. One or more crystalline phases are obtained depending on the original composition of glasses. Extensive studies have been carried out to obtain glass-ceramics with good physical properties and to optimize the pyroelectric and piezoelectric properties by varying the composition of glasses and by adding several modifying oxides to the above glass compositions. The details about the exact composition and properties can be found in references 1-5.

In the present study, the hydrostatic piezoelectric properties of glass-ceramics of fresnoite ( $\text{Ba}_2\text{TiSi}_2\text{O}_8$ ) and its modifications  $\text{Sr}_2\text{TiSi}_2\text{O}_8$  and  $\text{Ba}_2\text{Ge}_2\text{TiO}_8$  are reported. The properties of  $\text{Ba}_2\text{TiSi}_2\text{O}_8$  and  $\text{Ba}_2\text{TiGe}_2\text{O}_8$  single crystals were also measured. The hydrostatic piezoelectric coefficient  $d_H$ , hydrostatic voltage



coefficient  $g_h$  and acoustic impedances of these materials are compared with commonly used piezoelectric materials like lead zirconate titanate (PZT) and polyvinylidene fluoride  $[(CH_2F_2)_n \text{ or } PVF_2]$ . The advantages of glass-ceramics for hydrophone applications are discussed. In the last section, an explanation is given for the high value of  $g_h$  in fresnoite single crystals.

#### SAMPLE PREPARATION AND MEASUREMENTS

Glasses of different compositions were prepared by mixing reagent grade chemicals and melting in a platinum crucible. Glass-ceramic samples of approximately 1 cm diameter with oriented crystallites were prepared by recrystallizing the glasses in a temperature gradient. X-ray diffraction and microstructure studies indicated that needle-like crystals grow from the surface into the bulk of the sample along the direction of temperature gradient. Further details about sample preparation and characterization can be found in references 1-5. Single crystals of  $Ba_2TiSi_2O_8$  and  $Ba_2TiGe_2O_8$ , 1 cm in diameter were grown from melts of stoichiometric compositions by Czochralski method<sup>6,7</sup>.

For dielectric and piezoelectric measurements, sections were cut normal to the temperature gradient, then polished and coated with sputtered gold electrodes. The dimensions of the finished samples were approximately 1 cm in diameter and 0.5 mm in thickness.

The dielectric constant  $K$  and loss factors of samples were measured at a frequency of 1 KHz, using a Hewlett Packard automated capacitance bridge (Model 4270A). The piezoelectric  $d_{33}$  coefficient was measured with a  $d_{33}$ -meter (Channel Products, model CPDT 3300). The hydrostatic voltage coefficient  $g_h$  was measured by a dynamic method<sup>8</sup> which is basically a comparative technique. In this method, a PZT-5 sample of known value of  $g_h$  is used as a standard. After the sample and the standard are placed in the holder, the chamber is filled with oil and a static pressure is applied. A function generator set to the desired frequency drives an AC stress generator placed inside the test chamber. The voltage produced by the sample is displayed on an oscilloscope and compared to the voltage produced by the standard. By knowing the voltage responses and the dimensions of the sample and the standard, we can calculate the piezoelectric voltage coefficient  $g_h$  of the sample. From the measured values of  $d_{33}$ ,  $g_h$  and  $K$ , the piezoelectric voltage coefficient  $g_{33} = d_{33}/\epsilon_0 K$  and hydrostatic piezoelectric coefficient  $d_h = g_h \epsilon_0 K$  were calculated.

#### COMPOSITION OF GLASSES

The composition and crystalline phases of glass-ceramics are given in Table I along with their crystallization temperatures determined by exothermic peaks of DTA runs.

For all the systems examined in the present study, stoichiometric compositions did not give glass-ceramics with good physical and piezoelectric properties. Hence the compositions of glasses were optimized in order to obtain glass-ceramics with uniform

# GRAIN ORIENTED GLASS-CERAMICS:...

Table 1. Compositions and crystalline phases.

Composition	Crystallization Temp (°C)	Crystalline Phases
2BaO-3SiO <sub>2</sub> -TiO <sub>2</sub>	930	Ba <sub>2</sub> TiSi <sub>2</sub> O <sub>8</sub>
(1.98BaO-0.1PbO)-3SiO <sub>2</sub> -TiO <sub>2</sub>	920	Ba <sub>2</sub> TiSi <sub>2</sub> O <sub>8</sub>
2BaO-0.15CaO-2.85SiO <sub>2</sub> -TiO <sub>2</sub>	920	Ba <sub>2</sub> TiSi <sub>2</sub> O <sub>8</sub>
1.68BaO-0.4CaO-2.8SiO <sub>2</sub> -TiO <sub>2</sub>	930	Ba <sub>2</sub> TiSi <sub>2</sub> O <sub>8</sub>
1.68BaO-0.4SrO-3SiO <sub>2</sub> -TiO <sub>2</sub> -0.2CaO	930	Ba <sub>2</sub> TiSi <sub>2</sub> O <sub>8</sub>
2SrO-3SiO <sub>2</sub> -TiO <sub>2</sub>	950	Sr <sub>2</sub> TiSi <sub>2</sub> O <sub>8</sub>
(1.85SrO-0.2BaO)-2.8SiO <sub>2</sub> -TiO <sub>2</sub> -0.1CaO	940	Sr <sub>2</sub> TiSi <sub>2</sub> O <sub>8</sub>
BaO-GeO <sub>2</sub> -TiO <sub>2</sub>	800	Ba <sub>2</sub> TiGe <sub>2</sub> O <sub>8</sub>

crystallization and useful piezoelectric and pyroelectric properties. The optimized compositions for Ba<sub>2</sub>TiSi<sub>2</sub>O<sub>8</sub>, Sr<sub>2</sub>TiSi<sub>2</sub>O<sub>8</sub> and Ba<sub>2</sub>Ge<sub>2</sub>TiO<sub>8</sub> were 2BaO-3SiO<sub>2</sub>-TiO<sub>2</sub>, 2SrO-3SiO<sub>2</sub>-TiO<sub>2</sub> and BaO-GeO<sub>2</sub>-TiO<sub>2</sub> respectively. Addition of a small percentage of PbO, CaO and SrO helped in obtaining glass-ceramics with uniform crystallization and good mechanical strength. The crystallization temperature of the glasses were in the range 800-950°C. The crystalline phases of all the glass-ceramics are also listed in Table 1.

## HYDROSTATIC MEASUREMENTS

The measured values of dielectric constant, d<sub>33</sub> and g<sub>h</sub> are listed in Table 2, along with the calculated values of g<sub>33</sub>, d<sub>h</sub> and d<sub>h</sub>g<sub>h</sub>. The properties of Ba<sub>2</sub>TiSi<sub>2</sub>O<sub>8</sub> and Ba<sub>2</sub>Ge<sub>2</sub>TiO<sub>8</sub> single crystals are also listed in the table. A comparison of dielectric and hydrostatic properties of glass-ceramics with the corresponding properties of PVF<sub>2</sub> and PZT 50LA is given in Table 3. The values of g<sub>h</sub> and

Table 2. Hydrostatic measurements.

Composition	K	d <sub>33</sub> pC/N	g <sub>33</sub> (10 <sup>-3</sup> Vm/N)	g <sub>h</sub> (10 <sup>-3</sup> Vm/N)	d <sub>h</sub> pC/N	d <sub>h</sub> g <sub>h</sub> (10 <sup>-15</sup> m <sup>2</sup> /N)
2BaO-3SiO <sub>2</sub> -TiO <sub>2</sub>	9	7	88	110	8.8	970
(1.98BaO-0.1PbO)-3SiO <sub>2</sub> -TiO <sub>2</sub>	10	7	80	110	9.7	1070
2BaO-0.15CaO-2.85SiO <sub>2</sub> -TiO <sub>2</sub>	10	6	68	75	5.6	500
(1.68BaO-0.4CaO)-2.8SiO <sub>2</sub> -TiO <sub>2</sub>	10.5	6	65	85	7.9	670
(1.68BaO-0.4SrO)-3SiO <sub>2</sub> -TiO <sub>2</sub> -0.2CaO	9.8	6	70	100	9.7	970
2SrO-3SiO <sub>2</sub> -TiO <sub>2</sub>	11.5	14	138	85	9.7	740
(1.85SrO-0.2BaO)-2.8SiO <sub>2</sub> -TiO <sub>2</sub> -0.1CaO	10.6	10	107	100	9.4	940
BaO-GeO <sub>2</sub> -TiO <sub>2</sub>	15	6	45	70	9.3	550
BaTiSi <sub>2</sub> O <sub>8</sub> (Single Crystal)	11	8	82	130	12.7	1650
Ba <sub>2</sub> TiGe <sub>2</sub> O <sub>8</sub> (Single Crystal)	11.4	8	80	120	12.1	1450

Table 3. Comparison of piezoelectric properties.

Property	Glass-Ceramics	PVF <sub>2</sub>	PZT
K	10	13	1800
$d_{33}$ ( $10^{-2}$ C/N)	8-10	30	450
$d_{31}$ ( $10^{-12}$ C/N)	+1.5	-18	-205
$d_h$ ( $10^{-12}$ C/N)	3-10	10	40
$g_{33}$ ( $10^{-3}$ Vm/N)	100	250	28
$g_h$ ( $10^{-3}$ Vm/N)	100	100	2.5
$d_{h3h}$ ( $10^{-15}$ m <sup>2</sup> /N)	1000	1000	100
$Z$ ( $10^5$ rays)	18-25	2-3	30

$d_{h3h}$  of glass-ceramics are comparable to that of PVF<sub>2</sub> and much higher than the corresponding values of PZT. Even though the values of  $d_{33}$  and  $d_h$  of glass-ceramics are comparatively low, the magnitudes of  $g_{33}$  and  $g_h$  are high because of their low dielectric constant<sup>8-10</sup>. Acoustic impedance  $Z$  of glass-ceramics were calculated using the relation  $Z = \rho c$ , where  $\rho$  is the density of the material and  $c$  is the velocity of sound in the medium. Acoustic impedances of glass-ceramics are compared with those of PVF<sub>2</sub> and PZT in Table 3.

#### APPLICATION IN HYDROPHONES

A hydrophone is a passive device used as a hydrostatic pressure sensor. For hydrophone applications, the commonly used figure of merits are hydrostatic voltage coefficient  $g_h$  and  $d_{h3h}$ . For hydrophone applications, the desirable properties of a transducer material are:

1. High  $d_h$ ,  $g_h$  and  $d_{h3h}$ .
2. Low density for better acoustic matching with water.
3. High compliance and flexibility so that the transducer can withstand mechanical shock and it can be deformed to any desired profile.
4. No variation of  $g_h$  with pressure.

PZT ceramics are used extensively as piezoelectric transducer materials despite having several disadvantages. The values of  $g_h$  and  $d_{h3h}$  of PZT are low because of its high dielectric constant (~1800) and low  $d_h$ . In addition, the high density of PZT (~7900 kg/m<sup>3</sup>) makes it difficult to obtain good impedance matching with water. Moreover, for hydrophone applications, a more compliant material with better shock resistance would be desirable. To overcome the problems of PZT for use in hydrophones, a number of composites of PZT and polymer with different connectivities have been studied in recent years<sup>9</sup>. Very high values of  $g_h$  and  $d_{h3h}$  have been achieved with the composite approach.

However, among single phase materials PVF<sub>2</sub> seems to be an attractive candidate material for hydrophone applications. It has a low density (1760 kg/m<sup>3</sup>) and it is a flexible material. Although it has low  $d_{33}$  and  $d_h$ , the dielectric constant of this material is low enough that large values of piezoelectric voltage coefficients  $g_{33}$  and  $g_h$  are possible. Overall, this combination of properties seems to be very attractive and PVF<sub>2</sub> has received the attention of several

### GRAIN ORIENTED GLASS-CERAMICS:...

investigators<sup>10</sup>. However, the major problem in the use of PVF<sub>2</sub> is difficulty in poling PVF<sub>2</sub> sheets. A very high voltage is necessary to pole PVF<sub>2</sub> (about 10 to 100 MV/m) and this puts a limitation on the thickness of PVF<sub>2</sub> that can be poled.

From Table 3, it is clear that the piezoelectric coefficients  $d_{33}$  and  $d_h$  of glass-ceramics are comparable to those of PVF<sub>2</sub>, but much lower than that of PZT. However, values of  $g_{33}$  and  $g_h$  of glass-ceramics are much higher than that of PZT. Hence these glass-ceramics will be useful in passive devices like hydrostatic pressure sensors where  $g_h$  is more important. The variation of  $g_h$  with pressure was measured for glass-ceramics upto 3 MPa. There was no significant variation of  $g_h$  with pressure. In practical use, glass-ceramics may offer several advantages over PVF<sub>2</sub> and other ferroelectric materials for application in piezoelectric devices as discussed below.

Since all these glass-ceramics are nonferroelectric, there is no poling step involved, which is a major problem with PVF<sub>2</sub>. There will be no problem of depoling or ageing which are commonly encountered in most of the ferroelectric materials. Hence, these glass-ceramics can be used in devices operating at higher temperatures. Large area devices can be prepared easily by routine glass preparation techniques and hence the cost of the device can be significantly lowered compared to that of PVF<sub>2</sub>. Since acoustic impedances of these glass-ceramics ( $18-20 \times 10^6$  rayls) matches with that of aluminum, they can be used for non-destructive testing of aluminum. These glass-ceramics look attractive for use in piezoelectric devices in which glass fibers are used.

### POSITIVE $d_{31}$ IN FRESNOITE SINGLE CRYSTALS

The  $g_h$  values of Ba<sub>2</sub>TiSi<sub>2</sub>O<sub>8</sub> and Ba<sub>2</sub>TiGe<sub>2</sub>O<sub>8</sub> single crystals seem to be unusually high compared to most of the commonly used piezoelectric materials.

The hydrostatic piezoelectric coefficient  $d_h$  is given by the equation

$$d_h = d_{33} + 2d_{31} \quad (1)$$

Even though  $d_{33}$  and  $d_{31}$  coefficients of PZT are large (Table 3) its  $d_h$  value is low because of their opposite signs. Moreover, its high dielectric constant ( $\sim 1800$ ) further lowers the voltage coefficients  $g_{33}$  and  $g_h$  (Table 3). On the other hand, for fresnoite, even though  $d_{33}$  is low,  $d_h$  is slightly higher than  $d_{33}$  because of positive  $d_{31}$ . In addition, because the dielectric constant of fresnoite is very low ( $\sim 10$ ), the values of  $g_{33}$  and  $g_h$  are very high. The positive sign of  $d_{31}$  in fresnoite was confirmed by measurement with a  $d_{33}$ -meter. A model has been proposed to explain the positive sign of  $d_{31}$  in fresnoite based on its crystal structure and internal Poisson's ratio stress<sup>11</sup>.

### CONCLUSIONS

- (1) It has been shown that grain oriented glass-ceramics in the  $\text{BaO-SiO}_2\text{-TiO}_2$ ,  $\text{BaO-GeO}_2\text{-TiO}_2$  and  $\text{SrO-SiO}_2\text{-TiO}_2$  systems can be prepared by crystallizing glasses of optimized compositions in a temperature gradient.
- (2) Magnitudes of hydrostatic piezoelectric coefficient  $d_h$ , hydrostatic voltage coefficient  $g_h$  and dielectric constant of glass-ceramics are comparable to the corresponding values of  $\text{PVF}_2$ .
- (3) Acoustic impedances of these glass-ceramics are in the range  $18\text{-}20 \times 10^6$  rayls and hence good acoustic matching can be obtained with metals like aluminum and commonly used glasses.
- (4) These glass-ceramics are nonferroelectric and hence the problems associated with poling and ageing are avoided. Also, they can be used in devices operating at higher temperatures.

### REFERENCES

1. G.J. Gardopee, R.E. Newnham and A.S. Bhalla, Ferroelectrics **33**, 155 (1981).
2. A. Halliyal, A.S. Bhalla, R.E. Newnham and L.E. Cross, J. Mat. Sci. **16**, 1023 (1981).
3. A. Halliyal, A.S. Bhalla, R.E. Newnham and L.E. Cross, IEEE Ultrasonics Symposium, 315 (1981).
4. A. Halliyal, A.S. Bhalla, R.E. Newnham and L.E. Cross, J. Appl. Phys. **53**, 2871 (1982).
5. A. Halliyal, A.S. Bhalla and R.E. Newnham, Mat. Res. Bull. (submitted).
6. H. Schmid, P. Genequand, H. Tippmann, G. Pouilly and H. Guedu, J. Mat. Sci. **13**, 2257 (1978).
7. S. Haussühl, J. Cryst. Growth **40**, 200 (1977).
8. S.Y. Lynn, M.S. Thesis, The Pennsylvania State University (1981).
9. R.E. Newnham, L.J. Bowen, K.A. Klicker and L.E. Cross, Mat. Engg. **2**, 93 (1980).
10. G.M. Sessler, J. Acoust. Soc. Am. **70**, 1596 (1981).
11. A. Halliyal, A. Safari and R.E. Newnham, (to be published).

**APPENDIX 12**

Submitted April 1971

## Polar glass ceramics for sonar transducers

R.Y. Ting

Underwater Sound Reference Department, Naval Research Laboratory,  
P.O. Box 8337, Orlando, Florida 32856

A.G. Halliyal and A.S. Bhalla

Materials Research Laboratory, The Pennsylvania State University,  
University Park, Pennsylvania 16802

### Abstract

Glass ceramics are shown in this study as a new class of transduction materials for application in sonar transducers. It is found that the glass ceramics of  $\text{Ba}_2\text{TiSi}_2\text{O}_9$  have high hydrostatic voltage sensitivity, low dielectric loss and low dielectric constant. These

properties are also shown to be practically independent of pressure up to 35 MPa. The free-field voltage sensitivity of a glass-ceramic prototype hydrophone is higher than that based on a commonly used lead zirconate titanate (PZT) ceramic element.

PACS: 43.88.Fx; 43.30.Yj; 77.60.+v; 77.20.+y

## INTRODUCTION

Since the discovery of the ferroelectric barium titanate ( $\text{BaTiO}_3$ ) and lead zirconate titanate (PZT)<sup>1,2</sup>, ceramics have been rapidly replacing conventional piezoelectric crystals for hydrophone applications, and now PZT ceramics are used almost exclusively in the U.S. Navy's sonar transducers. However, PZT ceramics suffer several disadvantages: the values of their hydrostatic piezoelectric constants are relatively low, and dielectric constants very high. The density of these ceramics is also very high. Furthermore, PZT exhibits depoling or aging problems as commonly encountered in most of the ferroelectric materials.<sup>3</sup> Therefore, there has been a great deal of interest in recent years to develop new transduction materials that offer improved sensitivity and aging characteristics. Several different approaches such as PZT-polymer composites<sup>4</sup> and piezoelectric polymer<sup>5</sup> have been investigated. Recently a new family of materials (polar glass ceramics) has been studied for pyroelectric and piezoelectric applications.<sup>6-11</sup> Glass ceramics containing the crystalline phases of  $\text{Li}_2\text{SiO}_3$ ,  $\text{Li}_2\text{Si}_2\text{O}_5$ ,  $\text{Ba}_2\text{TiSi}_2\text{O}_3$ ,  $\text{Ba}_2\text{TiGe}_2\text{O}_3$ , and  $\text{Li}_2\text{B}_4\text{O}_7$  were shown to exhibit large pyroelectric responses comparable to those of respective single crystals. These materials also have low dielectric constant in the range of 10-20 and attractive piezoelectric



properties. In this report, grain-oriented  $\text{Ba}_2\text{TiSi}_2\text{O}_8$  glass ceramics (BST) are proposed as new materials for potential applications in sonar transducers.

## EXPERIMENTAL

Glass ceramic samples with oriented  $\text{Ba}_2\text{TiSi}_2\text{O}_8$  crystallites were prepared by recrystallizing the glasses of compositions in the  $\text{BaO-TiO}_2\text{-SiO}_2$  system in a temperature gradient. The detailed procedure for the preparation of glass ceramic samples was described in earlier references.<sup>6-11</sup> The oriented sections (after the recrystallization of the glasses) were cut normal to the temperature gradient and then polished to thickness  $\approx 0.04$  cm. Silver-paint electrodes were coated on both sides of the sample for testing. The piezoelectric and dielectric properties of the samples were characterized by using an acoustic reciprocity technique.<sup>12</sup> The theory of this calibration method has been well documented<sup>13</sup> and will not repeated here. The experiments were carried out in a castor-oil-filled acoustic coupler with temperature and pressure controlled to within  $\pm 0.1^\circ\text{C}$  and  $\pm 0.02$  MPa, respectively, and a sinusoidal acoustic pressure applied at 1 kHz. The glass ceramic specimen was in the form of a circular disk approximately 1.2 cm in diameter and 0.04-cm thick. A PZT-5 sample, 1.3 cm in diameter and 0.6-cm thick, was also tested as a reference. The properties of two commercially available piezoelectric polymer  $\text{PVF}_2$  samples, obtained from two different sources, were also measured for comparison. Each  $\text{PVF}_2$  sample was a 1.2 cm by 1.2 cm square piece. Their thicknesses were 0.056 cm and 0.070 cm, respectively. The experiments were performed over the temperature range of 5 to  $45^\circ\text{C}$ . A pressure cycle was carried out for each sample by increasing the static pressure in the coupler from ambient to 35 MPa at 5 MPa intervals, then followed with decreasing pressure at the same rate. During such a pressure cycle, the temperature of

the system was carefully controlled at 24.5°C.

The hydrophone characteristics of the glass ceramic sample were also evaluated in a prototype design using a standard NRL-USRD E8 high-frequency hydrophone assembly. The element was placed in the E8 mount with a rubber window attached to the face. The device was tested at the NRL-USRD Lake Facility to obtain its free-field voltage sensitivity (FFVS) as a function of frequency.

## RESULT AND DISCUSSION

Figure 1 shows the hydrostatic  $d_h$  constant of the materials tested as a function of pressure. The PZT-5 sample exhibited a  $d_h$  value of 21 pC/N at the ambient pressure, which also increased slowly with increasing pressure. The  $d_h$  values for both PVF<sub>2</sub> samples and the glass ceramic composite fall in the range of 9-10 pC/N. PVF<sub>2</sub> sample no. 1 showed a 1 dB reduction in  $d_h$  when the pressure was increased from 0.5 to 35 MPa, whereas the reduction for the PVF<sub>2</sub> sample no. 2 slightly exceeded 2 dB. The  $d_h$  of the glass ceramic material, however, was constant over the range of hydrostatic pressure of 0 to 35 MPa. During the decreasing portion of the pressure cycle, the  $d_h$  value also remained independent of pressure. This is in contrast to some ceramic-polymer composites which showed very large pressure-hysteresis effects.<sup>14</sup> The piezoelectric voltage constant  $g_h$  of the glass ceramic material, shown in Fig. 2, was also found to be independent of pressure up to 35 MPa. The  $g_h$  value of  $83 \times 10^{-3}$  V m/N is an improvement over that of PZT-5 by nearly two orders of magnitude. PVF<sub>2</sub> sample no. 1 exhibited an initial  $g_h$  value of  $112 \times 10^{-3}$  V m/N which was decreased to  $104 \times 10^{-3}$  V m/N at 35 MPa, representing a reduction of 0.6 dB. PVF<sub>2</sub> sample no. 2 gave a  $g_h$  less than that of the glass ceramic. It was also somewhat pressure sensitive; a 0.5 dB reduction was

found at 35 MPa. The  $d_h$  and  $g_h$  properties of these materials were also measured at 0.5 MPa over the temperature range between 5 and 45°C. The  $d_h$  value of the glass ceramic sample was independent of the test temperature, but  $g_h$  increased linearly with temperature by about 0.4 dB from 5°C to 45°C. The results on these samples are summarized in Table I.

The dielectric dissipation of these samples was also measured at 1 kHz. It can be seen from Table I that both the PZT and PVF<sub>2</sub> material have dissipation in the range of 0.01 to 0.02. But the glass ceramic samples have extremely low dissipation, varying from 0.00003 to 0.0006 depending on the sample composition. This would be very important if one would consider the material for active transduction applications.

The FFVS of the glass ceramic prototype <sup>hydrophone</sup> is shown in Fig. 3. A -211 dB sensitivity referenced to 1 V/ $\mu$ Pa was measured, and over the frequency range of 10 to 100 kHz, the response was reasonably flat. The PVF<sub>2</sub> elements gave a sensitivity of -202 and -207 dB, respectively. Although the FFVS of the glass ceramic is less than those of PVF<sub>2</sub>, it should be noted that this sensitivity parameter depends on both the  $g_h$  constant of the material and the thickness of the sample. The thickness of the glass ceramic sample is only 0.04 cm, as compared to 0.056 cm and 0.070 cm for the PVF<sub>2</sub> samples. Because of the high voltage required for poling, the thickness of poled PVF<sub>2</sub> that can be fabricated will be severely limited. On the other hand, thick glass ceramics can be readily prepared by routine glass fabrication techniques, and the FFVS then can be easily increased. As is, the glass ceramic sample is more sensitive than the 0.6 cm thick PZT-5, which gives a FFVS of -222 dB re 1 V/ $\mu$ Pa. Furthermore, the glass ceramics have low density (3-4 gm/cc) and thus lower mechanical impedance compared to that of PZT ceramics.

Finally, it is noted that the properties of the glass ceramics are approaching those of lithium sulphate crystals (see Table I). Lithium sulphate has been used in underwater transducers, and is still a favorite piezoelectric material for use in many of the Navy's standard transducers. However, the availability of lithium sulphate from commercial sources has declined rapidly in recent years. The glass ceramic would be a good candidate for its replacement.

#### REFERENCES

1. S. Roberts, Phys. Rev., 71, 890 (1947).
2. B. Jaffe, R.S. Roth, and S. Marzullo, J. Appl. Phys., 25, 809 (1954).
3. R.W. Timma, "Low Electrical Field Characteristics of Piezoelectric Ceramic Rings", NRL Report 7528 (1973).
4. R.E. Newnham, L.J. Bowen, K.A. Klicker, and L.E. Cross, Mater. Eng., 2, 93 (1980).
5. B. Woodward, Acustica, 38, 264 (1977).
6. G.J. Gardopce, R.E. Newnham, A.G. Halliyal, and A.S. Bhalla, Appl. Phys. Lett. 36, 817 (1980).
7. G.J. Gardopce, R.E. Newnham, A.S. Bhalla, Ferroelectrics, 33, 155 (1981).
8. A. Halliyal, A.S. Bhalla, R.E. Newnham, and L.E. Cross, J. Mater. Sci. 16, 1023 (1981).
9. A. Halliyal, A.S. Bhalla, R.E. Newnham, and L.E. Cross, Ferroelectrics, 38, 371 (1981).
10. A. Halliyal, A.S. Bhalla, R.E. Newnham, and L.E. Cross, IEEE Ultrasonics Symposium, 315 (1981).
11. A. Halliyal, A.S. Bhalla, R.E. Newnham, and L.E. Cross, J. Appl. Phys. 53, 2871 (1982).

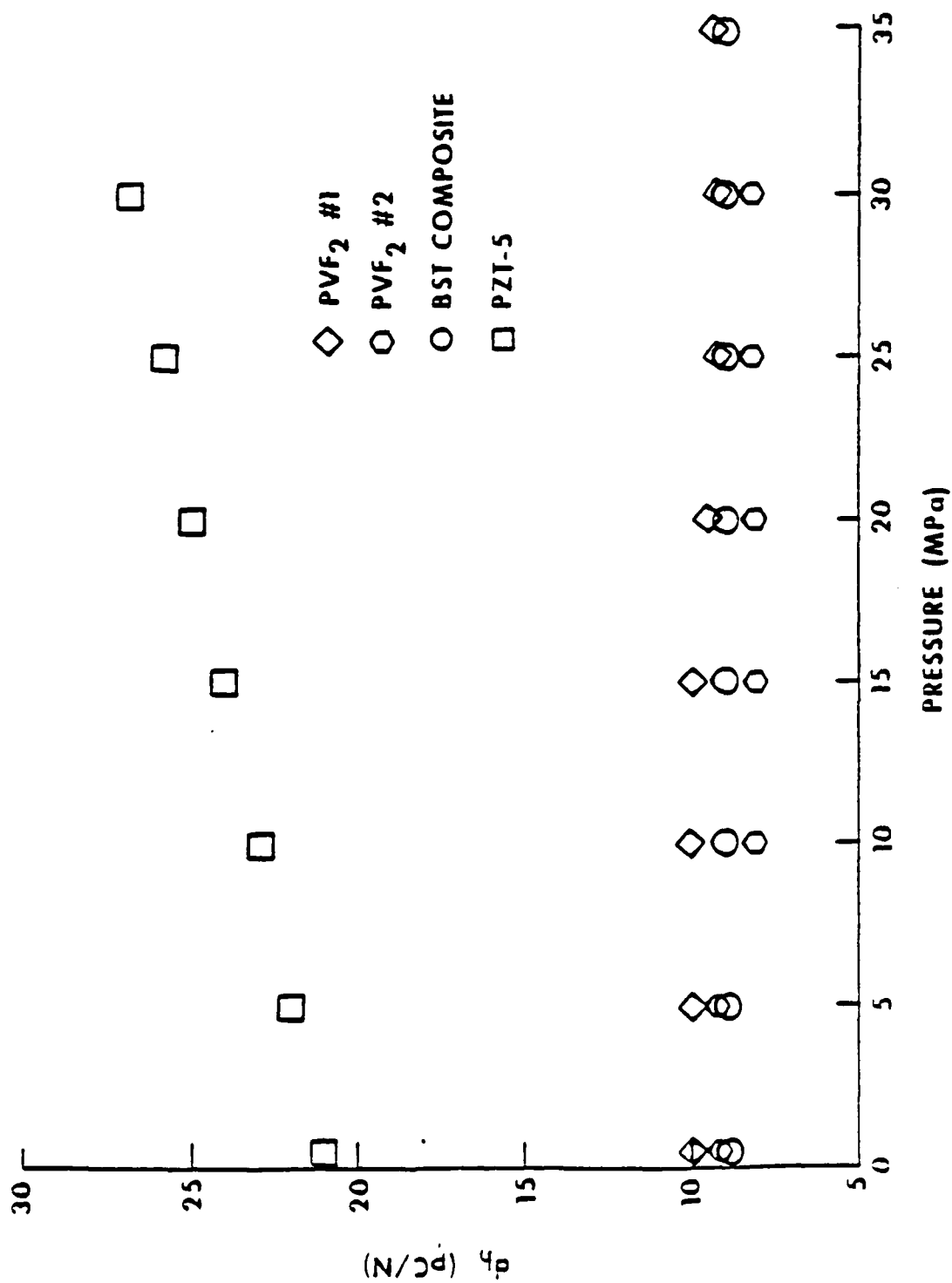
12. C.C. Sims and T.A. Henriquez, J. Acous. Soc. Am., 36, 1704 (1964).
13. R.J. Bobber, Underwater Electroacoustic Measurements (Government Printing Office, Wash, DC, 1970) pp. 27-41.
14. R.Y. Ting, Ferroelectrics, 49, 251 (1983).
15. T.A. Henriquez and L.E. Ivey, J. Acoust. Soc. Am., 47, 276 (1970).

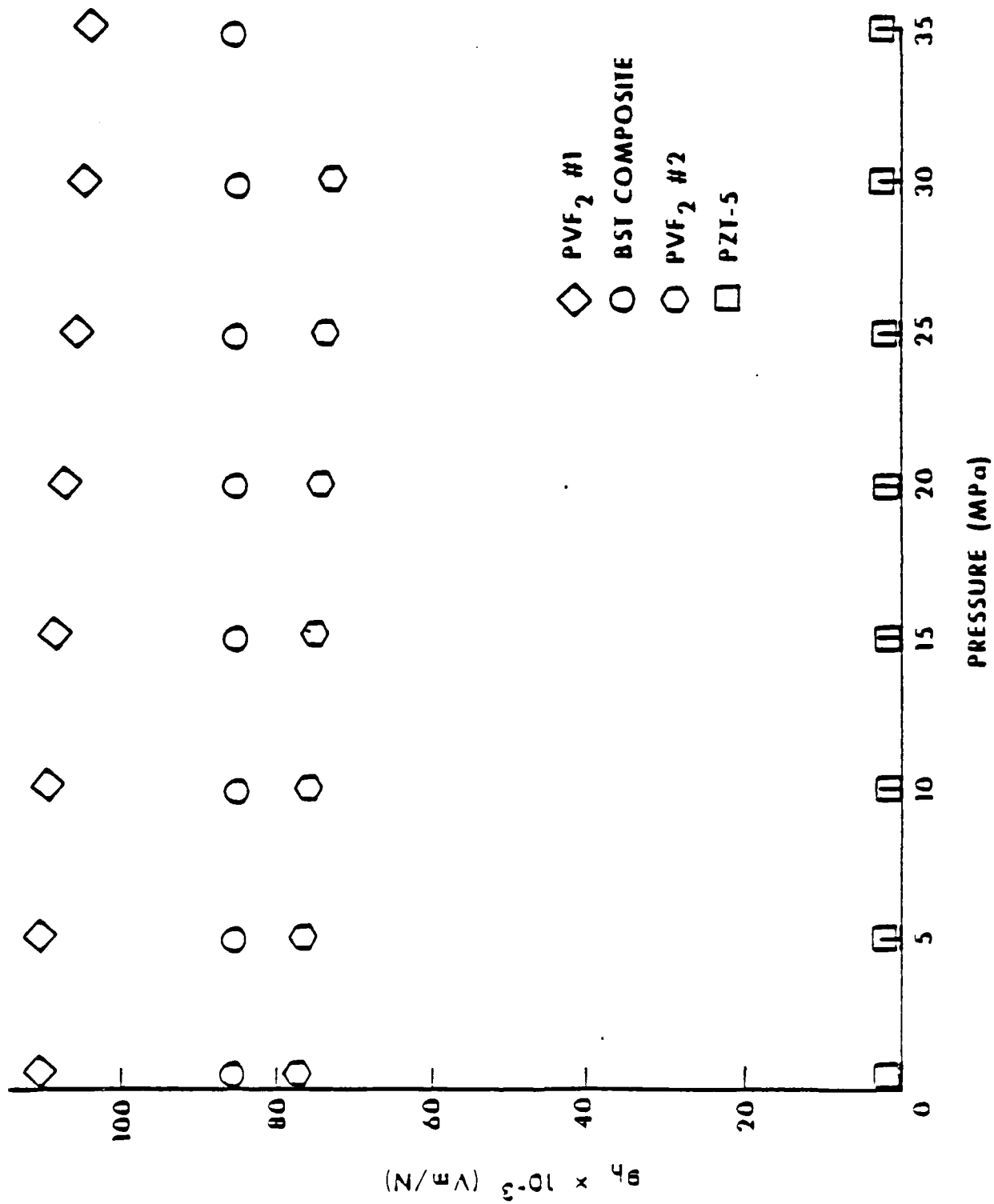
#### FIGURE CAPTIONS

Figure 1 - Hydrostatic piezoelectric strain coefficient  $d_h$  as a function of pressure (at 24.5°C).

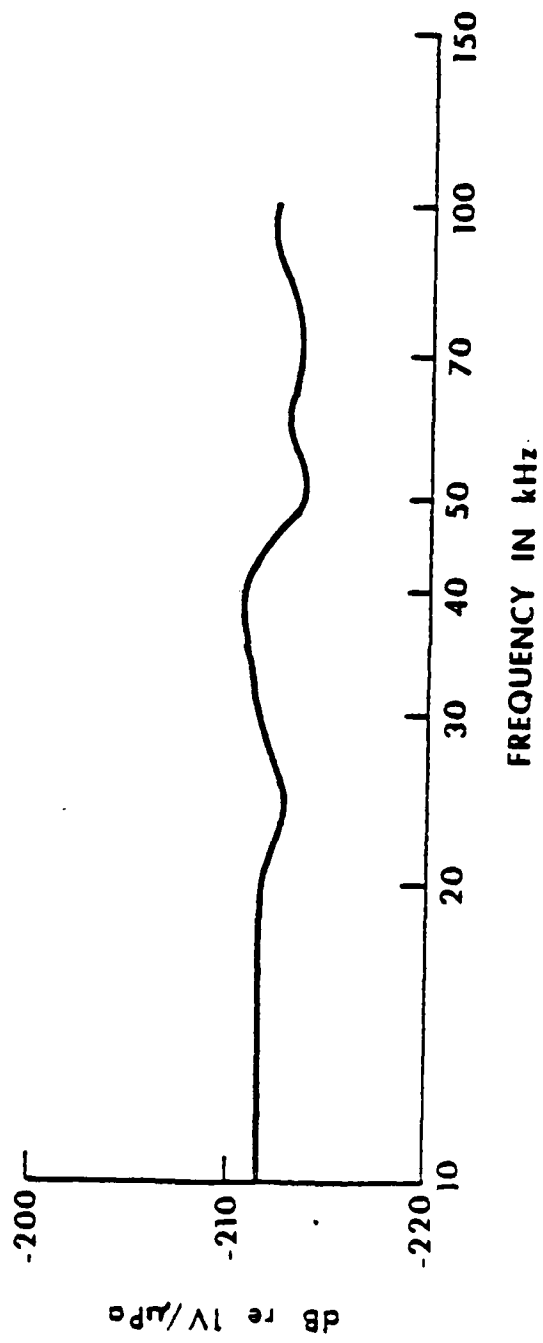
Figure 2 - Hydrostatic piezoelectric voltage coefficient  $g_h$  as a function of pressure (at 24.5°C).

Figure 3 - Free-field voltage sensitivity (FFVS) of the glass ceramic hydrophone as a function of frequency (at 24.5°C).









222R

-f .2 610 . 1.1

Table 1 - Properties\* of glass ceramic in comparison with those of PZT, PVF<sub>2</sub>, and Li<sub>2</sub>SO<sub>4</sub>.

Property	PZT-5	PVF <sub>2</sub> #1	PVF <sub>2</sub> #2	Glass Ceramic (Ba <sub>2</sub> TiSi <sub>2</sub> O <sub>8</sub> )	Li <sub>2</sub> SO <sub>4</sub> **
D ( $\times 10^{-2}$ )	1.73	1.05	1.81	0.003 - 0.06	--
$\kappa_{33}^T$	1688	10	12	12	10
$d_{31}$ (pC/N)	21	10	9	9	14
$g_{31}$ ( $\times 10^{-3}$ Vm/N)	1.5	112	78	83	148
Thickness (mm)	6	0.56	0.7	0.4	6.4
FFVS (dB re 1 V/ $\mu$ Pa)	-222	-202	-207	-211	-187

\*Measured at 1 kHz, 0.5 MPa, and 24.5°C.

\*\*Data from Reference 15.

**APPENDIX 13**

## GRAIN ORIENTED GLASS-CERAMICS FOR PIEZOELECTRIC DEVICES

A. Halliyal, A. Safari, A.S. Bhalla,\* R.E. Newnham\* and L.E. Cross\*

Materials Research Laboratory  
The Pennsylvania State University  
University Park, Pennsylvania 16802

### Abstract

Grain oriented glass-ceramics of  $\text{Li}_2\text{Si}_2\text{O}_5$ , fresnoite ( $\text{Ba}_2\text{TiSi}_2\text{O}_8$ ) and its isomorphs  $\text{Sr}_2\text{TiSi}_2\text{O}_8$  and  $\text{Ba}_2\text{TiGe}_2\text{O}_8$  have been prepared by recrystallizing glasses in a temperature gradient. Electromechanical and hydrostatic piezoelectric properties of these glass-ceramics were measured. Piezoelectric voltage coefficients  $g_{33}$  and hydrostatic voltage coefficient  $g_h$  of these glass-ceramics are comparable to those of  $\text{PVF}_2$  and an order of magnitude higher than the corresponding values of PZT. These glass-ceramics seem to be attractive candidate materials for hydrophones and several piezoelectric devices. Hydrostatic piezoelectric properties of  $\text{Ba}_2\text{TiSi}_2\text{O}_8$  and  $\text{Ba}_2\text{TiGe}_2\text{O}_8$  single crystals were also measured. The unusually high values of  $g_h$  in fresnoite single crystals and glass-ceramics are supposed to be due to positive  $d_{31}$  in these materials. A composite model has been proposed to explain the positive sign of  $d_{31}$  in fresnoite based on its crystal structure and internal poisson's ratio stress.

---

\*Member, the American Ceramic Society.

## I. Introduction

Recently a new technique for preparing glass-ceramics with oriented crystallites has been studied extensively.<sup>1-5</sup> In this technique glasses are recrystallized in a temperature gradient. It was shown in earlier studies that the technique is suitable for preparing inexpensive, large-area pyroelectric detectors and piezoelectric resonators. Using this method we have prepared glass-ceramics with both crystallographic and polar orientation.

The glass forming systems studied include  $\text{Li}_2\text{O-SiO}_2$ ,  $\text{Li}_2\text{O-SiO}_2\text{-B}_2\text{O}_3$ ,  $\text{BaO-SiO}_2\text{-TiO}_2$ ,  $\text{SrO-SiO}_2\text{-TiO}_2$  and  $\text{BaO-GeO}_2\text{-TiO}_2$ . Among the crystalline phases recrystallized from the glasses within these systems are  $\text{Li}_2\text{Si}_2\text{O}_5$ ,  $\text{Li}_2\text{B}_4\text{O}_7$ ,  $\text{Ba}_2\text{TiSi}_2\text{O}_8$ ,  $\text{Sr}_2\text{TiSi}_2\text{O}_8$  and  $\text{Ba}_2\text{TiGe}_2\text{O}_8$ . One or more of these crystalline phases are obtained depending on the composition of the glasses. All these crystalline phases are nonferroelectric and belong to one of the ten polar point groups. The compositions of the glasses were optimized by compositional variations and by the addition of various modifying oxides to obtain glass-ceramics with good physical properties. Extensive studies have been carried out to optimize the piezoelectric and pyroelectric properties of the glass-ceramics by adjusting the composition of the glasses and the crystallization conditions.<sup>1-5</sup>

It has also been shown that the polar growth behavior of the crystallites from the glass matrix depends on the original composition of the glass. A glass-ceramic is essentially a composite of a glassy phase and one or more crystalline phases. For glass-ceramics containing two crystalline phases, a connectivity model has been developed based on the principles of series and parallel connectivity models<sup>6,7</sup> to predict the piezoelectric and pyroelectric properties of glass-ceramic composites.

In the present study the hydrostatic piezoelectric properties of glass-ceramics of fresnoite ( $\text{Ba}_2\text{TiSi}_2\text{O}_8$ ) and its isomorphs  $\text{Sr}_2\text{TiSi}_2\text{O}_8$  and  $\text{Ba}_2\text{TiGe}_2\text{O}_8$  are reported. These glass-ceramics offer several advantages for hydrophone applications as will be discussed in a later section. The hydrostatic piezoelectric properties of  $\text{Ba}_2\text{TiSi}_2\text{O}_8$  and  $\text{Ba}_2\text{TiGe}_2\text{O}_8$  single crystals were also measured. The hydrostatic piezoelectric coefficient  $d_h$ , hydrostatic voltage coefficient  $g_h$ , and acoustic impedances of these materials are compared with commonly used piezoelectric materials like lead zirconate titanate (PZT) and polyvinylidene fluoride  $[(\text{CH}_2\text{F}_2)_n = \text{PVF}_2]$ . The advantages of these materials for application in piezoelectric devices are discussed. Finally, a simplified model based on the principles of series and parallel mixing of phases<sup>6</sup> is proposed to explain the high value of  $g_h$  in fresnoite single crystals and glass-ceramics.

## II. Experimental

Glasses of several different compositions were prepared by mixing reagent grade chemicals and melting in a platinum crucible. Glass-ceramic samples (approximately 1 cm diameter) with oriented crystallites were prepared by recrystallizing the glasses in a temperature gradient. The details of the sample preparation technique can be found in references 1-5. X-ray diffraction and microstructure studies indicated that needle-like crystals grow from the surface into the bulk of the sample along the direction of temperature gradient.

For piezoelectric and hydrostatic measurements, sections were cut normal to the temperature gradient, then polished and coated with sputtered gold electrodes. The dimensions of the finished samples were approximately 1 cm in diameter and 0.5 mm in thickness.

The dielectric constant ( $K$ ) and loss factors of the samples were measured

at a frequency of 1 kHz using an automated capacitance bridge.\* The piezoelectric  $d_{33}$  coefficient was measured with a  $d_{33}$ -meter.† The hydrostatic voltage coefficient  $g_h$  was measured by a dynamic method<sup>3</sup> which is basically a comparative technique. In this method, a PZT-5 sample of known  $g_h$  is used as a standard. After the sample and the standard are placed in the holder, the chamber is filled with oil and a static pressure is applied. A function generator set to the desired frequency drives an AC stress generator placed inside the test chamber. The voltage produced by the sample is displayed on an oscilloscope and compared to the voltage produced by the standard. By knowing the voltage responses and the dimensions of the sample and the standard, we can calculate the piezoelectric voltage coefficient  $g_h$  of the sample. Corrections were made for the stray capacitance of the sample holder. From the measured values of  $d_{33}$ ,  $g_h$  and  $K$ , the piezoelectric voltage coefficient  $g_{33} = d_{33}/\epsilon_0 K$  and hydrostatic piezoelectric coefficient  $d_h = g_h \epsilon_0 K$  were calculated. The electromechanical properties were measured by resonance-antiresonance technique using a spectrum analyzer.\*\*

Single crystals 1 cm in diameter of  $\text{Ba}_2\text{TiSi}_2\text{O}_8$  and  $\text{Ba}_2\text{TiGe}_2\text{O}_8$  were grown from the stoichiometric melts by the Czochralski method. Details concerning the growth procedure can be found in references 9-11.

### III. Results and Discussion

#### 3.1 Compositions and Crystalline Phases

The compositions and crystalline phases of the glass-ceramics are listed in Table I along with their crystallization temperatures determined

\*Hewlett Packard, Inc., Palo Alto Calif. (Model 4270A).

†Channel Products, Chesterland, Ohio (Model CPDT 3300).

\*\*Hewlett-Packard, Loveland, Columbia (Model 3585A).

from exothermic peaks in DTA runs.

It was not possible to obtain glass-ceramics with reasonable mechanical strength from a stoichiometric fresnoite glass composition ( $2\text{BaO}-2\text{SiO}_2-\text{TiO}_2$ ). The glass composition giving glass-ceramics with good physical properties and optimized piezoelectric and pyroelectric properties was  $2\text{BaO}-3\text{SiO}_2-\text{TiO}_2$ . Additions of a small percentage of  $\text{PbO}$ ,  $\text{CaO}$  and  $\text{SrO}$  helped in obtaining glass-ceramics with uniform crystallization and good mechanical strength. Similarly, the optimized glass compositions for  $\text{Sr}_2\text{TiSi}_2\text{O}_8$  and  $\text{Ba}_2\text{TiGe}_2\text{O}_8$  phases were  $2\text{SrO}-3\text{SiO}_2-\text{TiO}_2$  and  $\text{BaO}-\text{GeO}_2-\text{TiO}_2$  respectively. The optimized composition in the  $\text{Li}_2\text{O}-\text{SiO}_2-\text{B}_2\text{O}_3$  system was  $\text{Li}_2\text{O}-1.8\text{SiO}_2-0.2\text{B}_2\text{O}_3$ . Crystallization temperatures of the glasses ranged from  $600-950^\circ\text{C}$ . The crystalline phases of all the glass compositions are also listed in Table I.

### 3.2 Electromechanical Properties

A summary of electromechanical properties of optimized glass-ceramics is given in Table II. Values of temperature coefficient of resonance (TCR), measured by studying the variation of resonance frequency with temperature for radial mode are also listed in the table. The possibility of tailoring the electromechanical properties by varying the composition and heat treatment make these glass-ceramics attractive candidate materials for piezoelectric devices. Temperature variation of resonance frequencies can be further reduced by suitably modifying the composition of the glasses.<sup>5</sup>

### 3.3 Hydrostatic Measurements

The measured values of dielectric constant,  $d_{33}$  and  $g_h$  are listed in Table III, along with the calculated values of  $g_{33}$ ,  $d_h$  and  $d_h g_h$ . The properties of  $\text{Ba}_2\text{TiSi}_2\text{O}_8$  and  $\text{Ba}_2\text{TiGe}_2\text{O}_8$  single crystals are also presented in the table. A comparison of the dielectric and hydrostatic properties of glass-ceramics with the corresponding properties of  $\text{PVF}_2$  and PZT 50LA is given in Table IV.



The values of  $g_h$  and  $d_h g_h$  of glass-ceramics are comparable to  $PVF_2$  and much higher than PZT. Although the values of  $d_{33}$  and  $d_h$  of glass-ceramics are comparatively low, the magnitudes of  $g_{33}$  and  $g_h$  of glass-ceramics are high because of their low dielectric constant (8-10). A discussion of the advantages of these glass-ceramics in hydrophone applications will be given in section 3.5.

### 3.4 Acoustic Impedance

Acoustic impedance  $Z$  can be calculated from the relation  $Z = \rho c$ , where  $\rho$  is the density of the material and  $c$  is the velocity of sound in the medium. By measuring the thickness mode frequency constant  $N_c$  of the material, the velocity  $c$  can be calculated by the relation  $c = 2N_c$ . The values of density, velocity and acoustic impedance are listed in Table V. The corresponding properties of PZT,  $PVF_2$  and a number of commonly used materials are also listed in the table for comparison. A discussion of these properties is presented in the next section.

### 3.5 Application in Hydrophones

A hydrophone is a passive device used as a hydrostatic pressure sensor. For hydrophone applications, the commonly used figure of merits are the hydrostatic piezoelectric coefficient  $g_h$  and  $d_h g_h$ . For hydrophone applications, the desirable properties of a transducer material are

1. High  $d_h$  and  $g_h$ .
2. A density suited for acoustic matching with the pressure transmitting medium, usually water.
3. High compliance and flexibility such that the transducer can withstand mechanical shock, and can conform to any surface.

#### 4. No variation of $g_h$ with pressure.

PZT ceramics are used extensively as piezoelectric transducers despite having several disadvantages. The values of  $g_h$  and  $d_h g_h$  of PZT are low because of its high dielectric constant ( $\sim 1800$ ). In addition the high density of PZT ( $\sim 7900 \text{ kg/m}^3$ ) makes it difficult to obtain good impedance matching with water. PZT is also a brittle ceramic and for hydrophone applications, a more compliant material with better shock resistance would be desirable.

PVF<sub>2</sub> offers several advantages over PZT ceramic for hydrophone applications. It has a low density ( $1760 \text{ kg/m}^3$ ) and is a flexible material and although it has low  $d_{33}$  and  $d_h$ , the dielectric constant of this material is low enough that large values of piezoelectric voltage coefficients  $g_{33}$  and  $g_h$  are possible. Overall, this combination of properties seems to be very attractive and PVF<sub>2</sub> transducers are under intensive development.<sup>12</sup> However, a major problem in the use of PVF<sub>2</sub> is the difficulty in poling PVF<sub>2</sub> sheets. A very high voltage is necessary to pole PVF<sub>2</sub> (about 10 to 100 MV/m) and this puts a limitation on the thickness of PVF<sub>2</sub> that can be poled.

To overcome these problems, a number of composites of PZT and polymer have been studied in recent years. A detailed description of different kinds of composites and the principles involved can be found in reference 13. In a composite the polymer phase lowers density and dielectric constant and increases elastic compliance. Very high values of  $g_h$  and  $d_h g_h$  have been achieved with the composite approach.

From Table IV, it is clear that the piezoelectric coefficients  $d_{33}$  and  $d_h$  of glass-ceramics are comparable to PVF<sub>2</sub>, but much lower than that of PZT. However, because of low dielectric constant of glass-ceramics the values of  $g_{33}$  and  $g_h$  of glass-ceramics are much higher than that of PZT. Hence, these glass-ceramics will be useful in passive devices like hydrostatic pressure sensors where  $g_h$  is more important. The variation of  $g_h$  with pressure was

measured for glass-ceramics up to 3 Mpa. There was no significant variation of  $g_h$  with pressure. In practical use glass-ceramics may offer several advantages over  $\text{PVF}_2$  and other ferroelectric materials for application in piezoelectric devices.

Since all these glass-ceramics are nonferroelectric, there is no poling step involved, which is a major problem with  $\text{PVF}_2$ . There will be no problem of depoling or aging which are encountered in many ferroelectric materials. Hence, the glass-ceramics can be used in devices operating at high temperatures. Large area devices can be prepared by routine glass preparation techniques, and hence the cost of the device can be significantly lowered. Since acoustic impedances of the glass-ceramics are in the range  $18-20 \times 10^6$  rayls, good acoustic matching can be obtained with metals like aluminum. Non-destructive testing of aircraft metals over a wide temperature range is a possibility. These glass-ceramics also look attractive for use in devices in which glass fibers are used because of the good impedance matching.

#### IV. Explanation for the High Value of $g_h$ in $\text{Ba}_2\text{TiSi}_2\text{O}_8$

The  $g_h$  values of  $\text{Ba}_2\text{TiSi}_2\text{O}_8$  and  $\text{Ba}_2\text{TiGe}_2\text{O}_8$  single crystals and glass-ceramics are unusually large compared to other piezoelectric materials.

An explanation is offered here for the high value of  $g_h$  based on the crystal structure of fresnoite and an internal Poisson ratio stress.

The hydrostatic piezoelectric coefficient  $d_h$  is given by the equation

$$d_h = d_{33} + 2d_{31} \quad (1)$$

For PZT, the piezoelectric  $d_{33}$  coefficient is large ( $\sim 450$  pC/N), but  $d_h$  is low because the sign of  $d_{33}$  is positive and that of  $d_{31}$  is negative ( $\sim -205$  pC/N). Moreover, its high dielectric constant ( $\sim 1300$ ) further reduces the voltage coefficients  $g_{33}$  and  $g_h$  (Table III). On the other hand for fresnoite, even though  $d_{33}$  is low,  $d_h$  is slightly larger than  $d_{33}$  because of positive  $d_{31}$ .

In addition, because the dielectric constant of fresnoite is very low ( $\sim 10$ ), the value of  $g_h$  becomes exceptionally high. An explanation of the positive sign of  $d_{31}$  is given in section 4.2 by considering the crystal structure of  $\text{Ba}_2\text{TiSi}_2\text{O}_8$ .

#### 4.1 Composite Model

For a composite consisting of two phases, one dimensional solutions for dielectric and piezoelectric properties have been presented for both series and parallel connectivity.<sup>6,7</sup> In a number of composites it has been shown both theoretically and experimentally that the hydrostatic piezoelectric coefficients  $d_h$  and  $g_h$  can be increased by an order of magnitude over that of single phase PZT. Eventhough PZT-polymer composites are superior to single phase piezoelectric materials, some of the composites were not as sensitive as expected theoretically. The reason for this is an internal stress arising from Poisson's ratio. As an example, consider, the internal stress in composites prepared from PZT fibers and a stiff polymer.

In a 1-3 PZT-polymer composite (Fig. 1), the PZT fibers are aligned along the polar axis  $x_3$ , and the polymer matrix phase is self connected in all the 3 directions. Further, the PZT and polymer phases are connected in series along  $x_1$  and  $x_2$  and in parallel along  $x_3$ . Since the two phases are in series along  $x_1$  and  $x_2$ , they experience the same stress  $\sigma_1$ . This assumes that the two phases do not exert forces on one another and hence internal stresses are zero. This assumption is not justified for composites with small volume fraction of PZT, where interphase stress must be considered. Thus there are two contributions to  $d_{31}$  of composite: those arising from external stress  $\sigma_1$  and those arising from internal stress. In the equations which follow the piezoelectric coefficient  $d_{31}$ , volume fraction  $V$ , elastic compliances  $s_{11}$  and  $s_{33}$  and Poisson's ratio  $\nu$  of PZT and polymer are designated with a superscript 1 and 2, respectively.

Considering only the external stress  $\sigma_1$ , the polarization  $P_3$  appearing in the polar direction is given by the following equation

$$P_3 = d_{31}\sigma_1 = \frac{1}{V}d_{31}^1\sigma_1 \quad (2)$$

However, if internal stress is considered, a correction factor should be applied. This correction arises from Poisson's ratio and will be referred to as the Poisson's ratio stress.

When the composite is stretched along  $x_1$ , it contracts along  $x_3$  because of Poisson's ratio. This contraction is controlled by the compliance and Poisson's ratio. If the two constituent phases do not contract equally, an internal stress is generated. The magnitude of the internal stress can be estimated by assuming that the two phases remain mated together, or that the strains are equal along  $x_3$  ( $^1\epsilon_3 = ^2\epsilon_3$ ). For simplicity it is assumed that both the phases are elastically isotropic ( $s_{11} = s_{33}$ ). Under these assumptions, it can be shown that the internal stress on PZT phase ( $^1\sigma_3'$ ) is given by

$$^1\sigma_3' = \sigma_1 \frac{^1s_{11} - ^2s_{11}}{^1s_{11} + (^1V/2V)^2 s_{11}} \quad (3)$$

Since the polymer phase is generally far more compliant than PZT,  $^2s_{11} \gg ^1s_{11}$ , while the Poisson's ratios are comparable. Equation (3) then reduces to

$$^1\sigma_3' = \frac{-2V^2 s_{11} \sigma_1}{^1s_{11} + (^1V/2V)^2 s_{11}} \quad (4)$$

The minus sign indicates that the internal Poisson's ratio stress acts oppositely to the applied stress. That is when a tensile stress  $\sigma_1$  is applied, the internal stress  $^1\sigma_3'$  acting on PZT is compressive and vice versa. The internal stress  $^1\sigma_3'$  produces a piezoelectric effect by coupling through coefficient  $d_{33}$ . If both the external stress  $\sigma_1$  and the internal stress  $^1\sigma_3'$  are acting, the polarization along  $x_3$  is given by

$$P_3 = {}^1V^1d_{31}{}^1\sigma_1 + {}^1V^1d_{33}{}^1\sigma_3' \quad (5)$$

The first term on the right is the normal stress contribution while the second term is due to Poisson's ratio stress. Coefficient  $d_{31}$  of the composite is given by

$$\bar{d}_{31} = \frac{P_3}{\sigma_1} = \frac{{}^1V^1d_{31}{}^1\sigma_1 + {}^1V^1d_{33}{}^1\sigma_3'}{\sigma_1} \quad (6)$$

It is clear from the above equation that  $\bar{d}_{31}$  is greatly increased due to the internal Poisson's ratio stress. Because of this there will be a reduction in the magnitude of  $d_h$  (eq. (1)), lessening hydrostatic piezoelectric sensitivity of the composite.

#### 4.2 Positive $d_{31}$ in Fresnoite

The arguments concerning internal Poisson's ratio stress can be used to explain the positive sign of  $d_{31}$  in  $Ba_2TiSi_2O_8$  single crystals, based on a knowledge of its crystal structure.

The  $Ba_2TiSi_2O_8$  structure consists of  $(Si_2O_7)^{6-}$  tetrahedral pairs and  $(TiO_5)^{6-}$  square pyramids which are linked to give flat sheets parallel to  $\{001\}$  planes. These sheets are bonded together by  $Ba^{2+}$  ions. The structure can be visualized as made up of chains of deformed  $TiO_6$  octahedra linked together by a stiff silicate matrix as shown in Fig. 2. In the following discussion, the structure will be considered as a composite of two phases: piezoelectric phase consisting of  $TiO_6$  chains (phase 1) and a stiff silicate matrix which is non piezoelectric (phase 2) as shown in Fig. 3. All the properties with a superscript 1 and 2 refer to phases 1 and 2 respectively. Again for simplicity, elastic isotropy ( $s_{33} = s_{11}$ ) is assumed and Poisson's ratios of phases 1 and 2 are assumed to be comparable. Further, it is assumed that the piezoelectric phase 1 is much more compliant than phase 2, so that

$$l_{s33} = l_{s11} \gg 2s_{33} = 2s_{11} \quad (7)$$

$$\text{and } l_v = 2v. \quad (8)$$

Under these assumptions, the internal stress due to Poisson's ratio, given by equation (3) reduces to

$$l_{\sigma_3}' = l_v \sigma_1 \quad (9)$$

The polarization along  $x_3$ , due to both external and internal stresses is given by

$$\begin{aligned} p_3 &= l_v l_{d31} l_{\sigma_1}' + l_v l_{d33} l_{\sigma_3}' \\ &= l_v (l_{d31} + l_v l_{d33}) \sigma_1 \end{aligned} \quad (10)$$

Hence  $d_{31}$  of composite is given by

$$\bar{d}_{31} = l_{d31} + l_v l_{d33} \quad (11)$$

It is clear that  $\bar{d}_{31}$  of composite can be positive if  $l_v l_{d33} > l_{d31}$ . If the above argument is true, the sign of  $d_{31}$  in fresnoite should be positive, but its magnitude should be very small. The positive sign of  $d_{31}$  in fresnoite was confirmed by measurements with a  $d_{33}$ -meter and the magnitude of  $d_{31}$  was determined as 1.5 pC/N by standard resonance techniques. For most of the commonly used ferroelectric materials the value of  $d_{33}/d_{31}$  is approximately -3 whereas, for fresnoite it is approximately +5. From this discussion it is clear that the positive sign of  $d_{31}$  can be attributed to an internal Poisson's ratio stress acting in the same direction as external stress. This is the origin of the sizable hydrostatic sensitivity of  $\text{Ba}_2\text{TiSi}_2\text{O}_3$  and  $\text{Ba}_2\text{TiGa}_2\text{O}_3$  as well.

## V. Conclusions

- (1) It has been shown that grain oriented glass-ceramics in the  $\text{BaO-SiO}_2\text{-TiO}_2$ ,  $\text{BaO-GaO}_2\text{-TiO}_2$  and  $\text{SrO-SiO}_2\text{-TiO}_2$  systems can be prepared by crystallizing glasses of optimized compositions in a temperature gradient.
- (2) Magnitudes of hydrostatic piezoelectric coefficient  $d_h$ , piezoelectric voltage coefficient  $g_h$  and dielectric constant of glass-ceramics are comparable to the corresponding values of  $\text{PVF}_2$ .
- (3) Acoustic impedances of these glass-ceramics are in the range  $18\text{-}20 \times 10^5$  rayls and hence good acoustic matching can be obtained with metals such as aluminum and commonly used glasses.
- (4) An explanation is given for the high value of  $g_h$  in fresnoite and its isomorphs, based on the principles of series and parallel mixing of phases and crystal structure of fresnoite. The reason for the high value of  $g_h$  in fresnoite is the positive sign of  $d_{31}$  caused by an internal Poisson's ratio stress.



- (1) G.J. Gardopoe, R.E. Newnham, A.S. Bhalla, "Pyroelectric  $\text{Li}_2\text{Si}_2\text{O}_5$  Glass-Ceramics," *Ferroelectrics*, 33, 155 (1981).
- (2) A. Halliyal, A.S. Bhalla, R.E. Newnham and L.E. Cross, " $\text{Ba}_2\text{TiGe}_2\text{O}_8$  and  $\text{Ba}_2\text{TiSi}_2\text{O}_8$  Pyroelectric Glass-Ceramics," *J. Mater. Sci.* 16, 1023 (1981).
- (3) A. Halliyal, A.S. Bhalla, R.E. Newnham and L.E. Cross "Polar Glass-Ceramics," *Ferroelectrics*, 38, 781 (1981).
- (4) A. Halliyal, A.S. Bhalla, R.E. Newnham and L.E. Cross, "Piezoelectric and Elastic Properties of Barium Germanium Titanate and Lithium Borosilicate Glass-Ceramics," *Ultrasonics Symposium*, 315 (1981).
- (5) A. Halliyal, A.S. Bhalla and R.E. Newnham, "Polar Glass-Ceramics - A New Family of Electroceramic Materials: Tailoring the Piezoelectric and Pyroelectric Properties," *Mat. Res. Bull.* (accepted).
- (6) R.E. Newnham, D.P. Skinner and L.E. Cross, "Connectivity and Piezoelectric-Pyroelectric Composites," *Mat. Res. Bull.* 13, 525 (1978).
- (7) D.P. Skinner, R.E. Newnham and L.E. Cross, "Flexible Composite Transducers," *Mat. Res. Bull.* 13, 599 (1978).
- (8) S.Y. Lynn "Polymer-Piezoelectric Ceramic Composites with 3-1-0 Connectivity for Hydrophone Applications," M.S. Thesis, Pennsylvania State University (1981).
- (9) H. Schmid, P. Genequand, H. Tippmann, G. Pouilly and H. Guedu, "Pyroelectricity and Related Properties in the Fresnoite Pseudobinary System  $\text{Ba}_2\text{TiGe}_2\text{O}_8$ - $\text{Ba}_2\text{TiSi}_2\text{O}_8$ ," *J. Mater. Sci.*, 13, 2257 (1978).
- (10) S. Haussühl, "Growth and Physical Properties of Fresnoite  $\text{Ba}_2\text{TiSi}_2\text{O}_8$ ," *Jr. Crystal Growth*, 40, 200 (1977).
- (11) M. Kimura, K. Doi, S. Nanamatsu and T. Kawamura, "A New Piezoelectric Crystal:  $\text{Ba}_2\text{Ge}_2\text{TiO}_8$ ," *Appl. Phys. Lett.*, 23, 531 (1973).
- (12) G.M. Sessler, "Piezoelectricity in Polyvinylidene Fluoride," *J. Acoust. Soc. Am.*, 70, 1396 (1981).

- (13) R.E. Newnham, L.J. Bowen, K.A. Klicker and L.E. Cross, "Composite Piezo-electric Transducers," *Mat. Engg.*, 2, 93 (1980).

Table I. Compositions and Crystalline Phases

Composition	Crystallization Temp (°C)	Crystalline Phases
$2\text{BaO}-3\text{SiO}_2-\text{TiO}_2$	930	$\text{Ba}_2\text{TiSi}_2\text{O}_8$
$(1.9\text{BaO}-0.1\text{PbO})-3\text{SiO}_2-\text{TiO}_2$	920	$\text{Ba}_2\text{TiSi}_2\text{O}_8$
$2\text{BaO}-0.15\text{CaO}-2.9\text{SiO}_2-\text{TiO}_2$	920	$\text{Ba}_2\text{TiSi}_2\text{O}_8$
$1.6\text{BaO}-0.4\text{CaO}-2.8\text{SiO}_2-\text{TiO}_2$	930	$\text{Ba}_2\text{TiSi}_2\text{O}_8$
$1.6\text{BaO}-0.4\text{SrO}-3\text{SiO}_2-\text{TiO}_2-0.2\text{CaO}$	930	$\text{Ba}_2\text{TiSi}_2\text{O}_8$
$2\text{SrO}-3\text{SiO}_2-\text{TiO}_2$	950	$\text{Sr}_2\text{TiSi}_2\text{O}_8$
$(1.8\text{SrO}-0.2\text{BaO})-2.8\text{SiO}_2-\text{TiO}_2-0.1\text{CaO}$	940	$\text{Sr}_2\text{TiSi}_2\text{O}_8$
$\text{BaO}-\text{GaO}_2-\text{TiO}_2$	800	$\text{Ba}_2\text{TiGa}_2\text{O}_8$
$\text{Li}_2\text{O}-1.8\text{SiO}_2-0.2\text{B}_2\text{O}_3$	605, 680	$\text{Li}_2\text{Si}_2\text{O}_5 +$ $\text{Li}_2\text{B}_4\text{O}_7$

Table II. Electromechanical Properties

COMPOSITION	$k_p$ (%)	$k_t$ (%)	Q	TCR(Radial) ppm/°C
$Li_2O-1.8SiO_2-0.2B_2O_3$	15	20-25	1000-2000	70-100
$2BaO-3SiO_2-TiO_2$	14	20-25	1000-2000	100-120
$BaO-TiO_2-GaO_2$	6	8-10	2000-4000	60
$2SrO-3SiO_2-TiO_2$	11	25-30	1000-1500	50

Table III. Hydrostatic Measurements

Composition	K	$d_{33}$ pC/N	$B_{33}$ ( $10^{-3}$ Vm/N)	$B_h$ ( $10^{-3}$ Vm/N)	$d_h$ pC/N	$d_h B_h$ ( $10^{-15}$ m <sup>2</sup> /N)
2BaO-3SiO <sub>2</sub> -TiO <sub>2</sub>	9	7	88	110	8.8	970
(1.9BaO-0.1PbO)-3SiO <sub>2</sub> -TiO <sub>2</sub>	10	7	80	110	9.7	1070
2BaO-0.15CaO-2.9SiO <sub>2</sub> -TiO <sub>2</sub>	10	6	68	75	6.6	500
(1.6BaO-0.4CaO)-2.8SiO <sub>2</sub> -TiO <sub>2</sub>	10.5	6	65	85	7.9	670
(1.6BaO-0.4SrO)-3SiO <sub>2</sub> -TiO <sub>2</sub> -0.2CaO	9.8	6	70	100	8.7	870
2SrO-3SiO <sub>2</sub> -TiO <sub>2</sub>	11.5	14	138	85	8.7	740
(1.8SrO-0.2BaO)-2.8SiO <sub>2</sub> -0.1CaO-TiO <sub>2</sub>	10.6	10	107	100	9.4	940
BaO-GeO <sub>2</sub> -TiO <sub>2</sub>	15	6	45	70	9.3	650
BaTiSi <sub>2</sub> O <sub>8</sub> (Single Crystal)	11	8	82	130	12.7	1650
Ba <sub>2</sub> TiGe <sub>2</sub> O <sub>8</sub> (Single Crystal)	11.4	8	80	120	12.1	1450

Table IV. Comparison of Hydrostatic Properties

Property	Glass- Ceramics	PVF <sub>2</sub>	PZT
K	10	13	1800
$d_{33}$ ( $10^{-12}$ C/N)	8-10	30	450
$d_{31}$ ( $10^{-12}$ C/N)	+1.5	-18	-205
$d_h$ ( $10^{-12}$ C/N)	8-10	10	40
$g_{33}$ ( $10^{-3}$ Vm/N)	100	250	28
$g_h$ ( $10^{-3}$ Vm/N)	100	100	2.5
$d_h g_h$ ( $10^{-15}$ m <sup>2</sup> /N)	1000	1000	100

Table V. Comparison of Acoustic Impedances

MEDIUM	DENSITY (kg/m <sup>3</sup> )	VELOCITY (m/sec)	Z (10 <sup>6</sup> rayls)
Air	1.2	330	0.0004
Water	1000	1430	1.5
PZT	7600	4000	30
PVF <sub>2</sub>	1760	1450	2-3
Aluminum	2700	6300	17
Quartz	2640	5800	15.2
BaO-SiO <sub>2</sub> -TiO <sub>2</sub>	4000	4700	18-20
BaO-GeO <sub>2</sub> -TiO <sub>2</sub>	4780	5020	24
SrO-SiO <sub>2</sub> -TiO <sub>2</sub>	3600	5000	18

Figure Captions

Fig. 1. Internal stress in a composite of PZT fibers and a polymer.

Fig. 2. Simplified crystal structure of  $\text{Ba}_2\text{TiSi}_2\text{O}_8$ .

Fig. 3. Composite model for  $\text{Ba}_2\text{TiSi}_2\text{O}_8$ .



AD-A145 115

PIEZOELECTRIC AND ELECTROSTRICTIVE MATERIALS FOR  
TRANSDUCER APPLICATIONS(U) PENNSYLVANIA STATE UNIV  
UNIVERSITY PARK MATERIALS RESEARCH LAB

UNCLASSIFIED

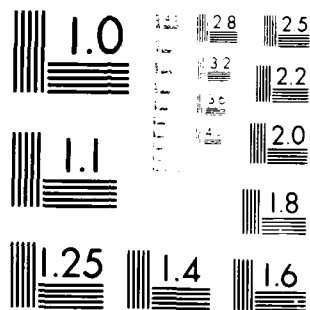
L F CROFT ET AL MAY 84 N00014 82-K-0339

F/G 20/3

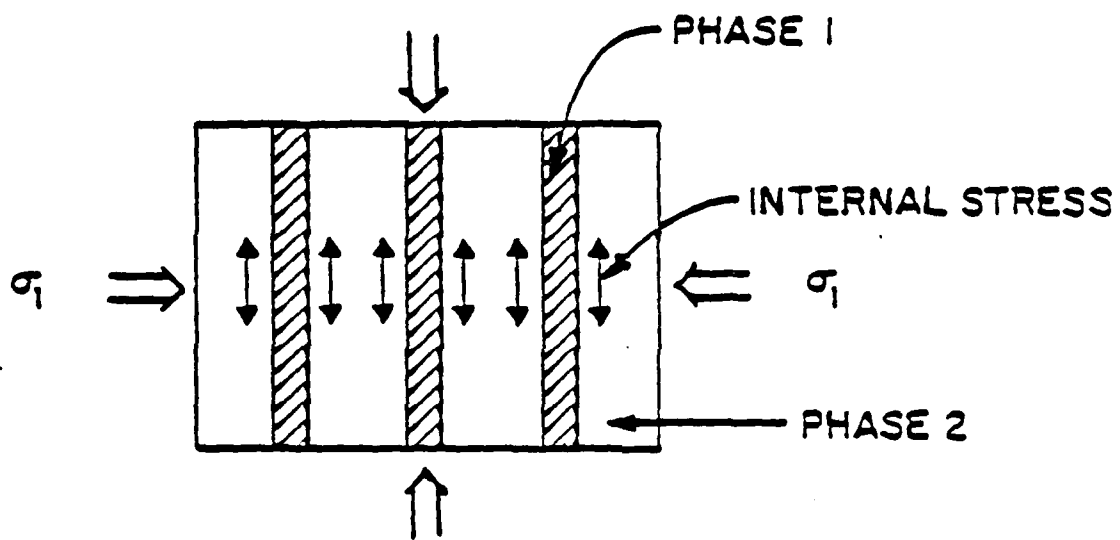
NL

3/4





MICROCOPY RESOLUTION TEST CHART  
 NATIONAL BUREAU OF STANDARDS-1963-A



PHASE 1 - PZT RODS  
PHASE 2 - POLYMER

Fig. 1. Internal Stresses in a composite of PZT fibers and a polymer.

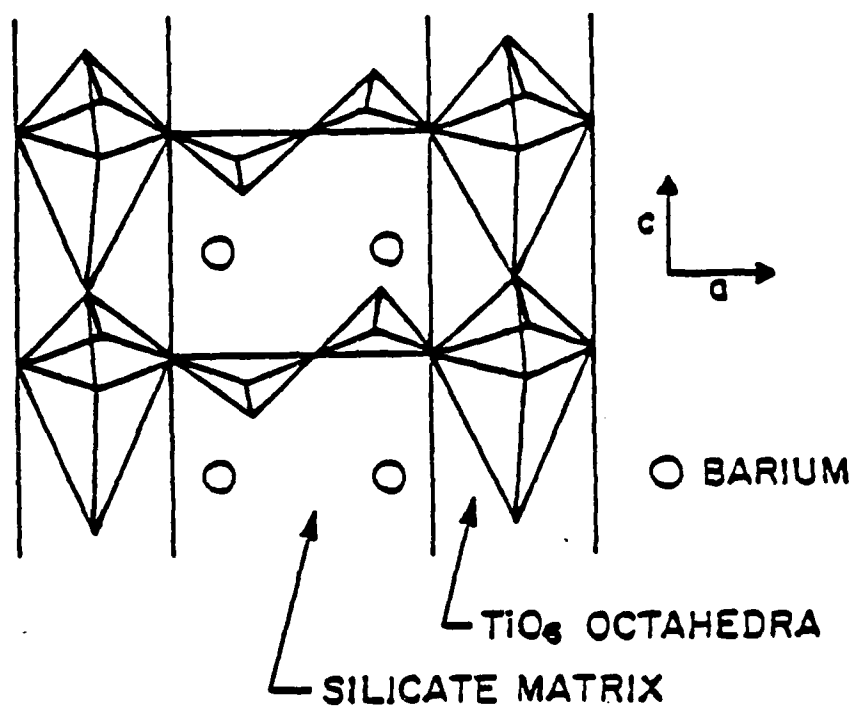
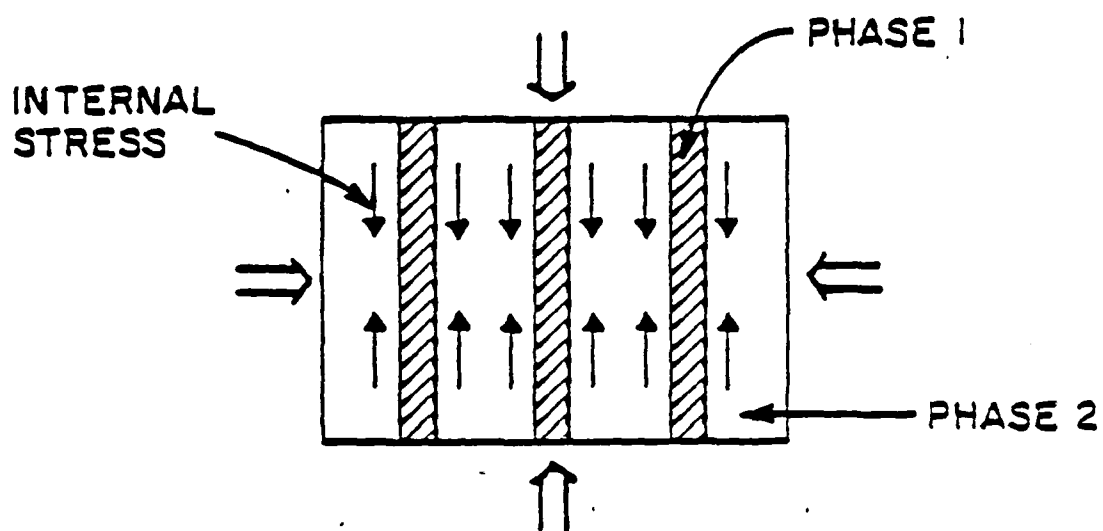


Fig. 2. Simplified crystal structure of  $\text{Ba}_2\text{TiSi}_2\text{O}_8$ .



PHASE 1 -  $\text{TiO}_6$  CHAINS  
 PHASE 2 - STIFF SILICATE MATRIX

Fig. 3. Composite model for  $\text{Ba}_2\text{TiSi}_2\text{O}_3$ .

**APPENDIX 14**

The Pennsylvania State University

The Graduate School

Electrostriction in Cubic Halide Compounds

A Thesis in  
Solid State Science

by

Kurt M. Rittenmyer

Submitted in Partial Fulfillment  
of the Requirements  
for the Degree of

Doctor of Philosophy

May 1984

I grant The Pennsylvania State University of nonexclusive right to use this work for the University's own purposes and to make single copies of the work available to the public on a not-for-profit basis if copies are not otherwise available.

---

Kurt M. Rittenmyer

## ABSTRACT

The electrostrictive properties have been reported previously of very few materials with low dielectric constants. They can be measured by using either the direct or converse electrostrictive effect. The converse effect involves measuring the stress dependence of the dielectric constant of the material. The direct effect is measured by determining the strain produced in a material by an applied electric field.

The hydrostatic electrostriction coefficients of several fluoride perovskite single crystals were determined from measurements of the converse effect using hydrostatic pressure. Non-linear behavior was observed in the dielectric constant-versus-pressure relationship. This indicates that higher-order electrostriction coefficients,  $\phi_{ijk}$ , are significant. The quadratic hydrostatic electrostriction coefficients,  $Q_H$ , of the fluoride perovskite materials are similar to those of other fluoride materials such as  $\text{LiF}$  and  $\text{CaF}_2$ . This comparison suggests that crystal structure is less important in determining the electrostrictive properties of a simple material than the kinds of ions in the structure.

An ultrasensitive dilatometer, which had been previously constructed, was modified to allow correct measurement of the electrostriction coefficients of single crystal materials with low dielectric permittivities. In order to obtain reliable results, it was necessary to rigidly mount the crystal between stiff metal electrodes.

The complete electrostriction tensor of  $\text{CaF}_2$  was calculated from measurements of the electrostriction coefficients of single crystals cut perpendicular to the (100), (110), and (111) crystallographic directions. These measurements were used in conjunction with the value of the hydrostatic



electrostriction coefficient obtained from the literature to calculate the values of the electrostriction tensor coefficients  $M_{11}$ ,  $M_{12}$ , and  $M_{44}$  using a least-squares method. The magnitude of the  $M_{11}$  coefficient is similar to those reported for alkali halide crystals. The values of  $M_{12}$  and  $M_{44}$  are relatively different from those determined by previous authors. However, the values in these previous papers are incorrect because of a calculation error.

Attempts at measuring electrostriction in sodium chloride were unsuccessful. The measured electrostriction coefficient was found to vary sharply with the frequency of the applied electric field. Subsequent investigations to determine the cause of this behavior were carried out. Electrostriction measurements were performed on a NaCl crystal which had been hot-forged and also on a crystal which had been irradiated with neutrons. Both of these measurements in addition to the experiments performed on  $\text{CaF}_2$  suggest that the movement of charged dislocations substantially increases the measured electrostriction coefficients of sodium chloride.

Measurements of other physical properties of several fluoride perovskite materials were completed. The measured properties include thermal expansion coefficients, temperature coefficients of the dielectric constants, and elastic constants. Values of these properties were used in conjunction with other published values of properties for a variety of materials to empirically relate electrostriction to other physical properties. Power-law relationships between isothermal compressibility, thermal expansion, and electrostriction were demonstrated. A linear relationship was observed between electrostriction and the pressure coefficient of isothermal compressibility. These empirical results are discussed in terms of the theory of anharmonic solids.

**APPENDIX 15**

Determination of the Electrostriction Tensor Components in Single  
Crystal  $\text{CaF}_2$  from the Uniaxial Stress Dependence of the  
Dielectric Permittivity

Z.Y. Meng\* and L.E. Cross\*\*

Materials Research Laboratory  
The Pennsylvania State University  
University Park, PA 16802

Abstract

The separated electrostriction tensor components have been measured for single crystal calcium fluoride by the converse effect, using a specially designed uniaxial elastic stressing jig. Values obtained for the individual components of the electrostrictive voltage (M) coefficients were  $M_{11} = -0.132$ ,  $M_{12} = 0.117$  and  $M_{44} = 0.507$  in units of  $10^{-20} \text{ m}^2/\text{v}^2$ . These values are smaller than those observed by direct measurement of electric field induced elastic strain (4), but are closer to expected values and likely to be more reliable.

---

\*On leave from the Department of Electronic Engineering, Xian Jiaotong University, Xian, Peoples Republic of China.

\*\*Also affiliated with the Department of Electrical Engineering.

## 1. Introduction

The quadratic electrostrictive effect is the basic electromechanical coupling phenomenon in all centric crystals and in amorphous insulators. Hydrostatic electrostriction coefficients have been measured for a number of insulator crystals with simple centric structures, but except in the case of high permittivity perovskite structure oxides, reliable values of the separated tensor components of electrostriction have not appeared in the literature. In the case of the simple alkali halides, even the signs of the coefficients are in doubt<sup>(1,2)</sup> and there is considerable uncertainty as to the influence of the dislocation structure upon the measured values<sup>(3)</sup>.

There are two alternative experimental approaches to the measurement of electrostriction, the direct method in which the elastic strain induced by a high electric field is measured directly by an ultra-dilatometer, and the converse method in which the thermodynamically equivalent change of dielectric stiffness under mechanical stress is measured. Both methods involve considerable experimental difficulty. In the case of the direct method, for normal simple low permittivity centric crystals, the electrostrictive strain levels which can be induced by a realizable high electric field, are only of the order  $10^{-8}$  so that in millimeter thick crystals displacements of the order of  $10^{-9}$  cm (0.1Å) must be measured with some precision so as to establish reliable values for the separate constants. For the converse methods, the need for sensitivity is now transferred to the dielectric measurement. Modern measuring systems like the General Radio 1620 bridge do have the sensitivity and stability required, but now there is also need for very precise temperature control and the requirement to establish a truly uniaxial stress upon the sample.

In this work, the converse method of measurement is used to measure the separated components of the electrostriction tensor for calcium fluoride.

Basic principles of the method are discussed in Section 2. A brief discussion of the design of a special uniaxial compression jig is given in Section 3, and data for the calibration of the system is presented in Section 4. Measured data for three orientations of the  $\text{CaF}_2$  crystal are presented and analysed in Section 5 and the results of measurements discussed in Section 6.

## 2. Basic Principles

The constitutive equations defining the phenomenological interaction between dielectric and elastic properties may be derived from the Gibbs free energy and from the elastic Gibbs function in the forms

$$x_{ij} = s_{ijkl}^E \epsilon_{kl} + M_{noij} E_n E_o \quad (1)$$

$$x_{ij} = s_{ijkl}^P \epsilon_{kl} + Q_{noij} P_n P_o \quad (2)$$

where  $x_{ij}$  and  $\epsilon_{ij}$  are the components of the elastic strain and elastic stress, respectively.  $E_n$ ,  $P_n$  the components of electric field and electric polarization.  $s_{ijkl}$  the elastic compliance tensor under the appropriate boundary condition (constant  $E$  or constant  $P$ ),  $M_{noij}$ ,  $Q_{noij}$  the electrostrictive coefficients in voltage and in polarization notation respectively.

From equations (1) and (2),  $M_{noij}$  and  $Q_{noij}$  may be defined by the relations

$$2M_{ijkl} = \left( \frac{\partial^2 x_{ij}}{\partial E_n \partial E_o} \right) \epsilon \quad (3)$$

$$2Q_{ijkl} = \left( \frac{\partial^2 x_{ij}}{\partial P_n \partial P_o} \right) \epsilon \quad (4)$$

and by application of the Maxwell relations to equations (3) and (4)

$$M_{ijkl} = \frac{1}{2} \left( \frac{\partial \eta_{kl}}{\partial X_{ij}} \right) P \quad (5)$$

$$Q_{ijkl} = - \frac{1}{2} \left( \frac{\partial \chi_{kl}}{\partial X_{ij}} \right) P \quad (6)$$

where  $\chi_{kl}$  and  $\eta_{kl}$  are the components of the dielectric stiffness and dielectric susceptibility respectively. It may be noted that

$$\chi_{kl} = \frac{1}{\eta_{kl}} = \frac{1}{\epsilon_0 (\epsilon_{kl} - 1)}$$

where  $\epsilon_0$  is the permittivity of free space and  $\epsilon_{kl}$  the components of the relative permittivity tensor. Thus

$$M_{ijkl} = \frac{\epsilon_0}{2} \left( \frac{\partial \epsilon_{kl}}{\partial X_{ij}} \right) P \quad (7)$$

$$Q_{ijkl} = \frac{1}{2\epsilon_0 (\epsilon - 1)^2} \left( \frac{\partial \epsilon_{kl}}{\partial X_{ij}} \right) P \quad (8)$$

and the measurement of either  $Q$  or  $M$  can be accomplished by the measurement of the change of permittivity under the appropriate stress, which itself can be related to the change of electrical capacitance for a suitably shaped sample.

### 3. DC Compression Fix for Capacitance Measurements

The scheme of the DC compressometer is outlined in Figure 1, which shows in projection the main parts of the sample holder and of the system for stress application. The system is designed to keep the pressure homogeneous and strictly uniaxial, the temperature stable for the period of a measurement, and the connections to the sample capacitance three terminal and completely electrically guarded.

The uniaxial stress is derived from a dead weight and is applied to the sample through a suitable lever arm. In the pressure cell, ram extenders are made from the same crystalline material, cut in the same orientation as the crystal sample under test. A very thin mylar gasket is used between crystal and crystal ram surfaces to take up any surface roughness. Complicated thermostatic control was not needed as it was found that the thermal capacity of the massive stressing jig was sufficient to smooth out any minor changes in the ambient in the thermostatically controlled clean room environment used for the measurements. All signal leads are coaxial and the design is such that there is not direct capacitance path other than through the sample.

A general view of the compressometer and associated equipment is shown in Figure 2. For measurement of the capacitance, a General Radio 1621 capacitance measuring assembly was used. This very high precision three terminal bridge provides stability and sensitivity quite adequate for the electrostriction measurement under reasonable stress loadings well inside the elastic range of the  $\text{CaF}_2$ .

#### 4. Calibration Measurements

##### 4.1 Elastic Stress

The compressive stress system was calibrated using a range of dead weights and replacing the sample with an Instron automatic load cell. In all cases, the pressure transfer from the lever arm was in excellent agreement with the lever principle, and the error in the force was less than 0.5%.

##### 4.2 Temperature Stability

To test the thermal stability, the sample was replaced with a similar size sodium chloride crystal with known temperature coefficient of capacitance. After the holder had come to thermal equilibrium several hours

after loading, the capacitance stability was explored. Maximum excursion  $\Delta C/C$  due to thermal drift was 0.6 ppm/min but under quiet conditions normal drift rates were much less than 0.3 ppm/min more than an order of magnitude smaller than the capacitance change due to pressure.

#### 4.3 Electrical Stability

After careful cleaning, the direct capacitance of the holder itself is less than 20 aF and the intrinsic conductance unmeasurable on a scale where the smallest increment is  $1 \times 10^{-7}$  nS. For the electrostriction measurement, the bridge was operated at 1 kHz with an applied drive of 30 volts. Electromagnetic screening was sufficiently perfect to prevent any observable perturbation from external electrical noise.

#### 4.4 Mechanical Vibration

No difficulty was experienced due to mechanical pickup, nonetheless, the system was operated on an air suspended table as is evident in Figure 1.

Considering worst possible combinations of all external perturbations, the capacitance resolution is better than 1 ppm and the absolute resolution of capacitance change  $\Delta C$  is of order 2 aF.

#### 5. Measurements on Calcium Fluoride

In these measurements, the dependence of the dielectric permittivity upon uniaxial stress is determined from the capacitance change of a disk shaped sample under homogeneous uniaxial pressure. In order to separate the tensor components  $M_{11}$ ,  $M_{12}$  and  $M_{44}$  for a centric cubic crystal, at least three and preferably four measurements must be made. In our case, it was chosen to measure the capacitance change for uniaxial pressure applied normal to the major faces of disks cut with (100), (110) and (111) axes normal to the major



face. In each case because of the geometry, the measuring field was being applied along the stress direction. Values for the hydrostatic coefficient  $M_h$  were taken from the literature<sup>(4)</sup>.

Using the equations for rotated cuts, it is simple to show that the general equations reduce to

$$M_h = M_{11} + 2M_{12} = \frac{\epsilon_0 \epsilon}{2} \left[ \left( \frac{1}{C} \frac{\partial C}{\partial X} \right)_h - (s_{11}^T + 2s_{12}^T) \right] \quad (9)$$

$$M'_{100} = M_{11} = \frac{\epsilon_0 \epsilon}{2} \left[ \left( \frac{1}{C} \frac{\partial C}{\partial X} \right)_{100} - (s_{11}^T - 2s_{12}^T) \right] \quad (10)$$

$$M'_{110} = \frac{1}{2} M_{11} + \frac{1}{2} M_{12} + \frac{1}{4} M_{44} = \frac{\epsilon_0 \epsilon}{2} \left[ \left( \frac{1}{C} \frac{\partial C}{\partial X} \right)_{110} + \frac{1}{2} (s_{44}^T - 2s_{12}^T) \right] \quad (11)$$

$$M'_{111} = \frac{1}{3} M_{11} + \frac{2}{3} M_{12} + \frac{1}{3} M_{44} = \frac{\epsilon_0 \epsilon}{C} \left[ \left( \frac{1}{C} \frac{\partial C}{\partial X} \right)_{111} + \frac{1}{3} (2s_{44}^T - s_{11}^T - 2s_{12}^T) \right] \quad (12)$$

From equations (9) to (12) the matrix components  $M_{11}$ ,  $M_{12}$  and  $M_{44}$  for the electrostriction constants can be deduced. They are related to the tensor components by  $M_{11} = M_{1111}$ ,  $M_{12} = M_{1122}$ ,  $M_{44} = 4M_{1212}$ .

Samples of calcium fluoride single crystal of high purity optical grade were purchased from Harshaw company and prepared in the form of flat cylindrical plates 23 mm in diameter 1.5 mm in thickness. Plates with  $\langle 100 \rangle$ ,  $\langle 110 \rangle$  and  $\langle 111 \rangle$  directions normal to the major surface were prepared, three samples of each orientation were prepared, two being used as pressure ram extenders and a central sample for dielectric measurement.

Electrodes for the capacitor sample were evaporated gold or aluminum, the guard region was 16 mm in diameter and the guard gap less than 0.2 mm. Contact strips for guard, guarded electrode and counter electrode, were carried over onto the edge of the sample by evaporation through specially machined masks. Guarded radial electrodes make contact with these contacting tabs.

All measurements were made at 22°C (room temperature). Capacitance change on both loading and unloading was taken to reduce the influence of slow thermal drift. Capacitance measurements were at 1 kHz with 30 volts applied to the G.R. 1621 measuring system. A typical graph for capacitance change on loading and unloading is given in Figure 3 for a  $\langle 100 \rangle$  oriented sample, and a corresponding curve for a  $\langle 110 \rangle$  sample in Figure 4. From measurements for a sequence of different load levels, the capacitance change  $\Delta c/c$  for pressures from 0 to 20 bar were constructed. It may be noted that the  $\langle 100 \rangle$  oriented sample increases in capacitance while  $\langle 110 \rangle$  and  $\langle 111 \rangle$  orientations decrease in capacitance with increasing stress.

Using a value for  $M_{11} = 1.017 \cdot 10^{-21} \text{ m}^2/\text{v}^2$  the slopes of the curves in Figure 5 give

$$M_{11} = -0.132 \times 10^{-20} \text{ m}^2/\text{v}^2$$

$$M_{12} = +0.117 \times 10^{-20} \text{ m}^2/\text{v}^2$$

$$M_{44} = +0.507 \times 10^{-20} \text{ m}^2/\text{v}^2 \quad (\text{i.e., } M_{1212} = -0.123 \times 10^{-20} \text{ m}^2/\text{v}^2)$$

## 6. Discussion

The major potential sources of error in these measured values are temperature drift, side lead and fringe field capacitance and lack of uniformity and homogeneity in the applied stress.

For the first two terms, the estimated total error is less than 3%.

It is difficult to estimate the effect of deviations from the ideal stress distribution, but successive measurements on the same orientation after removing and replacing the sample are repeatable to better than  $\pm 6\%$ . Direct measurements on similar samples which will be reported elsewhere give significantly higher values for the  $M_{11}$ , and we have no explanation for the

discrepancy. In favor of these measurements by the indirect method one may site

(a) The electric field levels are low so that there is no effect from Maxwell stresses which perturb the direct method.

(b) The dielectric change is directly proportional to the stress, so that inhomogeneity in the stress system tends to average out. In the direct method however, the strain is proportional to the square of the electric field and thus inhomogeneity in the field distribution will always tend to enhance the strain leading to spuriously high values of the  $M_{ijkl}$  coefficients.

Unfortunately as yet there is no reliable quantitative theory for electrostriction in fluorite structure crystals so that it is not possible to decide the merits of the two methods on theoretical grounds.

In general it may be noted that while the fluorite structure compounds are more polarizable and have higher dielectric permittivity than corresponding alkali halides, they are mechanically significantly stiffer and have lower thermal expansion. Thus in view of the general correlations observed between elastic and thermal expansion properties and electrostriction<sup>(5)</sup>, it would be expected that the fluorite structures would have lower magnitudes of electrostriction than the alkali halides, supporting the data values observed here by the converse method.

In conclusion, we believe that the converse method of measurement is a powerful technique for determining the sign and the magnitude of the separated electrostriction tensor components. The results for calcium fluoride are in accord with general expectations, but are significantly lower than recent values measured by the direct method. We are in the process of designing a new sample holder for direct measurements which will eliminate any possible perturbation from flexural strain induced by inhomogeneity in the electric field and are also developing a refined theoretical approach using techniques

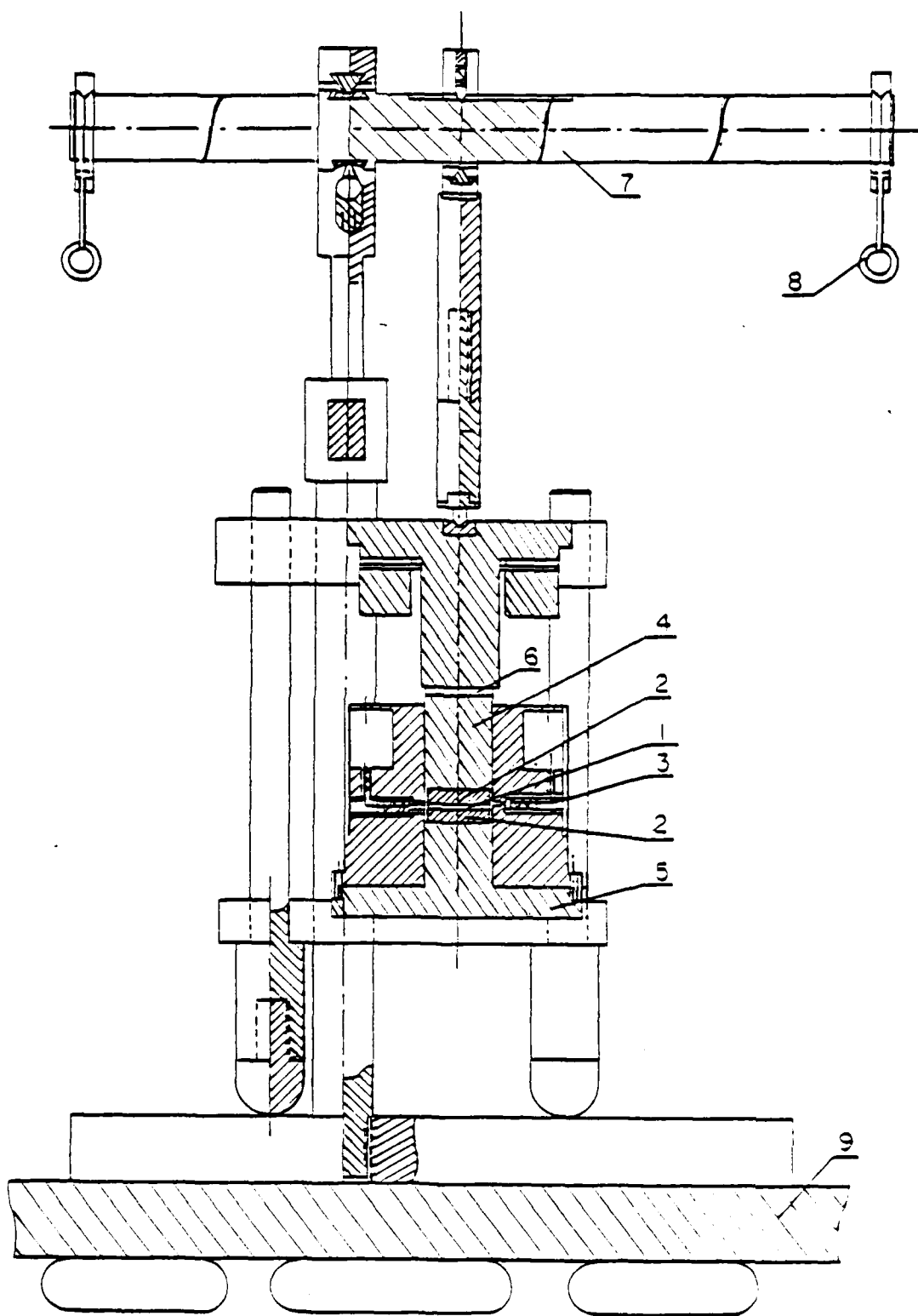
which have been applied successfully to the determination of electrostriction constants in perovskite structure halides<sup>(6)</sup>.

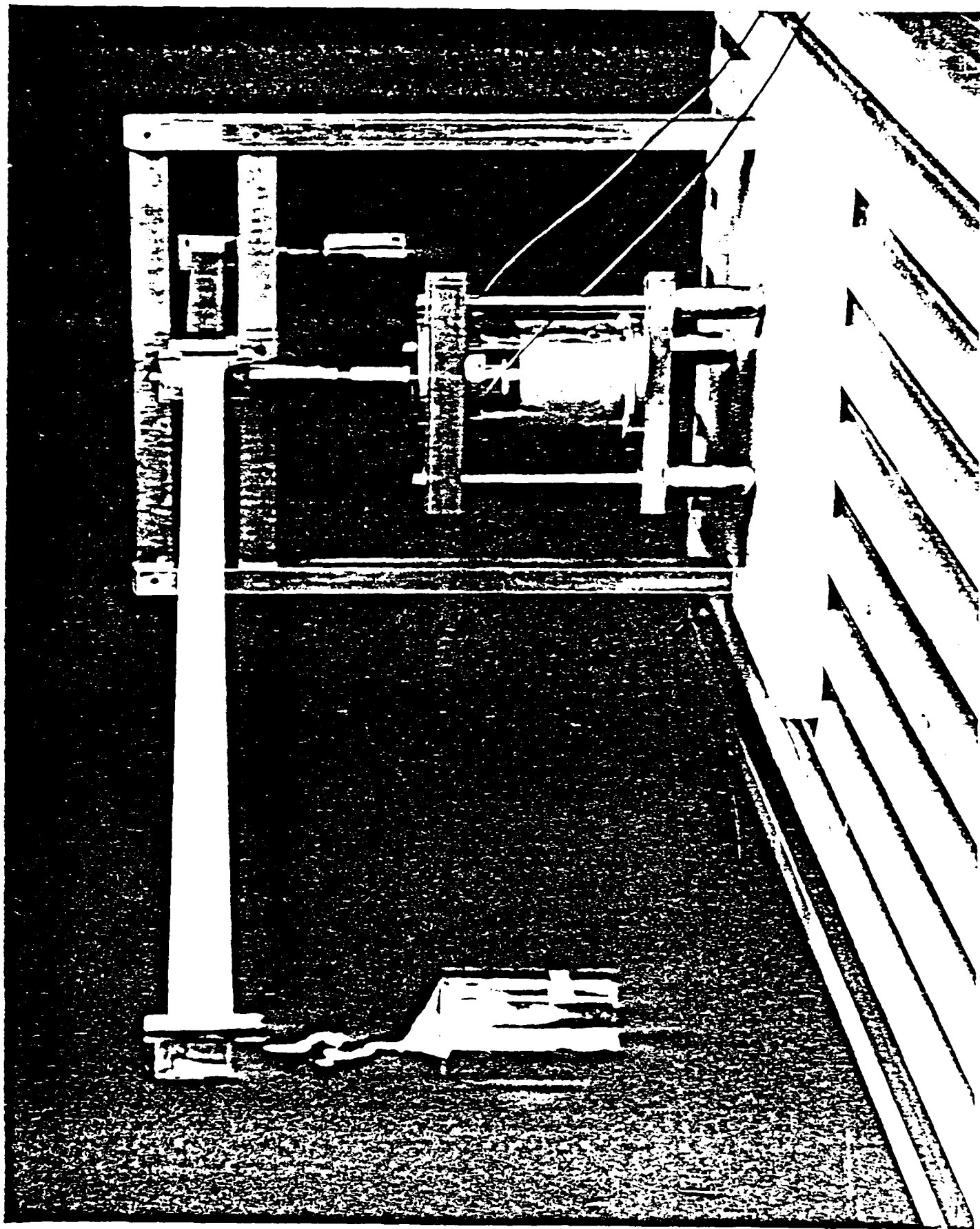
Acknowledgements

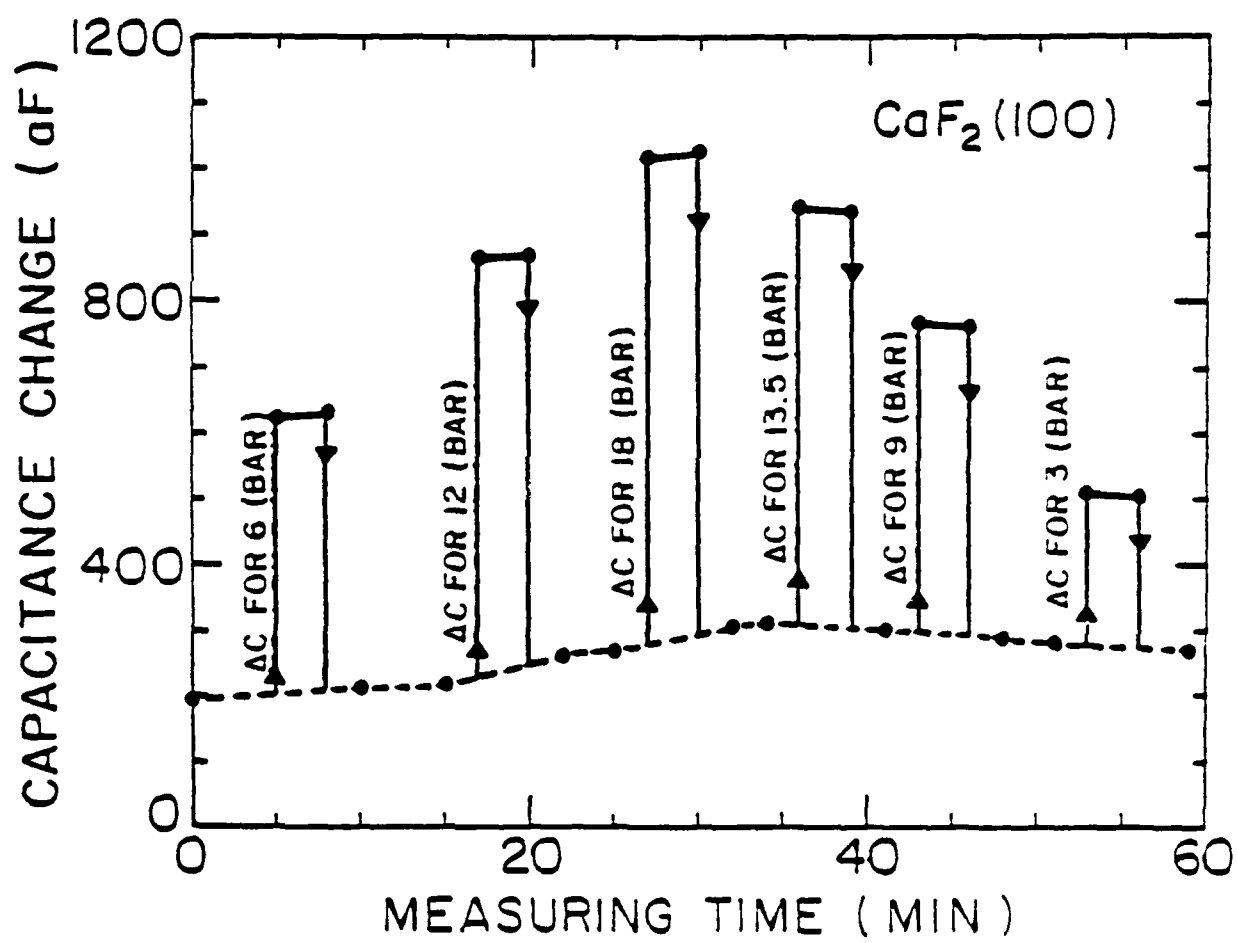
This work was supported by the Office of Naval Research under Contract No. N00014-82-K-0339.

### References

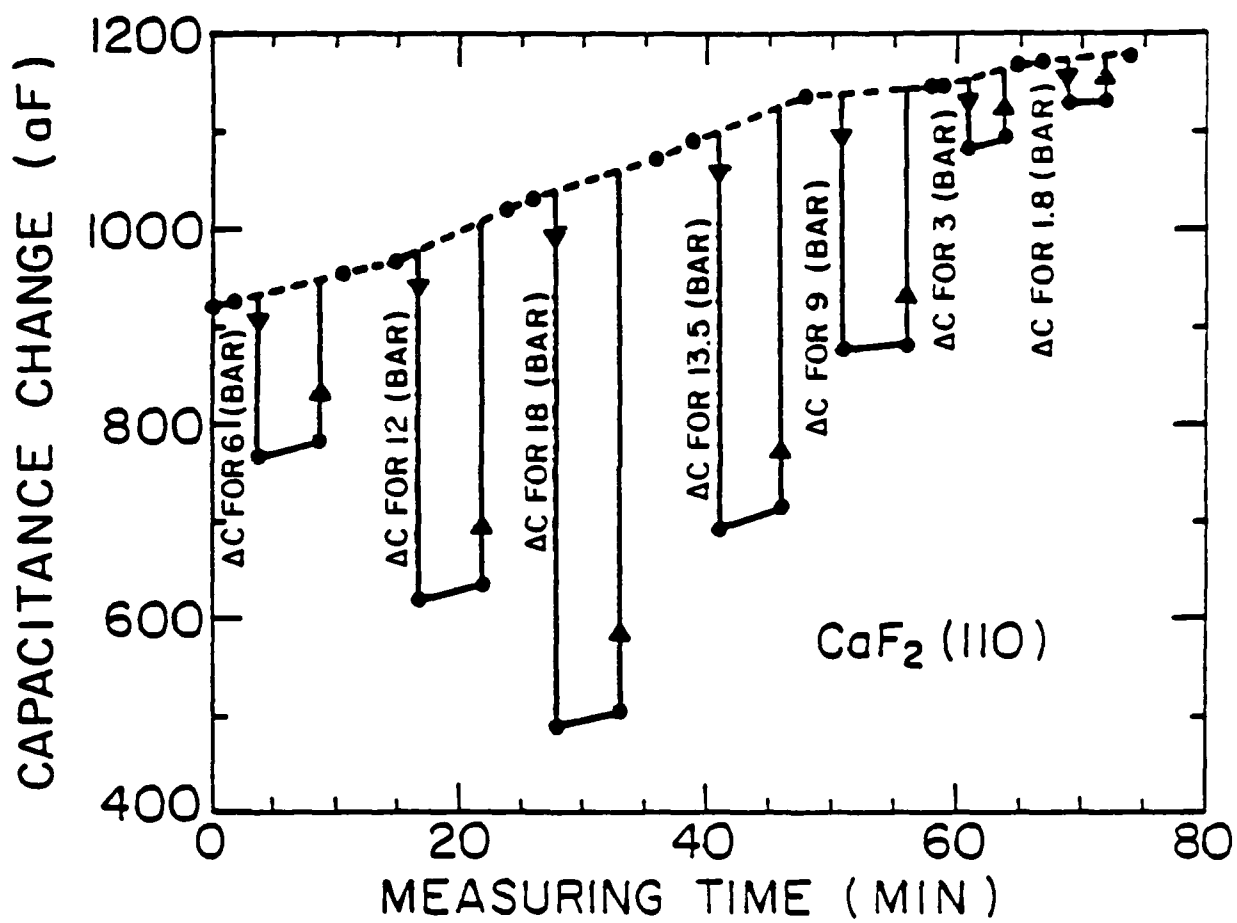
1. L. Bohaty and S. Hanssuhl, *Acta Cryst.*, A33, 114-118 (1977).
2. P. Preu and S. Hanssuhl, *Solid State Communications*, Vol. 45, No. 7, 619-623 (1983).
3. G. Balakrishnan, K. Srinivasan, and R. Srinivasan, *J. Appl. Phys.*, Vol. 54, No. 5, 2675-2677.
4. K. Rittenmyer, Ph.D. Thesis, Solid State Science, The Pennsylvania State University (May, 1984).
5. K. Uchino and L.E. Cross, *Jpn. J. Appl. Phys.*, Vol. 19, L171-L173 (1980).
6. B.N.N. Achar, G.R. Barsch and L.E. Cross, *Ferroelectrics*, Vol. 37, 495-497 (1981).

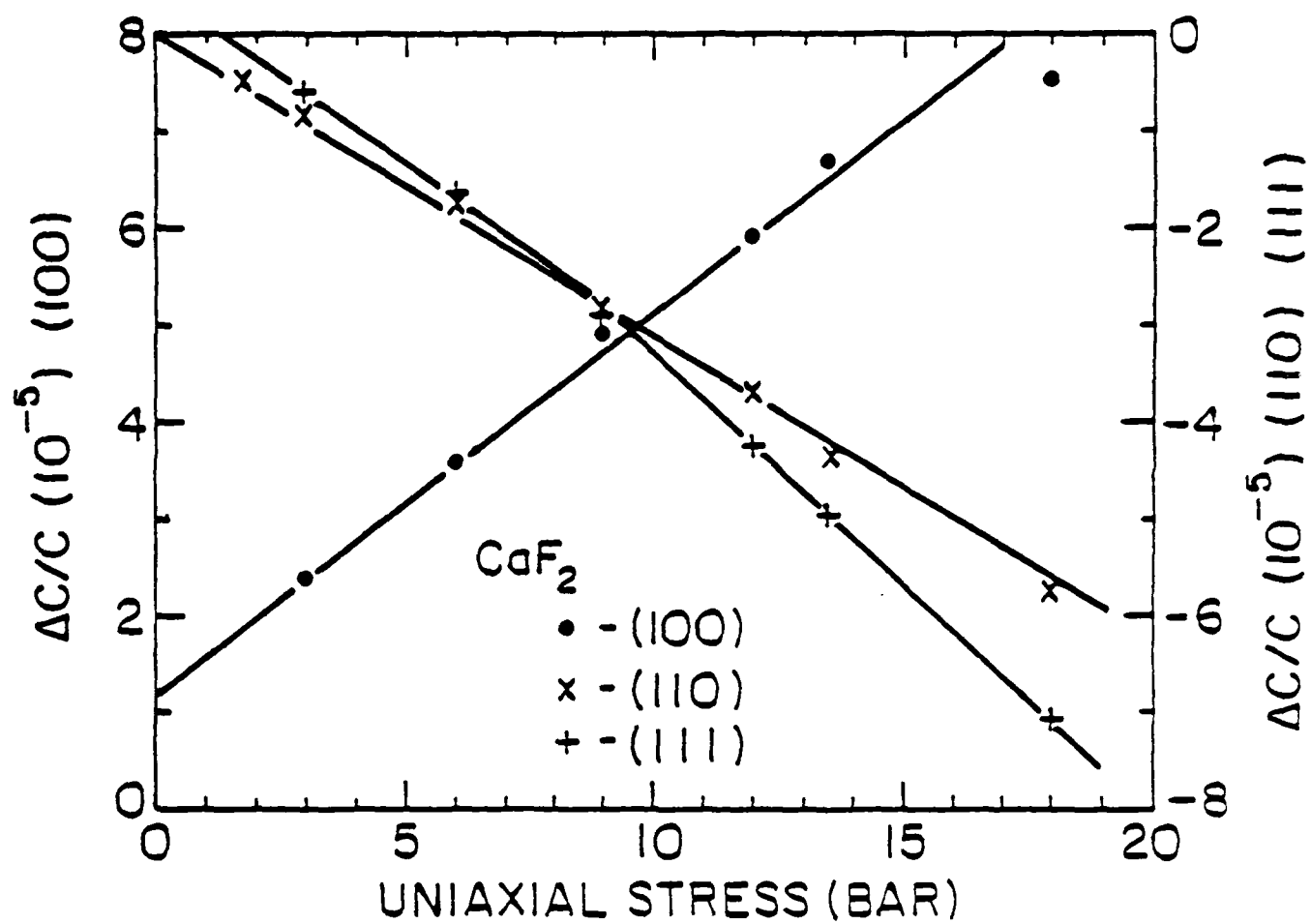












**APPENDIX 16**

The Pennsylvania State University  
The Graduate School  
Department of Electrical Engineering

A Simplified Temperature Compensated AC  
Dilatometer for Electrostriction Measurements

A Thesis in  
Electrical Engineering

by

Mojtaba Shishineh

Submitted in Partial Fulfillment  
of the Requirements  
for the Degree of  
Master of Science

December 1983

I grant The Pennsylvania State University the nonexclusive right to use this work for the University's own purposes and to make single copies of the work available to the public on a not-for-profit basis if copies are not otherwise available.

---

Mojtaba Shishineh

## ABSTRACT

In this thesis, the development, construction and experimental use of a very sensitive capacitance type AC dilatometer is presented. The need for the instrument arose from the requirement to be able to evaluate low level AC mechanical displacements produced in the paraelectric phase of a ferroelectric material under AC electric field through the electrostrictive coupling between dielectric polarization and lattice.

The design of the instrument was based on an earlier ultra sensitive dilatometer of Uchino and Cross (1980). A most important modification is the replacement of a DC servo system in their instrument by a thermal expansion compensation mechanical bridge (TECMB), which permits the instrument to be used at high sensitivity over a temperature range from 20°C to 200°C.

The instrument was calibrated using the known piezoelectric effect in a standard quartz crystal and maximum sensitivity better than 0.05Å ( $5 \times 10^{-12}$  meters) was obtained. Measurements on electrostrictive lead magnesium niobate-lead titanate (PMN-PT) ceramics, which have been previously evaluated by strain gauge methods, confirm this sensitivity.

The major effort has been directed to measuring the electrostrictive constant  $Q_{11}$  for single crystal  $\text{BaTiO}_3$  over a temperature range from 125°C to 190°C. These data clearly show and resolve the controversy associated with earlier conflicting data.

**APPENDIX 17**

The Pennsylvania State University

The Graduate School

Direct Measurement of the Temperature Dependence of  
Electrostrictive Coefficients in Strontium Barium Niobate

A Thesis in  
Solid State Science

by  
Carole Lynne Sundius

Submitted in Partial Fulfillment  
of the Requirements  
for the Degree of

Master of Science

May 1984

I grant The Pennsylvania State University the nonexclusive right to use this work for the University's own purposes and to make single copies of the work available to the public on a not-for-profit basis if copies are not otherwise available.

Carole Lynne Sundius  
Carole Lynne Sundius

# ABSTRACT

The electrostrictive effect in  $\text{Sr}_{.61}\text{Ba}_{.39}\text{Nb}_2\text{O}_6$  has been studied over a wide temperature range in the paraelectric region by direct measurement using an A.C. capacitance dilatometer. The dielectric properties in both the polar and non-polar directions have been thoroughly investigated, and procedures for measuring all six components of the electrostrictive tensor by direct methods are described. Measured values for  $Q_{33}$ ,  $Q_{13}$ , and  $Q_{11}$  coefficients are reported, followed by a discussion of the nature of direct measurement of electrostriction in relaxor ferroelectric materials.



**APPENDIX 18**

## ELECTROSTRICTION AND ITS RELATIONSHIP TO OTHER PROPERTIES IN PEROVSKITE-TYPE CRYSTALS

K. RITTENMYER, A.S. BHALLA, Z.P. CHANG AND L.E. CROSS  
Materials Research Laboratory, The Pennsylvania State University,  
University Park, PA 16802

**Abstract** Measurements of the fourth and sixth-order electrostriction constants have been performed on several fluoride perovskite single crystals. The results are compared with those observed in other similar materials, and the relationships between electrostriction and some physical properties are examined.

### INTRODUCTION

In a previous paper<sup>1</sup>, we presented measurements of the hydrostatic electrostriction constants,  $Q_{ij}$ , of several perovskite type single crystals based on fluorine octahedra rather than the oxygen octahedra on which all of the perovskite ferroelectrics are based. These fluoride perovskites ( $\text{KMnF}_3$ ,  $\text{RMgF}_3$ ,  $\text{KCaF}_3$ , and  $\text{KZnF}_3$ ) which are a lowered charge analog of the oxide perovskites, were found to have electrostriction and dielectric properties similar to those of other fluoride crystals such as  $\text{LiF}$  and  $\text{CaF}_2$ . In this paper, we present measurements of some physical properties of interest and further comparisons are made. First, a description of the various effects is necessary.

### ELECTROSTRICTION

Detailed phenomenological descriptions of the properties of linear dielectrics, including quadratic electrostrictive effects have been given elsewhere<sup>2</sup>. The higher order effects are derived here keeping only the terms necessary for this discussion. The total Gibbs function can be written in terms of the variables stress,  $X$ , and polarization,  $P$ , as

$$\Delta G = \frac{1}{2} X_{ij} P_i P_j + Q_{ijkl} P_i P_j X_{kl} + \frac{1}{2} s_{ijkl} X_{ij} X_{kl} + \phi_{ijklmn} P_i P_j X_{kl} X_{mn} \quad (1)$$

where  $X_{ij}$  is the inverse dielectric susceptibility, referred to from here on simply as susceptibility,  $Q_{ijkl}$  is the electrostriction tensor,  $s_{ijkl}$  is the elastic compliance tensor, and  $\phi_{ijklmn}$  is the sixth-order electrostriction term relevant to our measurements. Since most materials dealt with here are cubic, all tensor notation will be shortened in the usual manner.

In this work, the converse electrostrictive effect is used. By differentiating equation (1) twice with respect to polarization, an expression for the susceptibility is found:

$$X_i = \left( \frac{\partial E}{\partial P} \right)_X = \left( \frac{\partial^2 G}{\partial P_i^2} \right) = X_i(0) + 2Q_{ij} X_j + 2\phi_{ijk} X_j X_k \quad (2)$$

By taking the next two derivations and evaluating at zero stress, definitions for  $Q_{ij}$  and  $\phi_{ijk}$  coefficients are found to be,

$$Q_{ij} = \frac{1}{2} \left( \frac{\partial X_{ij}}{\partial X_j} \right); \quad \phi_{ijk} = \frac{1}{4} \left( \frac{\partial^2 X_i}{\partial X_j \partial X_k} \right) \quad (3)$$

Under a hydrostatic stress, a combination of transverse and uniaxial effects occur. Recalling that susceptibility and dielectric constant are related by

$$\chi = \frac{1}{(K-1)\epsilon_0}$$

we can define coefficients  $Q_h$  and  $\phi_h$  for electrostriction under hydrostatic pressure  $p$  as:

$$Q_h = Q_{11} + 2Q_{12} = \frac{-1}{2\epsilon_0(K-1)^2} \frac{dK}{dp} \quad (4)$$

$$\begin{aligned} \phi_h &= \phi_{111} + \phi_{122} + \phi_{133} + 2(\phi_{112} + \phi_{113} + \phi_{123}) \\ &= \frac{-1}{2\epsilon_0(K-1)^2} \left( \frac{1}{K} \frac{dK}{dp} + \frac{2}{(K-1)} \frac{dK}{dp} \right) \end{aligned}$$

## ELECTROSTRICTION AND ITS RELATIONSHIP TO OTHER PROPERTIES...

The first set of equalities show which tensor coefficients are involved and the terms of the right give the relationship to the pressure derivatives of the dielectric constant. Details of these kind of measurements have been given previously<sup>1,3</sup>. Measurements to separate the various tensor coefficients are difficult and has been done for few solids.

RESULTS AND DISCUSSIONSMeasurements of Dielectric Constant Versus Pressure

Results of these measurements showed a slightly non-linear relationship between  $K$  and pressure.  $Q_h$  and  $\phi_h$  can be calculated using equation (4) and (5) from the quadratic polynomials fitted to the data. The results are given in Table I along with values for other crystals. As mentioned previously, the  $Q_h$  values are similar to those of other fluoride

crystals, and are an order of magnitude larger than the oxide perovskites. The values of  $\phi_h$  for  $K\text{InF}_6$  and  $\text{KCaF}_3$  have not been corrected for pressure dependence of the compressibility,  $(\frac{\partial \chi_T}{\partial p})$ .

The low pressure compressibility is known, however, so the error caused by neglecting  $\frac{\partial \chi_T}{\partial p}$ , which typically accounts for less than ten percent of  $\phi_h$ , will be small compared to the error in the measurement. The values of  $\phi_h$  are essentially constant over a wide variety of oxides and fluorides. Only the alkali chlorides and bromides seem to show significantly different

Table I.  $Q_h$  and  $\phi_h$  values for several fluoride perovskites and other related single crystals.

$Q_h$ and $\phi_h$ for Some Solids		
Material	$Q_h, \text{a.u.}^2$	$\phi_h, \text{a.u.}^2$
$\text{NaF}$	0.93	$1.5 \times 10^{-4}$
$\text{LiF}$	0.40	1.1
$\text{NaCl}$	1.44	16.0
$\text{CaF}_2$	0.38	1.3
$\text{SrTiO}_3$	0.34	2.7
$\text{KInF}_6$	0.39	1.4
$\text{KCaF}_3$	0.29	3.5
$\text{KBrF}_4$	0.29	1.5

values for  $\phi_h$ . This indicates that  $\phi$  is principally a function of anion size rather than crystal structure or ionic charge. The one exception may be  $\text{KMnF}_3$ . The correction factor,  $\frac{d\kappa_T}{dp}$ , would have to be much larger than in the other fluoride crystals to account for the larger non-linearity. Since  $\text{KMnF}_3$  undergoes a structural transition at 186°K which causes a considerable anomaly in the elastic constants<sup>4</sup>, it is not inconceivable that this is indeed the case. However, the larger value of  $\phi$  could also be a result of a non-linear decrease of soft-mode frequency with increasing pressure.

#### Measurements of Dielectric Constant as a Function of Temperature

These measurements were carried out from 0-100°C in a computer controlled system described previously<sup>5</sup>, for  $\text{KlgF}_3$ ,  $\text{KZnF}_3$  and  $\text{KCaF}_3$ . The results for  $\text{KMnF}_3$  have been reported previously. The data for  $\text{KlgF}_3$  is shown in Figure 1. The other measurements are similar

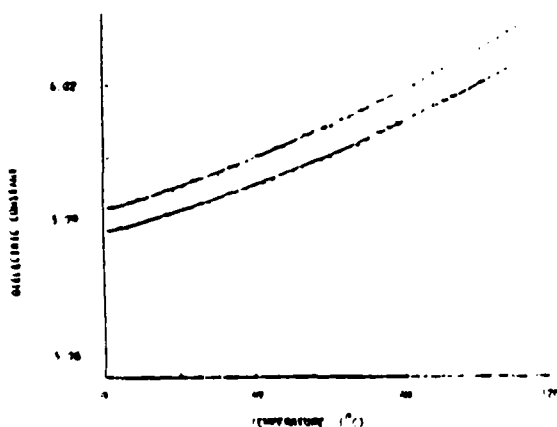


Figure 1. Plot of  $\kappa$  versus temperature for  $\text{KlgF}_3$ .

showing a slightly non-linear increasing dielectric constant with increasing temperature. The non-linearity in these measurements is similar to that of the pressure measurements<sup>1</sup>. The values of the temperature coefficients of dielectric constant,  $\frac{1}{\kappa} \frac{d\kappa}{dT}$ , are listed in Table II along with values for similar crystals. Unlike the pressure coefficients, these temperature coefficients are an order of magnitude smaller than other fluoride crystals and are, in fact, similar to that of quartz. The thermal expansion coefficients can

## ELECTROSTRICTION AND ITS RELATIONSHIP TO OTHER PROPERTIES...

account for only a fraction of this difference. Due to the soft-mode behavior at small wavevectors, the temperature coefficient for oxide perovskites are orders of magnitude larger

Table II. Dielectric constant and its temperature coefficient at constant pressure and volume.

Relationship Between $Q_h$ and Other Properties	TEMP. COEF. OF DIELECTRIC CONST.			
	Crystal	$K$	$(\frac{1}{K})_T$	$(\frac{1}{K})_V$
	NaF	5.1	$2.3 \cdot 10^{-4}$	$-0.73 \cdot 10^{-4}$
	LiF	9.0	1.1	0.35
	NaCl	5.9	3.2	1.9
	CaF <sub>2</sub>	5.9	1.4	0.99
	KMgF <sub>3</sub>	6.0	0.3	-0.55
	Quartz	4.6	0.3	-0.34

The relationship between properties such as dielectric constant, thermal expansion, and second and third-order elastic constants becomes apparent if the simple anharmonic (quasi-harmonic) model of solids is considered. Using the Lyddane-Sachs-Teller relation,

$$\frac{K_s}{K_\infty} = \prod_i \frac{W_{LO,i}^2}{W_{TO,i}^2} \quad (6)$$

where  $K_\infty$  and  $K_s$  are the optical and low frequency dielectric constants respectively, and  $W_{LO}$  and  $W_{TO}$  are respectively the longitudinal optic and transverse optic mode frequencies at long wavelengths, and the definition of volume isothermal compressibility

$$\chi_T = -\left(\frac{1}{V} \frac{dV}{dp}\right)_T \quad (7)$$

where  $V$  is the sample volume, the following expression for  $Q_h$  can be derived:

$$Q_h = \frac{-K_1 k}{2c_0 (K-1)^2} \left( \gamma_\infty + 2 \sum_i \gamma_{LO,i} - \gamma_{TO,i} \right) \quad (8)$$

where  $\gamma_{LO,i}$  and  $\gamma_{TO,i}$  represent the indicated gamma for each mode of the  $\omega$  versus  $k$  dispersion relation at long wavelengths. These are specific cases of the general mode gamma at wavevector  $\vec{k}$

K. RITTENMYER, A.S. BHALLA, Z.P. CHANG, L.E. CROSS

defined by

$$\gamma_l(k) = - \frac{v}{\omega_l(k)} \frac{d\omega_l(k)}{dv} \quad (9)$$

where  $l$  indicates which branch of the dispersion relation is being considered.  $\gamma_\infty$  is similarly defined as

$$\gamma_\infty = - \frac{v}{K_\infty} \frac{dK_\infty}{dv} \quad (10)$$

#### Relationship Between $Q_h$ , $K$ and $\chi_T$

If the mode gammas are considered to be independent of  $\chi_T$  and  $K$ , then the proportional relationships

$$Q_h \propto \frac{1}{K} \text{ and } Q_h \propto \chi_T \quad (11)$$

Uchino<sup>6</sup>, using ferroelectrics as examples of low  $Q_h$  materials, found the empirical relationship

$$Q_h \propto K^{-1.2} \text{ and } Q_h \propto \chi_T^{0.7} \quad (12)$$

Using the Born expression for lattice energy,

$$U(r) = \frac{A}{r^2} + \frac{B}{r^n} \quad (13)$$

where  $n$ , the Born exponent, has a value between 8 and 10 for the materials considered here, he derived the theoretical relationships

$$Q_h \propto K^0 \text{ and } Q_h \propto \chi_T \quad (14)$$

In Figure 2,  $Q_h$  is plotted as a function of dielectric constant. The upper line indicates a relationship like that of Uchino (equ. 12). A slope of -1 is a consequence of the Curie Weiss law for pressure and the result in (12) is expected. The lower line has no significant slope in agreement with equation 14. The compressibility plot (Fig. 3) for ordinary solids has a slope of 0.9 compared to 0.7 when ferroelectric materials are included.

## ELECTROSTRICTION AND ITS RELATIONSHIP TO OTHER PROPERTIES...

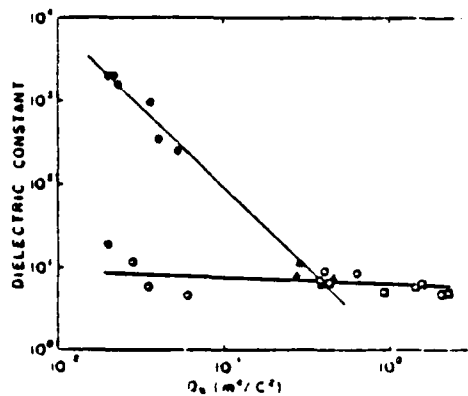


Figure 2. Log-log plot of dielectric constant versus  $Q_h$  for a variety of crystals: ●—oxide perovskite; ▲—fluoride perovskite; ○—diamond-type crystal; □—alkali halide; ○—fluorite-type crystal).

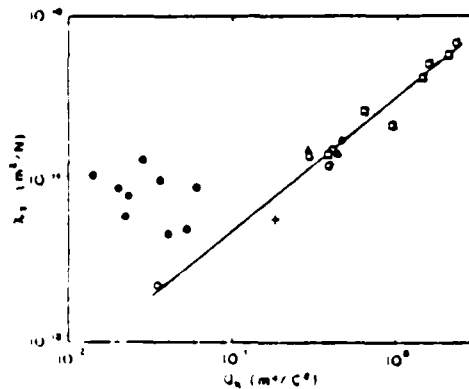


Figure 3. Log-log plot of volume compressibility versus  $Q_h$ . (Notation is same as in Fig. 2 except: +MgO).

In Figure 4, relative change in compressibility with pressure,  $\frac{1}{K_T} \frac{\partial K_T}{\partial p}$ , which is a combination of second and third order elastic constants, is plotted against  $Q_h$ . A strict linear relationship of the form, for  $p$  in  $N/m^2$ ,

$$Q_h = 0.13 + 1.5 \left( 10^{10} \frac{1}{K_T} \frac{\partial K_T}{\partial p} \right)$$

is demonstrated. This shows a clear, simple relationship between two third-order anharmonic effects.

#### Relationship Between $Q_h$ and Thermal Expansion ( $\alpha_V$ )

Grüneisen's theory was originally formulated to explain thermal expansion effects. The overall mode gamma, or Grüneisen constant, is defined as:

$$\gamma = \frac{\sum_i \gamma_i C_i}{\sum_i C_i} \quad (15)$$



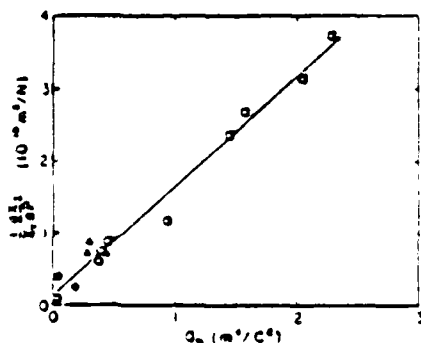


Figure 4. Linear plot of the pressure derivative of compressibility versus  $Q_h$  for various materials.

Depending on the corresponding  $C_i$ , it may or may not, however, dominate in equation 13.

Figure 5 shows the log-log plot of  $\alpha_v$  versus  $Q_h$ . The calculated value of the slope is 0.75

which implies that  $n \approx 9$  since the relationship

$$\alpha_v = Q_h^{n/(n+3)} \quad (16)$$

can be derived from equation 13.

For ferroelectric solids,  $n$  was shown to be about three or four<sup>6</sup>.

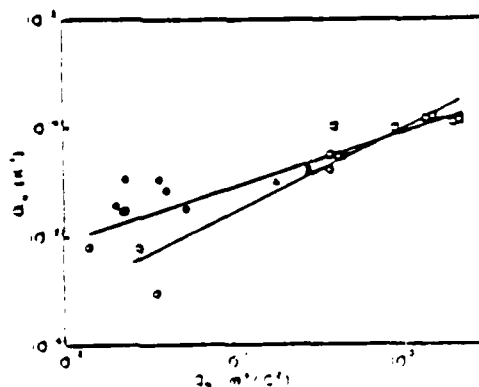


Figure 5. Log-log plot of volume thermal expansion versus  $Q_h$ . The line of lesser slope is fitted including perovskite materials. The steeper line excludes these ferroelectric-type crystals.

## ELECTROSTRICTION AND ITS RELATIONSHIP TO OTHER PROPERTIES...

References

1. K. Rittenmyer, A.S. Bhalla, Z.P. Chang and L.E. Cross, Ferroelectrics Letters (submitted).
2. J. Grindley, An Introduction to the Phenomenological Theory of Ferroelectricity, Pergamon Press, Oxford (1970).
3. J. Fontanella, C. Andeen and D. Scheule, Phys. Rev. **6**, 582-595 (1972).
4. K. Aleksandrov, L.M. Resnikova and B.V. Beznikov, Sov. Phys. Sol. St. **8**, 1904 (1967).
5. K. Rittenmyer, A.S. Bhalla and L.E. Cross, Physica Stat. Sol. (submitted).
6. K. Uchino and L.E. Cross, Jpn. J. Appl. Phys. **19**, L171-L173 (1980).

**APPENDIX 19**

## DIRECT MEASUREMENT OF ELECTROSTRICTION IN PEROVSKITE TYPE FERROELECTRICS

M. SHISHINEH, C. SUNDIUS, T. SHROUT AND L.E. CROSS  
Materials Research Laboratory, The Pennsylvania State University,  
University Park, PA 16802

**Abstract:** A simplified AC capacitance dilatometer based on the design of Uchino and Cross<sup>1</sup> has been constructed to measure directly the temperature dependence of electrostrictive strain in perovskite type ferroelectric crystals and ceramics. A mechanical bridge circuit is used to compensate for thermal expansion of the mechanical components, eliminating the need for DC servo stabilization. The instrument has been used in the temperature range from 20°C to 200°C. In the AC method, the electrostrictive strain under AC driving field is compared to the known strain induced in a quartz reference crystal under phase locked conditions. The method has been checked with the known piezoelectric behavior of quartz and of selected PZT disk samples. Measurements of Q constants will be reported for lead magnesium niobate (PMN), lead magnesium niobate:lead titanate solid solutions (PMN:PT), and lead iron niobate:lead iron tungstate (PFN:PTW).

### INTRODUCTION

Electrostriction, the effect by which all materials, upon application of an electric field, exhibit a strain proportional to the square of that field, is of interest to both design engineers and theoreticians. Measurements of electrostriction can be made by both direct and indirect methods.

The strain induced under high applied field conditions can be measured directly using optical detection systems<sup>2</sup>, such as, the interferometer, optical lever, laser probe, and optical grid; x-ray diffraction; electrical systems, including the capacitive dilatometer and the differential transformer dilatometer; and the strain gauge method<sup>3</sup>.

Indirect methods entail relating applied mechanical stress to variation in dielectric constant and employ either a pressure gauge or induced piezoelectric resonance techniques.

Of these methods, the AC capacitance dilatometer is the simplest and it is the best system for low frequency AC direct measurement of electrostriction.

The temperature dependence of electrostrictive coefficients in perovskite-type ferroelectrics is important for the clarification of electrostrictive mechanisms. Measurement of this dependence in

the high temperature, paraelectric phase, is preferable because the strain effect is wholly electrostrictive in this phase. (Measurements in the ferroelectric phase are complicated by the presence of piezoelectricity.)

The AC capacitance dilatometer described by Uchino and Cross<sup>5</sup> has been modified to facilitate its use for electrostrictive measurements over a large temperature range. It has been equipped with a mechanical bridge circuit designed to compensate for thermal expansion within the dilatometer, thereby eliminating the need for DC servo stabilization. The instrument has an operating range of 10°C to 200°C and can resolve low frequency, AC linear displacements of  $1 \times 10^{-12}$  m.

### THE INSTRUMENT

The sensing element of the dilatometer is a parallel plate capacitor composed of two pieces of Maccor glass ceramic with sputtered gold electrodes. The two samples to be measured, a piezoelectric quartz standard and an unknown, also have sputtered gold electrodes. Each sample is positioned between one glass ceramic plate and the upper/lower part of the dilatometer frame, as shown in Figure 1. The top plate is supported by three adjustable springs, while the bottom merely rests upon the sample as shown. Changes in plate separation are associated with a change in capacitance which is monitored by a capacitance bridge.

An AC signal of 7 Hz applied to an electrostrictive sample will cause the capacitor plates to vibrate at a frequency of 14 Hz. The output under these conditions is compared with the piezoelectric response of the quartz standard under phase-locked conditions of 14 Hz applied field, and the electrostrictive coefficient of the sample can be calculated. A block diagram of the system is given in Figure 2.

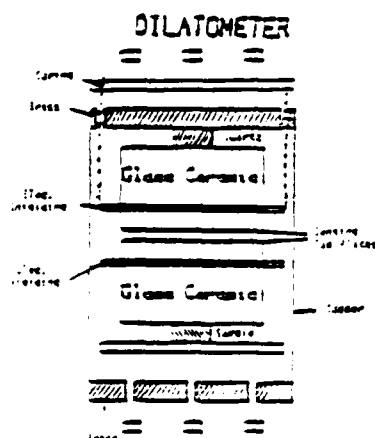
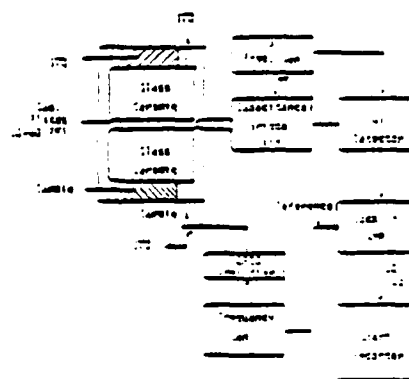


Figure 1. Dilatometer with the quartz on the top and sample on the bottom.



BLOCK DIAGRAM

Figure 2. Block diagram of the instrument.

## DIRECT MEASUREMENT OF ELECTROSTRICTION IN PEROVSKITE...

### THERMAL EXPANSION COMPENSATION BRIDGE

This system, as originally designed, was extremely sensitive to temperature variation, and the thermal expansion due to a  $1^{\circ}\text{C}$  -  $2^{\circ}\text{C}$  change in ambient temperature would cause the capacitance bridge to go out of balance. To compensate for this thermal drift, a DC servo system was used. While the DC servo provides adequate compensation for room temperature measurements, a more complete compensation device is required for high temperature operation.

The thermal effects within the dilatometer are two-fold. As the inside of the instrument, which is composed of glass ceramic, electrical shielding and brass supports, expands, the result is to bring the capacitor plates closer together, thereby increasing the stationary capacitance,  $C_0$ . The outside of the device, however, consists solely of a copper cylinder, 9.6 cm high, which is used for shielding and to support the upper half of the dilatometer. The effect of the expansion of the outer cylinder is to separate the two plates, causing  $C_0$  to drop. The second effect is much larger than the first and in the uncompensated dilatometer,  $C_0$  falls significantly with increasing temperature.

To compensate for the excessive thermal expansion of the outer part of the dilatometer, a mechanical bridge was designed and built. This bridge consists simply of three Super-invar rods, 12 cm long and .64 cm in diameter, with a thermal expansion coefficient  $<3.6 \times 10^{-7}/^{\circ}\text{C}$ . As shown in Figure 3, the rods are evenly spaced around the dilatometer and are clamped to a variable position brass ring, which in turn, is clamped to the copper cylinder. The portion of the cylinder below the ring now responds with the thermal expansion of Super-invar while the remainder behaves as before. By varying the length of Super-invar to copper, a point is found at which the thermal expansion of the outside is exactly equal and opposite to that of the inside.

### DERIVATION OF THE CONSTANTS

The coefficients used in this calculation are  $M$ , the electrostrictive voltage coefficient;  $Q$ , the electrostrictive polarization coefficient; and  $d$ , the piezoelectric coefficient. The subscripts,  $s$  and  $Q$ , are used to designate the electrostrictive sample and the quartz standard respectively.  $l$  is the thickness of the crystal,  $\Delta l$  is the induced displacement,  $\epsilon$  is strain,  $V$  is applied voltage,  $E$  is the external electric field and  $P$  is polarization.

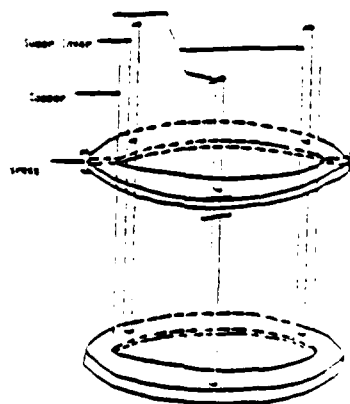


Figure 3: Thermal expansion compensation bridge.

M. SHISHINEH, C. SUNDIUS, T. SHROUT, L.E. CROSS

The strain due to an electric field applied across an electrostrictive sample is

$$\epsilon_s = \left(\frac{\Delta l}{l}\right)_s = M_s E_s^2.$$

That due to an applied field across a quartz standard is

$$\epsilon_Q = \left(\frac{\Delta l}{l}\right)_Q = d_Q E_Q.$$

The signal detected from the capacitance bridge is directly proportional to the change in capacitance, which is directly proportional to the displacement of the (sample, quartz). Therefore, for a given output signal,

$$\text{signal} \propto \Delta l = M_s E_s^2 l_s = d_Q E_Q l_Q.$$

Since,  $E = \frac{V}{l}$ ,

$$M_s \frac{V_s^2}{l_s} = d_Q V_Q$$

and

$$M_s = \frac{d_Q V_Q l_s}{V_s^2}$$

The electrostrictive polarization coefficient,  $Q$ , is defined by

$$\epsilon = Q P^2.$$

When  $P = P(E)$  is known,  $Q$  may be calculated from  $M$  using

$$Q = M \frac{V^2}{P^2 l}$$

#### SENSITIVITY AND PERFORMANCE

To check the AC sensitivity, a quartz crystal was driven at 14 Hz. The output of the lock-in amplifier as a function of applied voltage is given in Figure 4. The expected linear relation for piezoelectricity is clearly observed. The piezoelectric coefficient of the quartz was calculated using the absolute calibrator (variable air capacitor) described in detail by Uchino and Cross<sup>4</sup>, and is

$$d_Q = d_{33} = 2.34 \times 10^{-12} \text{ C/N}$$

(about 3% higher than the previously reported value,  $d_Q = 2.27 \times 10^{-12} \text{ C/N}^4$ ).

No significant change was observed in the calculated coefficient for quartz over the temperature range, 20°C-100°C, and the response remained linear in the electric field range .02-1.0 kV/cm.

The piezoelectric effect of a soft PCT ( $\text{PbZr}_{.10}\text{Ti}_{.90}\text{O}_3$ ) was measured at room temperature and calculated from

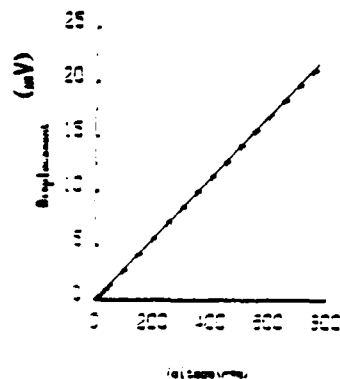
# DIRECT MEASUREMENT OF ELECTROSTRICTION IN PEROVSKITE...

$$d_s = d_{33} = \left(\frac{m_s}{m_Q}\right)d_Q$$

where:  $m_s$  is the slope of  $\Delta l$  vs  $V$  for the PZT,  
 $m_Q$  is the slope of  $\Delta l$  vs  $V$  for quartz and  
 $d_Q = 2.27 \times 10^{-2}$  C/N.

A value of  $d_{33} = 415$  C/N was found and is in good agreement with the value of 425 C/N measured by the Berlincourt  $d_{33}$ -meter.

## QUARTZ



## RESULTS AND DISCUSSION

The data from measurement of piezoelectricity and electrostriction in crystals and ceramics of quartz,  $Pb(Mg_{1/3}Nb_{2/3})O_3$ ,  $Pb(Mg_{1/3}Nb_{2/3})O_3$ -10%  $PbTiO_3$ , and PFW-PFN is listed in Table 1 along with the previously published data<sup>5</sup>.

The temperature dependence of the electrostrictive polarization coefficient,  $Q_{11}$ , of a  $PbTi$ -10%PT-5%MgO system was investigated above its Curie temperature, 40°C. A plot of  $Q_{11}$  versus temperature is shown in Figure 5 and shows the  $Q_{11}$  of this system to be independent of temperature. Future work will be on the measurement of electrostrictive properties of single crystal  $BaTiO_3$  (barium titanate) in paraelectric region.

Figure 4. A typical plot of the lock-in output (mv) as a function of voltage applied on quartz.

Table 1.  $Q_m$  measured by this system for the samples shown above compared with the reported data published earlier.

## RESULTS

SAMPLE	PURE PMN	PMN-10ZPT	PFW-PFN	Quartz
$k$	16.000	20.000	25.670	4.7
$r, ^\circ C/T_m$	-10/23	40/46	22/23	573
$q_{11} (m^2/V^2)$	$1.07 \cdot 10^{-14}$	$5.3 \cdot 10^{-14}$	$8.4 \cdot 10^{-14}$	—
$Q_{11} (m^2/C^2)$	$0.95 \cdot 10^{-2}$	$2.29 \cdot 10^{-2}$	$1.65 \cdot 10^{-2}$	—
$Q_{11} (m^2/C^2)$	$0.9 \cdot 10^{-2}$	$2.15 \cdot 10^{-2}$	—	—
REPORTED	—	—	—	—
$d_{11} (C/N)$	—	—	—	$2.34 \cdot 10^{-11}$

## REFERENCES

1. K. Uchino and L.E. Cross, Ferroelectrics **27**, 35 (1980).
2. J. Kuwata, K. Uchino and S. Nomura, Jpn. J. Appl. Phys. **19**, 2099 (1980).
3. S. Nomura, J. Kuwata, K. Uchino, S.J. Jang, L.E. Cross and R.E. Newnham, Phys. Stat. Sol. (a), **57**, 317 (1980).



M. SHISHINEE, C. SUNDIUS, T. SHROUT, L.E. CROSS

PMN-10ZPT-5XMgO

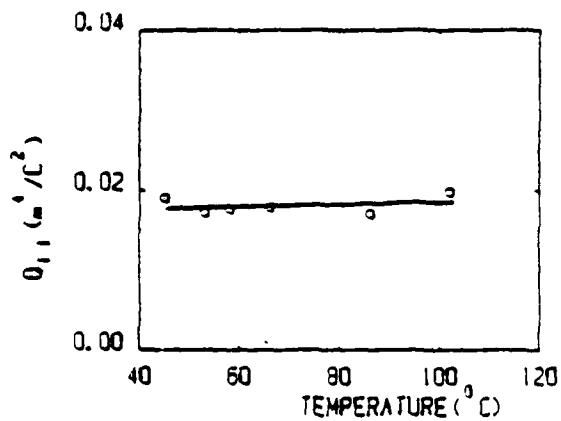


Figure 5.  $Q_{11} (m^4/C^2)$  as a function of temperature ( $^{\circ}C$ ) for a PMN-10ZPT-5XMgO sample.

4. V.E. Bottom, J. Appl. Phys. 41, 3941 (1970).
5. S.J. Jang, K. Uchino, S. Nomura and L.E. Cross, Ferroelectrics 27, 31-34 (1980).

**APPENDIX 20**

## POLARIZATION AND DEPOLARIZATION BEHAVIOR OF HOT PRESSED LEAD LANTHANUM ZIRCONATE TITANATE CERAMICS

YAO XI, CHEN ZHILI, AND L.E. CROSS

Materials Research Laboratory, The Pennsylvania State University, University Park, PA 16802

**Abstract**—Studies have been made of the polarization and depolarization behavior for lead lanthanum zirconate titanate ceramics with zirconia:titanium ratio 0.65/0.35 and  $\text{La}_2\text{O}_3$  content from 0.07 to 0.095 (7:65:35 to 9.5:65:35). Continuity of the dielectric dispersion on cooling unbiased freshly de-aged samples suggests that across this whole composition range for temperatures below the dielectric maxima, there are no macroscopic phase changes. Large remanent polarizations may be built up at low temperatures by cooling under suitable DC bias, but the ceramics will 'stand off' significant bias levels applied at low temperature and remain dispersive. Depoling on heating becomes progressively less abrupt with increasing  $\text{La}_2\text{O}_3$  content but is always accomplished well below the temperature of the dielectric maximum. A model involving the ordering and disordering of polar micro-regions under electrical and thermal fields accounts well for the observed properties.

### INTRODUCTION

The thermal depolarization behavior of electrically poled lead lanthanum zirconate titanate (PLZT) ceramics with compositions in the range of  $\text{PbZr}_{0.65}\text{Ti}_{0.35}\text{O}_3$  with  $\text{La}_2\text{O}_3$  additions of 6-, 7-, and 8-mole%  $\text{La}_2\text{O}_3$  have been of interest for the behavior of the pyroelectric current, dielectric response, and electro-optic characteristics<sup>1-3</sup>. It was clear from the early studies of Keve<sup>4</sup> that depolarization of a short-circuited PLZT of composition 7:65:35 occurs at a temperature well below that of the dielectric permittivity maximum. Dielectric data of Salaneck<sup>5</sup> suggest that the  $K'$  maximum is strongly dispersive as in ferroelectrics with diffuse phase transitions (relaxors). More recent measurements by Kimura, Newnham, and Cross<sup>6</sup> of the elastic shape memory effect suggest that the shape changing ferroelastic macrodomains are lost in these ceramics at the lower depoling temperature.

The present study was carried out to investigate more fully both poling and depoling characteristics of transparent hot pressed PLZTs covering the composition range from (7 to 9.5):65:35. Data for the 3%  $\text{La}_2\text{O}_3$  composition have been presented earlier<sup>7</sup>, but some are reproduced again here to compare with the 8.8 and 9.5%  $\text{La}_2\text{O}_3$  compositions.

### SAMPLE PREPARATION AND EXPERIMENTAL PROCEDURE

Ceramics used in these studies were provided by the Shanghai

Institute of Ceramics in China. Wafers used in the present study were cut from boules of near theoretical density, high optical transparency and mean grain sizes in the range 2 to 5  $\mu\text{m}$ .

Dielectric properties were measured on a computerized automatic measuring system using the HP LCR meters HP 4274A and 4275A under HP 9825 computer control. Pyroelectric currents were measured with an HP 4140B picoammeter. A Delta Design 2300 environment chamber covered the range -150 to 200°C and temperature were measured with a platinum resistance thermometer on a Fluke 8502A digital multimeter. Special software was developed for automatic measurement and all data were recorded on flexible magnetic disks.

### EXPERIMENTAL RESULTS

The temperature dependence of dielectric permittivity in 8:65:35 PZT cooling under zero bias, and under a DC bias of 3 kV/cm for a cooling rate of 3°C/min is shown in Figure 1a and 1b. Suppression of the dispersive behavior (relaxor character) under bias is clearly evident at temperatures below 55°C. Similarly for an 8:65:35 PLZT sample cooled to -75°C then biased to 3 kV/cm and heated at 3°C/min (Fig. 2), the persistence of the dispersion up to a temperature  $T_p$ , followed by a suppressed no dispersive region (2) a re-emergence of dispersion below  $T_m$  (3) and the conventional higher temperature non-dispersive regions (4) are quite evident. That  $T_p$  and  $T_m$  are poling and depoling temperatures is evidenced from the pyroelectric currents (Fig. 3), and the integrated current shows the corresponding build up and decay of macroscopic polarization.

Data has already been presented to show that  $T_p$  decreases with increasing bias field, and the kinetic nature of the change is evident from the dependence upon heating rate.

In the 8:8/65/35 PZT, on cooling a freshly de-aged sample again the dispersive character of a relaxor ferroelectric is clearly evidenced (Fig. 4a). Here, however, under even high DC bias of 15 kV/cm the relaxation is not completely suppressed and there is no evidence of an abrupt change such as that seen in the 8/65/35 compositions (Fig. 4b). That the polarization builds up and decays in a rather similar manner to that in the ceramics of lower lanthanum content is, however, evident from the integrated pyroelectric response for a sample cooled under field (Fig. 5[2]) as compared to that of a sample cooled without field to -100°C then biased to 3 kV/cm and heated at a constant rate of 3°C/minute (Fig. 5[1]).

It may be noted that the major changes with increased  $\text{La}_2\text{O}_3$  content is that the polarization levels are lower, the changes are more gradual and occur at lower temperature.

In the 9.5:65:35 this trend is continued (Fig. 6) and here a higher field of 6.6 kV/cm was used to produce comparable polarization changes. Larger polarization levels can be induced in both 8.8 and 9.5%  $\text{La}_2\text{O}_3$  compositions, but only by going to much higher field levels.

### DISCUSSION

The continuity of the dispersion curves in all samples below  $T_m$  suggests that in the absence of a driving field none of the materials goes through a normal macroscopic phase change below  $T_m$ . This would appear to be confirmed by recent measurements in Shanghai of W. Yin and colleagues<sup>(8)</sup> who show that in grain grown PLZTs of the 8:65:35 composition the individual grains have isotropic optical properties below  $T_m$  in the absence of an external field.

For the 8.8:65:35 and 9.5:65:35, the dispersion and poling: depoling behavior are remarkably similar to those observed in  $\text{Pb}(\text{Mg}_{1/3}\text{Nb}_{2/3})\text{O}_3$ ,  $\text{Pb}(\text{Se}_{1/2}\text{Ta}_{1/2})\text{O}_3$  and other relaxor ferroelectrics. It is thus tempting to apply the model of ordering of polar micro regions under field, and disordering under temperature to describe the observed build up and decay of polarization. That the 8:65:35 composition is optically isotropic grain by grain on cooling again suggests the model of disordered polar micro-regions. However, in this composition the disordering is rather abrupt and has many of the features of a phase change.

We suggest in speculation, that in analogy to magnetism, the PMN, PST, 8.8:65:35 and 9.5:65:35 compositions may be superparaelectric but that in the 8:65:35 the phenomena may be more analogous to that of critical superparamagnetism.

### REFERENCES

1. A.H. Meitzler and E.M. O'Bryan, J. Am. Ceram. Soc. 55, 54 (1972).
2. G.H. Haertling and C.E. Land, J. Am. Ceram. Soc. 54, 1 (1971).
3. G.H. Haertling, J. Am. Ceram. Soc. 54, 303 (1971).
4. E.T. Keve and K.L. Bye, J. Appl. Phys. 46, 810 (1975).
5. W.R. Salaneck, J. Appl. Phys. 43, 4468 (1972).
6. T. Kimura, R.E. Newham, and L.E. Cross, Phase Transitions 2, 113 (1981).
7. Yao Xi, Chen Zhili, and L.E. Cross, J. Appl. Phys. 54(6):339 (1983).
8. B.H. Chu, H.K. Ngao, X.S. Zheng, and Z.W. Yin, Joint US:China Seminar on Microstructure and Properties of Ceramic Materials, Shanghai, May, 1983 (to be published).

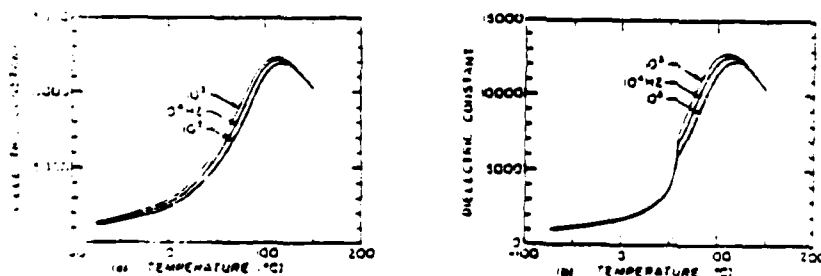


Figure 1. Temperature dependence of dielectric constant of PLZT 8:65:35 (a) without and (b) under dc bias of 5 kV/cm at cooling rate of 3°C/min.

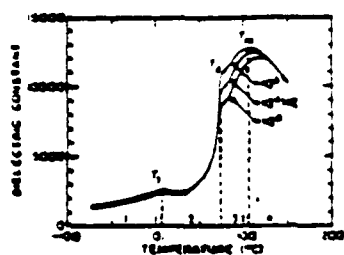


Figure 2. Temperature dependence of dielectric constant of PLZT 8:65:15 under a bias of 3 kV/cm at heating rate of 1°C/min.

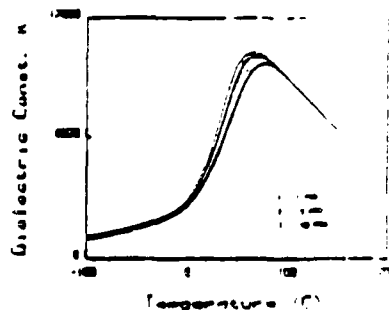


Figure 4(b). Dielectric permittivity in PLZT 8:65:15 at field 100 V/cm, heating rate 1 kV/cm, heating at 1°C/min.

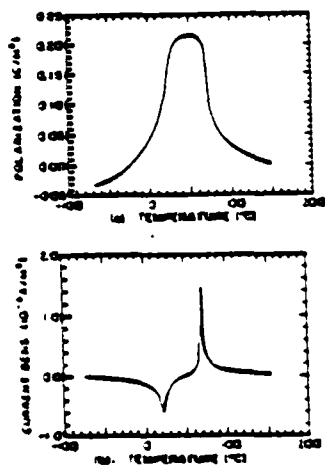


Figure 3. The buildup and decay of (a) the remnant polarization and (b) associated charging and discharging current of PLZT 8:65:15 under a bias of 3 kV/cm at constant heating rate.

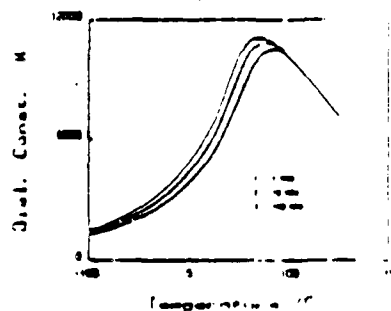


Figure 4(a). Dielectric permittivity in PLZT 8:65:15 at field 100 V/cm, heating rate 1°C/min.

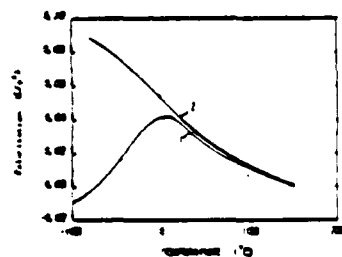


Figure 5. Polarization in PLZT 8:65:15  
(1) Depoled sample heated at 1°C/min (kV/cm)  
(2) Cooling under a field of 3 kV/cm.

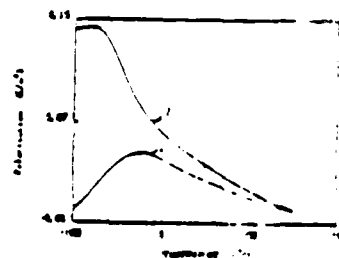


Figure 6. Poling and depoling in PLZT 8:65:15  
(1) Depoled sample heating at 1°C/min under bias of 3 kV/cm  
(2) Depoling after heating at 100 V/cm under 0 kV/cm in the same heating rate.

**APPENDIX 21**

REVERSIBLE PYROELECTRIC EFFECT IN  $\text{Pb}(\text{Sc}_{1/2}\text{Ta}_{1/2})\text{O}_3$  CERAMICS UNDER DC BIAS \*

CHEN ZHILI\*, YAO XI\*\* AND L.E. CROSS  
Materials Research Laboratory, The Pennsylvania State University  
University Park, PA 16802, USA

(Received for Publication December 27, 1982)

**Abstract**—It has been shown that quenched  $\text{Pb}(\text{Sc}_{1/2}\text{Ta}_{1/2})\text{O}_3$  (PST) disordered ceramics and crystals show diffuse dispersive dielectric properties, while well annealed ordered materials exhibit normal sharp first order transition. The pyroelectric depolarization measurements taken using a Hewlett Packard Model 4140B picoammeter/DC Source under computer controlled heating cycle also have shown different behaviors between disordered and ordered materials.

In this work pyroelectric measurements by Chynoweth method under DC bias up to 1.8 KV/mm within a temperature range of 70°C around the temperature of maximum dielectric constant have been studied. A very significant enhancement of the pyroelectric signal under DC bias is observed in thermally quenched disordered samples. The largest enhancement of the signal appears at temperatures some degrees below the temperature of maximum dielectric constant.

The existence of microdomains in disordered materials is believed to be responsible for this new extrinsic component of reversible pyroelectricity.

The large reversible pyroelectric effect is a promising phenomenon for developing new pyroelectric devices.

## 1. INTRODUCTION

In PST single crystals and ceramics which are of simple perovskite structure the combination of B-site cations in the  $\text{ABO}_3$  structure is close to the boundary between order and disorder<sup>1</sup>. The degree of ordering of the different B-site cations in these materials can be controlled thermally. Quenched disordered crystals and ceramics show diffuse dispersive dielectric properties, while well annealed ordered materials exhibit "normal" sharp first order ferroelectric transition. The influences of the ordering upon the dielectric, ferroelectric and elastoelectric properties of PST materials have been reported<sup>2,3</sup>. The effects of DC bias upon the dielectric properties of ordered and disordered PST ceramics have also been explored<sup>4</sup>.

Pyroelectric depolarization studies showed that the polarization of disordered samples drops down more smoothly, while ordered samples depolarize abruptly within the transition region<sup>2</sup>. In this work pyroelectric measurements by Chynoweth method<sup>5</sup> under DC bias up to 1.8 KV/mm within a temperature range of 70°C around the temperature of maximum dielectric constant have been studied.

\*Visiting scientist from Shanghai Institute of Ceramics, Shanghai, China.

\*\*Visiting scientist from Xian Jiaotong University, Xian, China.

\*Communicated by Professor L. E. Cross



## 2. EXPERIMENTAL

### 2.1 Preparation of Materials

All samples were prepared by conventional mixed oxide processing from stoichiometric proportion of  $PbO$ ,  $Sc_2O_3$ ,  $Ta_2O_5$  and  $Nb_2O_5$ . Compositions were ball milled in alcohol for 20 hours. The mixture was dried, then calcined for two hours at  $800^\circ C$ . The calcine powders were reground and pelletized. Then the pellets were fired at  $1300^\circ C$  for one hour, using  $PbZrO_3 + PbO$  for atmosphere control. A final sintering was performed at  $1560^\circ C$  followed by rapid quenching to induce the disordered structure. The degree of ordering in the B-site cations were controlled by thermal annealing the sample at  $1000^\circ C$ . Final densities achieved were 94% theoretical, with no more than 1% weight loss.

The degree of ordering was established by comparing base and superlattice reflection intensity in the x-ray powder pattern and using the relation for the degree of ordering  $S$

$$S^2 = \frac{I_{\text{superlattice}}}{I_{\text{base lattice/exp}}} \frac{I_{\text{base theory}}}{I_{\text{super}}} \quad \text{for } S = 1$$

The degrees of ordering are 0.37 for the samples annealed at  $1000^\circ C$  for 24 hours and 0.40 for the samples quenched at  $1560^\circ C$  to room temperature within 10 minutes.

### 2.2 Pyroelectric Measurements by Chynoweth Method

The pyro-signals were measured by a modified Chynoweth method. The schematic circuit for measurements is shown in Figure 1. The series circuit consists of a bias voltage supply, the sample, and a high resistance ( $10^9 \Omega$ ) across which a pre-amplifier was connected via a blocking capacitor ( $0.01 \mu f$ ). The output of the pre-amplifier was connected to a phase-lock amplifier model PAR HR-8. The magnitude of the pyro-signal can be read from the output voltmeter of the phase-lock amplifier. A Tektronix 545A cathode ray oscilloscope was used to monitor the wave form of the pyro-signal. A disk radiation chopper was used to control the heating frequency of the detector so as to be close to the charge mode of operation. In this mode the pyroelectric signal at

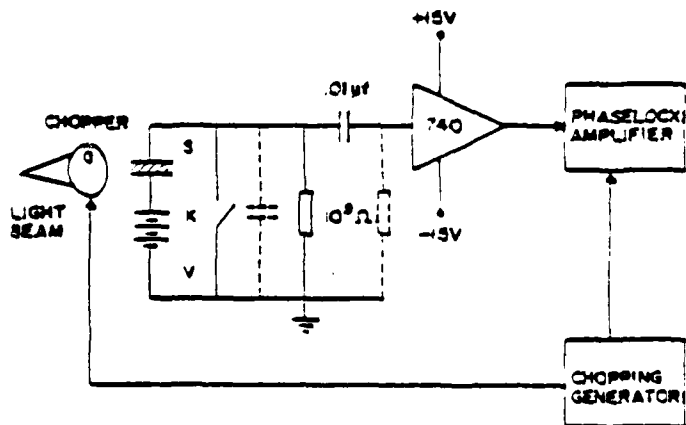


FIGURE 1. Schematic diagram of measurement. S - sample; 7 - bias source; 740 - pre-amplifier; K - charging switch.

fixed frequency is proportional to  $p/KC_p$ , here  $p$  - pyroelectric coefficient,  $K$  - dielectric constant,  $C_p$  - specific heat of the sample.

In all the experiments of this work the PST samples were about 0.25 mm in thickness. Circular gold electrodes were sputtered on to opposite faces of the samples, the diameter of the electrode was about 5 mm. Thin silver leads were attached to the gold electrodes by means of air-drying silver paste. An infrared projector lamp was used as the heat source to modulate the sample temperature. A Delta design MK 2300 environment chamber was used to change the ambient temperature about the bolometer chip.

Figure 2 shows the pyro-signal measured by Chynoweth method for the disordered and ordered PST ceramic samples without electric bias. The temperature range of measurement is  $70^\circ\text{C}$  around the temperature of the dielectric constant maximum  $T_m$  which is  $1.9^\circ\text{C}$  for the disordered PST ceramic sample, and is  $17^\circ\text{C}$  for the ordered one (Figure 3). It is obvious from the figures that the pyro-signal for ordered samples is much larger than that for the disordered one. The pyroelectric signal as a function of bias field at various temperatures is shown in Figure 4. If accurate absolute pyroelectric coefficients were needed, the pyro-signals would have to be corrected for the temperature variation of specific heat and the non-linearity departure of the rectifiers at small signal. These corrections were not performed since only relative magnitudes are to be used and thus they would not affect any of the interpretations and conclusions. It is clear that as the bias field increases the pyroelectric signal of the disordered PST sample increases more significantly than the ordered one. To compare the effect of electric bias field on the disordered and ordered materials the enhancement factor  $N_v$ , which is referred to as the ratio of the pyro-signal under a DC bias of 1.5 KV/mm and the pyro-signal under a DC bias of 0.1 KV/mm, is plotted as a function of the temperature difference  $T-T_m$  (Figure 5). The following feature of the experimental results are obvious: (1) The enhancement factor of the pyro-signal under DC bias for the disordered material is higher than that for the ordered one within the whole temperature range of measurements. (2) The highest enhancement factor occurs at the temperatures different from  $T_m$ . For the disordered sample the highest enhancement factor appears at the temperature about  $21^\circ\text{C}$  below  $T_m$ , while for the ordered sample it appears at the temperature about  $5^\circ\text{C}$  above  $T_m$ .

In contrast with the results for the PST samples, the electric bias field shows no significant effect on  $\text{LiNbO}_3$  single crystals at  $23^\circ\text{C}$  (Figure 6).

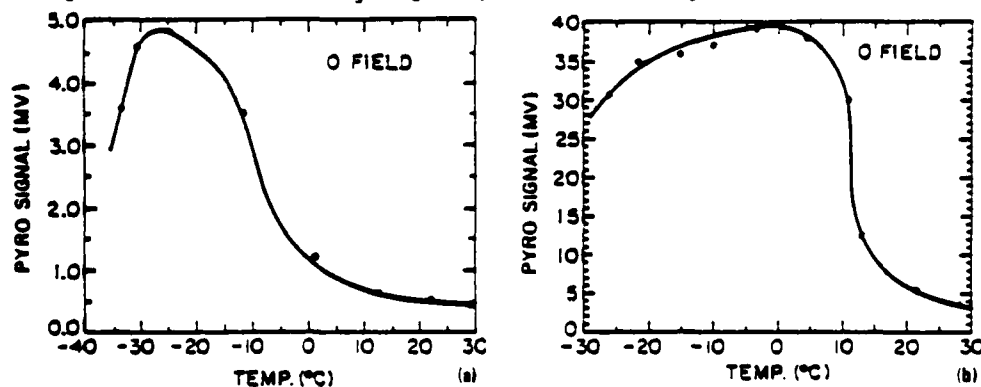


FIGURE 2. The temperature dependence of pyroelectric signal of the disordered (a) and ordered (b) ceramics.

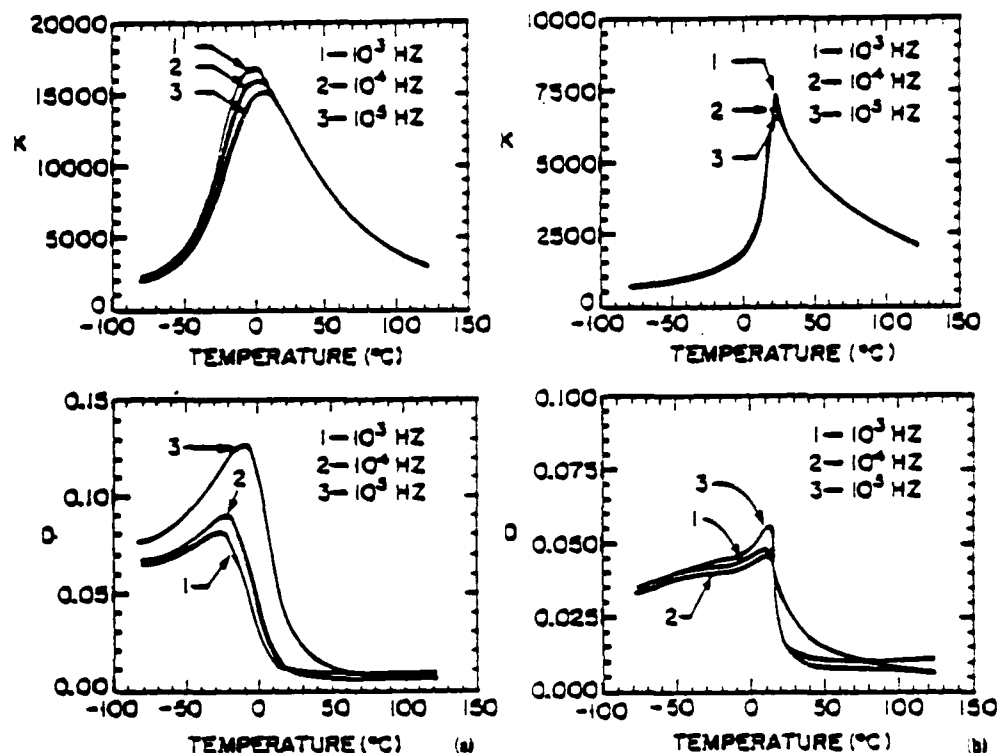


FIGURE 3. The temperature dependence of dielectric constant  $K$  and loss tangent  $D$  of the disordered (a) and ordered (b) PST ceramics.

### 3. DISCUSSION

The experimental results presented above show that the DC bias has a much stronger effect upon the pyroelectric behavior of disordered PST ceramic samples than the ordered one. An enhancement factor of 32 for the disordered PST sample was observed under a bias field of 1.5 KV/mm, while for the ordered one the highest enhancement factor is only 5. Since the pyro-signal measured in this work is proportional to the reciprocal of the dielectric constant  $K$ , the decreasing of  $K$  with respect to DC bias field for the ordered and disordered PST<sup>2</sup> should be partially responsible for the enhancement of the pyro-signal under DC biases. However, the ratio of the dielectric constants under DC biases of 0.1 KV/mm and 1.5 KV/mm is less than 5 within the entire-temperature range of the measurement<sup>2</sup>. It would appear that a new extrinsic component of reversible pyroelectricity induced by DC bias must be responsible for the very significant enhancement of the pyro-signal of the disordered PST ceramics under DC bias. The existence of microdomains in relaxor ferroelectrics in the temperature region lower than the temperature of the dielectric maximum  $T_m$  is suggested to be the origin of this new extrinsic component of the reversible pyroelectricity. Under DC bias fields,

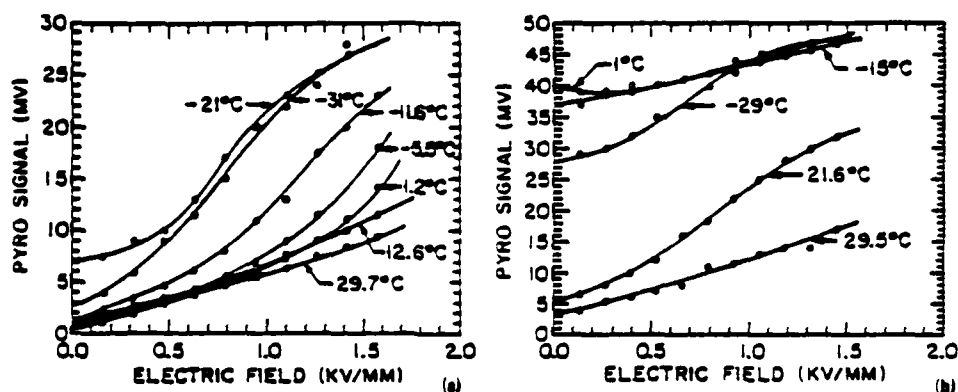


FIGURE 4. The pyroelectric signal as a function of bias field at various temperatures for the disordered (a) and ordered (b) PST ceramics.

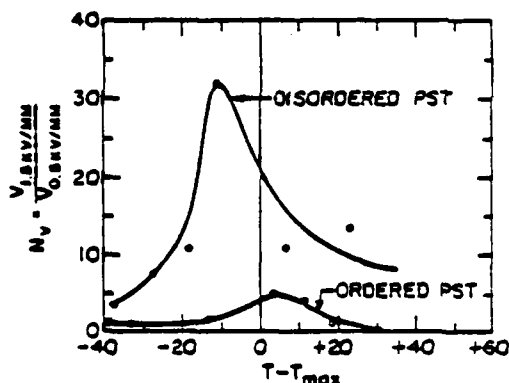


FIGURE 5. The enhancement factor as a function of the temperature difference  $T_{\text{max}} - T$  for the disordered and ordered PST ceramics.

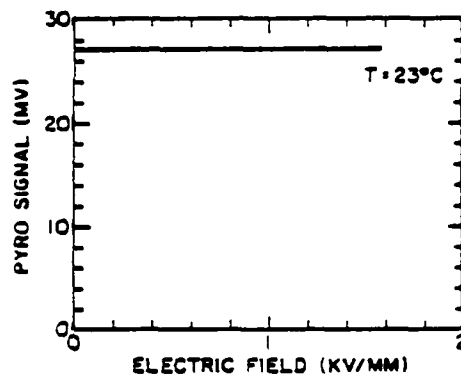


FIGURE 6. The pyroelectric signal as a function of bias field for  $\text{LiNbO}_3$  single crystals.

the large dipole moments of the microdomains, which are oriented in a random way, will experience strong orienting force and build up into macrodomains. Since disordering of the micro regions is a thermalization process, small reversible temperature change can modulate the state of microdomain order and thus contribute a new extrinsic component to the temperature dependence of the induced polarization. In disordered PST material, the direct measurement of the pyroelectric coefficient by Byer-Roundy<sup>6</sup> technique shows that the pyroelectric coefficient peak appears at  $-37^\circ\text{C}$  (Figure 7a), which

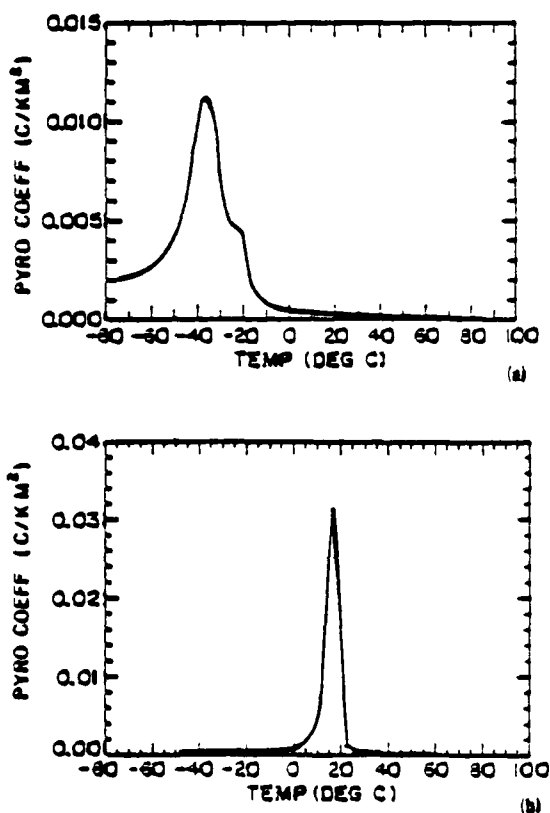


FIGURE 7. The temperature dependence of pyroelectric coefficient of the disordered (a) and ordered (b) PST ceramics.

is 39 degrees below  $T_c$  (1.3°C). The temperature region from -37°C to 1.3°C, which is supposed to be the most active temperature region of microdomains, is well coincident with the temperature region of large enhancement of the pyro-signal for the disordered PST sample, while for the ordered PST material the pyroelectric coefficient peak is 14°C (Figure 7b), which is only three degrees below  $T_c$  (17°C). Since the ordered PST material exhibits more or less normal ferroelectricity, no significant microdomain activity can be traced. The fact that only a factor of five of the largest enhancements of pyro-signal at the temperature five degrees higher than  $T_c$  has been observed in ordered PST samples, means that the DC bias can only induce a rather small displacive polarization in the absence of the microdomains.

The large and field-controllable reversible pyroelectric effect is a promising phenomenon for developing new pyroelectric devices.

#### REFERENCES

1. N. Setter and L.E. Cross, J. Mater. Sci. 15, 2478-2482 (1981).
2. N. Setter and L.E. Cross, J. Appl. Phys. 51 (8), 4356-4360 (Aug. 1980).
3. N. Setter and L.E. Cross, Phys. Stat. Sol. (a) 61, K71 (1980).
4. Chen Zhili, X. Yao and L.E. Cross, to be published.
5. A.G. Chynoweth, J. Appl. Phys. 27 (1), 78-85 (1956).
6. R.L. Byer and C.S. Roundy, Ferroelectrics 3, 133 (1972).

**APPENDIX 22**

# DEPOLARIZATION BEHAVIOR AND REVERSIBLE PYROELECTRICITY IN LEAD SCANDIUM-TANTALATE CERAMICS UNDER DC BIASES

CHEN ZHILI\*, YAO XI\*\* AND L.E. CROSS  
Materials Research Laboratory, The Pennsylvania State  
University, University Park, PA 16802

**Abstract** The depolarization behavior of ordered and disordered lead scandium-tantalate (PST) ceramics has been studied by Byer-Roundy and Chynoweth method. A sharp decrease of the spontaneous polarization takes place in a narrow temperature range very close to the Curie temperature  $T_C$  for the ordered PST materials. For the disordered PST materials, however, the depolarization takes place within a wide temperature range much lower than the temperature of maximum dielectric constant  $T_m$ . Evidence of microdomain activities has been observed in disordered materials. The reversible pyroelectric effect is discussed in terms of the micro-macro transition of the domains in disordered PST materials.

## INTRODUCTION

Earlier studies have shown that in the lead scandium-tantalate  $Pb(Sc_{1/2}Ta_{1/2})O_3$  (PST) single crystal and ceramics which are of simple perovskite structure, the B-site cations in the  $ABO_3$  structure are close to the boundary of order and disorder<sup>1</sup>. The degree of ordering of the B-site cations can be controlled thermally. The quenched materials with disordered structures are relaxor ferroelectrics with diffuse phase transitions, while the well annealed materials with ordered structure exhibit "normal" sharp first order ferroelectric transition. The dielectric and ferroelectric properties of PST materials have been reported<sup>2,3</sup>. The dielectric and pyroelectric properties under DC biases have also been studied<sup>4,5</sup>. A reversible pyroelectric effect under DC bias in disordered PST ceramics has been explored.

In this paper, the depolarization behavior of order and disorder PST materials using both Byer-Roundy<sup>6</sup> and Chynoweth<sup>7</sup> method are given. The ordering of microdomain region is believed to be responsible for the reversible pyroelectricity. The microdomain activity in disordered PST ceramics is very similar to that explored in PLZT ceramics<sup>8</sup>.

\*Visiting Scientist from Shanghai Institute of Ceramics, Shanghai, China.

\*\*Visiting Scientist from Xian Jiaotong University, Xian, China.

EXPERIMENTAL PROCEDURESSample Preparation

Samples used in this work were prepared by conventional mixed oxide processing. Stoichiometric proportion of  $\text{PbO}$ ,  $\text{Sc}_2\text{O}_3$ ,  $\text{Ta}_2\text{O}_5$  were ball milled in alcohol for 20 hours. The mixture was dried and precalcined at  $800^\circ\text{C}$  for 2 hours. After reground and pellerized, the samples were fired at  $1300^\circ\text{C}$  for one hour using  $\text{PbO}+\text{PbZrO}_3$  as atmosphere controller. A final sintering was performed at  $1560^\circ\text{C}$  followed by rapid air quenching to induce disorder structure. The ordering of the 3-site ions was achieved by thermal annealing at  $1000^\circ\text{C}$  for 24 hours. The degrees of ordering,  $S$ , for quenched and annealed samples are 0.40 and 0.87 respectively. The final density achieved was 94% theoretical with less than 3% weight loss.

The samples used in depolarization studies were 0.2-0.3 mm thick with sputtered gold electrode. The samples were heated to  $150^\circ\text{C}$  at first then poled at  $30^\circ\text{C}$ , 20 kV/cm for 10 min. and cooled under electric field down to  $-70^\circ\text{C}$ . The temperature of dielectric constant peaks of disordered and ordered PST ceramics are  $1.9^\circ\text{C}$  and  $17^\circ\text{C}$  at 1 KHz respectively.

Depolarization Measurements

For the modified Byer-Roundy method, the sample in series with a bias voltage supply was connected to a picoammeter HP 4140B. The sample was heated in a temperature chamber, Delta 2300. Linear temperature ramping with specified ramping rate  $dT/dt$  can be achieved under computer control using the HP 9825A desktop computer. Pyroelectric coefficient, which is proportional to the thermal current, can be measured directly. The depolarization curve can be obtained by integration of the thermal current with respect to time.

A modified Chynoweth method has been used in this work. The sample in series with a bias voltage supply was connected to a phase lock amplifier model PAR HR-8 through a preamplifier and a blocking capacitor. The sample was heated by a chopped light beam with chopping frequency around 5.5 Hz. The pyroelectric signal, which can be read from the output voltmeter of the phase-lock amplifier, is proportional to  $p/KC_p$ , here  $p$ -- pyroelectric coefficient,  $K$ -- dielectric constant,  $C_p$ -- specific heat of the sample.

EXPERIMENTAL RESULTS AND DISCUSSION

Figure 1 and 2 are the pyroelectric coefficients and depolarization curves of the ordered and disordered PST materials under different bias fields using the Byer-Roundy method. Although the spontaneous polarization of the ordered and disordered samples are the same, the depolarization behaviors are quite different. For the ordered sample, a sharp decrease of spontaneous polarization takes place in a narrow temperature range very close to the Curie temperature  $T_c$  ( $17^\circ\text{C}$ ) at zero bias field. Higher bias field shifts the transition toward higher temperature. However, the



# DEPOLARIZATION BEHAVIOR AND REVERSIBLE PYROELECTRICITY IN...

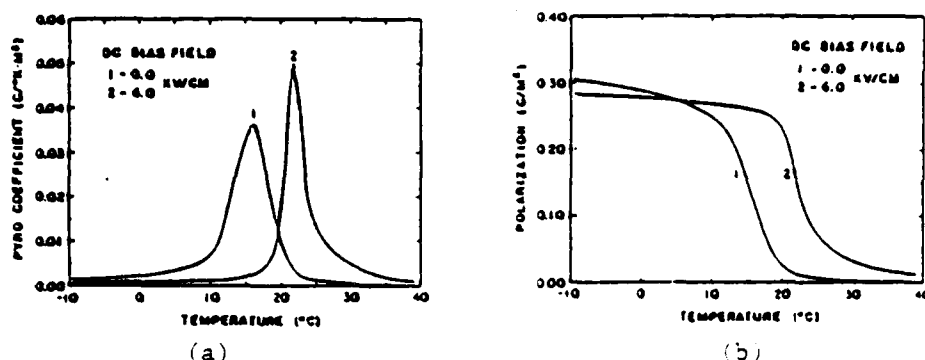


Figure 1. Pyroelectric coefficient (a) and depolarization curve (b) of ordered PST ceramics.

shape of the depolarization curve has no significant change. A first order transition for the ordered material is quite evident. For the disordered materials, the depolarization takes place in a wide temperature range much lower than the temperature of maximum dielectric constant  $T_m$  (1.9°C) at zero bias field. Higher bias field also pushes the depolarization toward higher temperature range. However, a sharp decrease of the spontaneous polarization and an elongated tail section of the depolarization curve under bias field are quite evident. The effect of the bias field is more evident on the temperature dependence of the pyroelectric coefficient as shown in Figure 2(a). Under zero bias field a concealed terrace is clearly shown in the low temperature region of the pyroelectric coefficient curve. Under small DC bias field, the concealed terrace disappears, the temperature dependences of the pyroelectric coefficient become more "normal". In this respect, we can assume that a DC bias drives a diffused phase transition of a relaxor ferroelectric toward a normal first order transition.

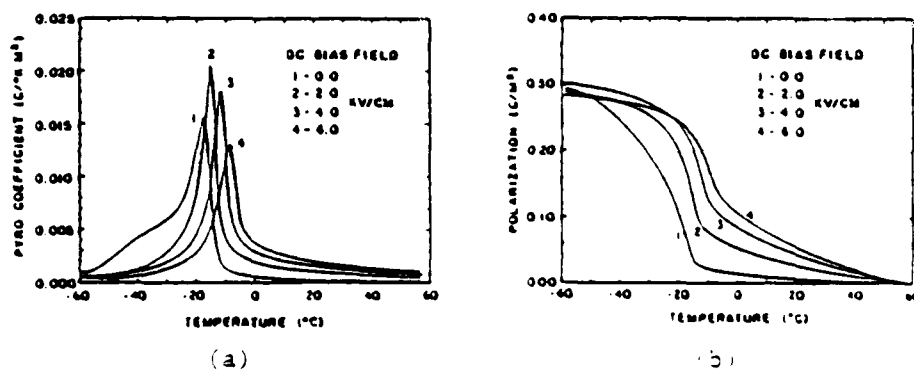


Figure 2. Pyroelectric coefficient (a) and depolarization curve (b) of disordered PST ceramics.

The depolarization curves of ordered and disordered PST materials taken from Chynoweth method also exhibit the same characteristic, as shown in Figures 3 and 4. A very sharp decrease of the pyrosignal is clearly shown in Figure 3 for the ordered materials, while a rather wide temperature range of the decreasing of the pyrosignal is observed in Figure 4 for the disordered sample.

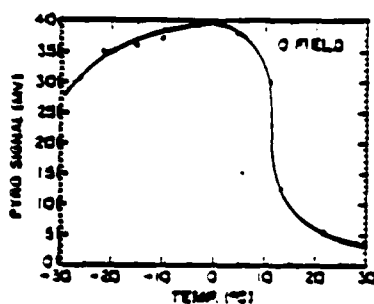


Figure 3. Pyrosignal of ordered PST ceramics (arbitrary scale).

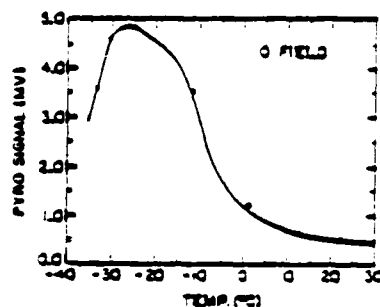


Figure 4. Pyrosignal of disordered PST ceramics (arbitrary scale).

A smooth and gentle decrease of the spontaneous polarization with respect to temperature change in the depolarization curve of a relaxor ferroelectric is very important for the reversible pyroelectric effect. It is in this temperature region that the highest enhancement of pyroelectric signal of disordered PST has been observed<sup>5</sup>.

The detailed mechanism of the reversible pyroelectricity is still not yet known, however, it is believed that the microdomain activity is of vital importance.

In our early works, the evidence of microdomain activities in PLZT ceramics has been given<sup>8</sup>. The depolarization behavior of disordered PST materials also presents apparent trace of the microdomain activities. The splitting of highly polarized macrodomains into random oriented microdomains may be responsible for the smooth decreasing of the polarization and the appearance of the high terrace of the pyroelectric coefficient at zero bias field in Figure 2. A small DC bias field drives the random oriented microdomains into highly polarized metastable macrodomains keeping the material in high polarization level. The DC bias also plays as a restoring force of the polarization during temperature fluctuation. Therefore, a high enhancement of pyrosignal accompanied with reversible effect results.

The kinetics of the micro-macro transition of the domains in relaxor ferroelectrics is another critical point for the reversible pyroelectric effect. In disordered PST materials, the micro-macro

## DEPOLARIZATION BEHAVIOR AND REVERSIBLE PYROELECTRICITY IN...

transition is fast enough to respond to a temperature fluctuation of 5.5 Hz (about 200 mS), while under the same condition no reversible ferroelectric effect has been observed in PLZT ceramics with composition 8:65:35. The experimental results on the kinetic behavior of the micro-macro transition in PLZTs<sup>3</sup> show that the transition is much slower than that of PST materials. An interesting question is how fast the micro-macro transition can respond to the temperature fluctuation. A detailed study on the kinetic behavior of the micro-macro transition of domains is now still continuing.

### SUMMARY

The depolarization of ordered PST materials takes place in a narrow temperature range close to its Curie temperature, while for the disordered materials the depolarization takes place in a wide temperature range much lower than the temperature of maximum dielectric constant.

Evidence of microdomain activity has been observed in disordered PST materials. The micro-macro transition of domains in relaxor ferroelectrics is believed to be responsible for the reversible pyroelectric effect.

### REFERENCES

1. N. Setter and L.E. Cross, J. Mat. Sci. **15**, 2473-2482 (1981).
2. N. Setter and L.E. Cross, J. Appl. Phys. **51**(3), 4356-4360 (1980).
3. N. Setter and L.E. Cross, Phys. Stat. Sol. (a) **61**, K71 (1980).
4. Chen Zhili, Yao Xi and L.E. Cross, to be published.
5. Chen Zhili, Yao Xi and L.E. Cross, to be published.
6. R.L. Byer and C.B. Roundy, Ferroelectrics **3**, 333 (1972).
7. A.G. Chynoweth, J. Appl. Phys. **27**(1), 73-85 (1956).
8. Yao Xi, Chen Zhili and L.E. Cross, to be published.

**APPENDIX 23**

# Polarization and depolarization behavior of hot pressed lead lanthanum zirconate titanate ceramics

Yao Xi,<sup>a)</sup> Chen Zhili,<sup>b)</sup> and L. E. Cross

Materials Research Laboratory, The Pennsylvania State University, University Park, Pennsylvania 16802

(Received 22 November 1982; accepted for publication 28 February 1983)

A detailed study of the polarization and depolarization behavior of 7:65:35 and 8:65:35 lead lanthanum zirconate titanate transparent ceramics under dc bias and constant heating rates has been carried out. The dielectric permittivity exhibits a new anomaly near 0 °C in freshly thermally depoled samples which is associated with a buildup of macrodomains and the development of a remanent polarization. From continuity of the dispersive behaviors it is suggested that the dielectric change at the so-called  $\alpha$ - $\beta$  transition  $T_d$  is not a conventional phase change, but rather is a loss of macro-ordering and a decay back to a disordered microdomain texture.

PACS numbers: 77.60. + v

## I. INTRODUCTION

The thermal depolarization behavior of electrically poled lead lanthanum zirconate titanate (PLZT) ceramics with compositions in the range of  $\text{PbZr}_{0.65}\text{Ti}_{0.35}\text{O}_3$  with  $\text{La}_2\text{O}_3$  additions of 6-, 7-, and 8-mole%  $\text{La}_2\text{O}_3$  have been of interest for the behavior of the pyroelectric current, dielectric response, and electro-optic characteristics.<sup>1-3</sup> It was clear from the early studies of Keve<sup>4</sup> that depolarization of a short-circuited PLZT of composition 7:65:35 occurs at a temperature well below that of the dielectric permittivity maximum. Dielectric data of Salaneck<sup>5</sup> suggest that the  $K'$  maximum is strongly dispersive as in ferroelectrics with diffuse phase transitions (relaxors). More recent measurements by Kimura, Newnham, and Cross<sup>6</sup> of the elastic shape memory effect suggest that the shape changing ferroelastic macrodomains are lost in these ceramics at the lower depoling temperature.

The present study was undertaken to explore more fully both the poling and depoling characteristics of transparent hot pressed PLZT's of 7:65:35 and 8:65:35 composition. Data presented here are for the 8:65:35 composition; however, the 7:65:35 material gives qualitatively similar results in every respect. To avoid, as far as possible, domain stabilization of the type demonstrated by Schulze, Biggers, and Cross,<sup>7</sup> all measurements were made on annealed and freshly thermally quenched samples.

## II. SAMPLE PREPARATION

Ceramics used in these studies were originally prepared at the Shanghai Institute of Ceramics in China. The designations 7:65:35 and 8:65:35 indicate in the conventional manner a zirconia:titania ratio of 65:35 mole% and a substitution of 7 and 8 mole% of  $\text{La}_2\text{O}_3$  for  $\text{PbO}$ . The samples were prepared from reagent grade nitrate salts of lanthanum and zirconium and reagent grade  $\text{TiCl}_3$ . The salts were dissolved in distilled water and the solutions mixed in the desired proportions. Mixed solutions were then coprecipitated by addi-

tion of ammonia to maintain a pH value of 8. After thorough washing to remove  $\text{NO}_3^-$  and  $\text{Cl}^-$  ions, the precipitates were spray dried at high temperatures. Reagent grade  $\text{PbO}$  powder in 10% excess of the required stoichiometric proportion was then added and the powders ball milled in polyethylene lined jars in acetone for 6 h. The slurry was again dried and cold pressed slugs of suitable dimensions were hot pressed in an  $\text{O}_2$  atmosphere at 1150 °C for 16 h under a uniaxial stress of 200 kg/cm<sup>2</sup>.

Boules of near theoretical density, high transparency, and a mean grain size of 2  $\mu\text{m}$  resulted.

## III. EXPERIMENTAL PROCEDURE

Samples of PLZT were cut with a string saw and then ground to the thickness used for dielectric measurements, generally 0.1 to 0.2 mm. Electrodes used were sputtered gold. The diameter of the electroded area was around 5 mm. Samples were annealed at 600 °C for 1 h and then followed by slow cooling.

The dielectric properties of PLZT were measured by a computerized automatic measuring system with Hewlett-Packard's new generation of microprocessor-based equipment. The biased temperature dependence of dielectric constant and loss tangent were measured by a multifrequency LCR meter, HP 4274A and 4275A in the frequency range of  $10^2$ – $10^7$  Hz, with basic accuracy of 0.1%. The biased pyroelectric currents were measured with the HP4140B picoampere meter. A Delta Design model 2300 environment chamber covered the temperature range from –150 to 200 °C, using liquid nitrogen as a coolant. Temperatures were measured with a Fluke 3502A digital multimeter via a platinum resistance thermometer mounting directly on the ground electrode of the sample fixture. A HP 9825A desktop computer was used for on-line control of automatic measurement through a HP 6904B multiprogrammer interface. All the data were recorded on flexible magnetic discs. Special software was developed for automatic measurement. Linear temperature change with specified rates was easily achieved. The reproducibility of measurements was excellent.

All the measurements were made on freshly thermally

<sup>a)</sup> Visiting scientist from Xian Jiaotong University, Xian, China.

<sup>b)</sup> Visiting scientist from Shanghai Institute of Ceramics, Shanghai, China.

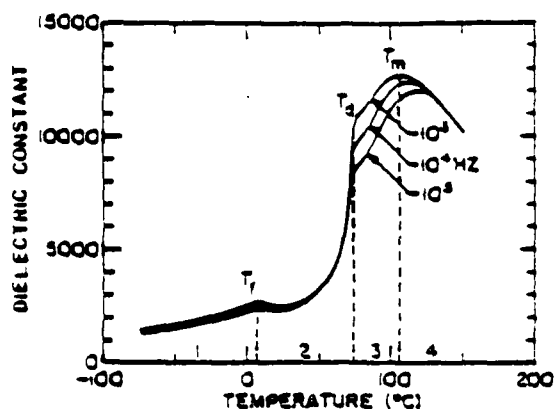


FIG. 1. Temperature dependence of dielectric constant of PLZT 3:65:35 under dc bias of 3 kV/cm at heating rate of 3 °C/min.

depoled samples. Samples were heated above 150 °C, then cooled down below -75 °C. Bias was applied at -75 °C and then the sample reheated from this temperature.

#### IV. EXPERIMENTAL RESULTS

The temperature dependence of the weak field dielectric permittivity at several frequencies applied to an 8:65:35 PLZT ceramic under a dc bias of 3 kV/cm applied at -75 °C and measured on slow heating (3 °C/min) is shown in Fig. 1. The peak labeled  $T_1$  observed near 0 °C is a new phenomenon heretofore unobserved in this system, and appears to divide the response into four distinct regions. There

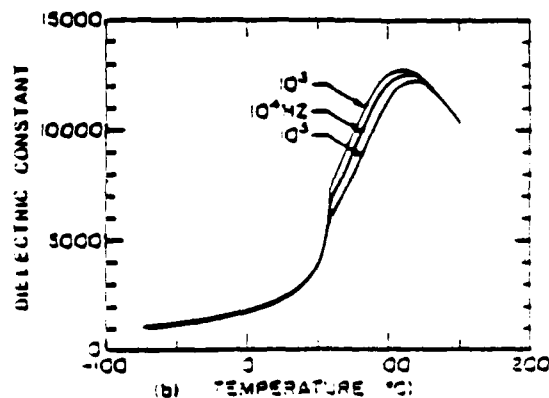
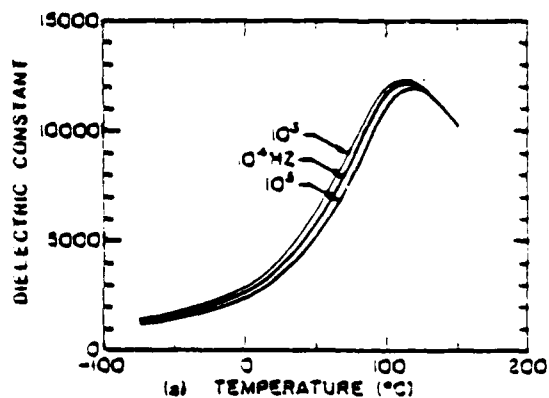


FIG. 2. Temperature dependence of dielectric constant of PLZT 3:65:35 (a) without and (b) under dc bias of 3 kV/cm at cooling rate of 3 °C/min.

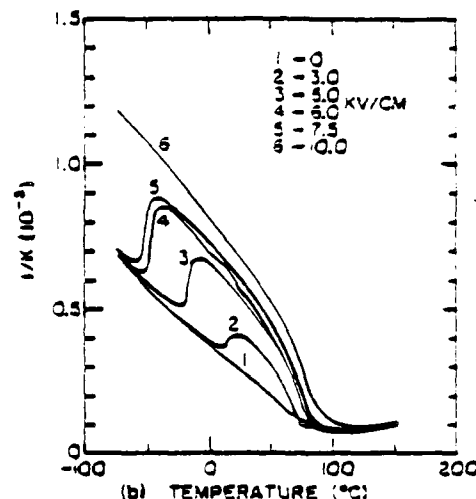
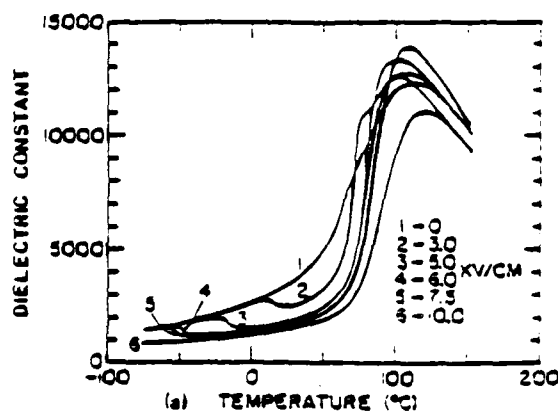


FIG. 3. Temperature dependence of (a) dielectric constant  $K$  and (b) dielectric stiffness  $1/K$  of PLZT 3:65:35 under different bias field at constant heating rate.

is a dispersive region below  $T_1$  (1), a largely nondispersive region between  $T_1$  and  $T_2$ , a temperature often referred to as the  $\alpha$ - $\beta$  phase change (2), a second dispersive region between  $T_2$  and  $T_m$ , the temperature of the dielectric maximum (3), and a second nondispersive region above  $T_m$  (4).

In a sample cooled without bias from above  $T_m$ , regions (1) and (3) cojoin filling the whole temperature range below  $T_m$  and appear to be of completely similar property [Fig. 2(a)]. On cooling under dc bias, however,  $T_2$  is reproduced.

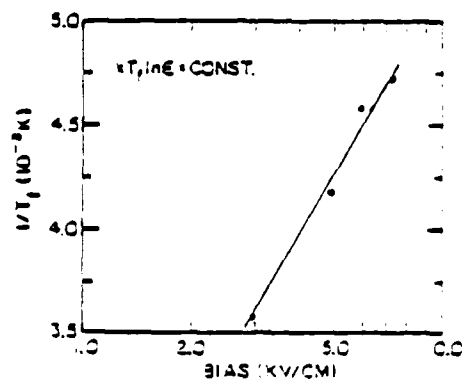


FIG. 4. Linear relation between logarithm of bias field in  $E$  and reciprocal of transition temperature  $1/T_1$ .

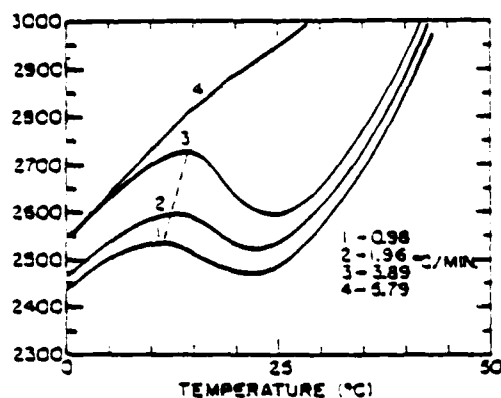


FIG. 5. Kinetic behavior of transition at  $T_g$  under different heating rates.

but region (2) now persists down to the lowest temperatures measured and region (1) is lost [Fig. 2(b)].

At a constant heating rate  $T_g$  shifts to a lower temperature with increasing bias [Fig. 3(a)] the "transition" being most obvious in the dielectric stiffness [Fig. 3(b)]. It would appear that the product  $kT_g \ln E$  is approximately constant over the field range studied (Fig. 4).  $k$  is an arbitrary constant.

For field below 1 kV/cm no  $T_g$  peak was observed, but at intermediate field levels it was clear that the temperature  $T_g$  depends on the heating rate, increasing with faster heating, but being difficult to observe for rates above 5 °C/min (Fig. 5).

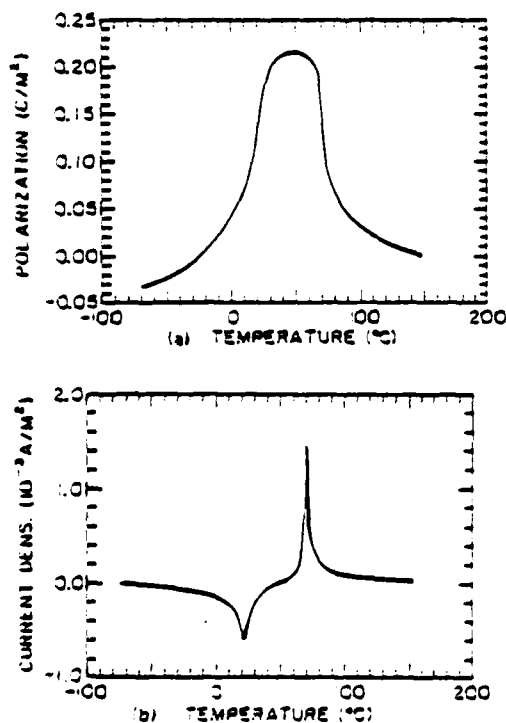


FIG. 6. The buildup and decay of (a) the remanent polarization and (b) associated charging and discharging current of PLZT 3:65:35 under dc bias of 3 kV/cm at constant heating rate.

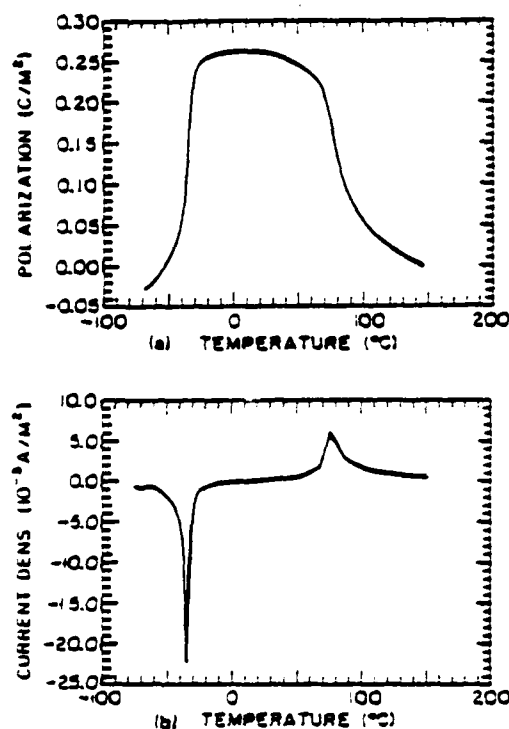


FIG. 7. The buildup and decay of (a) the remanent polarization and (b) associated charging and discharging current of PLZT 3:65:35 under dc bias of 5 kV/cm at constant heating rate.

Prepoled samples do not exhibit the  $T_g$  peak and in no sample could we detect this change on cooling from high temperature. A necessary preconditioning is that the sample be cooled in an unpoled state and the field applied at low temperature.

Aging the sample at temperatures below  $T_g$  appears to preferentially reduce the dispersive component of  $K'$  [Ref. 7] and for such samples the peak at  $T_g$  was smeared. In long aging at low temperature the  $T_g$  peak was often to the point where the change was difficult to discern at all.

That the dielectric changes are associated with the buildup and decay of macropolarization has been confirmed by pyroelectric measurements using the Byer-Roundey<sup>3</sup> technique.

The remanent polarization builds up rapidly in the vicinity of  $T_g$  for a sample heated from the depoled condition under a field of 3 kV/cm [Fig. 6(a)] and the charging current associated with this buildup is evident in the current curve in Fig. 6(b) and is in sharp contrast to the depoling current peak at  $T_g$ . Similar curves for a larger field of 5 kV/cm [Figs. 7(a) and 7(b)] confirm the dielectric trends for  $T_g$  and  $T_d$ .

The asymmetry on cooling is clearly evident in Figs. 3(a) and 3(b) which show that once the macropolarized state is established it does not decay again on cooling. Thus, only the poling current peak is evident in Fig. 3(b).

For a 3-kV/cm field the behavior of prepoled and depoled samples is contrasted directly in Fig. 8.

## V. DISCUSSION

The evidence presented above suggests strongly that neither  $T_f$  nor  $T_d$  are associated with conventional phase changes in the dielectric. The dispersive character below  $T_m$  in the virgin state is similar to that observed in many relaxor ferroelectrics and is attributed to heterophase micro regions which are disordered in the thermally depoled state. Since these "domains" are on a scale much smaller than the x-ray coherence length or the wavelength of light, the structure appears cubic below  $T_m$  to most macroscopic tests.

Under bias fields, the large dipole moments of the microdomains will experience strong orienting force and apparently at  $T_d$  microdomains can build into macrodomains with consequent distortion of the structure, the manifestation of optical birefringence, and the emergence of the shape memory of ferroelastic macrotwins.

Once established below  $T_d$ , the ordered state will persist down to absolute zero, and no lower change is to be expected. Clearly, however, the kinetics of microdomain rearrangement will slow up with reducing temperature. We suggest that for thermally depoled samples in the region below 0°C the kinetics is sufficiently slow that a dc bias is unable to effect reorientation in a reasonable time, and the disordered state persists. If, however, the biased disordered microdomain system is now heated at a constant rate, ordering can occur at a suitable temperature when the rates have speeded up sufficiently. Thus higher fields or slower heating rates will both serve to depress the temperature  $T_f$  of the change from micro- to macro-ordering.

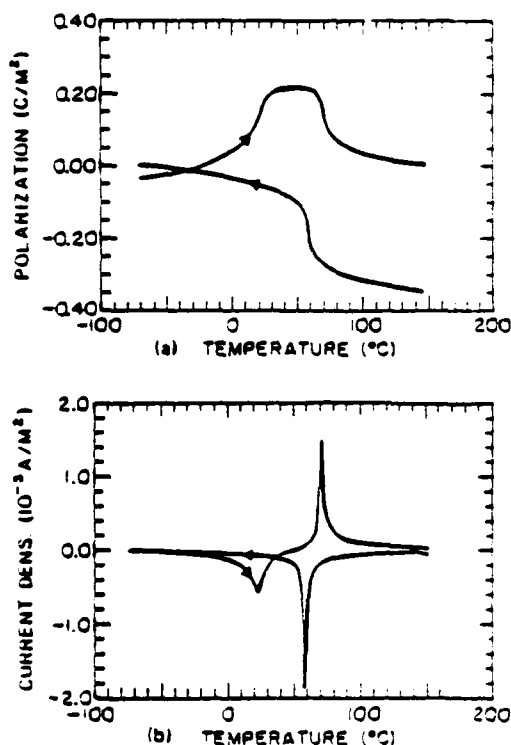


FIG. 3. (a) The remanent polarization and (b) charging-discharging current of PLZT 3:65:35 under dc bias of 5 kV/cm at heating and cooling measurement.

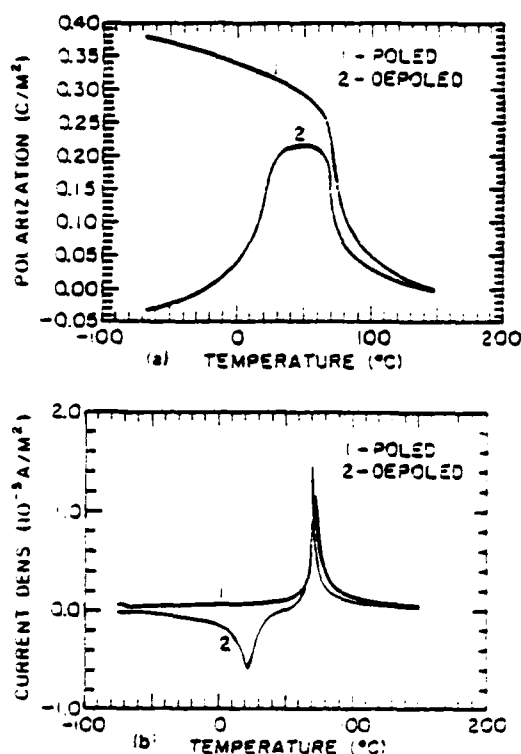


FIG. 3. (a) The remanent polarization and (b) charging-discharging current of prepoled and depoled PLZT 3:65:35 samples under dc bias of 5 kV/cm at constant heating rate.

The sequence of dielectric and pyroelectric observations are consistent with this suggested pattern. If  $T_d$  were an  $\alpha$ - $\beta$  phase change, as has been suggested earlier, then it would necessarily imply that the change at  $T_d$  was a conventional poling phenomenon. In this case the kinetics of the behavior would be difficult to explain, and the clear continuity of the dispersions in regions (1) and (3) for unbiased crystals would be a remarkable coincidence.

On balance we feel that the buildup and decay of macrodomains from polar microregions provide a valid description for all observed phenomena. A more subtle "phase change" explanation may be possible, however, bearing in mind the scale of the polar microregions postulated. Since the onset of a nonzero polarization will occur at a different temperature in each microregion over the temperature range of the dispersive dielectric permittivity peak, it may well be that on a global scale these local onsets should not be considered as phase changes.

In this view then, the crystal may be regarded as being macroscopically cubic over the whole temperature range. Below some temperature  $T_f$  between  $T_d$  and  $T_m$ , this "cubic" nonpolar phase becomes metastable with respect to a macroscopically polar phase and the crystal can be forced into the more stable state by a poling field. Thus  $T_d$  and  $T_f$  may be regarded as a field-forced phase change to a polar state and a thermal depoling into a macroscopically nonpolar state, respectively.

A question of major interest which remains unresolved is the nature of the subgrain heterogeneity in the PLZT which favors relaxor behavior. It may be suspected that the



very high levels of lanthanum doping could give rise to partially ordered planar defects which could serve to interrupt and limit the polarization on the appropriate scale, but much more detailed structure work is required to delineate this heterogeneity.

#### ACKNOWLEDGMENT

The authors wish to thank Mrs. Yin Weiping of the Shanghai Institute of Ceramics for providing the PLZT materials.

- <sup>1</sup>A. H. Meitzler and H. M. O'Bryan, *J. Am. Ceram. Soc.* **55**, 504 (1972).
- <sup>2</sup>G. H. Haertling and C. E. Land, *J. Am. Ceram. Soc.* **54**, 1 (1971).
- <sup>3</sup>G. H. Haertling, *J. Am. Ceram. Soc.* **54**, 303 (1971).
- <sup>4</sup>E. T. Keve and K. L. Byr, *J. Appl. Phys.* **46**, 810 (1975).
- <sup>5</sup>W. R. Salaneck, *J. Appl. Phys.* **43**, 4468 (1972).
- <sup>6</sup>T. Kimura, R. E. Newnham, and L. E. Cross, *Phase Transitions* **2**, 113 (1981).
- <sup>7</sup>W. A. Schulze, J. V. Biggers, and L. E. Cross, *J. Am. Ceram. Soc.* **61**, 41 (1978).
- <sup>8</sup>R. L. Byer and C. B. Roundy, *Ferroelectrics* **3**, 333 (1972).

**APPENDIX 24**

# Dielectric and piezoelectric properties of modified lead titanate zirconate ceramics from 4.2 to 300 K

X. L. ZHANG, Z. X. CHEN, L. E. CROSS, W. A. SCHULZE

*Materials Research Laboratory, The Pennsylvania State University, University Park, Pennsylvania 16802, USA*

The dielectric and piezoelectric properties (d-p properties) of four kinds of doped lead titanate zirconate piezoelectric ceramics (PZTs) have been measured from 4.2 to 300 K. The d-p properties of the materials converge with decreasing temperature down to liquid helium temperature, even though the properties have large differences at room temperature. The values of mechanical and electrical quality factors,  $Q_m$ ,  $Q_e$ , and of the frequency constant,  $N$ , of the materials increased at low temperature. It is evident from the freeze out in  $K'$  and the associate temperature: frequency-dependent maxima in  $\tan \delta$  that the relaxation processes including ferroelectric domain wall motion and thermal defect motion contribute to the d-p properties. The Navy type-III composition has a minimum temperature coefficient of d-p parameters and it is evident that PZT ceramics modified with  $Fe_2O_3$  can provide good stability and also give the strongest piezoelectric response at liquid helium temperature.

## 1. Introduction

PZT ceramics with composition close to the morphotropic phase boundary (MPB) have increased d-p properties [1, 2]. However, most of the practical PZT ceramics are modified by adding different dopants to maximize specific properties. These dopants can be divided into two groups as follows [3]:

(1) "softeners": which cause a decrease in the coercive field, electric and mechanical quality factors, while increasing the dielectric constant and piezoelectric coupling factors. The typical softeners are  $La_2O_3$ ,  $Nb_2O_5$ ,  $Ta_2O_5$  and  $Sb_2O_3$ ;

(2) "hardeners": which cause an increase in the coercive field and quality factors, and a decrease in dielectric constant. The typical hardeners are  $Fe_2O_3$ ,  $MgO$  and  $Sc_2O_3$ .

The mechanisms by which these modifiers act upon the properties are rather complex, but basically, their effects can be explained by the theory of vacancy compensation in the lattice of PZT [4] and of space charge effects [5].

Investigating the d-p properties of modified

PZT ceramics in a wide temperature range should provide some additional information about the mechanisms by which the dopants effect the properties of PZT ceramics and also some information about phase transitions in the PZT system.

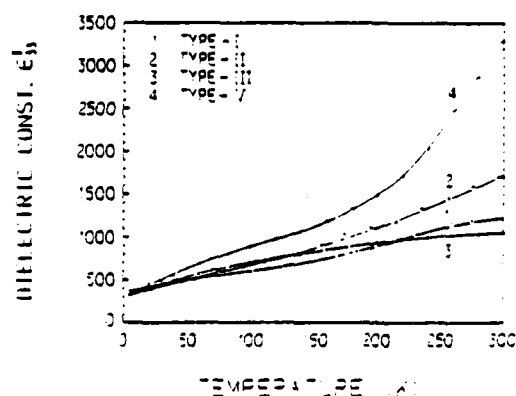


Figure 1 A plot of dielectric constant,  $\epsilon_r$ , against temperature measured at a frequency of 1 kHz, and electric field strength of 10 V/cm<sup>2</sup> for four types of doped PZT ceramics.

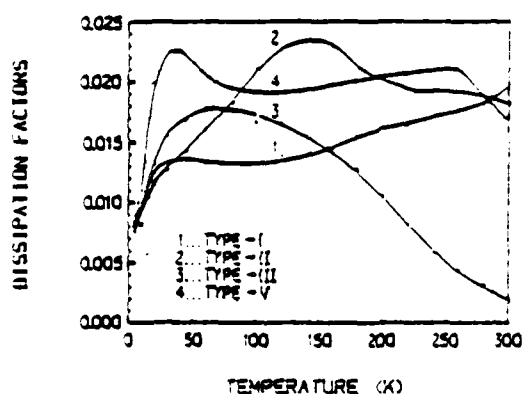


Figure 2 A plot of dissipation factor against temperature measured at a frequency of 1 kHz field strength,  $E_1$ , of  $10 \text{ V cm}^{-1}$  for four types of ceramics.

The study of commercial PZT will also give the application engineers a data base from which to choose PZT types for low-temperature applications.

## 2. Experimental procedure

The samples used in this study were a family of commercial PZT from one manufacturer that are categorized as Navy-type I, II, III, and V. The main compositions of the ceramics is lead titanate zirconate and each type is modified by different dopants. The samples were received in the form of prepoled and silvered discs. When possible, measurements were made on the undisturbed discs, but it was necessary to cut and repole bar-shaped specimens to fill the dimensional requirements of the IRE standards on piezoelectric crystals [6]. When the ceramics were reshaped,

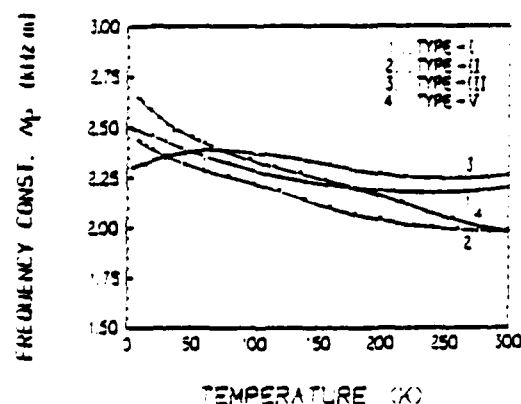


Figure 4 A plot of frequency constant,  $N_p$ , against temperature for four types of PZT ceramics.

fired or sputtered on silver or gold, electrodes were used. All shapes met the dimensional requirements of the standard and were suspended in vacuum by fine Cu or Ag wire.

The resonance measurements were made on a Hewlett Packard spectrum analyser model 3595A and dielectric measurements were made on an automatic capacitance bridge Hewlett Packard Model 4270 or 4275.

## 3. Results and discussion

Figs. 1 and 2 show the temperature dependences of the dielectric constant  $\epsilon_{33}^T$  and dissipation factor in the range 4.2 to 300 K. The  $\epsilon_{33}^T$  and  $\tan \delta$  decreased and converged at very low temperature. This shows that the base composition of the four kinds of ceramics is very close. At room temperature, the  $\epsilon_{33}^T$  were widely separated.

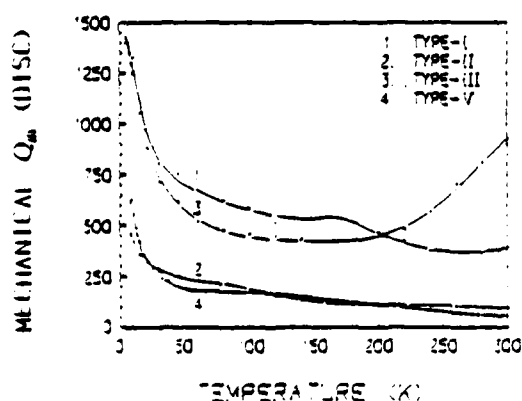


Figure 3 Mechanical  $Q_m$ -temperature dependence for four types of doped PZT ceramics.

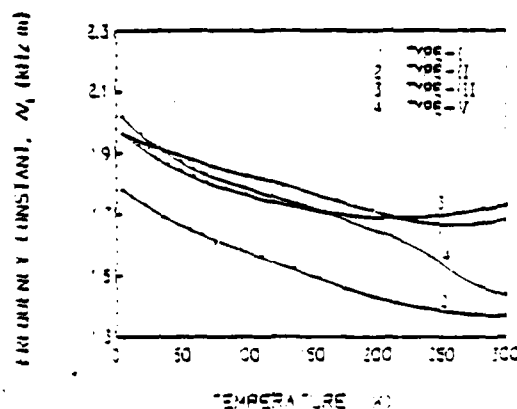


Figure 5 A plot of frequency constant,  $N_p$ , against temperature for four types of PZT ceramics.

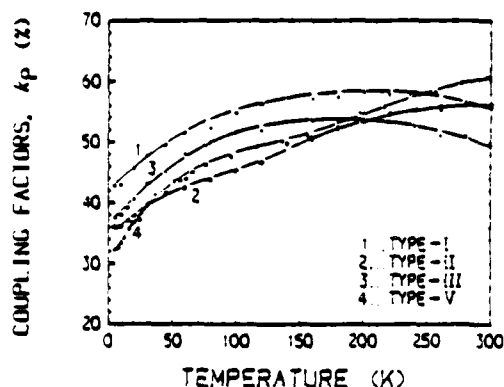


Figure 6 A plot of planar coupling factor,  $k_p$ , against temperature for four types of PZT ceramics.

clearly a result of the different dopants. For types I and III, which are the hard materials modified by hardeners NiO and  $\text{Fe}_2\text{O}_3$ , respectively, the permittivity is smaller. The soft materials, types II and IV, which were modified by softeners  $\text{Nb}_2\text{O}_5$  and  $\text{Sb}_2\text{O}_3$ , respectively, have higher permittivity. From Fig. 2 it can be seen that every sample has a characteristic  $\tan \delta$  peak; it suggested that there is at least one relaxation process for each sample in this range of temperature. The relaxation processes could be connected with the impurity ions and with domain walls or phase-boundary motion. At very low temperature, these thermally activated effects are "frozen" out which makes the  $\epsilon_{33}^T$  and  $\tan \delta$  converge to the average of the intrinsic single-domain properties.

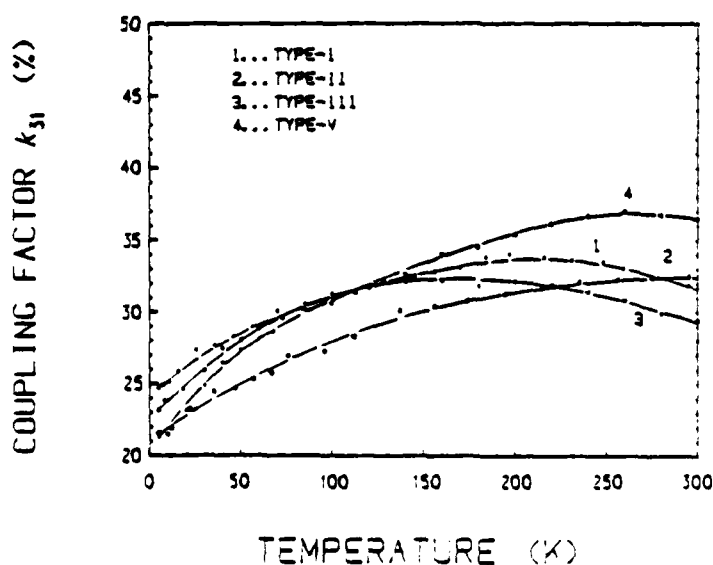


Figure 7 A plot of coupling factor,  $k_{31}$ , against temperature for four types of PZT ceramics.

Figs. 3 to 5 show the mechanical quality factor,  $Q_m$ , and frequency constant  $N_p$  (planar) and  $N_t$  (thickness). The  $Q_m$  of hard materials, types I and III, are much larger than those of the softer materials. Because the relaxation processes are "frozen" out,  $Q_m$  becomes very high for all of the samples at very low temperature. For hard materials I and III, the temperature coefficient of  $N_p$  and  $N_t$  are much smaller than for the softer materials. All of the frequency constants decreased with increasing temperature, except for type III: its  $N_p$  is anomalous in the 4.2 to 80 K range.

The PZT system has intrinsically p-type conductivity resulting from excess Pb vacancies [7]. If 5-valence ions replace  $\text{Zr}^{4+}$  or  $\text{Ti}^{4+}$ , or 3-valence ions replace  $\text{Pb}^{2+}$  (or vacancies of  $\text{Pb}^{2+}$ ), they behave as donors. The donors decrease the conductivity by electron-hole compensation. The aliovalent ions which enter the lattice and replace the  $\text{Pb}^{2+}$  or  $\text{Zr}^{4+}$  or  $\text{Ti}^{4+}$ , provide the relaxation ions that contribute to the dielectric polarization and piezoelectric properties. The motions of relaxing ions under stress is an intrinsically lossy process [8], and therefore reduces the electrical and mechanical quality factors,  $Q_e$  and  $Q_m$ , even though the d.c. resistivity is increased.

Because of additional polarizability associated with the defects, the "soft" materials have larger coupling factor values and piezoelectric constant values than "hard" materials at higher temperature, as can be seen in Figs. 6 to 10. "Hard" materials, types I and III, have smaller  $k$  and  $d$  values, and

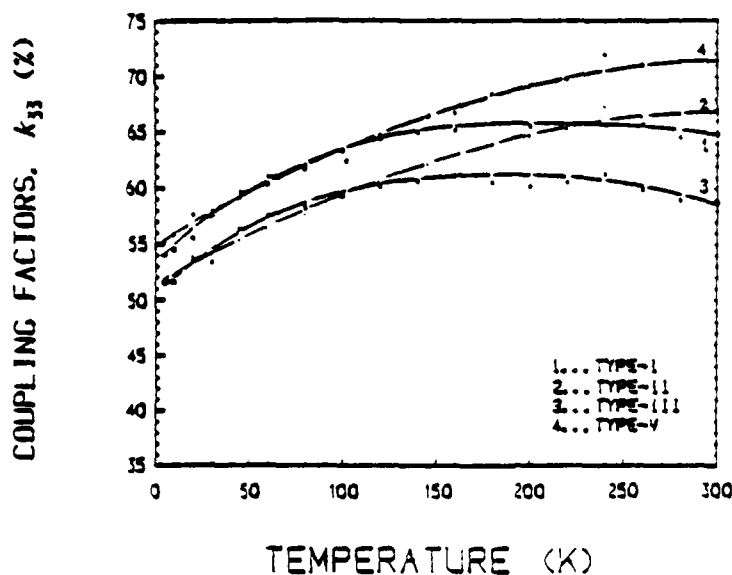


Figure 8 A plot of coupling factor,  $k_{33}$ , against temperature for four types of PZT ceramics.

also smaller temperature coefficient of  $\epsilon$ ,  $k$ , and  $d$  parameters. The effects of "hardeners" are in many ways opposite to that of the "softeners". They behave as acceptors, not as donors. For example, the impurity ion of type III as  $\text{Fe}^{3+}$  (or  $\text{Fe}^{2+}$ ). Since its ionic radius is very close to the radius of  $\text{Zr}^{4+}$  or  $\text{Ti}^{4+}$ , the  $\text{Fe}^{3+}$  ion enters the  $\text{Pb}(\text{Ti}_{1-x}\text{Zr}_x)\text{O}_3$  lattice to replace  $\text{Ti}^{4+}$  or  $\text{Zr}^{4+}$ . In this location it lacks an outer electron and acts as an acceptor to make the hole concentration increase, producing a more strongly p-type ceramic. The modification with  $\text{Fe}^{3+}$  creates oxygen vacancies and therefore tends to limit its own

solubility in the PZT lattice. Polarization stiffening has been postulated to occur by the orientation of slowly reorientable defect dipoles in the lattice and by space charge development at the grain boundary where the exsolved additional  $\text{Fe}^{3+}$  may be compensated by domain polarization or may give rise to a second phase. The acceptor dopant additions contribute little to the polarizability and actually stiffen out some of the extrinsic polarizability of the pure material. The limited stiffening of the hard material (types I and III) with reduced temperature is qualitatively explained by this effect.

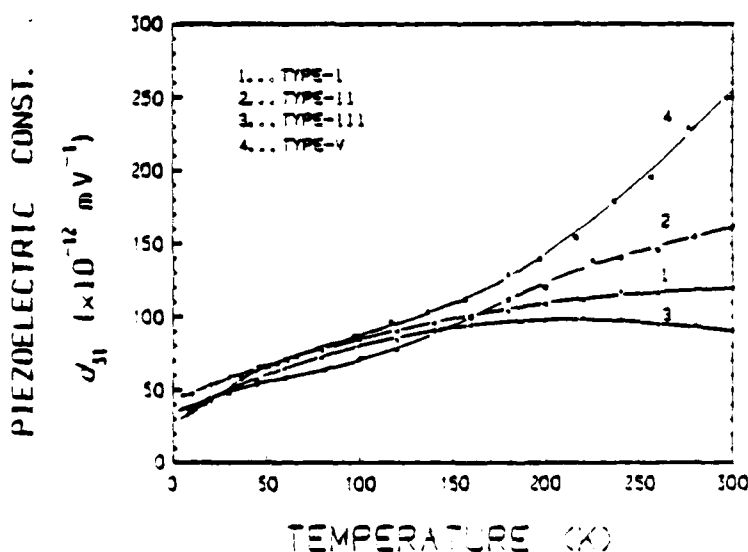


Figure 9 A plot of piezoelectric constant,  $d_{31}$ , against temperature for four types of PZT ceramics.

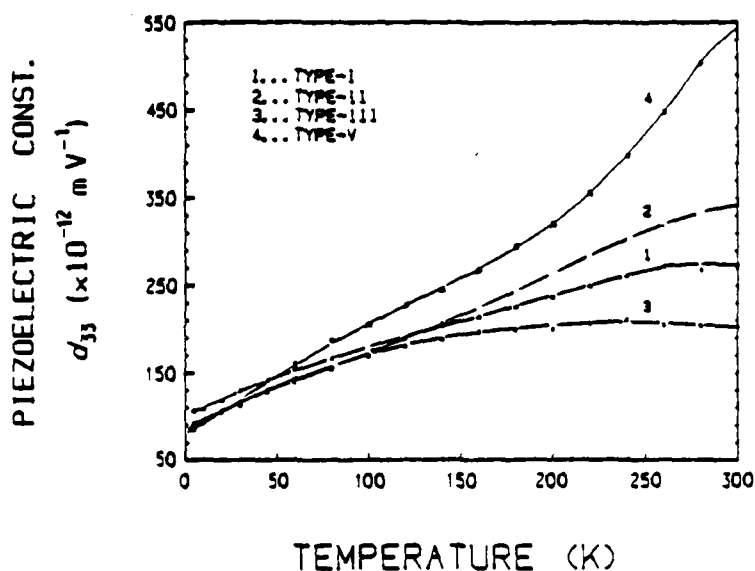


Figure 10 A plot of piezoelectric constant,  $d_{33}$ , against temperature for four types of PZT ceramics.

The second mechanism that may alter the d-p properties with reduced temperature is a change in phase content (tetragonal-rhombohedral) due to a finite temperature dependence of the morphotropic boundary. Some evidence for this shift may be contained in the temperature dependence of  $\tan \delta$ , but the maxima as observed in Fig. 2 could also be associated with minor dielectric relaxation processes.

#### 4. Conclusions

The main d-p properties of four kinds of doped PZT ceramics (two of them hard materials, another two soft materials) have been measured from 4.2 to 300 K. The hard materials (types I and III) have smaller dielectric and piezoelectric activities, but they also have smaller temperature coefficients of d-p parameters. For very low temperature application, they may, in fact, be preferable to the soft materials. In both types of doped materials, evi-

dence for dielectric relaxation mechanisms is given by the temperature-frequency course of the permittivity and  $\tan \delta$ , and it is clear that the processes are significantly different in the two cases.

#### References

1. B. JAFFE, W. R. COOK, Jr and H. JAFFE, "Piezoelectric Ceramics" (Academic Press, London, New York, 1971).
2. Y. H. XU, "Ferroelectric and Piezoelectric Materials" (in Chinese) (Scientific Publishing Co., Beijing, China, 1978).
3. H. THOMANN, *Ferroelectrics* 4 (1972) 141.
4. *Idem*, *Z. Angew. Phys.* 20 (1966) 554.
5. M. TAKAHASHI, *Jap. J. Appl. Phys.* 9 (1970) 1236.
6. "IRE Standard on Piezoelectric Crystals", *Proc. IRE* 46 (1958) 764.
7. M. TAKAHASHI, *Jap. Appl. Phys.* 10 (1971) 143.
8. R. GERSON, *J. Appl. Phys.* 33 (1962) 830.

Received 9 July

and accepted 12 July 1982

**APPENDIX 25**



# THE FERROIC PHASE TRANSITION BEHAVIOR OF $\text{Pb}(\text{Zr}_{0.6}\text{Ti}_{0.4})\text{O}_3$

A. AMIN

Advanced Development Laboratory, Texas Instruments, Inc.,  
Attleboro, MA 02703

L.E. CROSS

Materials Research Laboratory, The Pennsylvania State  
University, University Park, PA 16802

**Abstract** Neutron diffraction and diffuse neutron scattering experiments upon samples of chemically co-precipitated  $\text{Pb}(\text{Zr}_{0.6}\text{Ti}_{0.4})\text{O}_3$  PZT reveal an interesting diffuse behavior, and a modulation of the background intensity. The observations are consistent with the development of a short range order, either in the Zr:Ti distribution, or in the occurrence of a precursor for the ferroelectric tetragonal phase which becomes stable at the morphotropic composition. To test the latter hypothesis, a phenomenological energy function has been used to calculate the separation in free energy  $\Delta G$ , between tetragonal and rhombohedral forms over the whole temperature range below  $T_c$ .

## INTRODUCTION

The PZT crystalline solution system  $\text{Pb}(\text{Zr}_x\text{Ti}_{1-x})\text{O}_3$  between antiferroelectric lead zirconate ( $\text{PbZrO}_3$ ) and ferroelectric lead titanate ( $\text{PbTiO}_3$ ) embrace a number of extremely important compositions used in the electronic industry. These compositions are grouped close to the morphotropic phase boundary MPB ( $x \approx 0.5$ ) Figure 1. Transducer elements such as sonar transmitters and detectors are made of poled PZT compositions near the MPB where dielectric, piezoelectric, and electromechanical coupling coefficients are unusually high<sup>1</sup>. There are two ferroelectric compositional regions in the PZT phase diagram: (i) A ferroelectric tetragonal ( $P4_{mm}$ ) for  $x = 0$  to  $x \leq 0.5$ ; and (ii) A ferroelectric rhombohedral for  $x > 0.5$ . Furthermore, the rhombohedral region encompasses two crystallographically distinct rhombohedral phases, a high temperature ( $R3m$ ) phase, and a low temperature ( $R3c$ ) modification. The ferroelectric tetragonal and rhombohedral symmetries are derived from the ideal-high temperature-prototypic ( $Pm3m$ ) cubic perovskite structure.

Recent low temperature neutron diffraction and diffuse neutron scattering experiments on chemically coprecipitated  $\text{Pb}(\text{Zr}_{0.6}\text{Ti}_{0.4})\text{O}_3$ <sup>2</sup> revealed some interesting and unusual features: (i) The rhombohedral ( $R3c$ )-rhombohedral ( $R3m$ ) phase transition is

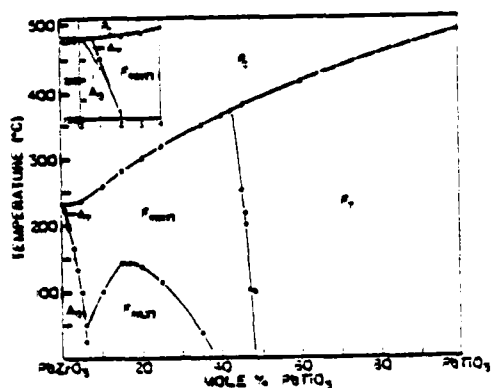


Figure 1. Lead zirconate ( $\text{PbZrO}_3$ )-lead titanate phase diagram (1).

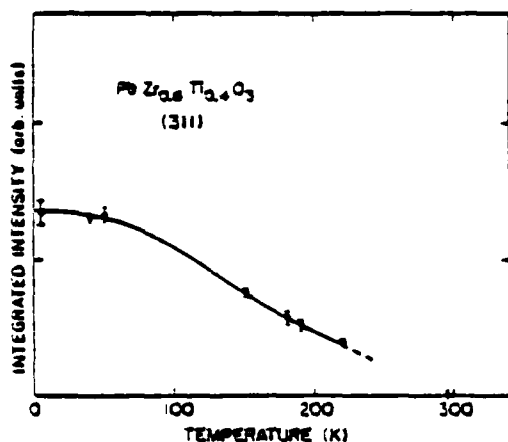


Figure 2. Temperature dependence of the integrated intensity of the pseudocubic 311 reflection.

rather broad, and the transition temperature is not well defined (somewhere between 250 and 300K) as determined from the temperature dependence of the strongest pseudocubic 311 reflection (Fig. 2); (ii) The diffuse neutron scattering data taken at 295 K with 1.65 Å neutrons revealed a quite distinct modulation to the background scattering as can be seen in Figure 3 (lower pattern). This type of background modulation most likely arises from static displacements in preferred directions, since random displacements would simply lead to a monotonically increasing background, as is characteristic of thermal diffuse scattering; (iii) Calculations showed that a simple model involving relaxation of about 0.1 Å of the six oxygen atoms in a  $\text{TiO}_6$  octahedron towards the small Ti atom is qualitatively consistent with the general shape of the curve. However, the 221 K data which were obtained with much better counting statistic (Fig. 3, inset) show some structure in the  $Q$  range  $0.9\text{--}3.0 \text{ \AA}^{-1}$   $Q = (4\pi \sin \theta) / \lambda$ , indicative of additional correlation. These may reflect a short range order which is a precursor of the tetragonal phase, or perhaps a tendency towards ordering of Zr and Ti atoms.

#### PHENOMENOLOGICAL ANALYSIS

In this work, it appeared desirable to use the recently extended thermodynamic phenomenology to examine the relative stability points of the rhombohedral ( $R3m$ ) and tetragonal ( $P4mm$ ) modifications of  $\text{Pb}(\text{Zr}_{0.6}\text{Ti}_{0.4})\text{O}_3$  over the temperature range from 100 K up to the critical point  $T_c$  (640 K). For simple-proper ferroelectrics derived from a prototypic  $Pm3m$  symmetry, the Landau-Ginzburg-Devonshire thermodynamic potential  $G$  takes the form (for Brillouin zone center nodes)

# THE FERROIC PHASE TRANSITION BEHAVIOR OF $\text{Pb}(\text{Zr}_{0.6}\text{Ti}_{0.4})\text{O}_3$

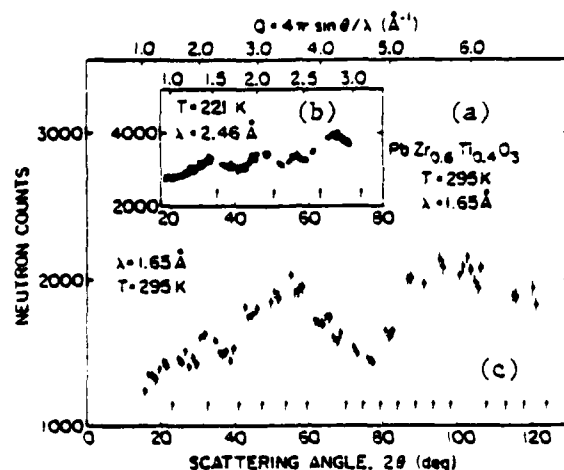


Figure 3. Diffuse neutron scattering from  $\text{Pb}(\text{Zr}_{0.6}\text{Ti}_{0.4})\text{O}_3$ . (a) Data taken at 295 K (1.65 Å neutrons). (b) Data taken with better counting statistics at 221 K (2.64 Å neutrons). Gaps in data corresponds to Bragg peaks. Arrows (c) indicate peak positions derived from a pseudocubic perovskite cell with  $a = 4.08$  Å.

$$\begin{aligned}
 G = & \alpha_1^x (P_1^2 + P_2^2 + P_3^2) + \alpha_{11}^x (P_1^4 + P_2^4 + P_3^4) \\
 & + \alpha_{12}^x (P_1^2 P_2^2 + P_2^2 P_3^2 + P_3^2 P_1^2) + \alpha_{111}^x (P_1^6 + P_2^6 + P_3^6) \\
 & + \alpha_{112}^x (P_1^4 (P_2^2 + P_3^2) + P_2^4 (P_3^2 + P_1^2) + P_3^4 (P_1^2 + P_2^2)) \\
 & + \alpha_{123}^x P_1^2 P_2^2 P_3^2 - \frac{1}{2} s_{11}^P (X_1^2 + X_2^2 + X_3^2) \\
 & - s_{12}^P (X_1 X_2 + X_2 X_3 + X_3 X_1) - \frac{1}{2} s_{44}^P (X_4^2 + X_5^2 + X_6^2) \\
 & - Q_{11} (X_1 P_1^2 + X_2 P_2^2 + X_3 P_3^2) \\
 & - Q_{12} (X_1 (P_2^2 + P_3^2) + X_2 (P_3^2 + P_1^2) + X_3 (P_1^2 + P_2^2)) \\
 & - Q_{44} (X_4 P_2 P_3 + X_5 P_3 P_1 + X_6 P_1 P_2)
 \end{aligned} \tag{1}$$

where  $\alpha_i^x$ ,  $\alpha_{ij}^x$ ,  $\alpha_{ijk}^x$  are related to dielectric stiffness and higher order stiffness coefficients;  $s_{11}^P$ ,  $s_{12}^P$ ,  $s_{44}^P$  are the elastic compliances measured at constant polarization;  $Q_{11}$ ,  $Q_{12}$ ,  $Q_{44}$  are the electrostriction coefficients written in polarization notation.

The expression is complete up to all sixth-power terms in polarization, but contains only first order terms in electrostrictive and elastic behavior.

Tensor coefficients in the free energy function (1) which fit the observed  $\text{PbZrO}_3$ - $\text{PbTiO}_3$  phase diagram and the observed physical properties (dielectric, piezoelectric, and other coupling coefficients) have been determined. In the analysis of the relative stability points as a function of temperature for the rhombohedral and tetragonal modifications of  $\text{Pb}(\text{Zr}_{0.6}\text{Ti}_{0.4})\text{O}_3$  it was assumed that all stresses are absent ( $X_{ij} = 0$ ).

### RESULTS AND DISCUSSION

The temperature dependence of the free energy function of the tetragonal ( $P4_{mm}$ ) and rhombohedral ( $R3m$ ) phases are depicted in Figure 4. The orthorhombic ( $3mm2$ ) modification of the prototypic ( $Pm3m$ ) symmetry is always metastable over the temperature range of interest, and therefore, omitted for clarity. It is obvious from Figure 4 that the rhombohedral phase is the most stable phase over the entire temperature range as suggested by the widely accepted phase diagram (Fig. 1). On the other hand, at temperatures well below the critical point, the tetragonal phase though less stable is close in free energy and this may be reflected as a short range

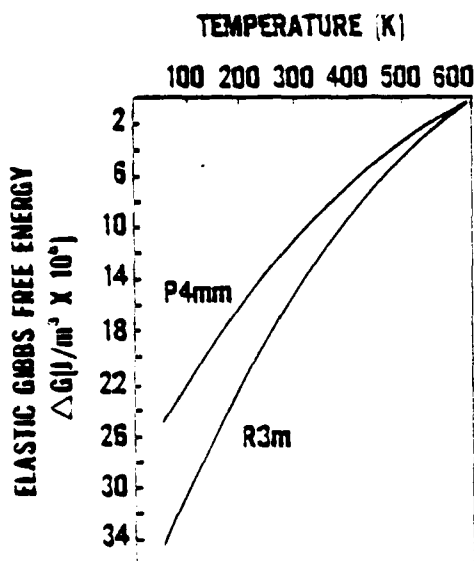


Figure 4. Temperature dependence of the elastic Gibbs functions of the rhombohedral ( $R3m$ ) and tetragonal ( $P4_{mm}$ ) modification of  $\text{Pb}(\text{Zr}_{0.6}\text{Ti}_{0.4})\text{O}_3$ .

precursor of this tetragonal phase occurring as suggested by the diffuse neutron scattering data. However, it is interesting to note that at a temperature 10 K below the critical point (640 K), there is a rhombohedral ( $R3m$ )-tetragonal ( $P4_{mm}$ ) degeneracy. Such a degeneracy implies that the two symmetries coexist with equal probability over a limited temperature range below the critical point. The concept of an extended "different symmetry region" in the lead zirconate-titanate phase diagram was discussed earlier by Isupov<sup>3,4</sup> with regard to the morphotropic phase boundary. Isupov showed that it is energetically possible to have stable tetragonal ( $P4_{mm}$ ) and rhombohedral ( $R3m$ ) phases in the interval from  $X_p$  to  $X_T$  where  $X_T > X_p$  throughout the temperature range from room temperature up to the critical point, although one of these phases can

## THE FERROIC PHASE TRANSITION BEHAVIOR OF $\text{Pb}(\text{Zr}_{0.6}\text{Ti}_{0.4})\text{O}_3$

be metastable relative to the other phase in one part of this interval and vice versa in the other part. Ari-Gur et al.<sup>5</sup> later reported a coexistence region of both rhombohedral and tetragonal morphotropic  $\text{Pb}(\text{Zr}_x\text{Ti}_{1-x})\text{O}_3$  structures. Based on x-ray profile-fitting analysis of morphotropic PZT compositions prepared from mixed oxides (dry technique), the coexistence region was found to extend from  $x = 0.49$  to  $x = 0.64$ . On the other hand, when these compositions were prepared by a "wet-dry combination technique" no coexistence of these two phases was found, and the coexistence behavior was explained in terms of compositional fluctuation<sup>6</sup>. In a recent study, Kakegawa et al.<sup>7</sup> developed a special technique to obtain monophasic-morphotropic PZT ceramic compositions exhibiting no coexistence and no compositional fluctuations in the B-site perovskite structure. The interesting finding of Kakegawa et al. work was that the monophasic compositions exhibited a sluggish  $R3m \rightarrow P4mm$  phase transition or vice-versa as a function of time after poling when they became made up of coexistent tetragonal and rhombohedral phases. In a future work, we intend to use the profile-fitting technique of temperatures close to the critical point of  $\text{Pb}(\text{Zr}_{0.6}\text{Ti}_{0.4})\text{O}_3$  to examine the rhombohedral-tetragonal degeneracy.

### REFERENCES

1. B. Jaffe, W.R. Cook, Jr. and H. Jaffe, Piezoelectric Ceramics, Academic Press, New York (1971).
2. A. Amin, R.E. Newnham, L.E. Cross and D.E. Cox, J. Solid State Chemistry **37**, 248 (1981).
3. V.S. Isupov, Sov. Physics - Solid State **12**(5), 1084 (1970).
4. V.S. Isupov, Solid State Commun. **17**, 1333 (1975).
5. P. Ari-Gur and L. Benguigui, Solid State Commun. **15**, 1077 (1974).
6. K. Kakegawa, J. Mohri, T. Takahashi, H. Yamamura and S. Shirasaki, Solid State Commun. **24**, 769 (1977).
7. K. Kakegawa, J. Mohri, S. Shirasaki and K. Takahashi, J. Amer. Ceram. Soc. **65**, 515 (1982).

**APPENDIX 26**

# CONTINUOUS POLING OF PZT FIBERS AND RIBBONS AND ITS APPLICATION TO NEW DEVICES

T. R. GURURAJA, D. CHRISTOPHER, R. E. NEWNHAM and W. A. SCHULZE

*Materials Research Laboratory, The Pennsylvania State University,  
University Park, PA 16802 USA*

*(Received February 22, 1983)*

A new technique has been developed for poling PZT fibers and ribbons along the length by gradually advancing them past two flexible surface electrodes maintained at the required potential difference. The limitation on poling very thick ribbons posed by the surface electrodes has been determined experimentally. New possibilities in designing composite piezoelectric devices using prepoled PZT fibers and ribbons are presented.

## INTRODUCTION

One of our major interests in the past few years has been in the development of diphasic composite transducer materials made from polymers and lead zirconate titanate (PZT) ceramics with highly improved hydrostatic pressure sensitivity.<sup>1-4</sup> The concept of phase connectivity (the manner in which the individual phases are interconnected) has been used to optimize the electric flux pattern and mechanical stress distributions in attaining remarkable improvement of hydrostatic strain coefficient ( $d_h$ ) and voltage coefficient ( $g_h$ ) over the corresponding values for solid PZT.

Of the several different connectivity patterns studied, PZT-polymer composites with 1-3 connectivity have been investigated most. In addition to its excellent low frequency properties for hydrophone applications, its adaptation to high frequency applications, such as ultrasonic medical diagnosis, appears very promising.<sup>5</sup> These composites with 1-3 connectivity consist of parallel PZT rods embedded in a three dimensional polymer matrix. A detailed procedure for fabricating composites with 1-3 connectivity has been reported by Klicker and co-workers.<sup>6</sup> In brief, PZT-501A\* rods were extruded using an organic binder and then fired at 1285°C for one-half hour. Fired rods were aligned using an array of appropriately spaced holes drilled in a pair of brass discs bolted parallel to each other. The array of PZT rods was then cast in a polymer matrix. The composite so formed was cut perpendicular to the length of the rod and polished to required thickness. The composite was electroded with silver paint on the major surfaces and poled conventionally by applying an electric field of 20 kV/cm across the electrodes for five min in a heated oil bath at 30°C. A high voltage power supply with a range of up to ten kV limits the thickness of the composites to approximately 4 mm. Composites thicker than 4 mm cannot be poled to saturation polarization using a 10 kV power supply. Also, the probability of dielectric breakdown is greater when poling thicker samples. These limitations on the conventional poling have been overcome with a recently developed continuous poling technique for

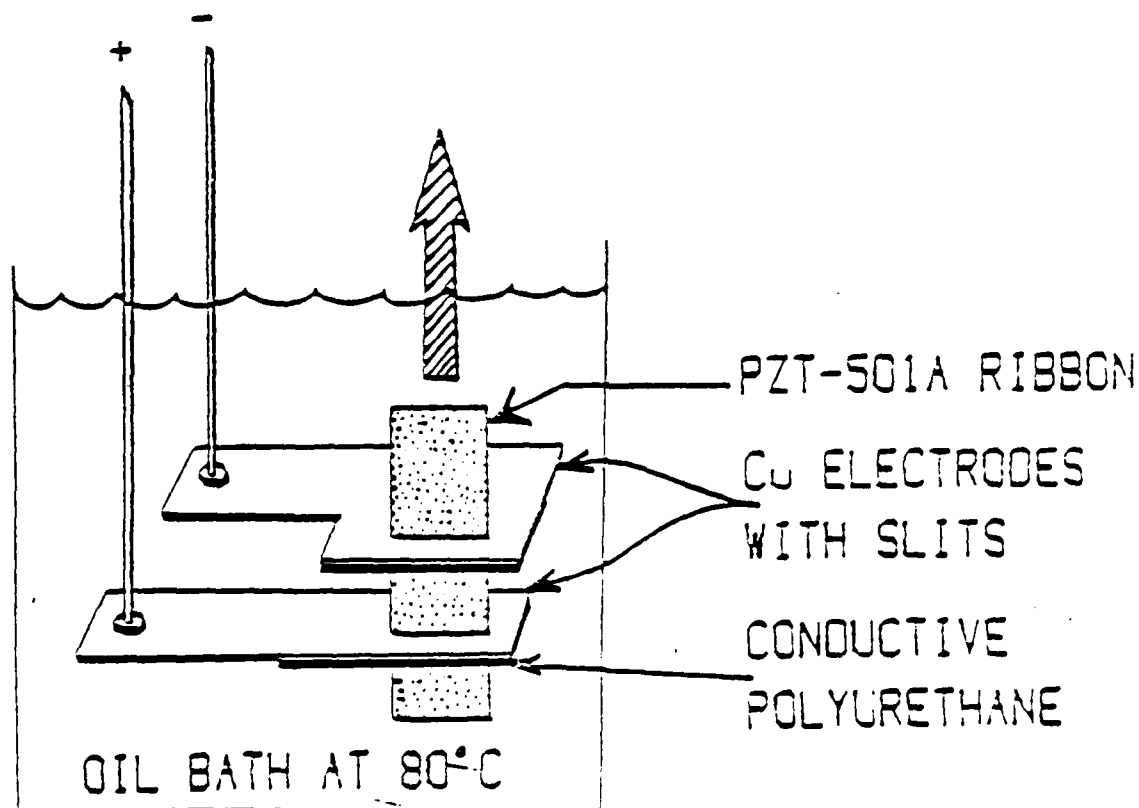
\*Ultrasonics Powders, Inc., South Plainfield, NJ

poling long PZT fibers.<sup>7</sup> In this paper we describe the technique and discuss its geometric limitations in poling large diameter fibers, and mention a few new possibilities for composite devices made from prepoled fibers and ribbons.

### CONTINUOUS POLING TECHNIQUE

The continuous poling technique uses the idea of gradually advancing PZT ribbons or fibers past two flexible surface electrodes maintained at the required potential difference. The experimental arrangement for continuous poling of PZT ribbon is shown in Figure 1. It consists of two metal plates with rectangular collinear slits separated by a distance of 2–4 mm. A carbon-loaded conductive polyurethane strip with an opening for the ribbon to move in the vertical direction was attached to the bottom of each metal plate using conductive silver epoxy. The openings in the metal plate and conductive polyurethane strip were made circular to pole PZT fibers. The conductive polyurethane strips serve as flexible surface electrodes for contacting the PZT ribbons or fibers. The entire system was immersed in an oil bath at 80°C. PZT ribbons were pulled through the openings in the conductive polyurethane and metal plates at a rate of 1 mm per min. An electric field of 20 kV/cm was applied between the two electrodes.

PZT-501A ribbons/fibers of 200 to 600  $\mu\text{m}$  in thickness/diameter and several centimeters long were poled to saturation polarization using this technique. Piezoelectric  $d_{33}$  coefficients, measured using a  $d_{33}$  meter, were in the range of 400 to 450 pC/N which compares favorably with reported  $d_{33}$  value of 400 pC/N of PZT-501A.





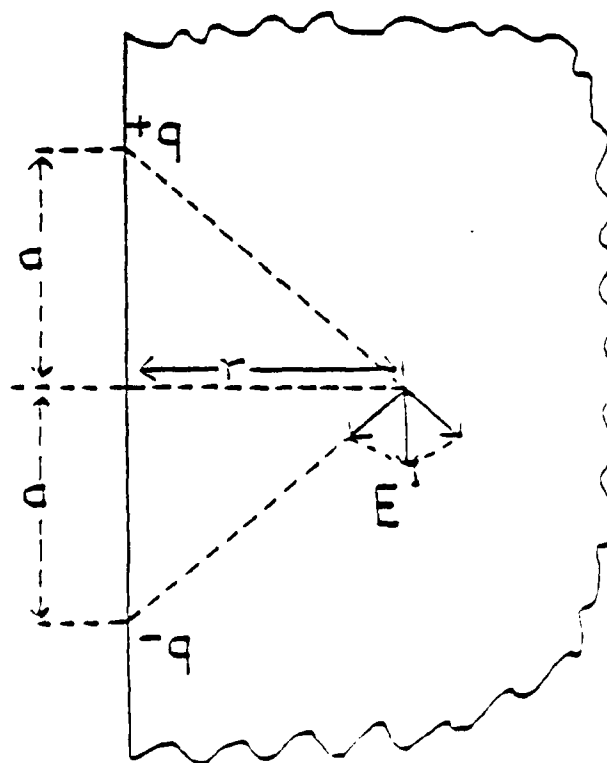
## GEOMETRIC LIMITATIONS

In the continuous poling technique, the conductive polyurethane serves as surface electrodes. The electric lines of force originating and terminating on the surface electrodes are the driving force for aligning the domains in the direction of the electric field. The magnitude of the electric field inside the ceramic for this electrode configuration decreases as a function of distance from the surface of the ceramic. This decrease in field limits the size of the rods and ribbons which can be poled to saturation polarization in the interior portions. However, in this method there is no limitation on the length of rods and fibers that can be poled.

It is possible, as shown in Figure 2(a), to calculate the electric field  $E'$  inside the ceramic as a function of the field  $E$  at the surface by treating the two surface electrodes as an electric dipole with positive and negative charges of equal magnitude. Such an analysis results in the following expression for field  $E'$  along the perpendicular bisector of the two electrodes as a function of depth  $r$ .

$$E' = E \frac{a^2}{(a^2 + r^2)^{3/2}}$$

where  $2a$  is the electrode separation,  $r$  the distance below the surface and  $E$  is the electric field at the surface ( $r = 0$ ). Figure 2(b) gives a plot of  $E'$  for an externally applied field of 20 kV/cm. Since PZT-501A requires an electric field of about 16–18 kV/cm for complete poling, a sample thickness of 0.5 to 0.7 mm can be poled. But since the surface electrodes contact both sides of the sample, it should be possible to pole samples of thickness 1 to 1.4 mm.



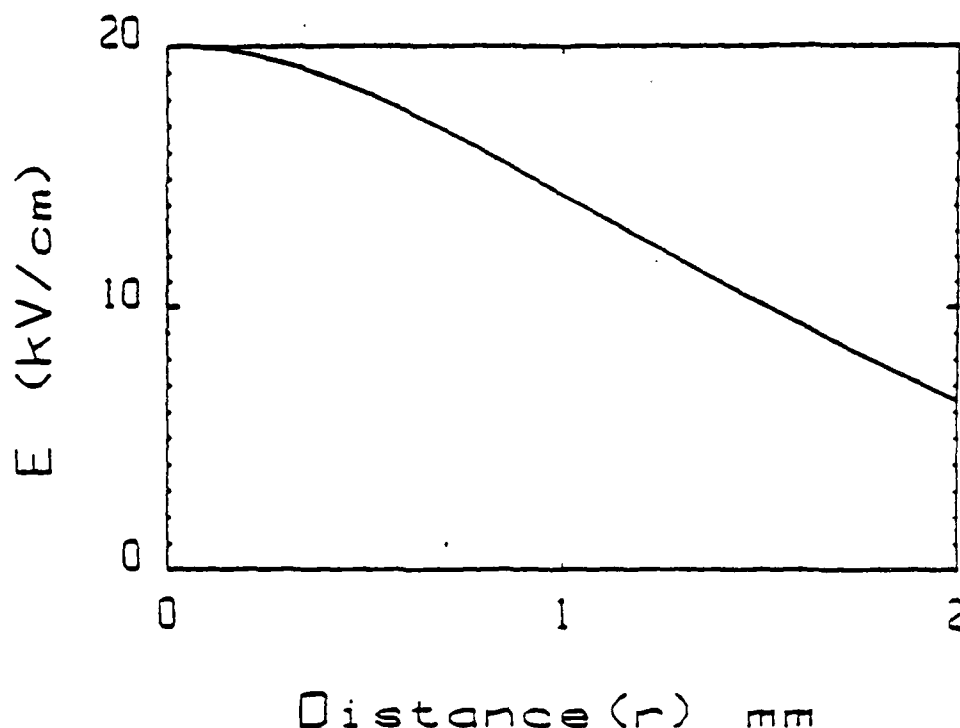


FIGURE 2b Inside field  $E'$  as a function of depth ( $r$ ) within the dielectric.

To determine the thickness limitation experimentally, PZT-501A ribbons ranging from 0.6 mm to 2.5 mm thick, prepared by conventional tape-casting technique, were poled by the continuous poling technique with a (surface) field  $E = 20$  kV/cm. The following tests were carried out to ascertain the extent of poling:

- $d_{33}$  measurements using Berlincourt  $d_{33}$  meter.
- measurement of thickness shear coupling coefficient ( $k_{15}$ ).
- microstructural studies of the ferroelectric domains.

Piezoelectric  $d_{33}$  coefficients measured with a  $d_{33}$  meter for samples of different thickness are listed in Table I. Thin samples less than 1.35 mm thick are poled to saturation but thicker samples are only partially poled. The degree to which the interior of the thick samples are poled was determined by slicing the ribbon to 0.5 mm thin sections parallel to poling direction. Piezoelectric results given in Table II show that the samples are well poled at the edges but the interior portions are only partially poled, as predicted from the field calculation.

By electroding the major faces of a continuously poled PZT ribbon and then applying an oscillating electric field of the proper frequency, the thickness shear resonance can be excited. Shear coupling coefficients can be determined by measuring the fundamental and overtone resonance frequencies. Small shifts in the resonant frequencies caused by electromechanical coupling have been related to  $k_{15}$  by Onoe *et al.*<sup>8</sup> The average shear coupling coefficient gives a measure of the degree of poling in the sample.<sup>9</sup>

Typical sample dimensions for the  $k_{15}$  measurements were: length: 7.5 to 10 mm; width: 5 mm; thickness: 0.5 to 2.15 mm. The frequencies corresponding to the fundamental ( $f_0$ ) and overtone frequencies ( $2f_0$ ,  $3f_0$ , etc.) of the thickness shear mode resonance were mea-

TABLE I

 $d_{31}$  measurements on continuously-poled PZT ribbon.

Ribbon thickness	Measured $d_{31}$
0.60 mm	400-440 pC/N
1.00 mm	370-380 pC/N
1.35 mm	340-380 pC/N
1.65 mm	340-380 pC/N
2.15 mm	300-325 pC/N

TABLE II

 $d_{31}$  measurements on 0.5 mm thin sections cut from thick PZT ribbons.

Ribbon thickness	Measured $d_{31}$	
	Edge section	Center section
1.65 mm	410 pC/N	355 pC/N
2.15 mm	310 pC/N	270 pC/N

TABLE III

 $K_{13}$  values obtained from fundamental and overtone resonance frequencies.

Ribbon thickness	$f_1$ MHz	$f_3$ MHz	$f_5$ MHz	$f_3/f_1$	$K_{13}$	$f_5/f_1$	$K_{13}$
0.60 mm	1.56	5.37	9.02	3.44	0.55	5.78	0.55
1.35 mm	0.75	2.49	4.23	3.32	0.49	5.64	0.51
1.65 mm	0.63	2.02	3.42	3.21	0.41	5.43	0.43
2.15 mm	0.51	1.60	2.71	3.14	0.34	5.31	0.38

 $f_1$  = fundamental resonance frequency;  $f_3$  = third overtone frequency;  $f_5$  = fifth overtone frequency.

from the table in Onoe's paper.<sup>1</sup> The results are presented in Table III. These samples have high  $k_{13}$  values, but smaller values were obtained for thicker samples. The decrease in the thickness shear coupling coefficient is consistent with the partial poling observed in the  $d_{31}$  experiments.

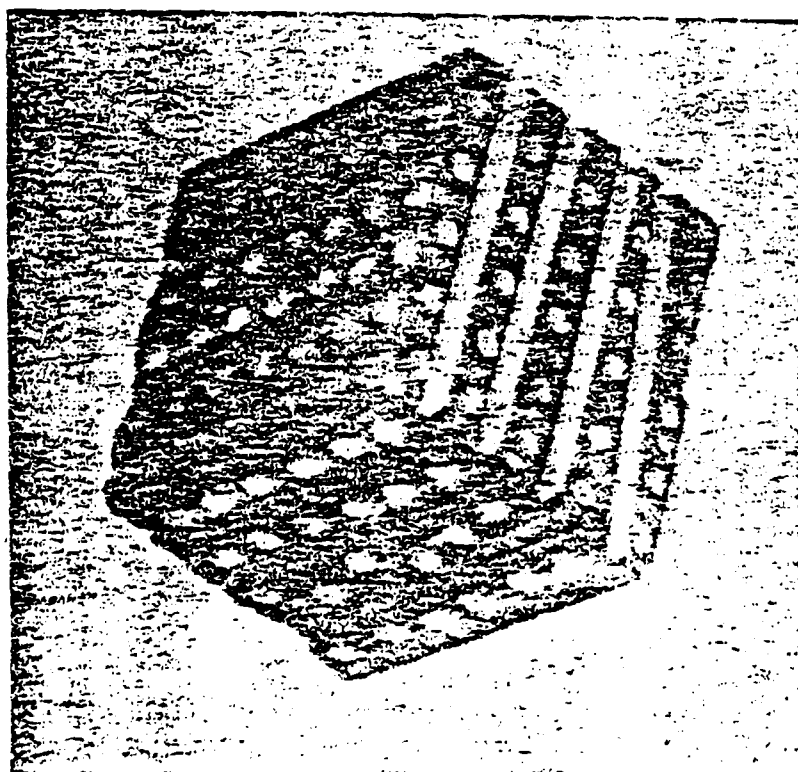
An unpoled ferroelectric sample with random orientation of domains has large number of domain walls which can be observed by preferential etching on a polished sample. Poling aligns the domain in the direction of electric field and reduces the number of domain walls. A microstructural study was carried out to estimate the extent of poling from the density of domains across the thickness of a continuously-poled ribbon. The samples were polished and etched for 30 s in 5% HCl and 4% HF solutions for SEM examination. There was a striking decrease in the density of domains in the continuously poled samples as compared to the unpoled sample, but it was difficult to differentiate any change across the thickness of the poled samples. This is probably because even the interior portions of the thick samples are poled to about 70% of the saturation value. This small difference in

## APPLICATIONS TO NEW DEVICES

## 1. MUPPETS

A variety of new piezoelectric devices can be constructed using prepoled fibers and ribbons (of any length) and joined together with polymer adhesives to give Multiply-Poled PiezoElectric Transducers (MUPPETS). Since the pieces are prepoled, they can be assembled like tinker toys to give complex poling patterns which are difficult to construct by conventional processing. Many of domain-divided piezoelectrics discussed in an earlier paper<sup>9</sup> can be built up from prepoled pieces in this way.

In lead zirconate titanate (PZT) ceramics, the hydrostatic piezoelectric coefficient  $d_h$  ( $= d_{33} + 2d_{31}$ ) is low because  $d_{33}$  and  $d_{31}$  are of opposite sign, even though the magnitudes of  $d_{33}$  and  $d_{31}$  are large. The voltage coefficients  $g_{33}$  ( $= d_{33}/\epsilon_3$ ) and  $g_h$  ( $= d_h/\epsilon_3$ ) are also small because of its high permittivity  $\epsilon_3$ . In a 1-3 composite, PZT rods are embedded in a continuous polymer matrix. Under the idealized situation in which the polymer phase is more compliant than PZT, the stress on the polymer phase will be transferred to the PZT rods. The stress amplification on the PZT phase along with reduced transverse coupling and permittivity greatly enhances the hydrostatic voltage coefficient.<sup>6</sup> This concept of stress amplification on the piezoelectric phase can be extended to three dimensions with the availability of prepoled fibers, using the new poling technique. Prepoled fibers can be arranged in a triple pillar configuration with PZT fibers oriented in three perpendicular directions and then cast in a polymer matrix (Figure 3). The active PZT fibers in the transverse direction perform two functions. First of all, they carry most of the transverse stress under hydrostatic loading, thereby decreasing  $d_{31}$  without appreciable reduction in



$d_{11}$ . Secondly, since they are poled PZT fibers, they add to the total charge collected. The charge coefficient should, in fact, be tripled. This is a major improvement over the method of transverse reinforcement of a 1-3 composite with stiff glass fibers and tubes.<sup>10</sup>

Modified lead titanate ceramics of compositions  $(\text{Pb}_{0.78}\text{Ca}_{0.24})(\text{Co}_{0.2}\text{W}_{0.2})\text{TiO}_3$  and  $(\text{Pb}_{0.85}\text{Sm}_{0.08})(\text{Ti}_{0.98}\text{Mn}_{0.02})\text{O}_3$  developed recently in Japan<sup>11,12</sup> have extremely low planar coupling coefficients. The anisotropy of the electromechanical coupling factors ( $k_t/k_p$ ) (where  $k_t$  is the thickness coupling coefficient and  $k_p$  is the planar coupling coefficient) in these compositions is as high as 15. As a result, they will be very sensitive to an acoustic beam with polarization in the direction of poling, and quite insensitive to any perpendicular vibrations. Prepoled fibers of these compositions arranged in a triple pillar configuration can be used as a polarization analyzer for acoustic waves. The signals from three orthogonal electrodes resolve the wave into its longitudinal component and two shear components.

Another application is an acoustic phase plate made by arranging prepoled pieces in a selected target array. A simple type of annular phase plate was demonstrated by Farnow and Auld.<sup>13</sup> The pattern might conform, for instance, to the Fourier transform of the shape of the object, or perhaps the elements are phased to detect a target moving with a preselected speed and direction. We refer to these composites as MUPPETS, MULTIply-Poled PiezoElectric TransducerS. They come in as many odd shapes and sizes as the Muppet characters seen on television.

## 2. DOFUSS

The DOFUSS (named for a comic strip dinosaur) is a composite device from prepoled PZT ribbon. By poling the ribbon parallel to its length, and later electroding the major faces of the ribbon, one obtains a shear sensor based on piezoelectric coefficient  $d_{13}$ . For many perovskite crystals and ceramics, coefficient  $d_{13}$  is very large. DOFUSS is an acronym for D-One-Five ( $d_{13}$ ) Ultrasonic Shear Sensor. These sensors are insensitive to all stress components except  $\sigma_3$ .

Hennig *et al.*<sup>14</sup> recently developed a device to measure the vertical contact stress generated between the planar surface of the foot and insole of a shoe during walking and running. The device consists of a flexible array of 499 tiny PZT transducers embedded in a thick layer of highly resistant silicone rubber, and positioned in the shoe insole. Similar construction can be used with shear sensors to get information about the shear stress distribution during walking and running.

## 3. Piezoelectric Transformer

Conventional piezoelectric transformers are composed of a long thin piezoelectric ceramic, the primary end of which is thickness poled, while the secondary end is longitudinally poled. When operated at the resonance frequency of the longitudinal mode, the secondary generates a high voltage through the piezoelectric  $d_{33}$  coefficient. The voltage step-up capability is determined by the relative lengths of the poled regions and the driving and loading condition. Bowen *et al.*<sup>15</sup> used an internal electrode multilayer as the primary linked to a PZT secondary with a significant improvement in the voltage step-up capability. The continuous poling technique helps to increase the length of the secondary for further

## SUMMARY

Ferroelectric ceramic fibers and tapes can be continuously poled by the method described in the paper. Flexible electrodes used in the poling technique provide only surface electrode and pose a limitation in poling very thick ribbons, but there is no limit on the length in the poling direction. Among the new types of composites which can be assembled from prepoled ceramics are multiply-poled piezoelectric transducers (MUPPETS) and  $d_{14}$  ultrasonic shear sensor (DOFUSS) devices.

## REFERENCES

1. R. E. Newnham, L. J. Bowen, K. A. Klicker and L. E. Cross, *Materials in Engg.*, **2**, 93 (1980).
2. K. Rittenmyer, T. R. Shrout and R. E. Newnham, *Ferroelectrics*, **41**, 189 (1982).
3. A. Safari, R. E. Newnham, L. E. Cross and W. A. Schulze, *Ferroelectrics*, **41**, 197 (1982).
4. A. Safari, A. Halliyal, L. J. Bowen and R. E. Newnham, *J. Am. Ceram. Soc.*, **65**, 207 (1982).
5. T. R. Gururaja, W. A. Schulze, T. R. Shrout, A. Safari, L. Webster and L. E. Cross, *Ferroelectrics*, **39**, 1245 (1981).
6. K. A. Klicker, J. V. Biggers and R. E. Newnham, *J. Am. Ceram. Soc.*, **64**, 5 (1982).
7. T. R. Gururaja, R. E. Newnham and L. E. Cross, *J. Am. Ceram. Soc.*, **64**, C8 (1982).
8. M. Onoe, F. Tiersten and Meitzler, *J. Acoust. Soc. Am.*, **35**, 36 (1963).
9. R. E. Newnham, C. S. Miller, L. E. Cross and T. W. Cline, *Phys. Stat. Sol. (a)*, **32**, 69 (1975).
10. M. J. Haun, M. S. Thesis, The Pennsylvania State University, 1983.
11. Y. Yamashita, K. Yokoyama, H. Honda and T. Takahashi, *Jpn. J. Appl. Phys., Supplement* **20-4**, 183 (1981).
12. H. Takeuchi, S. Iyomura, E. Yamamoto and Y. Ito, *J. Acoust. Soc. Am.*, **72**, 1114 (1982).
13. S. A. Farnow and B. A. Auld, *Appl. Phys. Lett.*, **25**, 681 (1974).
14. E. M. Hennig, P. R. Cavanagh, H. T. Albert and N. H. Macmillan, *J. Biomed. Eng.*, **4**, 213 (1982).
15. T. R. Shrout, W. A. Schulze, J. V. Biggers and L. J. Bowen, *Mat. Res. Bull.*, **15**, 551 (1980).

**APPENDIX 27**

## LOW FIELD POLING OF SOFT PZTs<sup>†</sup>

T.R. SHROUT, A. SAFARI, W.A. SCHULZE  
Materials Research Laboratory, The Pennsylvania State  
University, University Park, PA 16802, USA

(Received November 22, 1982)

**Abstract:** The inherent high electrical resistivity of donor doped or "soft" PZT's enables them to be poled using the field cooling method. The electric fields required for poling were reduced by a factor of five as compared to fields used in conventional poling. Dielectric and piezoelectric properties are reported.

### INTRODUCTION

It is well known that ferroelectric ceramic materials have no net polarization due to the random orientation of the axes of their constituent crystals. Such ceramics can be made piezoelectrically active by the application of an external dc electric field, this process being referred to as "poling." The effectiveness of the poling process depends primarily on the number of possible axial directions in which the polarization can be oriented. Other factors which limit the poling efficiency are intergranular stresses and imperfections, both of which tend to increase and distribute the field required for reorientation in a specific time (coercive field  $E_c$ ) and may later induce time dependent domain reorientation which causes "ageing" of dielectric and piezoelectric properties.<sup>(1,2)</sup>

Generally, the most effective poling process is when cooling from the paraelectric to ferroelectric phase under an applied field. This technique causes maximum alignment, since the dipoles are most easily aligned as they appear spontaneously at  $T_c$ , the Curie temperature. However, for the vast majority of ferroelectric ceramics poling is achieved by the application of a field, at a temperature significantly less than  $T_c$ , either for a continuous or an intermediate (pulse poling) time and at a temperature limited

<sup>†</sup>Communicated by Professor L. E. Cross



by the conductivity and breakdown characteristics. Also, due to the low dielectric breakdown strength of air-ceramic surfaces the poling operation is usually carried out in some insulating medium, e.g., silicone oil.

Presently, the most widely used ferroelectric ceramics for piezoelectric applications are based on lead zirconate titanate [ $\text{Pb}(\text{Zr}_{1-x}\text{Ti}_x)\text{O}_3$ ] compositions (designated PZT). The most useful range of compositions are ones with  $x$  ranging from 0.46 to 0.50 which lie close to the morphotropic phase boundary, in which both a tetragonal and rhombohedral forms coexist. Ceramics of these compositions can be efficiently poled due to the large number of possible directions in which the polar axes can be reoriented, i.e., 6 for the tetragonal and 8 for rhombohedral, thus giving a total of 14 directions. Poling of such ceramics is usually carried out by the application of a dc field of 20-60 kV/cm at temperatures (100-150°C) which are well below  $T_c$  (~350°C) and for various lengths of time (microseconds to minutes). The extremely strong piezoelectric effects exhibited by poled PZT ceramics can further be modified by small amounts of dopants. Additives such as  $\text{Fe}^{+3}$ ,  $\text{K}^{+1}$ ,  $\text{Mg}^{+2}$  are "acceptor" substitutes causing oxygen vacancies. Changes in characteristic properties include an increase in the coercive field, mechanical and electrical quality factors. Such modified ceramics are referred to as "hard" PZTs. Additives such as  $\text{Nb}^{+5}$ ,  $\text{Ta}^{+5}$ ,  $\text{La}^{+3}$  are "donor" substituents creating lead vacancies. The characteristic property changes are lowered  $E_c$ , increased dielectric constant, dielectric loss and electromechanical coupling coefficient. Such modified compositions are referred to as "soft" PZTs.

The "soft" PZTs not only have low  $E_c$ 's, which allows more thorough poling, but have electrical resistivities several orders of magnitude higher than that of undoped and "hard" PZTs. This suggests that "soft" PZTs may be able to support a relatively high dc electric field at high temperatures ( $>T_c$ ) without dielectric breakdown and thus may be poled more efficiently by field cooling

through  $T_c$ . Since the required poling field should be quite small ( $E_c$  decreases as you approach  $T_c$ ), the voltage necessary to pole large samples would be significantly reduced and there would no longer be a need to pole in any dielectrically insulating medium other than air.

The purpose of this investigation was to see if "soft" PZTs could, in fact, be poled more efficiently at reduced dc fields in conjunction with the field cooling method.

#### EXPERIMENTAL PROCEDURE

Two commercially available "soft" PZTs were chosen for the present study. Several sintered and electroded PZT disks were received from Don Bonnema of the Edo-Western Corporation. Also, in this study, samples were prepared using a commercially available PZT powder.\* Disks were prepared by firing at 1290°C for a soak period of 1/2 hour. The disks being fired in closed alumina crucibles with  $PbZrO_3$  added as a source of PbO. The fired disks were found to be at least 95% theoretically dense. The disks were polished parallel and electroded with a fired on silver paste electrode.

Preliminary electrical measurements included the dielectric constant ( $k$ )\* at room temperature (1 kHz) and as a function of temperature to determine the Curie transition. Electrical resistivity was determined using a HP model 4140B pico-ampmeter\*\* with an appropriate field (0.1-0.5 kV/cm) being applied across the samples. The resistivities were determined over a temperature range of 250°C to 550°C.

In order to determine the feasibility and/or effectiveness of the proposed field cooling method, various dc electric field levels were applied at a temperature well above  $T_c$  (in air) with the

---

\*Hewlett Packard (Model 4270A) Automated Capacitance Bridge, Hewlett Packard 1-59-1 Yoyogi, Tokyo, Japan 131.

\*\*Hewlett Packard (Model 4140B) pico-ampmeter, Hewlett Packard 1-59-1 Yoyogi, Tokyo, Japan 131.

AD-A145 115

PIEZOELECTRIC AND ELECTROSTRICTIVE MATERIALS FOR  
TRANSDUCER APPLICATIONS(1) PENNSYLVANIA STATE UNIV  
UNIVERSITY PARK MATERIALS RESEARCH LAB

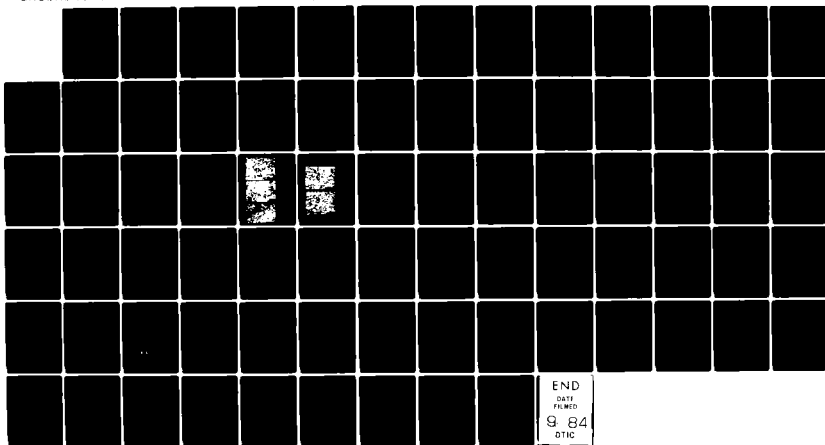
UNCLASSIFIED

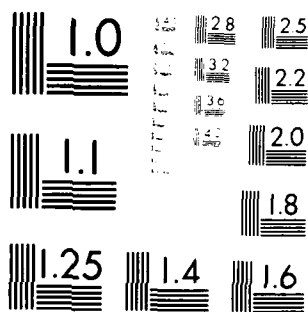
J E CRUMP ET AL. MAY 84 N00014-82-K-0339

F/G 20/3

NL

44





MICROCOPY RESOLUTION TEST CHART  
NATIONAL BUREAU OF STANDARDS-1963-A

samples then allowed to cool ( $\sim 10^\circ\text{C}/\text{min}$ ) to a temperature well below  $T_c$  before removing the field. For comparison, samples were also conventionally poled in a stirred silicone oil bath at  $140^\circ\text{C}$  by applying a dc field of 25 kV/cm for 5 minutes.

Immediately after poling, the piezoelectric charge constant ( $d_{33}$ ) was measured using a Berlincourt  $d_{33}$  meter.\* The planar coupling coefficient ( $k_p$ ) and mechanical  $Q$  were both determined using an HP model 3585A Spectrum Analyzer\*\* in accordance with the IEEE standards on piezoelectric crystals.<sup>(3)</sup> The room temperature value of the dielectric constant was again determined. The above measurements were then repeated after the samples had been allowed to age for 24 hours.

#### RESULTS AND DISCUSSION

Preliminary results clearly showed that the two commercial PZTs chosen for this investigation were indeed "soft" PZTs as evidenced by their relatively high dielectric constants ( $>1000$ ), reported in Table 1, and electrical resistivities (Fig. 1) similar in magnitude

TABLE 1. Dielectric and piezoelectric properties of "soft" PZTs poled with conventional (A) and field cooling methods (B) (aged 24 hrs).

PZT material	dielectric constant			piezo-electric $d_{33}$ ( $\times 10^{-12}\text{C/N}$ )		planar coupling coef. $k_p$ (%)		mechanical $Q$	
	unpoled	A	B	A	B	A	B	A	B
Edo-Western	1080	1620	1600	500	515	69.7	74.7	58	54
PZT-501A	1300	1940	2100	500	530	71.4	71.3	60	54

\*Berlincourt (Model 33)  $d_{33}$  Meter, Channel Products, Inc., 16722 Park Circle Drive, Chagrin Falls, OH 44020.

\*\*Hewlett Packard (Model 3585A) Spectrum Analyzer, Hewlett Packard 1-59-1 Yoyogi, Tokyo, Japan 151.

to that reported for other donor doped PZTs.<sup>(1)</sup> The Curie transition of both PZTs was found to be  $\sim 330^\circ\text{C}$ .

The dielectric constant, piezoelectric  $d_{33}$ , planar coupling coefficient ( $k_p$ ) and mechanical  $Q$  values determined on samples poled using the conventional method are also presented in Table 1. Again these values are representative of "soft" PZTs.

The results of the field cooling method

are presented in Figures 2 and 3, where it is clearly shown that efficient poling was possible using dc fields of less than 3 kV/cm with further enhancement being observed at higher fields. DC fields greater than 3 kV/cm were found to lead to dielectric breakdown. It is interesting to note that for both PZTs a maximum in  $k$  and  $d_{33}$  versus poling field was observed, with the dielectric constant dropping off more rapidly. The exact nature of this maximum is not understood, but may be attributed to the removal of  $180^\circ$  domain walls whose motion would contribute to the dielectric constant but not to  $d_{33}$ . Possible microcracking due to excessively large strains induced upon cooling through  $T_c$  could also lead to degradation in  $k$  and  $d_{33}$ . No maximum in the planar coupling ( $k_p$ ) was observed.

For a general comparison with that of conventional poling,

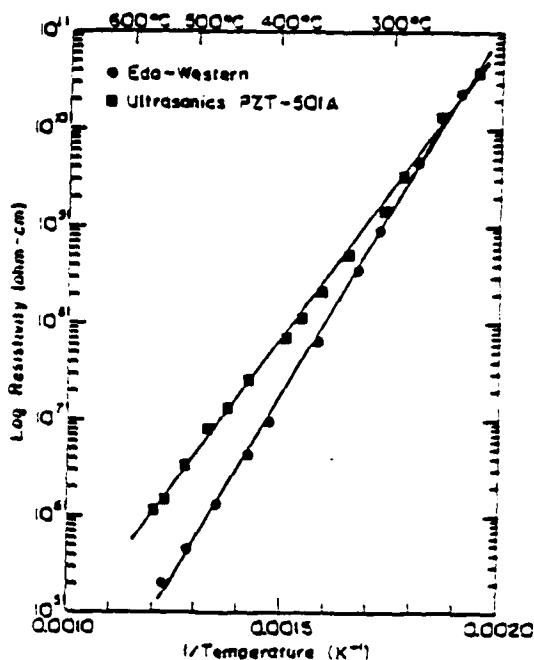


FIGURE 1. Electrical resistivity as a function of temperature for "soft" PZTs.

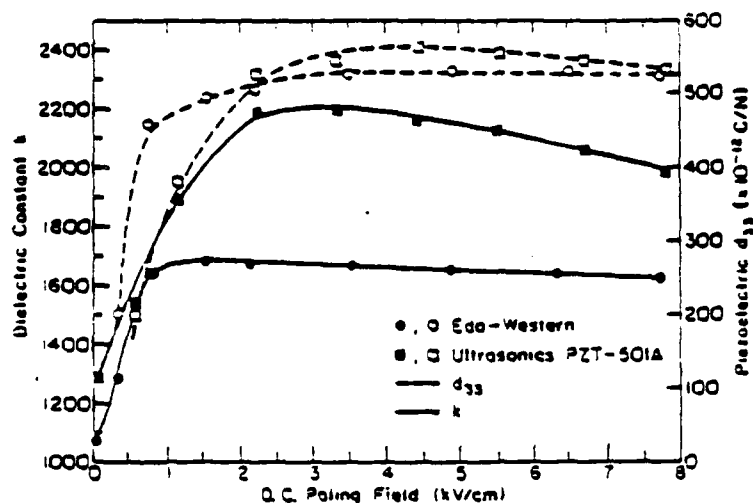


FIGURE 2. The dielectric and piezoelectric constants as a function of poling field.

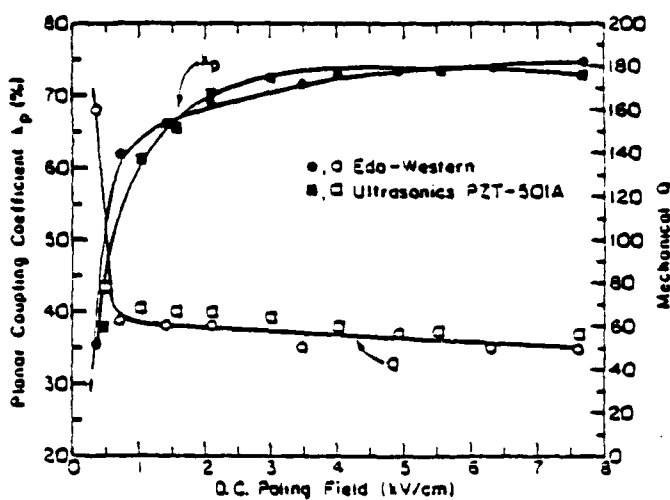


FIGURE 3. The planar coupling coefficient and mechanical  $Q$  as a function of poling field.

more than 20 samples were poled at specific levels (PZT-5 at 4 kV/cm and Edo-Western at 6 kV/cm) using the field cooling method with the averaged results being reported in Table 1.

As compared to the conventionally poled samples, the field

cooling method resulted in a substantial increase in the dielectric constant in the case of PZT-501A, while no appreciable change was observed for the Edo-Western samples. Both PZTs were found to have slightly enhanced  $d_{33}$  coefficients with similar decreases in mechanical  $Q$ .

In general, the piezoelectric coupling coefficient is directly related to the piezoelectric coefficient and inversely related to the square root of the dielectric constant, thus a significant increase in  $k_p$  was observed for the Edo-Western samples while only a slight increase was observed for the PZT-501 samples. This may also explain why no maximum in  $k_p$  (Fig. 3) was observed.

#### CONCLUSION

In this work, it was shown that due to their inherent high electrical resistivity, donor doped or "soft" PZT could be more efficiently poled using the field cooling method.

It was also found that the electric fields required for poling were reduced by a factor of five, as compared to fields used in conventional poling, thus allowing the poling process to be done in air. The reduced fields should also enable the poling of large shapes with reasonable voltages. Further investigation of the use of the field cooling method to pole "soft" PZTs and their resulting properties is still in progress.

#### REFERENCES

1. B. Jaffe, W.R. Cook, Jr., and H. Jaffe, Piezoelectric Ceramics (Academic Press, London and New York, 1971).
2. J.M. Herbert, Ferroelectric Transducers and Sensors (Gordon and Breach, Science Publishers, New York, London and Paris, 1982).
3. IRE Standards of Piezoelectric Crystals: Measurements of Piezoelectric Ceramics, 1961, Proc. IRE, 61, 1161 (1961).



**APPENDIX 28**

# Reaction Sequence in the Formation of Lead Zirconate-Lead Titanate Solid Solution: Role of Raw Materials

B. V. HIREMATH,\* ANGUS I. KINGON,\*\* and JAMES V. BIGGERS\*

Materials Research Laboratory, The Pennsylvania State University, University Park, Pennsylvania 16802

The reaction sequence in the formation of  $\text{Pb}(\text{Zr}_{0.6}\text{Ti}_{0.4})\text{O}_3$  (PZT 60/40) was investigated as a function of  $\text{PbO}$  and  $\text{ZrO}_2$  raw material variations, using powder X-ray diffraction. Particular emphasis was placed on the final stages of reaction in the formation of PZT solid solution. Based on the present work, a more detailed reaction sequence is being proposed for  $\text{Pb}(\text{Zr}_{0.6}\text{Ti}_{0.4})\text{O}_3$  and similar compositions. This reaction sequence is believed to account for many of the apparent discrepancies which have appeared in the literature.

## 1. Introduction

THERE is a continuing interest in lead zirconate-lead titanate (PZT) ceramics prepared by the mixed-oxide technique, particularly with regard to reducing the variability of the dielectric and electromechanical properties due to variation in processing and raw materials. The work described here is part of a larger program addressing this problem by attempting to identify those raw mate-

rial and processing factors which affect final properties. It includes a concerted effort to trace these effects from raw materials through the important processing steps, such as calcination, sintering, and the accompanying microstructural development, to the final properties.

The present work describes the effect of variations in raw materials on the reaction sequence in the formation of PZT solid solution. A detailed analysis of the initial stages of the reaction was done in the present study by calcining at different temperatures and durations.

The solid state reaction sequence in the system  $\text{PbO-ZrO}_2\text{-TiO}_2$  has been investigated by a number of workers.<sup>1-10</sup> There is no agreement among the results of various workers regarding reaction sequence and the formation of various intermediate products. There have been some apparently contradictory findings, particularly with respect to the presence or absence of intermediate products like  $\text{PbZrO}_3$  (PZ) and a  $\text{PbO}$  solid solution (Pss).

There is general agreement that the first step of the mixed-oxide reaction route for compositions near the morphotropic boundary<sup>11</sup> is the reaction of  $\text{PbO}$  with  $\text{TiO}_2$  to form  $\text{PbTiO}_3$  (PT). However, most of the previous workers<sup>1-11</sup> did not observe  $\text{PbZrO}_3$  as an intermediate product in the reaction. In contrast, Ohno *et al.*<sup>1</sup> reported formation of both  $\text{PbTiO}_3$  and  $\text{PbZrO}_3$ , with subsequent reaction to form a PZT solid solution. Yamaguchi *et al.*<sup>2</sup> reported the formation of  $\text{PbZrO}_3$  only under certain preparation conditions. Venkataramani and Biggers<sup>10</sup> reported that use of submicrometer-sized  $\text{ZrO}_2$  also resulted in  $\text{PbZrO}_3$  formation.

The reaction sequence proposed by Matsuo and Sasaki<sup>3</sup> is:

Step 1:  $\text{P} + \text{T} \rightarrow \text{PT}$   
Step 2:  $\text{PT} + \text{P} + \text{Z} \rightarrow \text{PT} + (\text{PZ}, \text{T}_{1-x})$   
Step 3:  $\text{PT} + (\text{PZ}, \text{T}_{1-x}) \rightarrow \text{PZT}$

where P refers to  $\text{PbO}$ , T to  $\text{TiO}_2$ , Z to  $\text{ZrO}_2$ , PT to  $\text{PbTiO}_3$ , and  $(\text{PZ}, \text{T}_{1-x})$  to  $\text{ZrO}_2$ -rich PZT. According to these workers, the first reaction product to form is  $\text{PbTiO}_3$ . A portion of  $\text{PbTiO}_3$  reacts with the remaining  $\text{PbO}$  and  $\text{ZrO}_2$  to form PZT solid solution as an intermediate reaction product. In the final step, the intermediate PZT solid solution reacts with the remaining  $\text{PbTiO}_3$  to form a single-phase PZT solid solution of desired composition.

Sper<sup>4</sup> reported the presence of an intermediate  $\text{PbO}$  (solid solution), which was a tetragonal solid solution of  $\text{PbO}$  with a small amount of  $\text{TiO}_2$ , and a trace of  $\text{ZrO}_2$ . The presence of  $\text{PbO}$  solid solution was confirmed by Hankey,<sup>5</sup> who obtained more quantitative data for the composition of the solid solution.

The reaction sequence given by Sper<sup>4</sup> and Hankey<sup>5</sup> and Biggers<sup>10</sup> is:

Step 1:  $\text{P} + \text{T} \rightarrow \text{PT}$   
Step 2:  $\text{P} + \text{PT} + \text{Z} \rightarrow \text{Pss}$   
Step 3:  $\text{PT} + \text{Pss} \rightarrow \text{PZT}$

The final stages of the reaction, particularly the composition of PZT solid solution, was not discussed by these workers. However, it is not clear how  $\text{PbO}$  solid solution as an intermediate product influences the final properties of PZT ceramic.

Chandrasekara *et al.*<sup>12</sup> recently reported interesting work on the reaction mechanism in the formation of PZT solid solution. They discussed the diffusion of various ionic species to form the solid solutions, but did not report the powder X-ray diffraction (XRD) patterns for the final stages of reaction in order to obtain quantitative data.

Kington<sup>13</sup> confirmed the formation of  $\text{PbO}$  (solid solution) under special experimental conditions, and also observed the formation of both  $\text{PbZrO}_3$ -rich and  $\text{PbTiO}_3$ -rich PZT solid solutions as intermediates, which homogenized to form PZT solid solutions of the

Received July 16, 1982; revised copy received February 3, 1983; approved March 22, 1983.

Supported by the U.S. Office of Naval Research under Contract No. N00014-82K-0339.

\*Member, the American Ceramic Society.

\*\*Permanent address: Ceramic Capacitors, B.E.L. Lalabali, Bangalore 560013, India.

Permanent address: National Physical Research Laboratory, CSIR, PO Box 395, Pretoria 0001, South Africa.

Table I. Properties of  $\text{ZrO}_2$  Raw Materials

Powder	Particle size* ( $\mu\text{m}$ )	Purity (%)	$\text{H}_2\text{O}$ (wt%)	Agglomeration
A	1.5	99.5	2.42	Little
B	1.7	99.8	1.37	Yes
Jet-milled B	1.7			Little
C	3.1	99.6	3.36	Yes

\*By SEM technique (mean value). \*Lot 1276, Harsco Chemical Co., Cleveland, OH. \*Lot 2-81, Harsco Chemical Co. \*Lot 1929, Astro Met Associates, Inc., Cincinnati, OH.

Table II. Properties of  $\text{PbO}$  Raw Materials

Powder	Particle size* ( $\mu\text{m}$ )
D	3.6
E	4.5
Jet-milled E	1.6

\*By SEM technique (mean value). \*Lot 1918, Hammond Lead Products, Inc., Hammond, IN. \*Lot 1148, Hammond Lead Products, Inc.

Table III. Raw Materials for PZT 60/40 Batches\*

Batch	$\text{PbO}$ source	$\text{ZrO}_2$ source
1	D	A
2	E	A
3	Jet-milled E	A
4	O	B
5	O	Jet-milled B
6	O	C

\* $\text{TiO}_2$  throughout was grade 333-77-20-4, Whitaker, Clark & Daniels, Inc., South Plainfield, NJ. \*\*Standard reagents.

desired composition. This observation is useful in explaining differing views regarding the coexistence of tetragonal and rhombohedral phases at and near the morphotropic boundary.<sup>12-15</sup>

In the present work, XRD patterns of calcined samples were more carefully analyzed in order to identify intermediate reaction products, particularly intermediate PZT solid solutions. The work was repeated using raw materials from different sources in order to understand their importance in the reaction sequence in the formation of PZT solid solutions.

## II. Experimental Procedure

In the present study,  $\text{TiO}_2$  from a single source<sup>1</sup> was used. The earlier work<sup>2</sup> had indicated that, since  $\text{TiO}_2$  reacts at relatively low temperatures to form  $\text{PbTiO}_3$ , it is unlikely that it would affect later stages of reaction. To determine if the other two oxides, namely  $\text{PbO}$  and  $\text{ZrO}_2$ , would influence the reaction sequence, various batch compositions were prepared using  $\text{PbO}$  and  $\text{ZrO}_2$  powders from several sources.

The properties of  $\text{ZrO}_2$  powders from different sources used in this study are listed in Table I. The particle sizes and size distributions were obtained by an automated SEM technique; only mean particle sizes are quoted. The extent of agglomeration was estimated by observing SEM<sup>4</sup> images of the powders. Table I shows that, in the case of powder B, the jet-milling<sup>5</sup> procedure reduced the extent of agglomeration, but did not affect the mean particle size. The  $\text{ZrO}_2$  C is a plasma-produced powder, highly agglomerated, with a relatively large particle size and a high hafnia content.

The mean particle sizes of  $\text{PbO}$  raw materials are listed in Table II. The manufacturer quotes a purity of at least 99.9% for these products.

A PZT composition with Zr/Ti 60/40, which is just away from the morphotropic boundary, was chosen for the present study. The batched compositions were corrected for impurities, loss on ignition, and  $\text{HfO}_2$  content. The  $\text{PbO}$  powder D and  $\text{ZrO}_2$  powder A were chosen as the "standard reactants" along with the  $\text{TiO}_2$ . Five other sets of raw materials were batched, varying  $\text{ZrO}_2$  and  $\text{PbO}$  sources as shown in Table III. Four hundred grams of each composition were weighed and mixed for 8 h in polyethylene containers using  $\text{ZrO}_2$  grinding media. Each batch was dried at  $120^\circ\text{C}$  for 24 h, remixed, and divided into 20 parts. The samples were reacted at different temperatures and durations by heating the samples to the desired temperature at  $\approx 400^\circ\text{C}/\text{min}$  and air-quenching after the required duration. The chosen conditions of temperature and duration were  $600^\circ$ ,  $700^\circ$ ,  $750^\circ$ ,  $800^\circ$ , and  $900^\circ\text{C}$  and 20, 40, 100, and 180 min at each temperature.

After calcination, all 120 samples were analyzed qualitatively by powder X-ray diffraction using an X-ray diffractometer.<sup>16</sup> Various crystalline phases were identified by comparing the XRD patterns with standard powder diffraction patterns. The composition of the PZT solid solutions was determined by the following method. From the reported unit cell dimensions,<sup>16</sup>  $d_{\text{calc}}$  values were calculated for all PZT solid solutions. The composition of different solid solutions was determined by comparing the observed  $d_{\text{obs}}$  values with the calculated values.

## III. Results and Discussion

The X-ray powder diffraction analyses showed that  $\text{PbTiO}_3$  was the only reaction product formed for all samples calcined at  $600^\circ\text{C}$ . This is in agreement with the observation of earlier workers.<sup>1-15,17</sup>

The results of XRD analyses for the standard reactants calcined at different temperatures and durations are shown in Table IV. Typical XRD patterns are shown in Fig. 1. It is important to note the reaction intermediates PZT(Z) and PZT(T), which are PZT solid solutions with a high and a low Zr/Ti ratio, respectively.

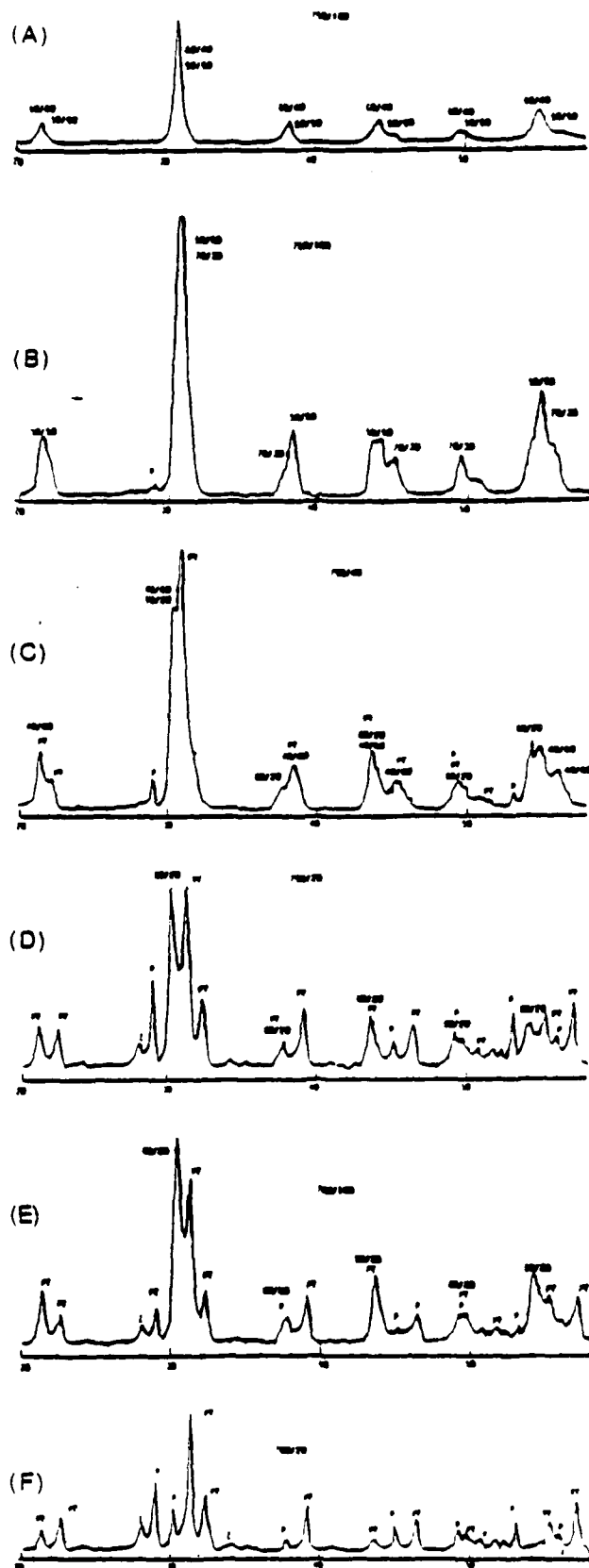


Fig. 1. X-ray diffraction patterns of standard reactants calcined at (A)  $750^\circ\text{C}$  for 180 min, (B)  $750^\circ\text{C}$  for 100 min, (C)  $750^\circ\text{C}$  for 40 min, (D)  $750^\circ\text{C}$  for 20 min, (E)  $700^\circ\text{C}$  for 180 min, and (F)  $700^\circ\text{C}$  for 20 min. Ratios indicate PZT with given Zr/Ti ratio, e.g. 60/40: P =  $\text{PbO}$ , T =  $\text{TiO}_2$ , Z =  $\text{ZrO}_2$ , PT =  $\text{PbTiO}_3$ .

<sup>1</sup>Grade 3328-77, J20-8, Whitaker, Clark & Daniels, Inc., South Plainfield, NJ.  
<sup>4</sup>Model JSM-50A scanning electron microscope, Japan Electron Optic Co., Tokyo, Japan.

<sup>5</sup>Model 4-MJ, Serial X9225, Microjet, Fluid Energy Processing and Equipment Co., Hatfield, PA.

<sup>16</sup>Type F,  $\text{CuK}\alpha$  radiation,  $\lambda = 0.154188$  nm, Picker International, Karlsruhe, Federal Republic of Germany.

Table IV. Products of Isothermal Calcination of Standard Reactants

Calcination temp (°C)	Time (min)			
	20	40	100	180
700	PT	PT	PT	PZT(Z)
	P	P	PZT(Z)	PT
	Z	Z	P	P
		PZT(Z)	Z	Z
750	PT	PZT	PZT	PZT
		(=40/60)	(=50/50)	(=60/40)
	P	PZT(T)	PZT	
			(=70/30)	
	PZT(T)	P	P $\alpha$	PZT
	Z	Z $\alpha$		(=50/50)

NOTE: P=PbO, Z=ZrO<sub>2</sub>, T=TiO<sub>2</sub>, PT=PbTiO<sub>3</sub>, PZ=PbZrO<sub>3</sub>, PZT(Z)=PZT rich in PZ, PZT(T)=PZT rich in PT, PZT (=60/40)=PZT with Zr/Ti ratio of =60/40;  $\alpha$ =trace. Products are listed in order of decreasing intensity of diffraction peaks.

Table V. Effects of PbO Raw Material

Calcination temp./time	PbO raw material		
	D	E	Jet-milled E
700°C/180 min	PZT(Z)	PZT(Z)	PT
	(85/15)	(80/20)	
	PT	PT	P
	P	P	PZT(Z)
750°C/40 min	Z	Z $\alpha$	(90/10)
			Z
	PZT	PZT(Z)	PZT(Z)
	(40/60)		
	PZT(Z)	PT	PT
	P	PZT	PZT
	Z $\alpha$	(40/60)	Z
		Z	

NOTE: Products are listed in order of decreasing intensity of diffraction peaks.

Table VI. Effects of ZrO<sub>2</sub> Raw Material\*

Powder A	Powder B	Powder B (Jet-milled)	Powder C
PZT(Z)	PT	PZT(Z)	PT
PT	P	PT	P
P	PZT(Z)	P	Z
Z	Z	Z	P(ss)

NOTE: Products are listed in order of decreasing intensity of diffraction peaks; P(ss)=PbO (solid solution) for products calcined at 700°C for 180 min.

PZT(Z) indicates a composition near that of PbZrO<sub>3</sub>(PZ) and PZT(T) indicates a composition near that of PbTiO<sub>3</sub>(PT).

In samples calcined at 700°C, the XRD analyses indicated an intermediate PZT(Z) solid solution of composition Pb(Ti<sub>0.20</sub>Zr<sub>0.80</sub>)O<sub>3</sub>. Here formation of PZ was not observed (Fig. 1). After 180 min of calcination at 700°C, this reaction had consumed a substantial amount of ZrO<sub>2</sub>. However, a small amount of unreacted PbO and ZrO<sub>2</sub> could still be observed even after calcination for 180 min.

The intermediate products identified in the 750°C isothermal reaction are also shown in Table IV. A PZT(Z) intermediate phase is once again observed (20 and 40 min), with the XRD peaks somewhat broader than in previous cases, indicating a wider range of Zr/Ti ratios. Also observed is a PZT(T) intermediate phase with a mean Zr/Ti ratio of approximately 40/60. After 40 min of calcination at 750°C, most of the original reactants were consumed. The XRD patterns corresponding to 100 and 180 min of calcination (Fig. 1) indicate homogenization of PZT intermediates. After 180 min at 750°C, the desired 60/40 (rhombohedral) composition is predominant. However, some peaks corresponding to a tetragonal phase are also observed. These can be assigned to a PZT composition with a Zr/Ti ratio of 50/50.

At higher calcination temperatures, the main rhombohedral peaks corresponding to PZT 60/40 sharpen with calcination time and the tetragonal peaks become less intense after longer calcination. However, the peaks corresponding to the tetragonal phase could still be observed after 180 min of calcination at 900°C.

It is clear that, for the system described above, the reaction sequence to form the final PZT 60/40 solid solution is via PZT intermediates of different compositions, near PZ and PT in composition, namely PZT(Z) and PZT(T), respectively. Thus, after the calcination step the final PZT solid solution does not have a composition which can be described by a Gaussian distribution of Zr/Ti ratios.

The following reaction sequence accounts for the species identified by XRD:

Step 1: P+T→PT

Step 2: P+Z+trace PT→PZT(Z) (85/15)

or P(ss)+Z→PZT(Z) (85/15)

Step 3: PT+P+Z→PZT(T) (40/60)

Step 4: PZT(T) (40/60)+PZT(Z) (85/15)→

PZT (60/40)+trace PZT (50/50)

Step 5: Homogenization

Note that steps 2 and 3 are competitive with normal calcination conditions, ensuring that step 2 does not go to completion. The competition between these reactions should clearly have a major influence in determining the compositional distribution (i.e. the range of Zr/Ti ratios) to be found in the PZT solid solution after calcination.

The reaction sequence presented here recognizes binodal distribution of PZT solid solutions and agrees with reported work by Kingon,<sup>12</sup> but differs from other earlier studies. It appears that two types of PZT solid solutions form as intermediate products, one rich in PZ and the other rich in PT. As the reaction progresses with calcination temperature and time, the two solid solutions approach each other in composition, giving a PZT solid solution of the desired composition after complete homogenization as described earlier.

How generally applicable is the reaction sequence proposed above? As described earlier, PZT (60/40) compositions were prepared using PbO and ZrO<sub>2</sub> from several sources (Table III) in order to study the effect of variations in raw materials on the reaction sequence. The XRD analyses of the remaining sets of reactants show that the above scheme is followed for all sets, except for that containing ZrO<sub>2</sub> powder C. However, small differences are apparent in the reaction rates, some specific examples being shown in Tables V and VI.

Table V shows the effect of PbO from different sources on the formation of PZ-rich intermediate PZT(Z), for the reaction carried out at 700°C for 180 min and 750°C for 40 min. The mean composition (i.e. Zr/Ti ratio) of this intermediate varies slightly, depending on the PbO source. In general, the reactions conform to steps 2 and 3 above, although reaction rates differ.

The effect of variations in the ZrO<sub>2</sub> powder source on the reaction sequence is shown in Table VI. The rates of reaction in the formation of a PZT(Z) intermediate are again seen to depend on the powder characteristics of ZrO<sub>2</sub>. More importantly, only the use of ZrO<sub>2</sub> powder C does not result in formation of a PZT(Z) intermediate at 700°C. The other three ZrO<sub>2</sub> powders gave a PZT(Z) phase, according to step 2. At 750°C, PbTiO<sub>3</sub> reacts directly with PbO and ZrO<sub>2</sub> to form a PZT solid solution with a very broad range of Zr/Ti ratios.

It is surprising that the raw material variations (for the first five sets) resulted only in differences in reaction rate; there were no significant differences in the composition (i.e. Zr/Ti ratios) of PZT intermediates. For example, one would expect that if step 2 goes to completion, step 3 would not occur, and one would need to add the following step to the sequence:

Step 4A: PT+PZT(Z)→PZT

The more general form of step 4 is therefore the reaction of PbTiO<sub>3</sub>-rich PZT (or PbTiO<sub>3</sub>) with PbZrO<sub>3</sub>-rich PZT (or PbZrO<sub>3</sub>) to form PZT. This is believed to be the situation when sub-micrometer-sized ZrO<sub>2</sub> is used as a precursor, as described by Venkataramani and Biggers.<sup>9</sup> In this case, step 2 occurs at an

extremely low temperature to form  $\text{PbZrO}_3$  ( $\approx 500^\circ\text{C}$ ), and the reaction goes to completion. The complete reaction is therefore via steps 1, 2, 4A, and 5 only, and step 3 is not competitive.

It is clear from the present results, and from earlier experience, that the temperature at which step 2 occurs depends on experimental conditions, particularly the physical properties of  $\text{ZrO}_2$  powder, including particle size, agglomeration, morphology, and powder packing. The results for the case of  $\text{ZrO}_2$  powder C can, therefore, also be treated as a special case of the above reaction sequence. In this case the properties of  $\text{ZrO}_2$  powder, probably its larger particle size and agglomeration, make step 2 uncompetitive, and the reaction occurs by steps 1, 3, and 5 only. Consequently, the PZT intermediate produced in step 3 is not PZ-deficient, but has a wide range of Zr/Ti ratios varying from PT to PZT 60/40 as the diffusion reaction proceeds. This is exactly the sequence postulated by Matsuo and Sasaki.<sup>1</sup>

There was some concern as very little PbO (solid solution) phase was observed by XRD for the materials and conditions used in the present study. A further experiment was therefore undertaken. A similar XRD analysis was carried out using two sets of raw materials. These were the standard reactants described above ( $\text{ZrO}_2$  powder A and PbO powder D), and the raw materials recently used by Hankey.<sup>4,7</sup> The preparation conditions were also altered to correspond exactly to those of Hankey, most notable being the lengthening of the reaction time to 24 h. The results of this study can be summarized as follows:

(i) PbO (solid solution) formed in both cases, a greater amount being observed in the case of raw materials used by Hankey.<sup>8</sup> This indicates that the formation of PbO (solid solution) is sensitive to the starting raw materials and mixing procedure. This is consistent with the results of Venkataramani,<sup>17</sup> who showed that formation of the PbO solid solution is also dependent on the packing density of the powders during calcination.

(ii) The presence of the PbO (solid solution) phase does not appear to affect the reaction sequence given above. The temperatures at which steps 2, 3, and 4 occur are decreased by  $\approx 50^\circ\text{C}$  compared to that of standard reactants. The same steps also occur over a narrower temperature range, making the analysis more difficult.

From the preceding discussion, it is clear that the reaction sequence in the formation of PZT solid solutions depends strongly on the raw materials used, powder characteristics, mixing method, and other experimental conditions. Discrepancies in the reaction sequence observed by several authors can be attributed to variations in experimental conditions. However, there is no doubt about the formation of a  $\text{PbTiO}_3$  phase at the beginning and intermediate PZT solid solutions of varying (Zr/Ti) ratio. The present study clearly shows that the reaction sequence can differ slightly, depending on the starting raw materials.

#### IV. Summary and Conclusions

The reaction sequence in the formation of PZT (60/40) composition was studied in detail by taking XRD patterns of powders calcined at different temperatures and times. The following reaction sequence is proposed.

- (1)  $\text{PbO}$  and  $\text{TiO}_2$  react to form  $\text{PbTiO}_3$ .
- (2)  $\text{PbO}$  or  $\text{PbO}$  (solid solution) reacts with  $\text{ZrO}_2$  to form  $\text{PbZrO}_3$ , or a  $\text{PbZrO}_3$ -rich intermediate product.
- (3) The  $\text{PbTiO}_3$  reacts with the remaining  $\text{ZrO}_2$  (and with some  $\text{PbO}$ ) to form a PZT-solid solution intermediate rich in PT. This reaction competes with step (2) above for the source of  $\text{ZrO}_2$ . This PZT intermediate is usually  $\text{PbTiO}_3$ -rich and has frequently been found to have a broad range of Zr/Ti ratios, centered around 40/60.
- (4) The intermediate products from either step (1) or step (3) above react with the product of step (2), if this reaction has oc-

curred. The resulting PZT solid solution has a distribution of Zr/Ti ratios determined by the previous steps.

(5) The solid solution homogenizes, resulting in a narrower compositional distribution.

Normally, all five of the above steps are observed, as shown for five combinations of raw materials from different sources. Step (2) is found to be particularly sensitive to the powder properties, and can vary in temperature. If it occurs at a low temperature, the reaction can consume all available  $\text{ZrO}_2$ , resulting in the elimination of step (3). Conversely, in the case of certain  $\text{ZrO}_2$  raw materials, step (2) is not observed, indicating that it may be shifted to such high temperatures as to make it noncompetitive. Reaction then occurs via steps (1), (3), (4), and (5), which corresponds to the reaction sequence of Matsuo and Sasaki.<sup>1</sup>

The PbO (solid solution) reported by other workers<sup>4,5,12</sup> was observed, but does not appear to significantly affect the reaction sequence in the formation of a final PZT solid solution of the desired composition.

The scheme presented above is believed to account for many of the discrepancies which have appeared in the literature in explaining the reaction sequence in the formation of a PZT solid solution, particularly with regard to the formation of the intermediate product,  $\text{PbZrO}_3$ . A clear understanding of the reaction sequence will help us explain the effects of variations of raw materials and calcination conditions on the ferroelectric properties of the PZT ceramics. This is, as one would expect, the compositional homogeneity and particularly the grain-boundary structure to be affected by the exact reactions which occur in the context of the scheme discussed in this paper.

**Acknowledgments:** The authors thank all colleagues at the Materials Research Laboratory for their useful discussions.

#### References

1. Mori, H., Miesada, K., Date, Y., Kikuchi, and T. Mizutani, "Study of Formation Process of  $\text{PbTi}_{1-x}\text{Zr}_x\text{O}_3$  Solid Solution with High Temperature X-Ray Diffractometry and Differential Thermal Analysis," *Nat. Tech. Rept. Matsushita Elec. Ind. Co., Osaka*, 10 (1) 32-40 (1964).
2. Y. Matsuo and H. Sasaki, "Formation of Lead Zirconate-Lead Titanate Solid Solutions," *J. Am. Ceram. Soc.*, 48 (6) 239-91 (1965).
3. N. H. Harris, "Solid State Reactions Forming the (Lead, Strontium) Titanate, Zirconate Solid Solution," Ph. D. Thesis, University of Illinois, Urbana-Champaign, 1967.
4. W. M. Spier, "Thermal Analysis of Processes Which Occur During the Calcining of Adulterated and Unadulterated Lead Zirconate-Lead Titanate," Ph. D. Thesis, Rutgers University, New Brunswick, NJ, 1969.
5. D. L. Hankey and J. V. Biggers, "Solid-State Reactions in the System  $\text{PbO}-\text{TiO}_2-\text{ZrO}_2$ ," *J. Am. Ceram. Soc.*, 64 (12) C-172-C-173 (1981).
6. D. L. Hankey, "Calcination Reaction Mechanisms and Kinetics in Lead Zirconate Titanate Powder Compacts," Ph. D. Thesis, The Pennsylvania State University, University Park, 1980.
7. S. S. Chandrasekhar, R. M. Fulrath, and J. A. Pask, "Reaction Mechanisms in the Formation of PZT Solid Solutions," *J. Am. Ceram. Soc.*, 64 (7) 422-25 (1981).
8. T. Ohno, M. Takahashi, and N. Tsubouchi, "Perovskite Formation Process in  $\text{PbTi}_{1-x}\text{Zr}_x\text{O}_3$  Ceramics Containing  $\text{SiO}_2$ ," *J. Jpn. Soc. Powder Metall.*, 20 (5) 154-60 (1973).
9. T. Yamaguchi, S. H. Cho, M. Makomori, and H. Kuno, "Effects of Raw Materials and Mixing Methods on the Solid State Reactions Involved in Fabrication of Electronic Ceramics," *Ceramurgia (Int.)*, 2 (2) 76-80 (1976).
10. S. Venkataramani and J. V. Biggers, "Reactivity of Zirconia in Calcining of Lead Zirconate-Lead Titanate Compositions Prepared from Mixed Oxides," *Am. Ceram. Soc. Bull.*, 59 (4) 462-66 (1980).
11. B. Jaffe, W. R. Cook, and H. Jaffe, *Piezoelectric Ceramics*, Academic Press, New York, 1971; p. 136.
12. A. I. Kingston, "Studies in the Preparation and Characterization of Selected Ferroelectric Materials," Ph. D. Thesis, University of South Africa, Pretoria, 1981.
13. V. A. Isupov, "Comments on the Paper: X-Ray Study of the PZT Solid Solutions Near the Monoclinic Phase Transition," *Solid State Commun.*, 17, 1331-33 (1975).
14. A. Gur and L. Bengurim, "X-Ray Study of the PZT Solid Solutions Near the Monoclinic Phase Transitions," *Solid State Commun.*, 15, 1077-79 (1974).
15. K. Kakagawa, J. Morita, T. Takanashi, H. Yamamura, and S. Shirasaka, "A Compositional Fluctuation and Properties of  $\text{PbZr}_{1-x}\text{Ti}_x\text{O}_3$ ," *Solid State Commun.*, 24, 69-72 (1977).
16. B. Jaffe, R. S. Roth, and S. Marzullo, "Properties of Piezoelectric Ceramics in the Solid Solution Series Lead Titanate-Lead Zirconate-Lead Oxide: Tin Oxide and Lead Titanate-Lead Titanate," *J. Res. Nat. Bur. Stand.*, 55 (5) 239-54 (1955).
17. S. Venkataramani, "Calcining and Its Effects on Sintering and Properties of Lead Zirconate Titanate Ceramics," Ph. D. Thesis, The Pennsylvania State University, University Park, 1981.

\*Lot #13  $\text{ZrO}_2$ , Harshaw Chemical Co., Cleveland, OH; or 36547 PbO, J. T. Baker Chemical Co., Phillipsburg, NJ; grade 3323-20-4  $\text{TiO}_2$ , Whitaker, Clark & Daniels, Inc.

**APPENDIX 29**

Reprinted from the Journal of the American Ceramic Society, Vol. 66, No. 10, October 1983.  
Copyright 1983 by The American Ceramic Society

## Products of Reaction Between PbO and Nb<sub>2</sub>O<sub>5</sub> in Molten KCl or NaCl

TOSHIO KIMURA,\* MASATAKA MACHIDA, AND TAKASHI YAMAGUCHI\*

Faculty of Science and Technology, Keio University, 3-14-1 Hiyoshi, Kohoku-ku, Yokohama 223, Japan

ROBERT E. NEWNHAM\*

Materials Research Laboratory, Pennsylvania State University, University Park, Pennsylvania 16802

*Lead oxide and niobium oxide were heated in molten KCl or NaCl to examine the participation of chlorides in the reaction between the oxides. Alkali ions partially replace Pb ions in PbNb<sub>2</sub>O<sub>6</sub>, and Cl ions form PbCl<sub>2</sub>. The substitution of alkali ions for Pb stabilizes the tetragonal form of PbNb<sub>2</sub>O<sub>6</sub>. The reactivity of NaCl with Nb<sub>2</sub>O<sub>5</sub> was much greater than that of KCl; the extended substitution resulted in the formation of an NaNbO<sub>3</sub> phase with incorporated Pb.*

**M**OLTEN salt synthesis is an important preparation method of ceramic powders and has been used to prepare ferrites and ferroelectrics.<sup>1</sup> This method yields oxides by the reaction between constitu-

ent oxides in the presence of molten salt. The molten salt has been considered to act as a pure solvent, and the salt content in the thoroughly washed products is quite small in some cases.<sup>1-3</sup> Recently, Arendt and Rosolowski<sup>4</sup> demonstrated that the orthorhombic form of PbNb<sub>2</sub>O<sub>6</sub> is obtained in molten NaCl-KCl mixtures at temperatures far below its transition temperature. Lead metaniobate has three modifications: rhombohedral, tetragonal, and orthorhombic.<sup>5</sup>

The former two are stable and the transition temperature between them is ~1150°C; the orthorhombic form is metastable. When the high-temperature stable phase (tetragonal) is cooled, it does not change to the low temperature stable phase (rhombohedral) because of the sluggish transition, but rather changes to the orthorhombic phase at 570°C. The results of Arendt and Rosolowski can be understood by assuming that the molten salt stabilizes the high-temperature or metastable phase.

This communication demonstrates the participation of the chlorides in the reaction between PbO and Nb<sub>2</sub>O<sub>5</sub> and proposes possible mechanisms of the phase stabilization. Although Arendt and Rosolowski<sup>4</sup> used NaCl-KCl mixed salts, a single salt was used in this experiment. Equimolar mixtures of PbO and Nb<sub>2</sub>O<sub>5</sub> were mixed with an equal weight of NaCl or KCl in an agate mortar and pestle for 1 h. The mixtures were heated in a furnace kept at a constant temperature between 750° and 1050°C. The salt was removed from the oxides by washing with hot deionized water several times; specimens were washed more than 20 times for chemical X-ray fluorescence analysis (XFA). Because the sodium content could not be measured by XFA, atomic absorption analysis was used. The phases were identified by X-ray

CONTRIBUTING EDITOR — P. K. GALLAGHER

Received June 30, 1983; approved July 12, 1983.  
Supported in part by the U. S. Army Research Office under Contract No. DAAG 39-80-C-0008.  
\*Member, the American Ceramic Society.

diffraction (XRD) using  $\text{CuK}\alpha$  radiation. Figure 1 shows typical XRD profiles of the products, and Table I summarizes the experimental conditions and product phases.

The product phase obtained between 750° and 1050°C in KCl was orthorhombic

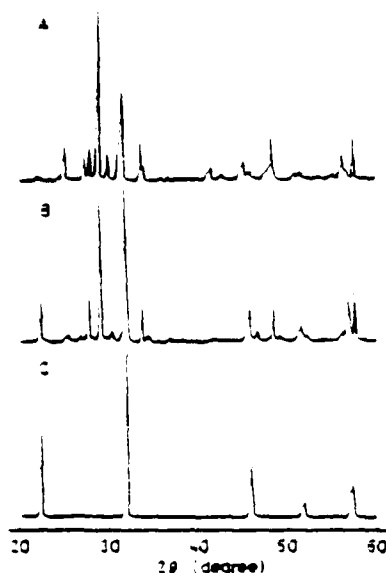
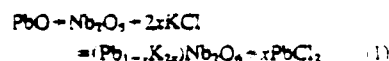


Fig. 1. X-ray diffraction patterns of products of samples heated for 1 h in (A) KCl at 950°C, (B) NaCl at 950°C, and (C) NaCl at 1050°C.

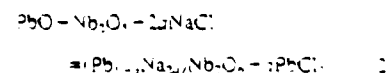
$\text{PbNb}_2\text{O}_6$ . Even at 750°C, well below the melting point of KCl, there was complete reaction to form  $\text{PbNb}_2\text{O}_6$ . In a sample fired under the same conditions but in the absence of KCl, however, the reaction was incomplete, and the resulting  $\text{PbNb}_2\text{O}_6$  phase was rhombohedral. Table II shows XFA results. In all cases the Cl content was less than the analytical limit (<0.1 wt%), and the difference between 100% and the sum of the weight percent of each ion was assigned to oxygen. A potassium ion can substitute for the Pb ion in the form  $(\text{Pb}_{1-x}\text{K}_x)\text{Nb}_2\text{O}_6$ ,<sup>4</sup> and calculated  $x$  values are shown in Table II. These results indicate that KCl participates in the reaction between  $\text{PbO}$  and  $\text{Nb}_2\text{O}_5$  and that K ions substitute for Pb in  $\text{PbNb}_2\text{O}_6$  lattice. The fact that Pb ions were detected by adding  $\text{K}_2\text{CrO}_4$  aqueous solution to the first supernatant washing water supports the proposed substitution of K for Pb. The substitution is accompanied by the formation of  $\text{PbCl}_2$ . The reaction can be summarized as follows:



Incorporation of potassium ions in the lead metaniobate structure stabilizes the tetragonal form. The transition temperature from the rhombohedral to the tetragonal form is  $\approx 1150^\circ\text{C}$ , and the piezoelectric orthorhombic form can be obtained only when the tetragonal form cools to the

tetragonal-orthorhombic transition temperature (ferroelectric Curie temperature).<sup>5</sup> The fact that the orthorhombic form at room temperature was obtained by firing even at 750°C indicates that the tetragonal form is stabilized by the incorporation of K into the  $\text{PbNb}_2\text{O}_6$  lattice. The reported evidence that the Curie temperature decreases with increasing K-ion content eliminates the possibility of the stabilization of the orthorhombic form by K ion.<sup>6</sup> The tetragonal form has  $\frac{1}{4}$  empty sites in the Pb position, but the rhombohedral form has no such vacant sites.<sup>7</sup> The  $x$  value near 0.2 obtained for samples fired between 350° and 1050°C corresponds with all vacant sites being occupied by K ions. By replacing one Pb ion with two K ions, the predicted value agrees with the reported solubility limit ( $x=0.25$ ).<sup>8</sup> The stabilization of the tetragonal form by the incorporation of a K ion is probably explained in terms of its open structure.

The reaction products obtained in NaCl were different from those in KCl. The typical XRD profiles of the products are shown in Fig. 1(B) and (C), and the product phases are summarized in Table I. At 750°C the product was rhombohedral  $\text{PbNb}_2\text{O}_6$ . At 350° and 950°C, mixtures of orthorhombic  $\text{PbNb}_2\text{O}_6$  and a phase with cubic structure were obtained. The intensity of the diffraction lines of the cubic form increased with increasing temperature up to 1050°C at which a single-phase cubic form was obtained. The diffraction pattern of the cubic form coincided with pseudocubic  $\text{NaNbO}_3$ .<sup>9</sup> Diffraction lines (200), (210), and (220) ( $2\theta=46.0^\circ$ ,  $51.9^\circ$ , and  $57.3^\circ$ , respectively) split slightly, indicating that this phase was slightly distorted. Again Pb ions were detected in the first supernatant washing water. Table III shows the Na, Pb, and Nb contents and composition. The formula  $(1-x)\text{NaNbO}_3 - x\text{PbNb}_2\text{O}_6$  was adopted to compare with the data of Francombe and Lewis.<sup>10</sup> Because the accuracy in determining the Na content was less than that in determining the Pb content, the  $y$  value was calculated based on the molar ratio of Pb/Nb. The  $y$  values in the samples obtained between 350° and 1050°C indicate that the samples are in the two-phase region ( $\text{NaNbO}_3$  and  $\text{PbNb}_2\text{O}_6$ ), even for the single-phase specimen with the pseudocubic structure obtained at 1050°C. It is possible that the  $\text{NaNbO}_3$  phase region extends into the  $\text{NaNbO}_3$ - $\text{PbNb}_2\text{O}_6$  system. These results indicate that NaCl also participates in the reaction and that Na ions in  $\text{PbNb}_2\text{O}_6$  stabilize the tetragonal structure. Furthermore, the extent of the exchange of the alkali ion for the Pb is greater in the case of NaCl than in KCl. The reaction can be summarized as follows:



and

Table I. Preparation Conditions and Product Phases

Temp. (°C)	Time (h)	Salt	Product phases*
750	1	KCl	Ortho
350	1	KCl	Ortho
950	1	KCl	Ortho
1050	1	KCl	Ortho
1050	5	KCl	Ortho
750	1	NaCl	Rhombo
350	1	NaCl	Cubic-ortho
950	1	NaCl	Cubic-ortho
1050	1	NaCl	Cubic
1050	5	NaCl + KCl	Ortho

\*Ortho=orthorhombic  $\text{PbNb}_2\text{O}_6$ , rhombo=rhombohedral  $\text{PbNb}_2\text{O}_6$ , cubic=pseudocubic  $\text{NaNbO}_3$ .

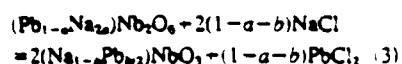
Table II. Results of X-Ray Fluorescence Analysis for Samples Heated for 1 Hour in KCl

Temp. (°C)	Content (wt%)			$x$ in $(\text{Pb}_{1-x}\text{K}_x)\text{Nb}_2\text{O}_6$
	K	Pb	Nb	
750	2.1	34.2	38.6	0.12
350	3.4	35.7	40.1	0.20
950	3.7	35.1	40.3	0.22
1050	3.8	34.8	40.5	0.23

Table III. Results of X-Ray Fluorescence and Atomic Absorption Analyses for Samples Heated for 1 Hour in NaCl

Temp. (°C)	Content (wt%)			$y$ in $(1-y)\text{NaNbO}_3 - y\text{PbNb}_2\text{O}_6$
	Na	Pb	Nb	
750	0.2	40.3	38.2	0.94
350	4.7	30.2	43.4	0.63
950	5.7	26.2	45.3	0.52
1050	6.3	24.9	46.2	0.48



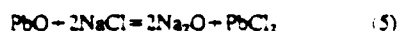


Pure  $\text{NaNbO}_3$  is orthorhombic at room temperature and the Curie temperature is  $640^\circ\text{C}$ . Since the substitution of Pb for Na decreases the Curie temperature,<sup>9</sup> the pseudocubic  $\text{NaNbO}_3$  phase obtained in this experiment is caused by the incorporation of the Pb ion.

Because standard free-energy changes for the following reactions



and



are positive<sup>10</sup> (370 and 266 kJ at  $298^\circ\text{C}$  for the reactions (4) and (5), respectively), the difference in the product phases is related to the reactivity of the chlorides with  $\text{Nb}_2\text{O}_5$ . Niobium oxide was mixed with NaCl or KCl and heated at  $1050^\circ\text{C}$  for 1 h. No reaction was detected in the case of KCl, whereas the  $\text{Na}_2\text{Nb}_4\text{O}_{11}$  or  $\text{NaNb}_2\text{O}_6$  phases were obtained in NaCl (since the XRD patterns of these two niobates are almost the same,<sup>11</sup> it could not be deter-

mined which of the phases was formed). This result indicates that NaCl is more reactive with  $\text{Nb}_2\text{O}_5$  than KCl.

Granahan *et al.*<sup>12</sup> prepared grain-oriented  $\text{PbNb}_2\text{O}_6$  ceramics from powder reacted in NaCl-KCl-mixed salt at  $1050^\circ\text{C}$  for 5 h. In the present experiments, an orthorhombic phase of  $\text{PbNb}_2\text{O}_6$  was obtained under the same conditions, as shown in Table I. Orthorhombic  $\text{PbNb}_2\text{O}_6$ , obtained at  $1050^\circ\text{C}$  in KCl and washed with water, was mixed with NaCl and heated at  $1050^\circ\text{C}$  for 1 h. The resultant powder contained the pseudocubic  $\text{NaNbO}_3$  phase. These experiments indicate that the presence of KCl in the NaCl-KCl mixture suppresses the reaction between the orthorhombic  $\text{PbNb}_2\text{O}_6$  and NaCl.

#### ACKNOWLEDGMENT

The authors would like to acknowledge K. Utsuru for performing the X-ray fluorescence and atomic absorption analyses.

#### REFERENCES

- R. H. Arendt, J. H. Rosolowski, and J. W. Savinazzi, "Lead Zirconate Titanate Ceramics from Molten Salt Solvent Synthesized Powders," *Water Res. Bull.*, 14 (5) 703-709 (1979).
- T. Takahashi, N. Mogushi, T. Kimura, and T. Yamaguchi, "Formation Mechanism of Ferrite Powders in Flux," *Yuppon Kagaku Kaishi*, 1981, No. 9, 391-95.
- Y. Inoue, T. Kimura, and T. Yamaguchi, "Sintering of Glass-Like  $\text{Bi}_2\text{Ti}_2\text{O}_7$  Powders," *Am. Ceram. Soc. Bull.*, 62 (6) 704-707, 711 (1983).
- R. H. Arendt and J. H. Rosolowski, "Molten Salt Synthesis of Orthorhombic Lead Metaniobate Powder," U.S. Pat. 4,234,558, November 18, 1980.
- R. S. Roth, "Phase Equilibrium Relations in the Binary System Lead Oxide-Niobium Pentoxide," *J. Res. Nat. Bur. Stand.*, 62 (1) 27-38 (1959).
- E. C. Subbarao and G. Shirane, "Nonstoichiometry and Ferroelectric Properties of  $\text{PbNb}_2\text{O}_6$ -Type Compound," *J. Chem. Phys.*, 32 (6) 1846-51 (1960).
- R. Mahe, "Structure of Rhombohedral Lead Metaniobate II," *Bull. Soc. Chim. Fr.*, 1967, 61, 879-84 (1967).
- Powder Diffraction File, Card No. 19-1221 Joint Committee on Powder Diffraction Standards, Swarthmore, PA.
- M. H. Francombe and B. Lewis, "Structure and Phase Transitions of Ferroelectric Sodium-Lead Niobate and of Other Sodium Niobate-Type Ceramics," *J. Electrochem. Soc.*, 104 (4) 387-403 (1957).
- O. Kubaschewski and E. L. Evans, *Metallurgical Thermochemistry*, 3d ed., Pergamon, London, 1958.
- Powder Diffraction File, Card No. 13-129 and 21-1367 Joint Committee on Powder Diffraction Standards, Swarthmore, PA.
- M. Granahan, M. Holmes, W. A. Schultze, and R. E. Newnham, "Grain-Oriented  $\text{PbNb}_2\text{O}_6$  Ceramics," *J. Am. Ceram. Soc.*, 64 (4) C-68-C-69 (1981).

**APPENDIX 30**

*to appear in Nov 1983 J Am Cer Soc*

## FABRICATION OF GRAIN ORIENTED $\text{PbBi}_2\text{Nb}_2\text{O}_9$

Sheng-He Lin<sup>\*</sup>, S.L. Swartz, W.A. Schulze and J.V. Biggers

Materials Research Laboratory  
The Pennsylvania State University  
University Park, PA 16802

### ABSTRACT

This paper describes a process for the fabrication of grain oriented  $\text{PbBi}_2\text{Nb}_2\text{O}_9$  ceramics. A molten salt technique was used to synthesize crystallites of  $\text{PbBi}_2\text{Nb}_2\text{O}_9$  with a high degree of shape anisotropy. Tape casting and subsequent uniaxial hot pressing resulted in ceramics with grain orientation of greater than 90% with densities greater than 96% theoretical.

---

Address: Department of Inorganic Materials Science and Engineering,  
South China Institute of Technology, Guangzhou, China.

## I. Introduction

$\text{PbBi}_2\text{Nb}_2\text{O}_9$  (PBN) is a member of the high Curie temperature bismuth oxide layer structure compounds. It was first synthesized in 1949 by Amriviillins<sup>1</sup>, and its ferroelectric nature was discovered by Smolenskii<sup>2</sup>, et al. in 1959. Subbarao<sup>3</sup>, in 1961, published a set of dielectric and piezoelectric measurements on PBN ceramics, reporting a  $d_{33}$  coefficient of  $15 \times 10^{-12}$  C/N. Ikegami and Ueda<sup>4</sup> followed up with a set of piezoelectric measurements in 1974, and reported a coupling factor,  $K_t$ , of 17%. These seemingly low values of  $d_{33}$  and  $K_t$  can be explained by the anisotropic crystal structure of PBN. There exists only two polar axes in PBN, as opposed to the multiple domain states of the perovskite ferroelectrics; so that in a randomly oriented polycrystalline ceramic, efficient poling is difficult to achieve.

If PBN could be fabricated with substantial grain orientation and sufficient density, efficient poling would become possible. This might lead to applications as high sensitivity transducer devices for temperatures in excess of 400°C. To this end, there have been several attempts at achieving grain orientation in PBN<sup>5,6</sup> and other bismuth oxide layer structural ferroelectrics<sup>7-11</sup>. These workers employed hot forging techniques to develop grain orientation. They were quite successful in achieving good density and substantial grain orientation; however, hot forging should inevitably result in deleterious orientation gradients.

This paper describes the preparation of grain oriented PBN ceramics by a modification of the molten salt synthesis-tape casting technique, which has been used successfully in the past to fabricate grain oriented ceramics of  $\text{Bi}_4\text{Ti}_3\text{O}_{12}$ <sup>12-14</sup>,  $\text{Bi}_2\text{WO}_6$ <sup>12-15</sup> and  $\text{PbNb}_2\text{O}_6$ <sup>16,17</sup>.

## II. Fabrication of Grain Oriented $\text{PbBi}_2\text{Nb}_2\text{O}_9$

### A. Structure of $\text{PbBi}_2\text{Nb}_2\text{O}_9$

The family of bismuth oxide layer structures can be represented by the general formula:



where Me can be any of several mono-, di-, or tri-valent cations ( $\text{Na}^+$ ,  $\text{Pb}^{2+}$ , etc.), and R represents a tetra-, penta-, or hexa-valent cation ( $\text{Ti}^{4+}$ ,  $\text{Nb}^{5+}$ ,  $\text{W}^{6+}$ , etc.). The structure can be described as a combination of a perovskite type layers interleaved with  $\text{Bi}_2\text{O}_2^{2-}$  layers. The coefficient m can range from 1 to 5 and is equal to 2 for the compound  $\text{PbBi}_2\text{Nb}_2\text{O}_9$ .

The structure of  $\text{PbBi}_2\text{Nb}_2\text{O}_9$  is shown in Figure 1. It is often referred to as 'pseudotetragonal,' but is actually orthorhombic with lattice parameters a, b, and c equal to 5.492, 5.503, and 25.53Å, respectively<sup>18</sup>. The spontaneous polarization lies in the a-b plane at about 45° between the a and b axes. Thus, if grain orientation is to enhance the piezoelectric properties of PBN, then the orientation must be such that the a and b directions are aligned perpendicular to the c direction in the ceramic.

### B. Molten Salt Synthesis

The molten salt synthesis technique consists of reacting oxides in a suitable salt system at a temperature at which the salts are molten. The salts act as a transport medium for the diffusion of the oxides. The advantage of molten salt processing over solid state reaction is that it produces a homogeneous powder with the particle size and morphology being easily controlled by the reaction temperature. This process has been used

in the past to produce homogeneous powders of  $\text{PZT}^{19}$ ,  $\text{BaFe}_{12}\text{O}_{19}^{20}$  and  $\text{NiFe}_2\text{O}_4^{21}$  and more recently has been adopted at this laboratory for the fabrication of grain oriented ceramics. The usefulness of the molten salt synthesis technique in the fabrication of grain oriented ceramics is due to the tendency of certain growth directions to be favored during formation of crystallites in the molten salt. Molten salt synthesis of the bismuth oxide layer structure compounds results in crystallites with plate-like morphologies<sup>12-15</sup>, while molten salt synthesis of the tungsten bronze  $\text{PbNb}_2\text{O}_6$  results in crystallites with needle-like morphologies<sup>16,17</sup>. These crystallites can then be aligned by tape casting, prior to the sintering step. The advantage of achieving grain orientation by tape casting prior to sintering (or hot pressing) is that the problem of orientation gradients in the final ceramic is eliminated.

### C. Tape Casting

Tape casting is a process whereby a slurry, consisting of a ceramic powder and organic binder system, is poured on a moving glass plate and forced under a doctor blade to form a thin flexible sheet (or tape)<sup>22</sup>. This process is useful for the fabrication of grain oriented ceramics because of the tendency of the platelets (in the case of the bismuth oxide layer structured compounds) or needles (in the case of  $\text{PbNb}_2\text{O}_6$ ) to lie flat during the casting process. This tendency to lie flat during tape casting is due to the mechanical or flow forces exerted by the doctor blade and possibly gravitational settling forces.

The orientation developed by tape casting of platelets (in the case of the bismuth oxide layer structured compounds) is such that the c-direction is perpendicular to the plane of the tape. Recalling that the polar direction of PBN lies in the a-b plane, the piezoelectric properties

will be enhanced in the direction parallel to the plane of the tape. Thus, it is required to laminate several layers of tape to develop a thickness that is large enough so that properties can be measured in the a-b oriented direction of what will eventually become the grain oriented ceramic. This is achieved by warm pressing several layers of tape together<sup>23</sup>. The applied pressure and temperature are large enough to cause the binder to flow and completely laminate the layers of tape. This step is believed to further increase the orientation of the crystallites in the green pressed tape.

#### D. Binder Burnout and Hot Pressing

Due to the large volume percent of organics and relatively large density of the pressed tapes, extreme care must be exercised during the binder burnout. If the heating rate is too fast as the organics volatilize, the gases do not have enough time to escape the pressed tape, and bloating occurs. This problem is alleviated by the use of ultra-slow heating rates in the range of temperature where the binder volatilization is greatest.

It was found that in the fabrication of grain oriented  $\text{Bi}_4\text{Ti}_3\text{O}_{12}$  ceramics by the molten salt synthesis-tape casting method, conventional sintering was sufficient to achieve substantial grain orientation with acceptable density (92-94% theoretical)<sup>14</sup>. However, in the case of PBN, the molten salt-tape casting method, followed by conventional sintering, resulted in ceramics with large grain orientations, but disappointingly low densities (80-85% theoretical)<sup>24</sup>. For this reason, it was decided to employ mild hot pressing conditions to help in the densification of grain oriented PBN ceramics.

### E. Characterization of Grain Oriented Ceramics

Two important parameters to consider are the density and the degree of grain alignment. Density can be measured by geometry or by the Archimedes method. The degree of grain orientation can be monitored by scanning electron microscopy and x-ray diffraction.

Lotgering<sup>25</sup> developed a quantitative measure of the degree of grain orientation from x-ray diffraction data, by defining an orientation factor  $f$ ,

$$f = (P - P_0) / (1 - P_0)$$

where  $P = \sum I_{(002)} / \sum I_{(hk2)}$ ,  $\sum I_{(002)}$  is the sum of intensities of the (002) reflections,  $\sum I_{(hk2)}$  is the sum of intensities of all (hk2) reflections, and  $P_0$  is the value of  $P$  for random orientation. Lotgering's orientation factor  $f$  is equal to zero for random orientation and one for complete orientation. Thus, the use of Lotgering's orientation factor allows one to normalize the degree of orientation to 100%.

### III. Experimental Procedure

Reagent grade oxides were batched according to the PSN stoichiometry, with a 3 mole% excess of PbO added to account for volatilization during firing. The salt system selected was equi-molar NaCl-KCl, and the salts were weighed out with the oxides so that the weight ratio of oxides to salts was unity. The mixture was ball milled in alcohol for 12 hours in a malgene jar with zirconia media, followed by drying overnight at 100°C.

The unreacted powder was loaded into alumina crucibles and heated to 350°C for 3 hours to insure that all organics were removed. Lids were placed on the crucibles and the powder was heated at a rate of 100°C/hour to the molten salt synthesis reaction temperatures which ranged from 300



to 1150°C. After a 2 hour soak time, the furnace was turned off and allowed to cool.

Salt removal was a tedious but very important step. The sintered oxide-salt mass was placed in a beaker with distilled water. Boiling was sufficient to break up the chunks, and a magnetic stirrer was added to facilitate the salts going into solution. After 1-2 hours of boiling and stirring, the beaker was removed from the hot plate and the material allowed to settle, followed by decanting. The material was subjected to at least 20 such washings and then allowed to dry.

Molten salt PBN powder synthesized at 1050°C was selected for tape casting and subsequent production of grain oriented PBN ceramics. Prior to tape casting, a slurry consisting of 67% by weight of PBN powder and 33% of a commercial organic binder system<sup>26</sup> was prepared. After ball milling for 24 hours, tapes were cast on to a moving glass plate with the doctor blade set at a height of 0.4 mm. After drying, the single layer tapes were cut into disc shapes of 1.43 cm diameter. Between 30 and 50 layers were stacked in a steel die and laminated by warm pressing for 15 minutes at 60°C and 700 MPa. Binder burnout was accomplished by heating the pressed discs from room temperature to 600°C in 3 days. A heating rate of ~3°C/hour was utilized in the range of 200-300°C where binder volatilization is greatest.

The hot pressing was conducted in a simple resistance heated lever-arm press with an air ambient. The samples were isolated from the alumina rams by Pt foil. The three main hot pressing parameter variables included the hot pressing temperature (1055-1095°C), pressure (13.6-21.4 MPa), and time (0.5-2.5 hours). A typical hot pressing temperature-pressure-time profile is given in Figure 2. Densities of the hot pressed PBN ceramics were measured by the Archimedes method. Lotgering orientation factors

were calculated from x-ray diffraction patterns. The degree of orientation was determined by averaging the orientation factors calculated from both the top and bottom faces (ground with 600 grit) of the hot pressed PBN pellets. SEM micrographs were taken on fractured surfaces perpendicular to the hot pressing direction.

#### IV. Results and Discussion

The molten salt synthesized powders were subjected to chemical, x-ray diffraction, and scanning electron microscopy analyses. Chemical analysis revealed the presence of less than 0.05 wt% of  $K^+$ ; however, 0.50 wt% of  $Na^+$  was detected. Whether the sodium is going into the PBN structure or whether this simply indicates incomplete washing is not known at this time. X-ray diffraction confirmed that single phase  $PbBi_2Nb_2O_9$  was formed for all molten salt synthesis reaction temperatures (800–1150°C).

Presented in Figures 3a, b, and c are typical SEM micrographs of PBN powder synthesized at 800, 1050, and 1150°C, respectively. The morphology of the crystallite was plate-like over the entire range of molten salt reaction temperatures, with aspect ratios of 10–20. The expected result of an increase of crystallite size with increasing reaction temperature was observed. The increase of platelet size with increasing temperature was more pronounced from 1050 to 1150°C than the gradual increase of platelet size observed between 800 to 1050°C.

The microstructures of PBN ceramics, made by the molten salt-tape casting method and densified by conventional sintering (1060°C, 2 hours) and hot pressing (1075°C, 17.5 MPa, 2 hours), may be compared in Figure 4. An increase of density (6.7 to 8.0 g/cc) and orientation (58 to 90%) was observed with hot pressing. This demonstrates the importance of the hot pressing step. The same hot pressing conditions were applied to a pressed

tape made of calcined (equi-axed) PBN powder. This resulted in a PBN ceramic with a density of 7.9 g/cc and orientation of only 45%, demonstrating the importance of the molten salt-tape casting processing.

The dependence of the density and orientation of PBN ceramics on the hot pressing temperature, pressure, and time are demonstrated in Figures 5a, b, and c, respectively. The trends are similar for the three parameters. Both the density and orientation increase to some saturation level as the hot pressing temperature, pressure, and time are increased within the range of hot pressing conditions employed.

#### V. Summary

The results of this investigation are summarized below:

1. Molten salt synthesis was used to produce tiny plate-like crystallite of  $\text{PbBi}_2\text{Nb}_2\text{O}_9$  with reaction temperatures ranging from 800 to 1150°C.
2. Tape casting of molten salt PBN powder and subsequent warm pressing resulted in a substantial grain orientation in the green body.
3. Uniaxial hot pressing of the green pressed tapes resulted in PBN ceramics with densities of greater than 96% theoretical and grain orientation of over 90%.
4. The specific hot pressing conditions employed (temperature, pressure, time) were found to have a significant effect on the density and orientation of grain oriented PBN ceramics.

#### ACKNOWLEDGEMENTS

The authors are greatly indebted to Dr. Cross and Dr. Newnham for their advice in the fabrication of  $\text{PbBi}_2\text{Nb}_2\text{O}_9$  ceramics and to Mr. H.C. Chen for his help in the  $\text{PbBi}_2\text{Nb}_2\text{O}_9$  powder preparation.

#### REFERENCES

1. B. Aurivillius, 'Mixed Bismuth Oxides with Layer Lattices: I. The Structure Type of  $\text{CaNb}_2\text{Bi}_2\text{O}_9$ ,' *Arkiv fur Kemi*, 1 [54], 463-480 (1949).
2. G. Smolenskii, V.A. Isupov, and A.I. Agranovskaya, 'A New Group of Ferroelectrics (with Layered Structure),' *Soviet Physics Solid State*, 1 [1], 149-150 (1959).
3. E.C. Subbarao, 'Ferroelectricity in Mixed Bismuth Oxides with Layer-Type Structure,' *Journal of Chemical Physics*, 34 [2], 695-696 (1961).
4. S. Ikegami and I. Ueda, 'Piezoelectricity in Ceramics of Ferroelectric Bismuth Compound with Layer Structure,' *Japanese Journal of Applied Physics*, 13 [10], 1572-1577 (1974).
5. H. Igarashi, K. Matsunaga, T. Taniai, and K. Okazaki, 'Dielectric and Piezoelectric Properties of Grain-Oriented  $\text{PbBi}_2\text{Nb}_2\text{O}_9$  Ceramics,' *Bulletin of the American Ceramic Society*, 57 [9], 815-817 (1978).
6. Y. Nakamura, H. Igarashi, T. Taniai, and K. Okazaki, 'Grain Orientation Effects on Strength in  $\text{PbBi}_2\text{Nb}_2\text{O}_9$ ,' *Bulletin of the American Ceramic Society*, 53 [9], 853-855 (1979).
7. T. Takenaka, K. Shoji, H. Takai, and K. Sakata, 'Ferroelectric and Dielectric Properties of Press Forged  $\text{Bi}_4\text{Ti}_3\text{O}_{12}$  Ceramics,' *Proceedings of the Japan Congress on Materials Research*, 19, 230-233 (1979).

3. T. Takenaka, K. Shoji, and K. Sakata, 'Grain Orientation and Microstructure of Hot-Forged  $\text{Bi}_4\text{Ti}_3\text{O}_{12}$  Ceramics,' Proceedings of the Japan Congress on Materials Research, 20, 212-214 (1977).
9. K. Sakata, T. Takenaka, and K. Shoji, 'Hot-Forged Ferroelectric Ceramics of Some Bismuth Compounds with Layer Structure,' Ferroelectrics, 22 [1/2], 825-826 (1978).
10. T. Takenaka and K. Sakata, 'Grain Orientation and Electrical Properties of Hot-Forged  $\text{Bi}_4\text{Ti}_3\text{O}_{12}$  Ceramics,' Japanese Journal of Applied Physics, 19 [1], 31-39 (1980).
11. T. Takenaka and K. Sakata, 'Electrical Properties of Grain-Oriented Ferroelectric Ceramics in Some Lanthanum Modified Layer-Structure Oxides,' Ferroelectrics, 38 [1/2/3/4], 769-772 (1981).
12. M. Holmes, 'Grain-Oriented Ferroelectric Ceramics,' M.S. Thesis, The Pennsylvania State University, University Park, PA (1980).
13. M. Holmes, R.E. Newnham and L.E. Cross, 'Grain-Oriented Ferroelectric Ceramics,' Bulletin of the American Ceramic Society, 58 [9], 872 (1979).
14. S.L. Swartz, W.A. Schulze and J.V. Biggers, 'Fabrication and Electrical Properties of Grain Oriented  $\text{Bi}_4\text{Ti}_3\text{O}_{12}$  Ceramics,' Ferroelectrics, 38 [1/2/3/4], 765-768 (1981).
15. T. Kimura, M. Holmes and R.E. Newnham, 'Fabrication of Grain-Oriented  $\text{Bi}_2\text{WO}_6$  Ceramics,' Journal of the American Ceramic Society, 65 [4], 223-226 (1982).
16. M. Granahan, 'Effect of Molten Salt Processing and Tape Casting on the Ferroelectric Properties of Lead Metaniobate,' B.S. Thesis, The Pennsylvania State University, University Park, PA (1980).

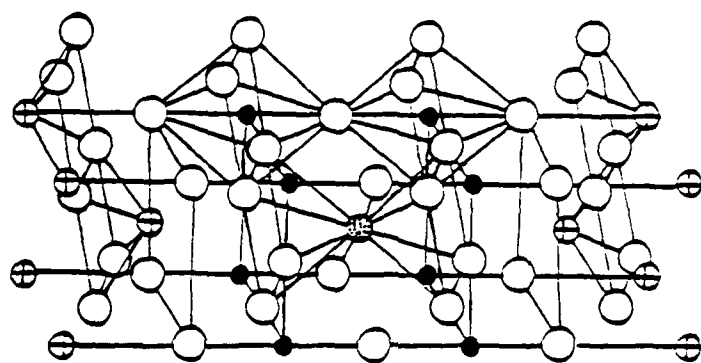
17. M. Granahan, M. Holmes, W.A. Schulze and R.E. Newnham, 'Grain-Oriented  $\text{PbNb}_2\text{O}_6$  Ceramics,' *Journal of the American Ceramic Society*, 64 [4], C68-C69 (1981).
18. B. Jaffe, W.R. Cook and H. Jaffe, *Piezoelectric Ceramics*, Academic Press, New York (1971).
19. R.H. Arendt, J.H. Rosolowski and J.W. Szymaszek, 'Lead Zirconate Titanate Ceramics from Molten Salt Synthesized Powders,' *Materials Research Bulletin*, 14 [5], 703-709 (1979).
20. R.H. Arendt, 'The Molten Salt Synthesis of Single Magnetic Domain  $\text{BaFe}_{12}\text{O}_{19}$  and  $\text{SrFe}_{12}\text{O}_{19}$  Crystals,' *Journal of Solid State Chemistry*, 8 [4], 339-347 (1973).
21. T. Kimura, T. Takahashi and T. Yamaguchi, 'Preparation and Characteristics of Ni-Ferrite Powders Obtained in the Presence of Fused Salts,' *Journal of Materials Science*, 15 [6], 1491-1497 (1980).
22. J.C. Williams, 'Doctor-Blade Processes,' in *Treatise on Materials Science and Technology*, Volume 9, Ceramic Fabrication Processes, Edited by F.Y. Wang, Academic Press, New York (1976).
23. J.V. Biggers, T.R. Shrout and W.A. Schulze, 'Densification of PZT Cast Tape by Pressing,' *Bulletin of the American Ceramic Society*, 58 [5], 516-518 (1979).
24. S.L. Swartz, unpublished data.
25. F.X. Lotgering, 'Topotactical Reactions with Ferrimagnetic Oxides Having Hexagonal Crystals Structures-I,' *Journal of Inorganic Nuclear Chemistry*, 2 [2], 113-123 (1959).
26. Cladan B-62, Cladan, Inc., San Marcos, California.

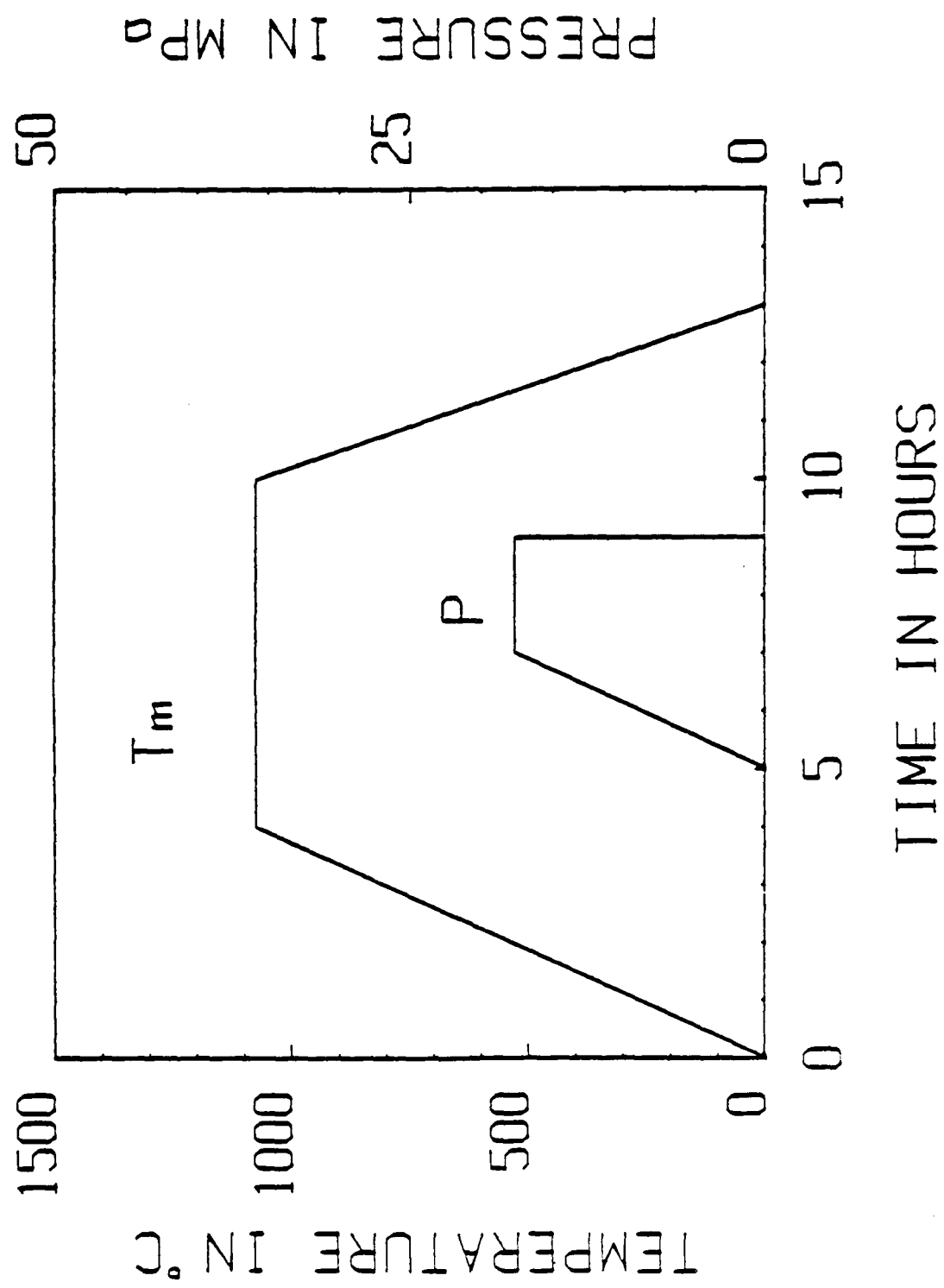
Sheng-He Lin is a lecturer at the Department of Inorganic Materials Science and Engineering, South China Institute of Technology, Guangzhou, China. Since 1965, he has been teaching and conducting research on piezoelectric ceramics. In 1982, he was a visiting scholar at the Materials Research Laboratory, The Pennsylvania State University.

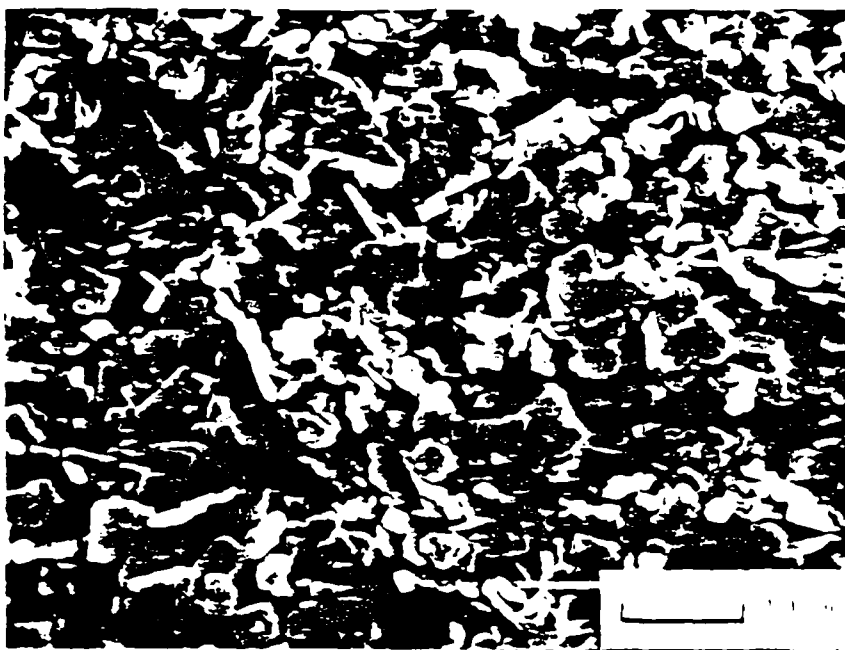
## LIST OF FIGURES

- Figure 1.  $\text{PbBi}_2\text{Nb}_2\text{O}_9$  structure in pseudotetragonal form.
- Figure 2. Time dependence of temperature and pressure during a hot-pressing cycle.
- Figure 3. Typical SEM micrographs of molten salt synthesizing  $\text{PbBi}_2\text{Nb}_2\text{O}_9$  powders reacted at a)  $800^\circ\text{C}$ , b)  $1050^\circ\text{C}$ , and c)  $1150^\circ\text{C}$ .
- Figure 4. Typical fracture micrographs looking parallel to the tape cast layers for ceramic that was a) conventionally sintered at  $1060^\circ\text{C}$  for 2 hours, and b) hot pressed at 17.5 MPa at  $1075^\circ\text{C}$  for two hours.
- Figure 5. Dependence of orientation factor and density on a) hot pressing temperature, b) hot pressing pressure, and c) duration at pressure.



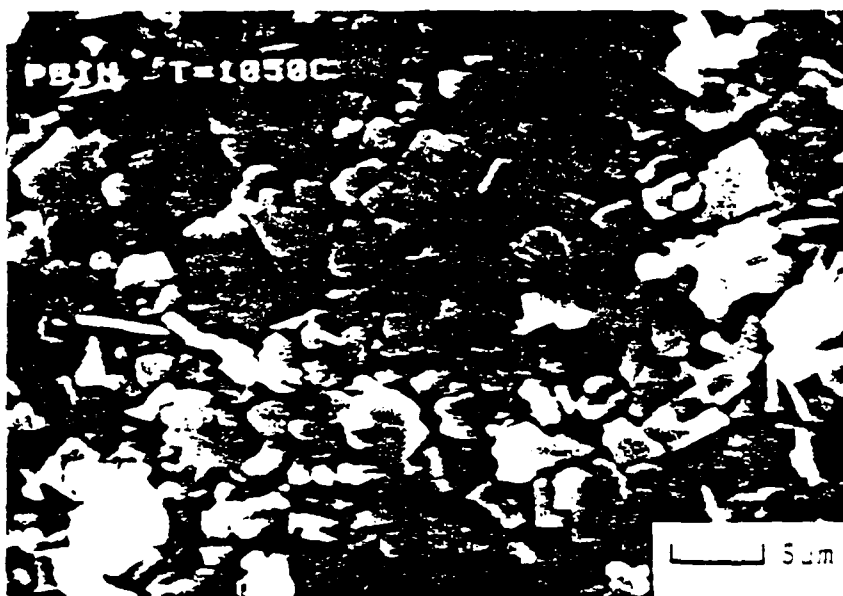






FIGURE

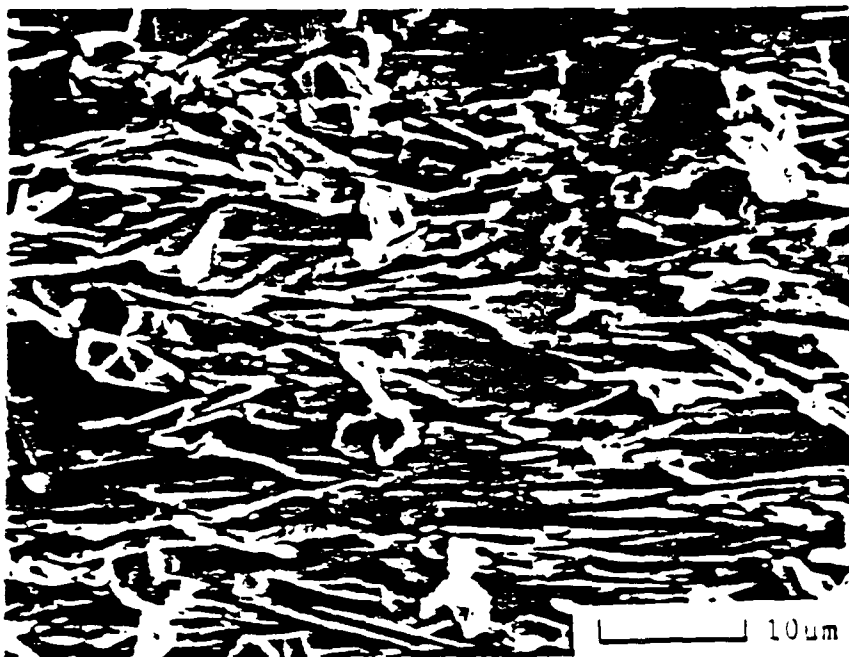
3a



3b

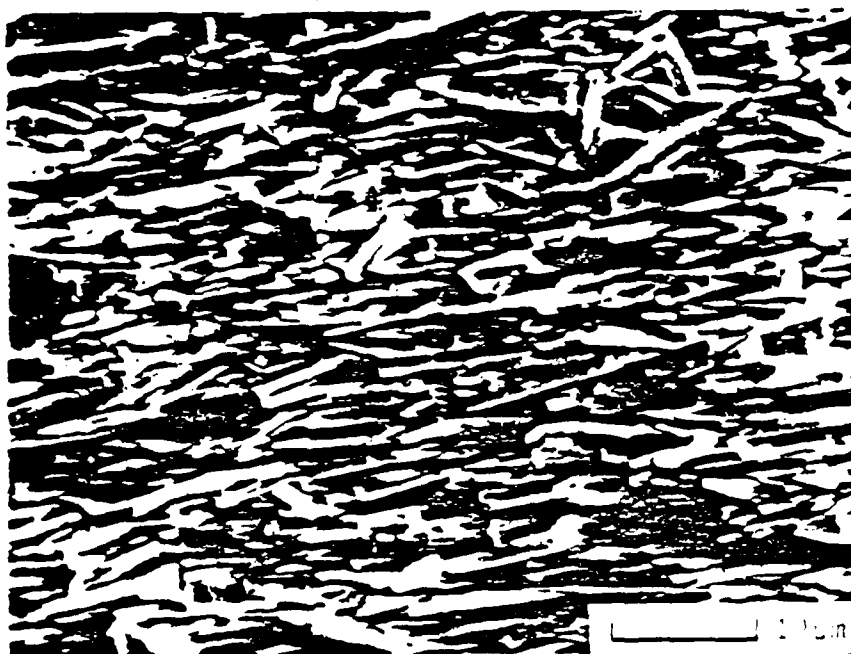


3c

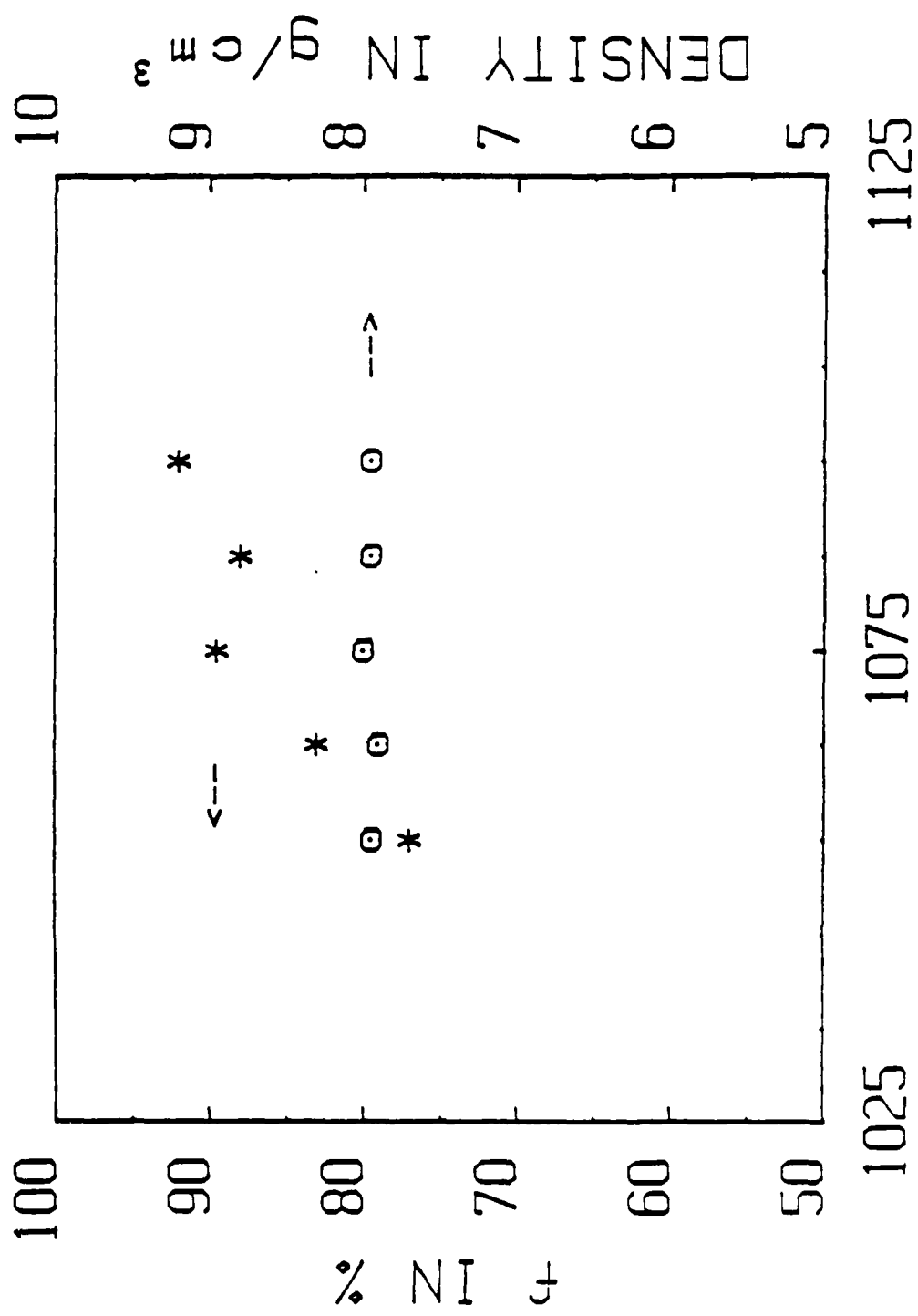


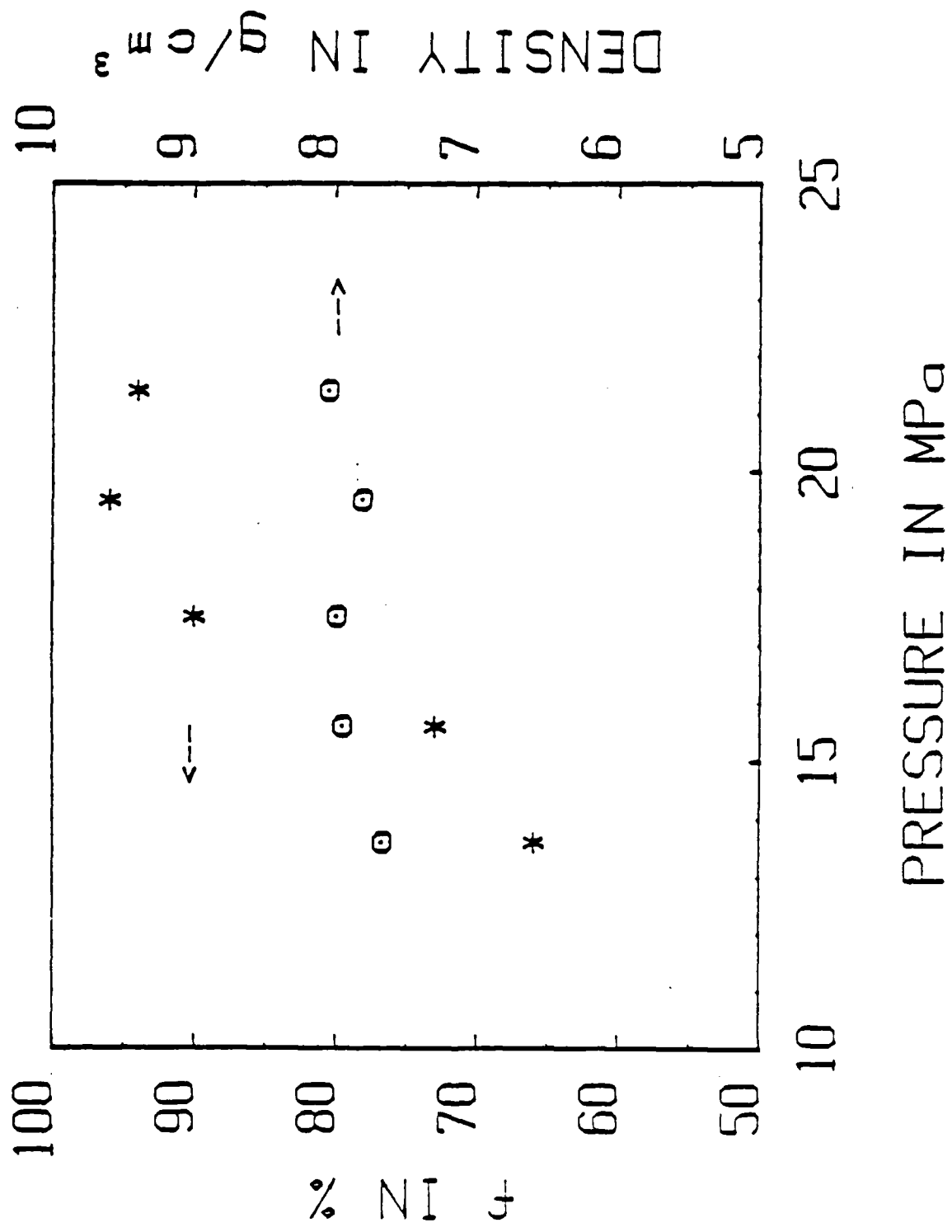
FIGURE

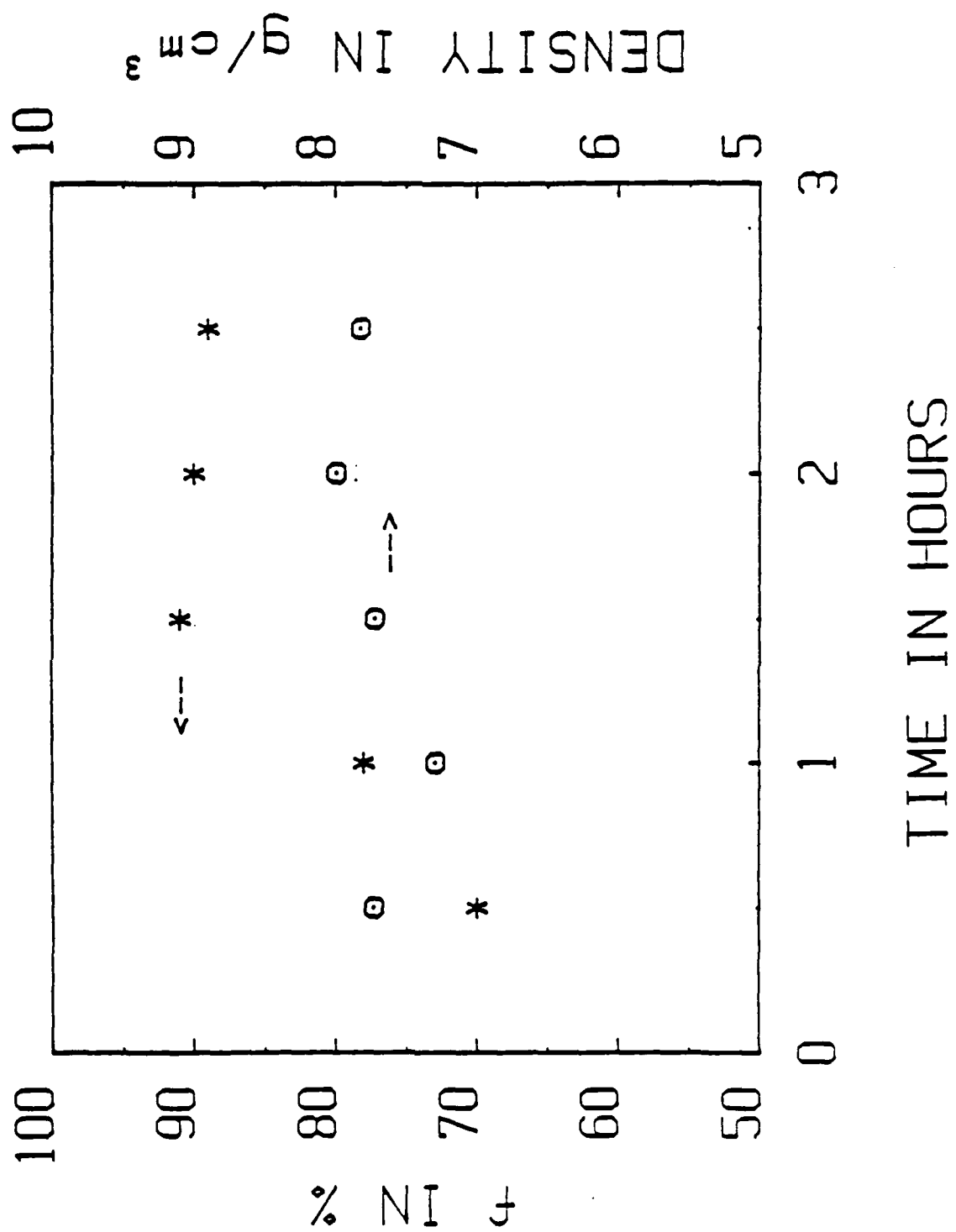
49



46







**APPENDIX 31**



## THE EFFECTS OF VARIOUS B-SITE MODIFICATIONS ON THE DIELECTRIC AND ELECTROSTRICTIVE PROPERTIES OF LEAD MAGNESIUM NIOBATE CERAMICS

D.J. VOSS, S.L. SWARTZ AND T.R. SHROUT  
Materials Research Laboratory, The Pennsylvania State  
University, University Park, PA 16802

**Abstract:** Sintering characteristics, dielectric properties, and electrostrictive  $Q_{12}$  coefficients are reported for fourteen dopant cations incorporated in the perovskite  $A(B', B'')O_3$  structure of lead magnesium niobate  $[Pb(Mg_{1/3}Nb_{2/3})O_3]$ . Two trends in the dielectric properties were found: the maximum permittivity appears to be directly proportional to the transition temperature, and secondly, the percent change in capacitance at 20 kV/cm is proportionally larger for the higher permittivity samples.

Two methods to estimate the frequency dependence of the diffuseness of the phase transition showed good correlation with each other, but revealed no general trend with ionic size or valence of the modifier cations. Electrostrictive  $Q_{12}$  coefficients were found to generally decrease with increasing diffuseness of the phase transitions.

### INTRODUCTION

Perovskite lead magnesium niobate  $[Pb(Mg_{1/3}Nb_{2/3})O_3]$ , hereafter abbreviated P<sub>1</sub>MN is a well-known relaxor ferroelectric exhibiting the characteristic frequency dispersion of the dielectric maximum, i.e., the maximum permittivity increases and shifts to lower temperatures as the frequency is decreased. This relaxation character has been attributed to a statistical inhomogeneity in the distribution of the  $Mg^{+2}$  and  $Nb^{+5}$  cations in the P<sub>1</sub>MN structure<sup>1</sup> creating microregions of varying transition temperatures ( $T_c$ ).

A wide variety of properties have been measured in polycrystalline samples of P<sub>1</sub>MN and numerous homotypes<sup>2</sup> revealing that the P<sub>1</sub>MN family are promising candidates for both dielectric and electrostrictive strain applications<sup>3,4</sup>. Crystallographic studies of the P<sub>1</sub>MN family have shown that ordering in the B sites of the perovskite  $A(B', B'')O_3$  structure depends on the relative differences in the sizes and valences of the B' and B'' cations<sup>5</sup>. However, the magnitudes of other physical properties, particularly the dielectric properties, have not been satisfactorily correlated to the ionic size, valence, or other properties of the various cations.

For this reason, the purpose of this study was to introduce various cations into the B site of the P<sub>1</sub>MN structure in hopes of

possibly correlating resultant dielectric properties with characteristic properties of the cations. Upon analysis, these results should be helpful in selecting PMN-based materials having optimum properties for various dielectric and electrostrictive applications.

The properties examined included the sintering characteristics, the frequency-related diffuseness, temperature and E-field dependence of the permittivity, resistivity, and electrostrictive behavior.

#### EXPERIMENTAL PROCEDURE

A very successful method to fabricate polycrystalline samples of perovskite PMN with minimal pyrochlore phase has been reported<sup>6</sup>. The first step is to prereact the refractory oxides MgO and Nb<sub>2</sub>O<sub>5</sub> to form columbite MgNb<sub>2</sub>O<sub>6</sub>; this product is then reacted with PbO to form perovskite Pb<sub>3</sub>(MgNb<sub>2</sub>O<sub>9</sub>) (PMN). This fabrication scheme was employed for the following +2-valent cations used in this study: Ni, Mg (pure PMN), Ca, Co, Zn, Mn and Cd. The columbite precursors were prepared by ball milling reagent-grade oxides or carbonates with optical grade Nb<sub>2</sub>O<sub>5</sub> in ethanol for 12-24 hr, drying the slurries, and reacting the powders in open Al<sub>2</sub>O<sub>3</sub> crucibles at 300°-1000°C for 2-8.5 h. X-ray diffraction confirmed the products were single phase.

The following cations were also investigated and are grouped according to valence: (+1) Li; (+3) Al, Cr, Fe, Sc, and Ti; (+4) Ge, Mn, Ti, Mo, W, Te, Sn, Hf, Zr and Ce; (+5) V and Ta; and (+6) W. Of these, precursors were prepared for the following five: Li<sup>+1</sup> as LiNbO<sub>3</sub>, Cr<sup>+3</sup> as CrNbO<sub>4</sub>, Fe<sup>+3</sup> as FeNbO<sub>4</sub>, Ti<sup>+4</sup> as PbTiO<sub>3</sub> and Ta<sup>+5</sup> as MgTa<sub>2</sub>O<sub>6</sub>.

Following precursor formation, appropriate amounts of the oxides and/or precursors for the modifier cations were mixed and reacted with PbO in a similar procedure as described above. The substitution of all 3-sites was 3.3 mol% [this corresponds to 30 mol% PMN + 10 mol% Pb( $\frac{1}{3}$ Nb $\frac{2}{3}$ O<sub>3</sub>)] for the seven cations with +2 valency. All non-+2 cations were introduced on 10 mol% of all 3 sites. Other dopant levels tried were Cd<sup>+2</sup> at 5 mol% and Zn<sup>+2</sup> at 10 mol%. The amount of substitution was limited to low levels to minimize distortion of the perovskite structure yet produce detectable changes in the macroscopic properties.

The calcinations were performed once at 300°C for 4 h, except for Al<sup>+3</sup>, Cr<sup>+3</sup> and Mo<sup>+4</sup> which were reacted at 700°C for 4 h. X-ray analysis of the products showed that Ti<sup>+3</sup> and Mn<sup>+4</sup> yielded less than 50% perovskite phase by intensity ratios.

Pellets, 1.59 cm in diameter and 3-4 mm thick, were pressed from the other twenty-four calcined products to which 3 wt% of a polyvinyl alcohol binder was added. A PbO atmosphere was maintained during sintering to minimize PbO loss. Surfaces were ground parallel with 12  $\mu$ m Al<sub>2</sub>O<sub>3</sub> powder and geometrical densities were calculated. Densities less than 90% of theoretical were obtained for all sintered Mo<sup>+4</sup>-doped pellets. A polished surface of the sintered pellets was x-rayed for phase analysis.

## THE EFFECTS OF VARIOUS 3-SITE MODIFICATIONS ON THE DIELECTRIC...

Dielectric Measurements

The faces of those pellets with densities greater than 90% of theoretical were electroded, first with sputtered Au and then with air-dry Ag. The weak-field dielectric measurements were made from 100 to  $-75^{\circ}\text{C}$  with a cooling rate of  $3^{\circ}/\text{min}$ . The measurement system has been described elsewhere<sup>4</sup>.

For ferroelectrics with a diffused phase transition, the law  $1/\epsilon \propto (T-T_0)^2$  has been shown to hold over a wide temperature range instead of the normal Curie-Weiss law. Uchino et al. have shown that when the local Curie temperature distribution is Gaussian, the diffuseness and/or broadness of the phase transition can be measured by the diffuseness parameter  $\delta$ <sup>7</sup>. The temperature difference between the  $T_c$ 's measured at 0.1 and 100 KHz is a second estimation of the frequency dependence of the diffuseness.

The broadness of the dielectric maximum can also be realized from the temperature dependence of the dielectric permittivity. For this, the magnitudes of the decreases in the permittivity  $60^{\circ}\text{C}$  above and  $15^{\circ}\text{C}$  below the KHz  $T_c$  were normalized with the maximum value found at  $T_c$ . This particular temperature range was chosen because it corresponds to the range of  $10^{\circ}\text{C}$  to  $35^{\circ}\text{C}$  being normalized with room temperature, commonly used for capacitor materials.

The dielectric permittivity as a function of E-field was determined on samples being maintained at their respective 10 KHz  $T_c$ . This temperature was arbitrarily chosen for comparison basis only. The permittivity was recorded with increasing and decreasing field; the maximum field being 20 KV/cm.

The electrical resistivity ( $\rho$ ) was measured by applying 100 volts across selected samples being maintained at  $\sim 100^{\circ}\text{C}$ . Current values were recorded 10 min. after application of the voltage.

Electrostrictive Measurements

The electrostrictive  $Q_{12}$  coefficients were indirectly measured from induced piezoelectric resonance of the ceramic disks by the application of dc fields of various strengths. The selected samples were maintained in air at approximately  $50^{\circ}\text{C}$  above their respective 10 KHz  $T_c$ 's, being far removed from possible nonlinear effects commonly found near  $T_c$ . Details of this method are described by Nomura et al.<sup>8</sup>.

RESULTS AND DISCUSSION

Relatively broad, frequency-dependent permittivity-temperature curves were obtained for all modifier cations. However, not all cations were successfully incorporated into the PMN structure. This was evident from an insignificant change in  $T_c$  as compared to pure PMN, and the presence of other phases, primarily pyrochlore, in the x-ray analyses. These samples typically had low dielectric maximum ( $<5000$ ) which can be attributed to the low-permittivity second phase(s). Interestingly, however, these compositions had low dissipation factors; relatively high resistivities, and low temperature

coefficients of dielectric constants which does not preclude their use for possible dielectric application.

The dielectric behavior, resistivity, and other properties for the samples in which the modifier cations were successfully incorporated into the structure are presented in Table I. Most compositions were found to densify (>90% theoretical) at sintering temperatures as low as 1050°C with the compositions containing  $\text{Cd}^{+2}$ ,  $\text{Sn}^{+4}$ ,  $\text{W}^{+6}$  and 10% Zn being densified at  $\leq 950^\circ\text{C}$ .

Resistivities at 100°C were relatively high with the exceptions of  $\text{Fe}^{+3}$ ,  $\text{Co}^{+2}$ , and  $\text{Mn}^{+2}$ -doped specimens. The low value for these particular ions may be due to electronic conduction made possible by multiple valence states.

The dielectric properties, particularly K, were found to be a function of sintering conditions, particularly for the modifier  $\text{Ti}^{+4}$  in which K greatly increased with increasing sintering temperature. One possible explanation for such findings is a grain size dependency as reported by Swartz et al.<sup>9</sup>. In the compositions having  $\text{Cd}^{+2}$ ,  $\text{Zn}^{+2}$  and  $\text{Co}^{+2}$ ,  $T_c$  was found to decrease with increasing sintering temperature. This suggests that less of the cation is being incorporated into the PMN structure, further evidenced by an increasing amount of pyrochlore phase at the high sintering temperatures.

A wide range of  $T_c$ 's are found in Table I with the  $T_c$  for  $\text{W}^{+6}$  being the lowest near  $-55^\circ\text{C}$  and the  $T_c$  for  $\text{Ti}^{+4}$  being the highest near  $+50^\circ\text{C}$ . Likewise, there is a correspondingly wide range of maximum permittivities. Figure 1 shows good correlation between  $T_c$  and the largest of the  $K_{\text{max}}$  values listed for each ion in Table I. There also appears to be a corresponding increase in the temperature coefficients of the permittivity with increasing dielectric maximum.

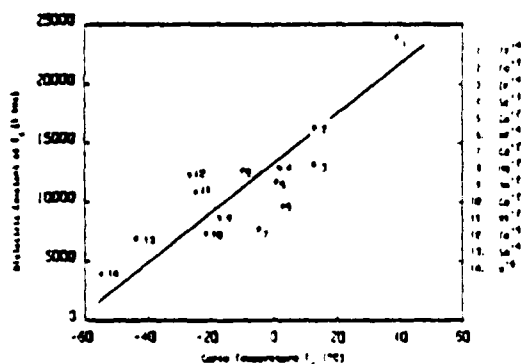


Figure 1. Dielectric constant at  $T_c$  (1 KHz data for fourteen compositions in Table I.

A strong correlation of  $K_{\text{max}}$  with the percentage change in permittivity at a field strength of 20 KV/cm is shown in Figure 2. This shows the difficulty in finding a single phase material exhibiting a high K along with good field stability.

The main characteristic of a relaxor ferroelectric is the temperature breadth of the dielectric maximum at different frequencies. Listed in Table I are the differences in temperature at the 0.1 and 100 KHz  $T_c$ 's for the various cations. Another measure of the frequency dependence of the diffuseness is the diffuseness coefficient  $\delta$  which is

## THE EFFECTS OF VARIOUS B-SITE MODIFICATIONS ON THE DIELECTRIC...

Table 1. Properties of Doped PMN.

Ion <sup>a</sup>	Sintering temperature (°C)	T <sub>c</sub> (°C)	ΔT <sub>c</sub> (0.1 and 100 kHz)	ε <sub>max</sub> (1 kHz)	1947, -15° ± 0.5		ε <sub>max</sub> (1 kHz)	-107, -60° ± 0.5		δ (%)	T <sub>0</sub> (°C)	Δε <sub>0</sub> (10 <sup>4</sup> × 10 <sup>-12</sup> C <sup>2</sup> )
					ε <sub>max</sub>			ε <sub>max</sub>				
					(1 kHz)	(1 kHz)		(1 kHz)	(1 kHz)			
Ba <sup>2+</sup>	1050	-20	15	8,100	-11	-30	60					
	1150	-25	11	10,000	-16	-37	50					
	1250	-25	17	10,900	-18	-43	56	8 × 10 <sup>-10</sup>	50			
Pb <sup>2+</sup>	1050	-6	16	10,900	-18	-44	53					
	1150	-9	15	11,300	-17	-45	51	4 × 10 <sup>-11</sup>				
	1250	-10	15	12,700	-19	-47	52	1 × 10 <sup>-12</sup>	50			
Ca <sup>2+</sup>	1050	3	3	6,400	-5	-36	60	2 × 10 <sup>-7</sup>				
	1150	-10	7	8,500	-4	-36	50	6 × 10 <sup>-7</sup>				
	1250	-21	17	7,300	-12	-39	55	1 × 10 <sup>-8</sup>	52			
Zn <sup>2+</sup>	1050	4	16	11,100	-16	-45	52					
	1150	2	14	11,200	-16	-44	54	5 × 10 <sup>-11</sup>				
	1250	1	14	11,700	-18	-45	52	6 × 10 <sup>-11</sup>	50			
10 mol %	950	39	11	10,300	-16	-42	50	2 × 10 <sup>-11</sup>				
	1050	34	11	15,300	-16	-50	47	2 × 10 <sup>-10</sup>				
	1150	33	12	13,000	-16	-47	50	2 × 10 <sup>-10</sup>				
Mn <sup>2+</sup>	1050	19	1	3,300	-3	-27	73					
	1150	29	2	4,000	-3	-31	60					
	1250	-17	13	8,600	-6	-36	56	6 × 10 <sup>-7</sup>				
Ce <sup>2+</sup>	950	2	18	6,000	-11	-31	70	6 × 10 <sup>-10</sup>				
	1050	-1	18	6,100	-11	-30	72	9 × 10 <sup>-10</sup>				
	1150	-5	16	7,700	-12	-34	60	8 × 10 <sup>-11</sup>				
	1250	-13	18	6,900	-13	-25	65	4 × 10 <sup>-10</sup>	50			
5 mol %	900	9	21	7,500	-12	-32	75	3 × 10 <sup>-11</sup>				
	1050	3	21	7,200	-12	-31	74	2 × 10 <sup>-11</sup>				
Fe <sup>3+</sup>	1150	13	12	16,300	3	-52	43	2 × 10 <sup>-8</sup>				
Sc <sup>3+</sup>	1250	2	14	12,800	-20	-47	51	8 × 10 <sup>-11</sup>	45			
Ti <sup>4+</sup>	1050	51	7	7,700	-5	-37	54					
	1150	61	10	13,500	-14	-46	48					
	1250	70	10	23,900	-24	-63	36	7 × 10 <sup>-11</sup>	61			
La <sup>4+</sup>	950	-37	19	5,400	-11	-20	71					
	1050	-30	20	4,700	-9	-23	79					
	1150	-41	20	6,900	-12	-30	69					
	1250	-44	21	6,900	-15	-30	73	3 × 10 <sup>-10</sup>	47			
W <sup>6+</sup>	1250	3	13	9,700	-12	-40	59	4 × 10 <sup>-11</sup>	40			
Zr <sup>4+</sup>	1150	10	8	7,000	-4	-37	50					
	1250	13	14	13,200	-16	-47	51	6 × 10 <sup>-11</sup>	50			
Ta <sup>5+</sup>	1150	-26	15	10,900	-18	-45	52					
	1250	-27	16	12,500	-19	-47	51	1 × 10 <sup>-11</sup>	48			
U <sup>6+</sup>	950	-50	19	3,400	-11	-23	87	9 × 10 <sup>-9</sup>				
	1050	-53	19	3,800	-12	-25	81					
	1150	-55	20	3,900	-15	-24	80					
	1250	-54	19	2,300	-12	-23	80					

<sup>a</sup>For +2-valent ions, amount of substitution on total B-sites was 1/2 mol% except where noted for La<sup>2+</sup> and Ce<sup>2+</sup>. Amount of substitution was 10 mol% of total B-sites for cations with +3 or higher valence.

also listed in Table 1. These two parameters show good correlation with each other in that a wide T<sub>c</sub> or large δ indicate a wide Gaussian distribution of T<sub>c</sub>'s and thus lower temperature coefficients of the permittivity.

The values of δ for the fourteen samples used in Figure 1 have been plotted in Figure 3 as a function of the ionic radius<sup>10</sup> of the modifier cations. When grouped according to common valences, there

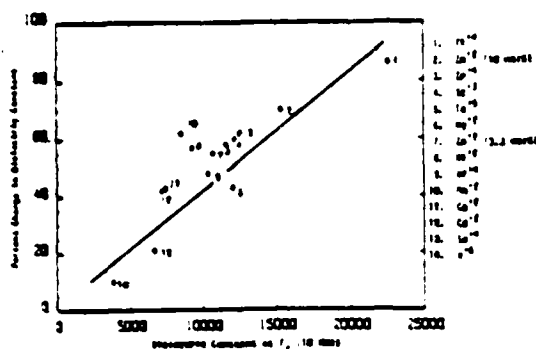


Figure 2. Decrease in dielectric constant at an E-field of 20 KV/cm. Samples were maintained at 10 KHz  $T_C$ 's during measurement.

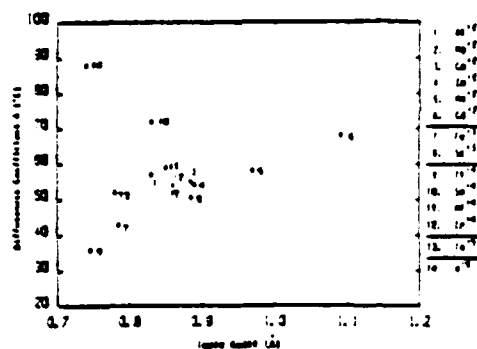


Figure 3. Diffuseness coefficient  $\delta$  as a function of ionic radius for 14 compositions in Table I.

appears to be only a slight increase in the magnitude of  $\delta$  with increasing ionic radius.

The single data points for the cations with +5 and +6 valency are insufficient to show any trends. However, upon consideration of ionic size alone, no general trend was observed.

The electrostriction  $Q_{12}$  coefficients are also reported in Table I with a  $Q_{12}$  value of  $-0.0050 \text{ m}^2/\text{C}^2$  for pure PMN. In general, the larger the  $\delta$  coefficient, the smaller the  $Q_{12}$ .

#### REFERENCES

1. V.A. Bokov and I.E. Myl'nikova, Sov. Phys. Solid State **2**, 613-623 (1961).
2. Landolt Bornstein, Ferroelectrics and Related Substances, New Series, Vol. 16 (1981).
3. B.A. Malkov and Y.N. Venevtsev, Inorg. Mat. **13**, 1189-1192 (1977).
4. L.E. Cross, S.J. Jang, R.E. Newnham, S. Nomura and K. Uchino, Ferroelectrics **23**, 187-192 (1980).
5. F. Galasso and J. Pyle, Inorg. Chem. **2**, 482-484 (1963).
6. S.L. Swartz, T.R. ShROUT, Mat. Res. Bull. **17**, 1245-1250 (1982).
7. K. Uchino, S. Nomura, L.E. Cross, S.J. Jang and R.E. Newnham, J. Appl. Phys. **51**(2), 1142-1145 (1980).
8. S. Nomura, K. Tonooka, J. Kuwata, L.E. Cross and R.E. Newnham, Proc. Second Meeting Ferroelectric Materials and Their Applications (FMA2), Kyoto, Japan, 133-138 (1979).
9. S. Swartz, T. ShROUT, W. Schulze and L.E. Cross, (submitted for publication).
10. O. Muller and R. Roy, The Major Ternary Structural Families, Springer-Verlag, New York (1974).

**APPENDIX 32**

# FERROELECTRIC PROPERTIES OF TUNGSTEN BRONZE LEAD BARIUM NIOBATE (PBN) SINGLE CRYSTALS

..... SHROUT and L.E. CROSS

Materials Research Laboratory, The Pennsylvania State University, University Park, PA 16802

D.A. HUKIN

Clarendon Laboratory, Oxford University, Oxford, England OX1 3PU

**Abstract**—A ferroelectric tungsten bronze single crystal of  $\text{Pb}_{0.33}\text{Ba}_{0.70}\text{Nb}_2\text{O}_6$  was grown from a melt using the Czochralski technique. The crystal belongs to the tetragonal point group  $4mm$  with the spontaneous polarization parallel to the 'c' axis. The room temperature lattice parameters were  $a = 12.50 \text{ \AA}$  and  $c = 3.995 \text{ \AA}$ . The spontaneous polarization was found to be  $0.40 \text{ C/m}^2$ . The Curie transition was  $350^\circ\text{C}$  as determined from the temperature dependence of the dielectric constants. The pyroelectric properties were found to be typical of other tetragonal ferroelectric bronzes. Dielectric constant  $\epsilon_{11}$  and piezoelectric constant  $d_{15}$  show a strong enhancement from the approach of the tetragonal:orthorhombic morphotropic phase boundary and it is clear that crystals with composition in the tetragonal phase field closer to this boundary will be of major interest for piezoelectric and electro-optic applications.

## INTRODUCTION

Single crystal ferroelectric tungsten bronzes, in general, are known for their excellent electro-optic<sup>(1,2)</sup>, pyroelectric<sup>(3)</sup>, and piezoelectric<sup>(4)</sup> properties, making them promising candidates for use in various device applications; e.g. laser modulators, pyroelectric infrared detectors, S.A.W. devices, etc. This plus the fact that there are over 100 individual end member bronze compositions, with numerous possible solid solutions<sup>(4)</sup>, makes the tungsten bronze family one of the most extensive, versatile and potentially useful families of oxygen octahedra based ferroelectrics.

Typically, the bronze ferroelectrics which are of most practical interest are ones of complex composition and/or solid solutions, which are inherently difficult to grow in single crystal form.

The present paper reports single crystal growth in the  $\text{Pb}_{1-x}\text{Ba}_x\text{Nb}_2\text{O}_6$  solid solution bronze system. Of particular interest are compositions near  $x = 0.4$  which is very close to the reported morphotropic phase boundary<sup>(5,6)</sup>. For polycrystalline ceramics, it has been demonstrated, as in the  $\text{PbTiO}_3$ - $\text{PbZrO}_3$  perovskite system<sup>(7)</sup>, that compositions near morphotropy have very strong piezoelectric properties<sup>(8)</sup>. Measurements of physical and ferroelectric related properties are presented which contain this expected enhancement in the single crystal material.



## EXPERIMENTAL AND DISCUSSION OF RESULTS

### Crystal Growth

The materials used were Specpure<sup>†</sup> grade PbO, BaCO<sub>3</sub>, and Nb<sub>2</sub>O<sub>5</sub>. These were weighed out according to the stoichiometry Pb<sub>1-x</sub>Ba<sub>x</sub>Nb<sub>2</sub>O<sub>6</sub> (x = 0.40) and then wet ball milled in ethanol for 12 hrs. The resulting slurry was air dried and then fired in an alumina crucible at 650°C for 24 hrs. This procedure was adopted to ensure that the lead was in a fully oxidized state before being loaded into the platinum pulling crucible. The crucible was 40mm in both diameter and height and was supported in a fibrous alumina insulating jacket and covered with a similar radiation shield. The furnace used was R.F. induction heated at 370 kHz.

Crystals were grown by the Czochralski technique being pulled at a rate of 2 mm/hr with a rotation of 10 rpm. The grown crystal was annealed in situ by programming the temperature down over 12 hrs.

Under these pulling conditions, transparent and very pale yellow crystals were obtained. The grown boules were typically cracked containing 3 or 4 single crystals with dimensions up to 10 x 5 x 8 mm.

Chemical analysis revealed that the initially grown crystal contained 16.6 wt% PbO, 24.6 wt% BaO and 60.1 wt% Nb<sub>2</sub>O<sub>5</sub>, which correspond to Pb<sub>0.33</sub>Ba<sub>0.70</sub>Nb<sub>1.98</sub>O<sub>6</sub> rather than Pb<sub>0.60</sub>Ba<sub>0.40</sub>Nb<sub>2</sub>O<sub>6</sub>, the starting composition. The significant difference in compositions was probably attributed to volatilization of PbO during the growth process. The apparent loss of PbO was also evident from other crystals grown from the same melt having continuously decreasing Pb:Ba ratios.

Physical and ferroelectric properties presented in this work were only determined for single crystals having the composition Pb<sub>0.33</sub>Ba<sub>0.70</sub>Nb<sub>1.98</sub>O<sub>6</sub>. Properties of single crystals containing lower amounts of PbO were all found to be somewhat similar, as reported for polycrystalline ceramics of similar compositions<sup>(8)</sup>.

X-ray powder diffraction analysis showed that the grown crystals had the tungsten bronze structure and belonged to the tetragonal point group system 4mm. The lattice parameters at room temperature for the composition Pb<sub>0.33</sub>Ba<sub>0.70</sub>Nb<sub>1.98</sub>O<sub>6</sub>, designated PBN, were found to be a = 12.50 Å and c = 3.995 Å (see Table 1).

### Sample Preparation

Crystals belonging to tetragonal point group 4mm, have three piezoelectric, one pyroelectric and two dielectric independent constants, thus requiring various sample shapes and orientations.

Bar and plate shape specimens, [100] and [001], were cut with an abrasive wire saw from the single crystal boule following orientation using back laue reflection. Samples were lapped and polished down to 3 μ alumina powder. The samples were then carefully cleaned with acetone in preparation for application of sputtered on gold electrodes.

Prior to most measurements, the crystals were poled by the field cooling method under a DC field of 1-2 Kv/cm along the [001] or 4 fold polar axis. The completeness of poling was checked using a Berlincourt (Model 333) piezoelectric d<sub>33</sub> meter.

<sup>†</sup>Johnson Matthey Chemicals Limited, Orchard Road, Rayston, Hartfornshire 568 5HE England.

<sup>—</sup>Berlincourt (Model 333) d<sub>33</sub> meter, Channel Products, Inc., 16722 Park Circle Drive, Chagrin Falls, OH 44020.

# FERROELECTRIC PROPERTIES OF TUNGSTEN BRONZE LEAD BARIUM NIOBATE (SBN)

TABLE 1

Physical Properties of  $\text{Pb}_{0.33}\text{Ba}_{0.70}\text{Nb}_{1.967}\text{O}_6$  at Room Temperature

Lattice Constants	$a = 12.50 \text{ \AA}$ $c = 3.995 \text{ \AA}$
Spontaneous Polarization	$P_s = 0.40 \text{ C/m}^2$
Dielectric Constants	$\epsilon_{11}^T = 360 \quad \tan \delta < 0.002$ $\epsilon_{33}^T = 140 \quad \tan \delta^* < 0.007$ $(170)^* \quad (0.04)$ $\epsilon_{11}^S \approx 340 \quad \tan \delta = 0.005$ $\epsilon_{33}^S \approx 95 \quad \tan \delta \approx 0.02$
Pyroelectric Coefficient	$\rho_p = 1.7 \times 10^{-4} \text{ C/m}^2\text{ }^\circ\text{C}$
Piezoelectric Coefficients	$d_{31} \approx 12 \times 10^{-12} \text{ C/N} \quad k_{31} = 15\%$ $d_{33} = 60 \quad k_{33} \approx 52\%$ $d_{15} \approx 50 \times 10^{-12} \text{ C/N} \quad k_{15} = 25\%$

\*Unpoled values.

## Spontaneous Polarization

The most commonly used technique for observing ferroelectricity and determining spontaneous polarization ( $P_s$ ) is based on the polarization field hysteresis loops generated using the Sawyer and Tower method(9).

Typical hysteresis loops taken from repeated switching experiments at low frequencies (0.1 Hz) and at other various frequencies in PBN crystals showed a recession of the high remanent polarization obtained in the first cycle of the applied field, suggesting that a major fraction of the total polarization rapidly locks into non-switching domain configurations (Note: the remanent polarization ( $P_R$ ) is essentially equivalent to  $P_s$  in single crystals). This recession of the hysteresis loop has been observed in several other tetragonal tungsten bronze;  $\text{Sr}_{0.5}\text{Ba}_{0.5}\text{Nb}_2\text{O}_6$ (10),  $\text{K}_{0.2}\text{Na}_{0.2}\text{Sr}_{0.5}\text{Ba}_{0.5}\text{Nb}_2\text{O}_6$ (11) and  $\text{K}_{0.2}\text{Sr}_{0.9}\text{Nb}_2\text{O}_6$ (12).

Thus the polarization ( $P_s$ ) was determined statically, by taking a poled sample, and thermally depoling by submersion in a hot furnace ( $>600^\circ\text{C}$ ), which is well above the Curie transition ( $T_C$ ), while charge is collected using an electrometer. The  $P_s$  determined, for room temperature, was found to be  $\sim 40 \times 10^{-2} \text{ C/m}^2$  (Table 1).

## Dielectric Properties

The temperature dependence of the dielectric constants (relative permittivities)  $\epsilon_{33}^T$  and  $\epsilon_{11}^T$  (constant and zero stress) and loss ( $\tan \delta$ ) were determined from poled and unpoled [001] and [100] plates at frequencies 1, 10, 100, and 1000 KHz using a Hewlett Packard††† (HP) 4274A and 4275A frequency LCR Meters under full program control in an HP 9825 bus controlled system. The temperature range was  $-75^\circ\text{C}$  to  $500^\circ\text{C}$  with a heating rate of  $3^\circ/\text{min}$ .

†††Hewlett Packard, 1-50-1 Yoyogi, Tokyo, Japan 151.

The temperature dependence of the dielectric constants  $\epsilon_{33}^T$  and  $\epsilon_{11}^T$ , at 100 KHz, are shown in Figures 1 and 2 respectively. Both  $\epsilon_{33}^T$  and  $\epsilon_{11}^T$  showed marked anomalies at a transition point ( $T_c$ ) of 350°C. The temperature behavior and large anisotropy of  $\epsilon_{33}^T$  and  $\epsilon_{11}^T$  is typical of most tetragonal ferroelectric bronzes<sup>(4)</sup>. Little frequency dependence of the constants was observed.

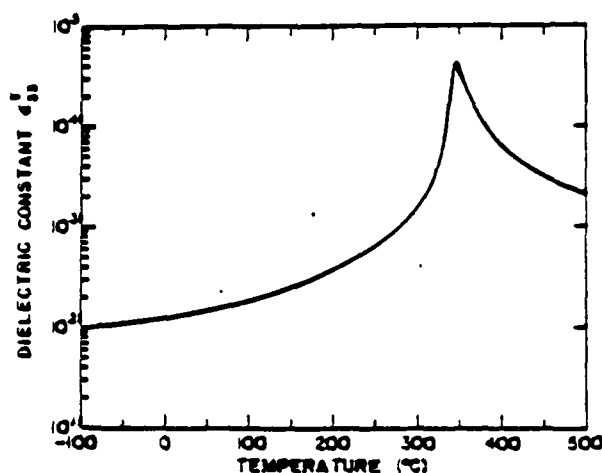


Figure 1. Dielectric constant  $\epsilon_{33}^T$  as a function of temperature for PBN at 100 kHz.

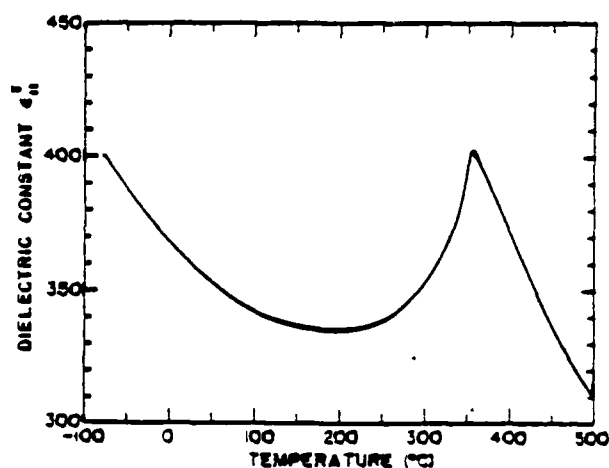


Figure 2. Dielectric constant  $\epsilon_{11}^T$  as a function of temperature for PBN at 100 kHz.

Room temperature dielectric and loss values for both poled and unpoled samples are given in Table 1. The reported difference in the dielectric constant  $\epsilon_{33}$  and loss between poled and unpoled states is probably attributed to multi domain (180°) wall motions<sup>(10)</sup>. The room temperature values of the clamped dielectric constants  $\epsilon_{33}$  and  $\epsilon_{11}$  (zero and constant strain) and loss are also reported in Table 1. These values were determined at 100 meagHz using a Model 4191A HP Impedance Analyzer.

The Curie Weiss constants, the relationship between the reciprocal dielectric constants  $\epsilon_{33}$  and  $\epsilon_{11}$  and temperature above  $T_c$ , were  $2.5 \times 10^5$ °C and  $1.9 \times 10^5$ °C, respectively. The Curie constant obtained are quite characteristic of other oxygen-octahedra ferroelectrics<sup>(4)</sup>.

### Pyroelectricity

The pyroelectric coefficient  $p_3$  of PBN, as a function of temperature between 0°C and 100°C, is shown in Figure 3. The room temperature value of  $p_3$  ( $1.7 \times 10^{-4}$  c/m²°C) reported in Table 1 is similar to that of other bronzes having approximately the same transition temperatures<sup>(4)</sup>.

The pyroelectric coefficient was determined by measuring the DC discharging current of a poled sample at a controlled rate of change of temperature. The current was measured using a HP 4140B pA meter and the temperature and data acquisition was using an automatic measuring system similar to that used for determining the dielectric behavior.

# FERROELECTRIC PROPERTIES OF TUNGSTEN BRONZE LEAD BARIUM NIOBATE (SBN)

## Piezoelectric Properties

Piezoelectric coefficients  $d_{31}$ ,  $d_{33}$ ,  $d_{15}$  and equivalent coupling coefficients  $k_{31}$ ,  $k_{33}$ , and  $k_{15}$  for PBN are reported in Table 1. The piezoelectric  $d_{33}$  coefficient was simply determined on a poled [001] plate using a Berlincourt  $d_{33}$  meter. The piezoelectric coupling coefficient  $k_{31}$  was determined on a poled [100] bar using the resonance-antiresonance technique based on the IRE Standards of Piezoelectric crystals(13). The piezoelectric coupling coefficient  $k_{15}$  was determined using the relationship (1)

$$\epsilon_{11}^S = (1 - k_{15}^2) \epsilon_{11}^T \quad (1)$$

relating the free ( $\epsilon_{11}^T$ ) and clamped ( $\epsilon_{11}^S$ ) dielectric constants(13).

The coefficients  $k_{33}$ ,  $d_{31}$  and  $d_{15}$  were simply calculated from other experimentally determined values through the relationship (2)

$$k_{ij}^2 = \frac{d_{ij}^2}{\epsilon_{ii}^T \cdot \epsilon_0 s_{jj}^E} \quad (2)$$

where  $\epsilon_0$  is the permittivity of free space ( $8.854 \times 10^{-12}$  F/m) and  $s_{jj}^E$  the appropriate elastic constant. Elastic constant values used were those typical of other tetragonal tungsten bronzes(4).

## SUMMARY

Single crystal growth, physical, and ferroelectric related properties of PBN were investigated. PBN was characterized as a tetragonal tungsten bronze type ferroelectric with the spontaneous polarization parallel to the tetragonal [001] or 'c' axis. From the measured results, particularly the temperature dependence of  $\epsilon_{11}^T$  and magnitudes of  $d_{15}$  and  $k_{15}$  it is clear that the approach towards the morphotropic composition at  $\text{Pb}_{0.60}\text{Ba}_{0.40}\text{Nb}_2\text{O}_6$  is lowering the transverse Curie temperature and softening the transverse dielectric stiffness. With further lead addition composition with exceedingly interesting  $d_{15}$  and electro-optic  $r_{41}$  coefficients should be possible.

Work to reduce the PbO volatilization problem and further optimize growth in the  $\text{Pb}_{1-x}\text{Ba}_x\text{Nb}_2\text{O}_6$  solid solution system, especially for compositions closer to morphotropy at the  $x = 0.4$  value are now in progress.

## ACKNOWLEDGEMENT

This work was supported by the Air Force Office of Scientific Research through Contract No. F49620-78-6-0093.

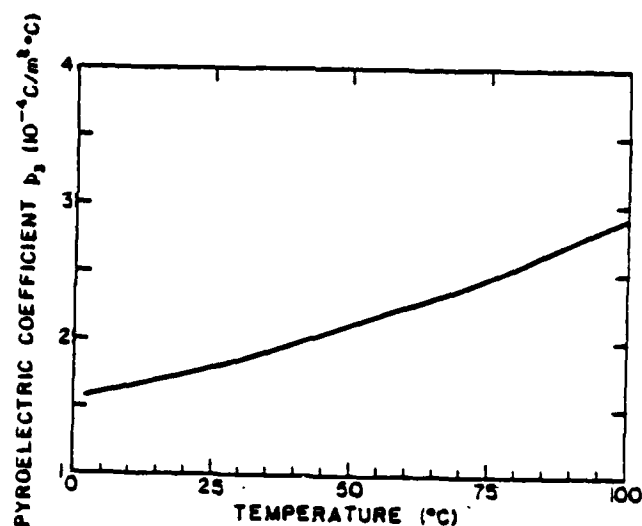


Figure 3. Pyroelectric coefficient  $p_3$  as a function of temperature for PBN.

REFERENCES

1. H. Hirano, H. Takei, and S. Koide, Jon. J. Appl. Phys., **8**, 972 (1969).
2. J.E. Geysic, J.H. Levinstein, J.J. Rubin, S. Singh, and L.G. Van Uitert, Appl. Phys. Lett., **11**, 269 (1967).
3. A.M. Glass, J. Appl. Phys., **40**, 4699 (1969).
4. Landolt Bornstein, Ferroelectrics and Related Substances, New Series, Vol. 16 (1981).
5. E.C. Subbarao, G. Shirane, and F. Jona, Acta Cryst., **13**, 226 (1960).
6. V.A. Isupov and V.I. Kosiakov, Soviet Physiks Tech. Phys., **3**, 2002 (1958).
7. B. Jaffe, W.R. Cook, Jr., and H. Jaffe, Piezoelectric Ceramics, Academic Press, London and New York (1971).
8. R. Baxter and N.H. Hellicar, J. Amer. Ceram. Soc., **43**, 578 (1960).
9. C.B. Sawyer and C.H. Tower, Phys. Rev., **35**, 269 (1930).
10. T. Cline, Ph.D. Thesis, The Pennsylvania State University (1977).
11. H.C. Chen, Private Communication.
12. F.W. Ainger, J.A. Beswick, and S.G. Porter, Ferroelectrics, **3**, 321 (1972).
13. IRE Standards of Piezoelectric Crystals: Measurements of Piezoelectric Ceramics, Proc. IRE, **61**, 1161 (1961).

**APPENDIX 33**

# DIELECTRIC AND PIEZOELECTRIC PROPERTIES OF $\text{Pb}_{1-x}\text{Ba}_x\text{Nb}_2\text{O}_6$ FERROELECTRIC TUNGSTEN BRONZE CRYSTALS

T.R. SHROUT, HUANCHU CHEN, AND L.E. CROSS

Materials Research Laboratory, The Pennsylvania State University, University Park, PA 16802

**Abstract**—Tungsten bronze single crystals in the  $\text{Pb}_{1-x}\text{Ba}_x\text{Nb}_2\text{O}_6$  system were grown from a melt using the Czochralski technique. The dielectric, piezoelectric and pyroelectric properties were determined. The dielectric constant  $K_1$  and piezoelectric coefficient  $d_{15}$  showed a strong enhancement upon approaching the tetragonal:orthorhombic morphotropic phase boundary as predicted by thermodynamic phenomenology. It is clear that crystals with a composition in the tetragonal phase field near this boundary will be of major interest for various piezoelectric device applications.

## INTRODUCTION

Single crystal ferroelectric tungsten bronzes are promising candidates for use in various device applications; e.g. acousto-optic, pyroelectric detectors, S.A.W. devices, etc. Not only do these materials possess relatively high piezoelectric, electro-optic and pyroelectric properties, but it has been shown thermodynamically using the Landau:Ginsburg:Devonshire (LGD) phenomenology and confirmed experimentally for the tungsten bronze  $\text{Sr}_{.61}\text{Ba}_{.39}\text{Nb}_2\text{O}_6$  (SBN) and possibly all other tetragonal bronzes, the existence of temperature compensation<sup>(1,2)</sup>. It was also found that the LGD phenomenology could be used to give a good description of the dielectric, piezoelectric and thermal behavior of SBN.

Another important aspect of SBN is the ease in which large single crystals can be grown<sup>(3)</sup>, however, even though the piezo values are high for  $d_{33}$ , they are very small for  $d_{15}$  and correspondingly the shear coupling coefficient  $k_{15}$  is low. The low value of this constant may be traced in the phenomenology to the very low value of the transverse Curie temperature  $\theta_1$ , the temperature at which  $1/K_2$  when extrapolated from high temperature values is equal to zero. To improve the piezo coupling,  $d_{15}$  and  $k_{15}$ , it would be desirable to move into a composition field in the bronze structure where the  $\theta_1$  can be enhanced.

It has been reported<sup>(4)</sup> that a cross over between  $\theta_1$  and  $\theta_3$  is found to occur in the  $\text{Pb}_{1-x}\text{Ba}_x\text{Nb}_2\text{O}_6$  solid solution family for compositions in the vicinity  $x = 0.4$ . Near this composition a morphotropic phase boundary occurs between a ferroelectric orthorhombic (mm2) and a tetragonal (4mm) structure as shown in Figure 1. Thus tetragonal compositions with large  $\theta_1$  values and

correspondingly large  $\bar{\epsilon}_1$  and  $d_{15}$ , should exist near the morphotropic phase boundary.

It was the purpose of this investigation to grow single crystals in the  $\text{Pb}_{1-x}\text{Ba}_x\text{Nb}_2\text{O}_6$  system near the morphotropic phase boundary to verify the existence of tetragonal compositions with greatly improved transverse properties.

Various dielectric, piezoelectric and physical properties of a wide range of  $\text{Pb}_{1-x}\text{Ba}_x\text{Nb}_2\text{O}_6$  compositions are also reported.

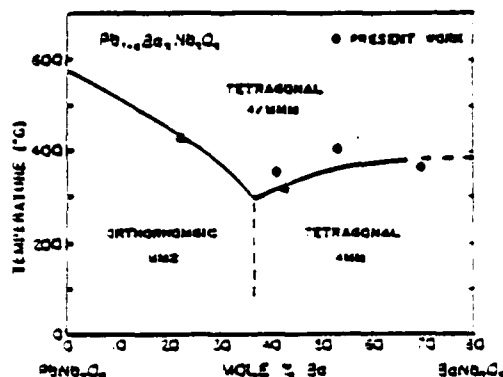


Figure 1. Phase Diagram of  $\text{Pb}_{1-x}\text{Ba}_x\text{Nb}_2\text{O}_6$

#### EXPERIMENTAL PROCEDURE

Single crystals of various  $\text{Pb}_{1-x}\text{Ba}_x\text{Nb}_2\text{O}_6$  were grown using the Czochralski technique. The crystals grown were typically small ( $<1 \text{ cm}^3$ ) but sufficient in size to characterize the dielectric and piezoelectric properties.

For each crystal grown, a chemical analysis was performed, along with the determination of the density using a pycnometer method and the lattice parameters found using powder x-ray diffraction. To determine the various dielectric and piezoelectric properties, plate shaped samples with major surfaces normal to the a and c or 1 and 3 axes of the tetragonal prototype were prepared for crystals with  $x > 0.4$ . For compositions in the orthorhombic phase, the samples were cut with major faces normal to c, but for a and b cuts (1 and 2 axes), with major faces making an angle of  $45^\circ$  to the tetragonal a axis. Sputtered on gold electrodes were used. The crystals were poled by the field cooling method under a DC field of 1-2 kV/cm along the 'c' axis for tetragonal compositions and the 'b' axis for orthorhombic compositions.

Further details of the crystal growth and property measurement techniques can be found in reference (5).

#### RESULTS AND DISCUSSION

The single crystals grown are indicated by the circles imposed on the  $\text{Pb}_{1-x}\text{Ba}_x\text{Nb}_2\text{O}_6$  phase diagram shown in Figure 1. The  $T_c$ 's were determined from the peak in  $\bar{\epsilon}_c$  for tetragonal compositions and the peak in  $\bar{\epsilon}_a$  or  $\bar{\epsilon}_b$  (equivalent above  $T_c$ ) for the orthorhombic one. The compositions, as determined by chemical analysis, are reported in Table 1 listed in order of decreasing Ba content and/or increasing density. It is apparent that most of the crystals grown were deficient in Pb due to the volatilization of PbO during crystal growth. The exact effect of PbO deficiency on the various properties is not known.



Table 1. Properties of  $\text{Pb}_{1-x}\text{Ba}_x\text{Nb}_2\text{O}_6$  Crystals.

COMPOSITION	DENSITY (g/cm <sup>3</sup> )	LATTICE PARAMETERS a, b, c (Å)	T <sub>m</sub> °C	CURIE TEMP AND CONST. θ <sub>1</sub> , C <sub>1</sub> (°C, 10 <sup>10</sup> esu)	DIELECTRIC CONSTANT K <sub>a</sub> , K <sub>b</sub> , K <sub>c</sub>	PIEZO COEFF. d <sub>33</sub> , d <sub>15</sub> (C/N)	PYROELECTRIC COEFF. (10 <sup>-6</sup> C/m <sup>2</sup> °C)
$\text{Pb}_{0.33}\text{Ba}_{0.67}\text{Nb}_2\text{O}_6$ (2.72) <sup>(4)</sup>	5.48 (5.48)	12.400 12.400	1.795 400	-110 1.0	100 (100) <sup>(5)</sup>	100 (100,000) <sup>(5)</sup>	60 15
$\text{Pb}_{0.37}\text{Ba}_{0.63}\text{Nb}_2\text{O}_6$ (5.62)	5.72 (5.62)	12.400 12.400	1.900 400	150 1.0	100 (100)	70 (77,000)	45 13.5
$\text{Pb}_{0.40}\text{Ba}_{0.60}\text{Nb}_2\text{O}_6$ (6.17)	6.05 (6.17)	12.400 12.400	1.900 350	140 1.1	100 (10000)	100 (10,000)	110 150
$\text{Pb}_{0.40}\text{Ba}_{0.60}\text{Nb}_2\text{O}_6$ (6.12)	6.10 (6.12)	12.400 12.400	1.970 167	150 1.1	100 (1000)	110 (10,000)	140 110
$\text{Pb}_{0.40}\text{Ba}_{0.60}\text{Nb}_2\text{O}_6$ (6.12)	6.10 (6.12)	12.400 12.400	1.975 115	100 1.1	100 (1000)	100 (10,000)	100 100
$\text{Pb}_{0.33}\text{Ba}_{0.67}\text{Nb}_2\text{O}_6$ (6.12)	6.45 (6.12)	17.67 17.78	7.78 400	- 1.0	100 (10,000)	110 (10,000)	70 (100)
$\text{PbNb}_2\text{O}_6$ <sup>(4)</sup>	6.61	17.65 17.78	7.74 100	- 1.0	100 (10,000)	100 (10,000)	100 (1,000)

(4) Calculated density.  
(5) Data from reference 1.

(6) Pyro mean constant  $\bar{p}_1 = 110^\circ\text{C}$ .  
(7) Data from reference 1.

Also tabulated in Table 1 are the room temperature and peak values of the dielectric constants ( $K_a$ ,  $K_b$ ,  $K_c$ ), Curie Weiss temperatures ( $\theta_1$ ) and constant ( $C_1$ ), the piezo  $d_{33}$  and  $d_{15}$  and pyro coefficients ( $p$ ) for the various compositions. For completion, reported values for the end member  $\text{PbNb}_2\text{O}_6$  were also included. The values for the orthorhombic composition and the compositions well in the tetragonal field are typical of those for other bronzes<sup>(6)</sup>.

From Table 1 it can be seen that most of the properties increase slightly, e.g.  $K_c$ ,  $d_{33}$ , with  $p$  decreasing as one moves across the tetragonal phase region toward the morphotropic boundary. The transverse Curie temperature  $\theta_1$ ,  $K_a$  and  $d_{15}$ , however, were found to increase markedly.

From the LGD phenomenology, the dielectric stiffness ( $\chi_{11} = 1/(K_a - 1)$ ) for the prototype 4/mmm tetragonal case with the spontaneous polarization along the 4-fold axis can be expressed by the following equation:

$$\chi_{11} = \frac{T - \theta_1}{C_1} + 2\alpha_{13}P_3^2 + 2\alpha_{133}P_3^4 + 2\alpha_{1333}P_3^6 \quad (1)$$

where  $\alpha$ 's are dielectric stiffness parameters. Given a room temperature spontaneous polarization ( $P_3$ ) of  $0.40 \text{ C/m}^2$  as determined for the composition  $\text{Pb}_{0.33}\text{Ba}_{0.67}\text{Nb}_{1.99}\text{O}_6$ <sup>(5)</sup> a  $C_1$  of  $2.0 \times 10^5^\circ\text{C}$  and using the derived  $\alpha$  terms found for SBN<sup>(1)</sup>, with  $2\alpha_{13} = 4.2 \times 10^{-3}$ ,  $2\alpha_{133} = 4.22 \times 10^{-2}$  and  $2\alpha_{1333} = 4.98 \times 10^{-2}$  (MKS units), the dielectric stiffness and thus  $K_a$  were determined as a function of  $\theta_1$  as shown in Figure 4.

The piezo coefficient  $d_{15}$  as a function of  $\theta_1$  is also shown in Figure 4, having been determined from the expression

$$d_{15} = Q_{44}P_3\epsilon_0(K_a - 1) \quad (2)$$

Note: An electrostriction  $Q_{44}$  value of  $4 \times 10^{-2} \text{ m}^4/\text{C}^2$  was used, having been calculated from data in Table 1 for the composition  $\text{Pb}_{0.7}\text{Ba}_{0.33}\text{Nb}_{1.99}\text{O}_6$ .

As expected, both  $K_a$  and  $d_{15}$  were found thermodynamically to increase markedly with increasing  $\delta_1$  being in quite good agreement with the experimentally determined values found for the various tetragonal compositions, being also shown in Figure 2.

### CONCLUSION

Single crystals with various compositions in the ferroelectric tungsten bronze  $\text{Pb}_{1-x}\text{Ba}_x\text{Nb}_2\text{O}_6$  system were grown using the Czochralski technique. Particular attention was made near  $x = 0.4$  in which a morphotropic boundary separates orthorhombic and tetragonal phases. The various dielectric, piezoelectric and pyroelectric properties were determined and reported. From the measured results, it was found that upon approaching the morphotropic boundary from the tetragonal side, the transverse Curie temperature  $\theta_1$  increased resulting in markedly improved transverse dielectric ( $K_a$ ) and piezoelectric ( $d_{15}$ ) properties as expected from the LGD phenomenology. It is also interesting to note the excellent agreement between the experimental and thermodynamically determined values even when higher order dielectric stiffness parameters found for the bronze SBN were used. Thus, tetragonal crystals with compositions close to morphotropy will be of interest for various piezoelectric applications.

It is necessary, however, to further optimize crystal growth to reduce  $\text{PbO}$  volatilization and to produce larger crystals.

### REFERENCES

1. T.R. Shrout, Ph.D. Thesis, The Pennsylvania State University (1981).
2. T.R. Shrout, L.E. Cross, P. Moses, H.A. McKinstry and R. Neurgaonkar, Proc. Ultrasonics Symposium, IEEE, 414 (1980).
3. R.R. Neurgaonkar, Mat. Res. Bull., **15**, 1305 (1980).
4. E.C. Subbarao, G. Shirane, and F. Jona, Acta Cryst., **13**, 225 (1960).
5. T.R. Shrout, D.A. Hukin, and L.E. Cross, Ferroelectrics Letters, **44**, 325 (1983).
6. Landolt Bornstein, Ferroelectrics and Related Substances, New Series, Vol. 16 (1981).

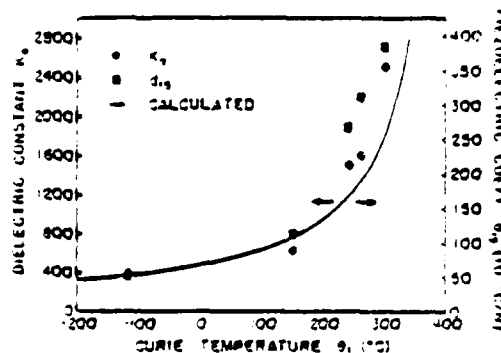


Figure 2. Experimental and calculated values of  $K_a$  and  $d_{15}$  as a function of  $\theta_1$ .

**APPENDIX 34**

# Longitudinal Piezoelectric Strain Measurements of Poly(vinylidene Fluoride) Films

K. UCHINO, *Department of Physical Electronics, Tokyo Institute of Technology, Ookayama, Meguro-ku, Tokyo 152, Japan*, and L. E. CROSS, *Materials Research Laboratory, The Pennsylvania State University, University Park, Pennsylvania 16802*

## Synopsis

The longitudinal piezoelectric strain of poly(vinylidene fluoride) (PVF<sub>2</sub>) films has been measured at room temperature using a high-sensitivity ac capacitance-type dilatometer. The dc bias field dependence of the piezoelectric strain coefficient  $d_{33}$  has been determined. The polarization-related electrostrictive coefficient  $Q_{33}$  obtained is several hundred times larger than the value in normal piezoelectric oxide crystals and is of opposite sign.

## INTRODUCTION

Poly(vinylidene fluoride) (PVF<sub>2</sub>) has been extensively studied since the discovery of its large piezoelectric coefficients in 1969.<sup>1</sup> Rolling and stretching films at elevated temperatures during preparation enhances the crystallization of the polar phase (form I) with polymer chains oriented preferentially along the tensile stress axis. After an electric field of sufficient magnitude (about  $10^8$  V m<sup>-1</sup>) is applied normal to the film at elevated temperatures, large piezoelectric coefficients can be measured. Though the transverse piezoelectric effect is rather easily detected, few studies have been attempted of the longitudinal piezoelectric strain  $x_3$  or stress  $X_3$  induced by an applied electric field  $E_3$  because of the thinness of films (usually less than 100  $\mu$ m). The first direct observation of the piezoelectric coefficient  $d_{33}$  (defined by  $x_3 = d_{33}E_3$ ) was made by Burkard and Pfister using a capacitance-type dilatometer.<sup>2</sup> They carried out static measurements at 0.3 K to avoid length fluctuations due to thermal expansion. Kepler and Anderson constructed an ac interferometric dilatometer and obtained the induced longitudinal strain.<sup>3</sup> On the other hand, the piezoelectric stress coefficient  $e_{33}$  ( $X_3 = e_{33}E_3$ ) was determined by Ohigashi.<sup>4</sup>

Using a newly developed high-sensitivity ac dilatometer,<sup>5,6</sup> we have measured precisely the longitudinal piezoelectric coefficients of PVF<sub>2</sub> films at room temperature. Moreover, we have observed the dc bias electric field dependence of the piezoelectric coefficient  $d_{33}$  (i.e., the electrostrictive effect).

## EXPERIMENTAL

Samples (30  $\times$  30 mm) were cut from 193- $\mu$ m-thick unoriented and 69- $\mu$ m-thick oriented Kynar 7200 sheets (Pennwalt Chemicals Co.) and from 25- $\mu$ m-thick oriented sheets obtained from Kureha Chemical Industries, after the samples

TABLE I  
Electromechanical Properties of Polarized PVF<sub>2</sub> Films (Compared with LiNbO<sub>3</sub>)

Coefficients	Unoriented Kynar	Oriented Kynar	Oriented Kureha	LiNbO <sub>3</sub>
$\epsilon_0$	9.9	11	12	28.7 <sup>a</sup>
$d_{31}$ ( $\times 10^{-12}$ m V <sup>-1</sup> )	4.3	16.1	21.2	-0.85 <sup>b</sup>
$d_{32}$ ( $\times 10^{-12}$ m V <sup>-1</sup> )	4.2	1.9	2.4	...
$d_{33}^{\text{eff}}$ ( $\times 10^{-12}$ m V <sup>-1</sup> )	-9	-19	-25	...
$d_{33}^{\text{eff}}$ ( $\times 10^{-12}$ m V <sup>-1</sup> )	-5.5 $\pm$ 0.2	-20.2 $\pm$ 0.4	-24.2 $\pm$ 0.6	6.73 <sup>c</sup>
$M_{33}$ ( $\times 10^{-10}$ m <sup>2</sup> V <sup>-2</sup> )	-3.6	-13.6	-34.1	...
$Q_{33}$ ( $\times 10^4$ C <sup>-2</sup> )	-5	-15	-30	0.016 <sup>a</sup>
$2Q_{33}\epsilon_0 d_{33}$ ( $\times 10^{-12}$ m V <sup>-1</sup> )	-4.4	-15	-31	5.3

<sup>a</sup> Reference 10.

<sup>b</sup> Reference 11.

<sup>c</sup> Measured with the present instrument.

had been poled in the manner described above. All the samples were kindly supplied by Dr. J. C. Hicks of the Naval Ocean Systems Center.

Two systems were used to measure the electric-field-induced strain in these sample films. For the transverse piezoelectric effect, a strain gauge technique was applied, the sample being placed so that the deformation produced a stress on a strain gauge. The piezoelectric coefficients  $d_{31}$  and  $d_{32}$  obtained are listed in Table I. The piezoelectric coefficient  $d_4$  ( $= d_{31} + d_{32} + d_{33}$ ) was determined with the conventional method of applying a time-varying hydrostatic pressure to the film. The values of  $d_4$  are roughly the same for the three specimens ( $d_4 \approx -1 \times 10^{-12}$  m V<sup>-1</sup>). From the values of  $d_{31}$ ,  $d_{32}$ , and  $d_4$ , we can evaluate the piezoelectric coefficient  $d_{33}$ , values of which are also shown in Table I.

For the longitudinal piezoelectric measurement we applied a newly developed high-sensitivity ac dilatometer whose minimum resolvable displacement is less

Block Diagram

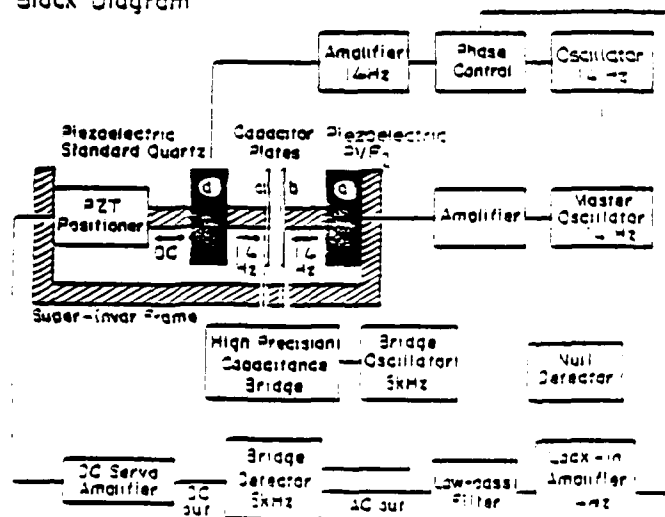


Fig. 1. Block diagram of high-sensitivity ac capacitance-type dilatometer.

than  $10^{-3}$  Å rms. Figure 1 shows the block diagram of this system, the details of which have been reported in our previous papers.<sup>5,6</sup> To measure the piezoelectric strain, an alternating electric field at 14 Hz is applied to the PVF<sub>2</sub> sample film through a suitable oscillator-amplifier combination, which sets the capacitor plate vibrating at 14 Hz. The lock-in amplifier, which is phase locked to the 14-Hz driving frequency, senses any component in the bridge output (capacitance modulation), which is at 14 Hz and in phase with the driving oscillator. To check the output calibration factor, a standard quartz crystal is then driven at 14 Hz without applying a voltage to the film.

To avoid separation changes of the sensing capacitor plates due to thermal expansion, the dc imbalance signal of the capacitance bridge is fed back to the PZT pushers through an amplifier. This servo-system is the key to the high sensitivity and stability of the instrument.

In Figures 2(a) and 2(b) we show the observed longitudinal strain (root-mean-square value) for oriented and unoriented Kynar and oriented Kureha films under a sinusoidal electric field at 14 Hz. The piezoelectric coefficient  $d_{33}$  is calculated from the slope of the linear relation between strain and electric field near zero field. Deviation from the straight line at higher electric fields is caused by the hysteresis effect and the nonlinear (higher-order) coupling. Determination of the negative sign of  $d_{33}$  is made from the 180° phase difference between the lock-in amplifier outputs of the PVF<sub>2</sub> films and the standard quartz crystal.

To obtain the electrostrictive effect separately from the hysteresis effect, we measured the dc bias field dependence of the piezoelectric coefficient  $d_{33}$ . When a dc electric field  $E_{dc}$  is superposed with a sinusoidal electric field  $\sqrt{2}E_{ac} \sin \omega t$ , the induced strain  $x_3$  is represented as

$$x_3 = d_{33}(E_{dc} + \sqrt{2}E_{ac} \sin \omega t) + M_{33}(E_{dc} + \sqrt{2}E_{ac} \sin \omega t)^2 \quad (1)$$

where  $M_{33}$  is the field-related electrostrictive coefficient. The root-mean-square value of the strain at a frequency of  $\omega$ ,  $x_3(\omega)$ , is given as

$$x_3(\omega) = d_{33}^{eff}(E_{dc})E_{ac} \quad (2)$$

where

$$d_{33}^{eff}(E_{dc}) = d_{33}[1 + (2M_{33}/d_{33})E_{dc}] \quad (3)$$

The lock-in amplifier output for a constant ac electric field ( $E_{ac} \approx 10^5$  V m<sup>-1</sup>) was plotted as a function of the dc electric field. Figures 3(a) and 3(b) show the change of the effective piezoelectric coefficient  $d_{33}^{eff}$  with the dc bias field  $E_{dc}$ . An obvious hysteresis curve could be obtained in the relation between  $d_{33}^{eff}$  and  $E_{dc}$  for all samples. The average change in  $d_{33}^{eff}$  (neglecting the hysteresis) with the dc field is considered to give the electrostrictive effect approximately. The piezoelectric coefficient  $d_{33}$  (experimentally observed) and the field-related electrostrictive coefficient  $M_{33}$  for three specimens are listed in Table I. For comparison, the electrostrictive coefficient  $M_{33}$  of the unpoled 69- $\mu$ m-thick oriented Kynar film was determined by the same technique as  $M_{33} = -5.5 \times 10^{-20}$  m<sup>2</sup> V<sup>-2</sup>.

It should be noted here that the electrostatic force between a pair of electrodes sometimes gives an extra displacement, especially in elastically soft materials with low permittivity. In the case of our measurements correction of the  $M_{33}$

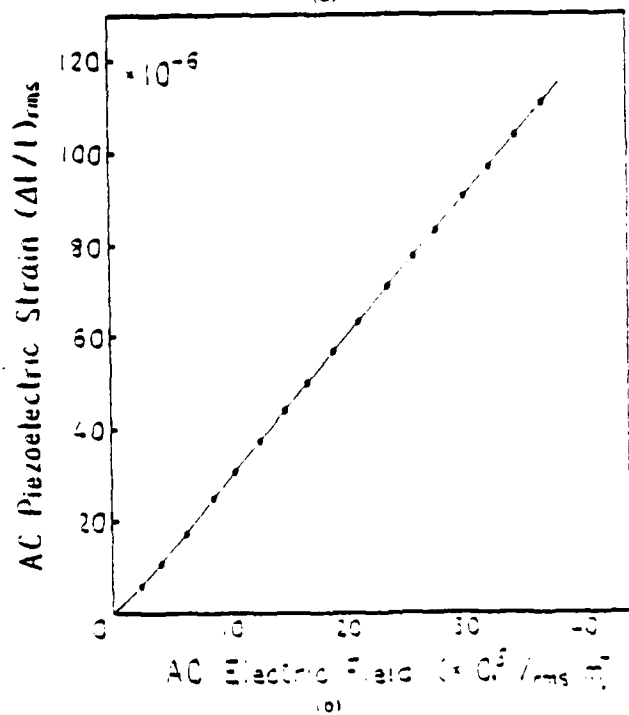
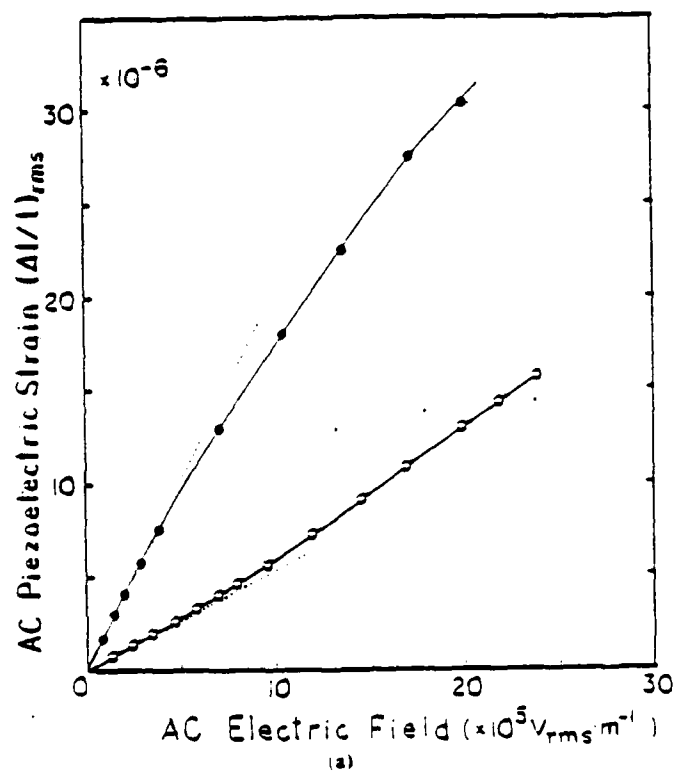


Fig. 2. Induced longitudinal strain under a sinusoidal electrical field at 14 Hz: (a) oriented Kynar (69  $\mu m$ ) and unoriented Kynar (200) (193  $\mu m$ ) and (b) oriented Kurena film (15  $\mu m$ ).

value due to the Maxwell stress is estimated as less than 10% of the apparent value.

### DISCUSSION

Oshiki and Fukada determined precisely the piezoelectric stress coefficient  $e_{31}$  and the electrostrictive stress coefficient  $\gamma_{31}$  (transverse effect) of PVF<sub>2</sub> by applying a sinusoidal electric field and detecting the induced stresses.<sup>7</sup> They reported a marked hysteresis curve of  $e_{31}$  with the cyclic change of the dc bias field, which is very similar to that in Figure 3, showing the dependence of  $d_{33}$  on the dc bias field. The low-frequency piezoelectric stress coefficient  $e_{31}$  decreases by about one order of magnitude from its room-temperature value of ca.  $10^{-2}$  C m<sup>-2</sup> on cooling the sample down to 123 K. At 0.3 K the longitudinal piezoelectric strain coefficient  $d_{33}$  measured by Burkard and Pfister is of the order of  $-10^{-13}$  to  $-10^{-12}$  m V<sup>-1</sup>.<sup>2</sup> The difference of one to two orders of magnitude between their data and our  $d_{33}$  values (which are close to the room-temperature results of Kepler and Anderson<sup>3</sup>) is explained by the large temperature dependence of  $d_{33}$ . Their electrostriction data were not so reliable as ours, but are still consistent with our measurement.

Using the piezoelectric resonance method, Ohigashi determined the piezoelectric strain coefficients ( $d_{31}$  and  $d_{32}$ ) and the piezoelectric stress coefficient  $e_{33}$  at high frequency.<sup>4</sup> At room temperature the  $d_{33}$  value (ca.  $-15 \times 10^{-12}$  m V<sup>-1</sup>) estimated from the approximate relation  $d_{33} \approx e_{33}/c_{33}^D$ , is almost of the same order as that from our low-frequency data. No electrostriction data could be obtained by the resonance method.

We discuss now a phenomenological interpretation of the piezoelectricity in poled PVF<sub>2</sub> in terms of electrostriction which was first introduced by Oshiki and Fukada.<sup>7</sup> After poling, a preferred orientation of dipoles is produced in the film, and results in the remanent polarization  $P_r$  and the remanent strain  $x_r$ . The coupling of the electrostriction (which may be determined by the film preparation technique) with this remanent polarization produces piezoelectricity. In the phenomenological expression, the strain  $x_3$  in the poled film of PVF<sub>2</sub> under a small electric field  $E_3$  is given by using the electrostrictive coefficient  $Q_{33}$  as

$$x_3 = Q_{33}(P_r + \epsilon_0 \epsilon_3 E_3)^2 \quad (4)$$

where  $\epsilon_3$  is the permittivity of PVF<sub>2</sub> and  $\epsilon_0 = 8.854 \times 10^{-12}$  F m<sup>-1</sup>. Then, by analogy with eq. (1) we may describe

$$x_r = Q_{33}P_r^2 \quad (5)$$

$$d_{33} = 2Q_{33}\epsilon_0\epsilon_3P_r \quad (6)$$

and

$$M_{33} = Q_{33}\epsilon_0\epsilon_3^2 \quad (7)$$

The polarization-related electrostrictive coefficient  $Q_{33}$  was calculated approximately as follows:

$$Q_{33} = M_{33}/\epsilon_0\epsilon_3^2 \quad (7')$$

By using  $P_r \approx 0.5 \times 10^{-2}$  cm<sup>-2</sup>, as roughly estimated by Hicks and Jones<sup>8</sup> in describing the effect of ac annealing on the remanent polarization, we can eval-



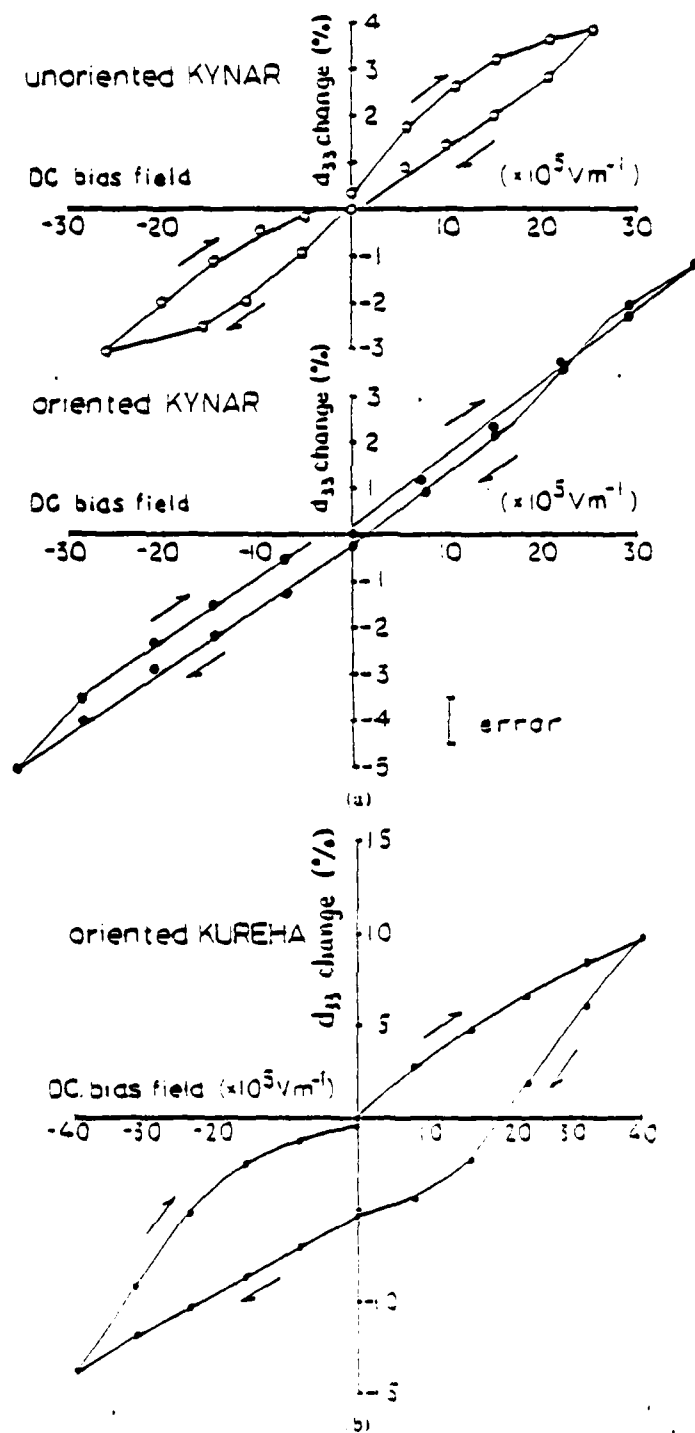


Fig. 3. Change of effective piezoelectric coefficient  $d_{33}$  with dc bias field  $E_{dc}$ : (a) in oriented and unoriented Kynar 7200 and (b) in oriented Kureha film.

uate the piezoelectric strain coefficient from eq. (6). Good agreement between the product  $2Q_{33}\epsilon_0\epsilon_3P_r$  and the observed  $d_{33}$  for all three specimens shown in Table I suggests the validity of the phenomenological treatment.

It is worth noting here, however, that the electrostrictive coefficient  $M_{33}$  of the unpoled oriented Kynar film is about half the value for the poled specimen. This is consistently explained by the commonly accepted assumption that an electrical poling process (as well as rolling and stretching) changes the microstructural conformation of PVF<sub>2</sub> in addition to the orientation of dipoles (see, e.g., ref. 9), and consequently varies the electrostrictive  $M_{33}$  coefficient. The validity of the phenomenological treatment should probably be discussed within the context of the same crystal structure.

Electromechanical data for a normal piezoelectric oxide LiNbO<sub>3</sub> are listed in Table I, for comparison. In addition to the sign difference of  $d_{33}$  and  $Q_{33}$ , it is interesting that the  $Q_{33}$  values in PVF<sub>2</sub> are two to three orders of magnitude larger than in LiNbO<sub>3</sub>, while the  $P_r$  values are two to three orders of magnitude smaller. In consequence, the piezoelectric coefficient  $d_{33}$  has almost the same magnitude (though with the opposite sign).

The authors would like to express their sincere thanks to Dr. J. C. Hicks of Naval Ocean Systems Center in San Diego, CA for supplying ready-poled PVF<sub>2</sub> samples. They also wish to thank the Office of Naval Research for their support of our work through Contract No. N00014-78-C-0291.

### References

1. H. Kawai, *Jpn. J. Appl. Phys.*, **8**, 975 (1969).
2. H. Burkard and G. Pfister, *J. Appl. Phys.*, **45**, 3360 (1974).
3. R. G. Kepler and R. A. Anderson, *J. Appl. Phys.*, **49**, 4490 (1978).
4. H. Ohigashi, *J. Appl. Phys.*, **47**, 949 (1976).
5. K. Uchino and L. E. Cross, Proc. 33rd. Annual Symposium on Frequency Control, U.S. Army Electronics Command, Fort Monmouth, NJ, 1979, p. 110.
6. K. Uchino and L. E. Cross, *Ferroelectrics*, **27**, 35 (1980).
7. M. Oshiki and E. Fukada, *J. Mater. Sci.*, **10**, 1 (1975).
8. J. C. Hicks and T. E. Jones, Proc. Meeting of Amer. Phys. Soc., No. 77.30, 1979.
9. N. Takahashi and A. Odajima, *Rep. Prog. Polym. Phys. Jpn.*, **22**, 151 (1979).
10. R. T. Smith and F. S. Welsh, *J. Appl. Phys.*, **42**, 2219 (1971).
11. T. Yamada, *J. Appl. Phys.*, **43**, 329 (1972).

Received July 30, 1982

Accepted November 29, 1982

**APPENDIX 35**

## SOME INTERESTING PROPERTIES OF DISLOCATION-FREE AND La-MODIFIED $\text{Sr}_{0.5}\text{Ba}_{0.5}\text{Nb}_2\text{O}_6$

S.T. Liu  
Honeywell Corporate Technology  
Center  
Bloomington, MN 55420

A.S. Bhalla  
Materials Research Laboratory  
The Pennsylvania State University  
University Park, PA 16802

Some properties of dislocation-free and rare-earth modified  $\text{Sr}_{0.5}\text{Ba}_{0.5}\text{Nb}_2\text{O}_6$  (SBN) ferroelectric crystals have been evaluated. The polarization of the dislocation-free SBN and some La-modified (82 atomic %) SBN crystals can survive repeated thermal cycles close to their Curie temperatures without being thermally depoled. Interesting properties relevant to pyroelectric, surface acoustic wave, and electro-optic devices are discussed.

### INTRODUCTION

Pure and lanthanum-modified ( $\text{Sr}_{0.5}\text{Ba}_{0.5-x}\text{La}_x\text{Nb}_2\text{O}_6$ ,  $x$  from 0 to 0.03) are interesting materials because they can be grown relatively easily in single crystals. These crystals are known to exhibit large pyroelectric effect, piezoelectric effect, and electro-optic effects.<sup>1</sup> These and most other ferroelectrics become partially depoled when operated close to their Curie temperature. However, we found recently that the polarization of the dislocation-free crystals<sup>2</sup> and some La-modified (82 atomic %) SBN crystals can survive repeated thermal cycle a few degrees within their Curie temperatures without being thermally depoled. This is shown in Fig. 1 for the pyroelectric properties:  $p$  and  $P_r$ .

The unusual stability displayed by the polarization will enable devices made from these crystals to operate over a wide range of temperature. The purpose of this paper is to reexamine the properties of these SBN crystals and to assess their potential applications as pyroelectric, surface acoustic wave and electro-optic devices.

### PYROELECTRIC PROPERTIES

Three different criteria have been used in selecting pyroelectric materials.<sup>3</sup> First,  $p/\sqrt{K}$  is used for minimizing the

pyroelectric voltage response in pyroelectric vidicon or pyroelectric/CCD. Second,  $p/c^E \sqrt{K \tan \delta}$  is used for minimizing the signal-to-noise ratio of pyroelectric detectors where the dielectric noise dominates in the normal mode point detectors. Third,  $p/c^E$  is used for selecting materials for transverse mode point detectors where fast response and wide bandwidth are important. Table 1 gives these three properties of the dislocation-free and La-modified SBN as compared to the most widely used pyroelectric materials; namely TGS<sup>6</sup> and LiTaO<sub>3</sub><sup>7</sup> (values of  $\tan \delta = 0.005$  used for TGS, 0.001 for others). From Table 1, it is clear that the dislocation-free SBN is a good choice for normal mode point detector application and La-modified SBN is an excellent choice for the transverse mode point detectors. The stability of the polarization of these crystals will enable these detectors to operate over a wide temperature range close to  $T_c$ .

Table 1

Materials	$(10^{-8} \frac{p}{cm^2 o_K})$	K	$\frac{C^E}{(e^3 o_K)} \times 10^{-11}$	$\frac{p}{C^E K} \times 10^{-11}$	$\frac{p}{C^E \sqrt{K \tan \delta}} \times 10^{-8}$	$\frac{p}{C^E} \times 10^{-8}$
SBN-50	5.5	400	2.34	5.88	3.72	2.35
LSBN-50 (2 atomic %)	11.7	1600	2.34	3.13	3.95	5.0
TGS	4.0	35	2.5	45.7	3.82	1.6
LiTaO <sub>3</sub>	1.9	46	3.2	12.9	2.75	0.39

#### SAW PROPERTIES

SAW devices have become an important application of piezoelectrics recently in signal processing areas such as filters, delay lines and convolvers. The two most important parameters are the SAW coupling factor ( $K^2$ ) for efficiency and the temperature coefficient of the delay time (TCD) for stability. These criteria are often not met in the piezoelectric materials except some with zero temperature compensation.

In a recent study by Shorrocks et al.<sup>9</sup>, it was predicted that the pure SBN-50 possesses a number of zero TCD orientations with reasonably high SAW coupling coefficient ( $K^2$ , approximately 0.03). A low TCD (7 ppm/°C) and high  $K^2$  (approximately 0.021) combination exists on ZX-SBN. Although TCD and  $K^2$  of dislocation-free SBN have not been measured, it is plausible to infer from nearly the same electro-elastic properties [9, 10] that the dislocation-free SBN-50

crystals will have nearly the same SAW properties. These properties together with the non-depoling property of these crystals make them the most promising materials for SAW devices.

#### ELECTRO-OPTIC PROPERTIES

The linear electro-optic effect in  $\text{Sr}_{1-x}\text{Ba}_x\text{Nb}_2\text{O}_6$  crystals has been studied by Lenzo et al.<sup>11</sup> By lowering the Ba content from  $x = 0.75$  toward 0.25 they show that the larger the dielectric constant is, the larger the electro-optic effect. We observe similar behavior in La-modified SBN by increasing the La-content.

Table 2 shows the effective linear electro-optic effect of La-modified SBN from measurement of half-wave voltage by propagating a He-Ne laser light along the a-axis of SBN crystal of length  $l$  while applying an electric field parallel to the c-axis. The reduced half-wave voltage is given by

$$V_{\lambda/2} = \lambda / (n_3^2 r_3) \quad (1)$$

where  $r_3 = r_{33} - (n_1/n_3)^3 r_{11}$  and  $n$ 's and  $r$ 's are indices of refraction and electro-optic coefficients respectively. The subscripts 1 and 3 refer to a-axis and c-axis of the crystals.

Samples for electro-optic measurement were rectangular parallelepipeds, typically 2mm on the side with the faces parallel to the principal axes. Samples for refractive index measurements were prisms with  $15^\circ$  apex angle, cut and oriented with c-axis parallel to the apex so that both  $n_3$  and  $n_1$  can be measured by a minimum deviation technique.<sup>12</sup> Also listed in Table 2 are pyroelectric and dielectric data.

Table 2

$y$	$n_1$	$n_3$	$K_{33}$	$p_3 (10^{-8} \frac{\text{C}}{\text{cm}^2 \text{k}})$	$V_{\lambda/2} (\text{V})$	$r_3 (10^{-8} \frac{\text{cm}}{\text{V}})$
0	2.27	2.23	400	5.5	396	1.45
0.002	2.27	2.23	425	5.7	375	1.52
0.008	2.28	2.24	780	7.6	280	2.01
0.02	2.29	2.24	1600	11.7	183	3.03
0.03	2.30	2.25	8000	25.0	83	6.70

From Table 2, the variation of  $r_j$  vs  $K_{jj}$  is seen to be similar to  $p_j$  vs  $K_{jj}$  and suggests a direct relationship between the two may exist. With the ferroelectrics treated as biased paraelectrics,  $r_j$  is related to  $K_{jj}$  by<sup>13</sup>

$$r_j = 2 K_{jj} \epsilon_0 g p_j \quad (2)$$

Where  $g$  is a generalized quadratic electro-optic coefficient. It has been shown that  $p_j$  is related to  $K_{jj}$  by<sup>14</sup>

$$p_j = K_{jj} P_g / C_c \quad (3)$$

where  $C_c$  is the Curie constant. Therefore,  $r_j$  and  $p_j$  are related by

$$r_j = 2 \epsilon_0 g C_c p_j \quad (4)$$

As a consequence, the figure of merit of electro-optic devices  $r_j^2/K_{jj}$  is proportional to  $p_j^2/K_{jj}$ . It has been shown that  $p_j^2/K_{jj}$  is relatively constant<sup>15</sup> so that  $r_j^2/K_{jj}$  will be relatively constant for these materials. Therefore, crystals of La-modified SBN provide good materials for the study of ferroelectric relationships. Because of the striation, these crystals of La-modified SBN have not been useful as electro-optic devices. They are still promising and may find applications as electro-optic devices if the striation problem were solved.

#### CONCLUSIONS

From the preceding discussions, we conclude that (1) both the dislocation-free and the La-modified SBN crystals are very good for pyroelectric detector applications; (2) the dislocation-free crystals are expected to be very good for SAW device applications; and (3) both dislocation-free and La-modified SBN-50 crystals are very good materials for the study of ferroelectric property relationships.

#### REFERENCES

- 1A. A.M. Glass, J. Appl. Phys. 40, (1969).
- 1B. S.T. Liu and R.B. MacIsaac, IEEE Int. Electron Device Meeting, Technical Digest, 259-262 (1973), Washington, D.C.
2. S.T. Liu and L.E. Cross, Phys. Stat. Sol. (a) 41, 831 (1977).
3. S.T. Liu, Am. Ceram. Society/IEEE Joint Fall Meeting, September 1978, Dallas, TX (unpublished).
4. R.B. MacIsaac, F.L. Schaffer, and S.T. Liu, J. Electron. Mat. 5, 415 (1976).

5. S.T. Liu and D. Long, *Proc. IEEE* **66**, 14 (1978).
6. H.P. Beerman, *Infrared Phys.* **15**, 225 (1975).
7. A.M. Glass, *J. Appl. Phys.* **40**, 4699 (1969).
8. A.J. Slobodnik, Jr., *Acoustic Surface Waves* (edited by A.A. Oliver, 1978, Springer) pp. 275-303.
9. N.M. Shorrocks, R.W. Whatmore, and S.T. Liu, *J. Phys. D: Appl. Phys.* **15**, 2469 (1982).
10. S.T. Liu, *Ferroelectrics* **22**, 709 (1978).
11. P. V. Lenzo, E.G. Spencer and A.A. Ballman, *Appl. Phys. Lett.* **11**, 23 (1967).
12. W.L. Bond, *J. Appl. Phys.* **36**, 1674 (1965).
13. J.D. Zook, D. Chen and G.N. Otto, *Appl. Phys. Lett.* **11**, 159 (1967).
14. S.T. Liu and J.D. Zook, *Ferroelectrics* **7**, 171 (1974).
15. J.D. Zook and S.T. Liu, *Ferroelectrics* **11**, 371 (1976).

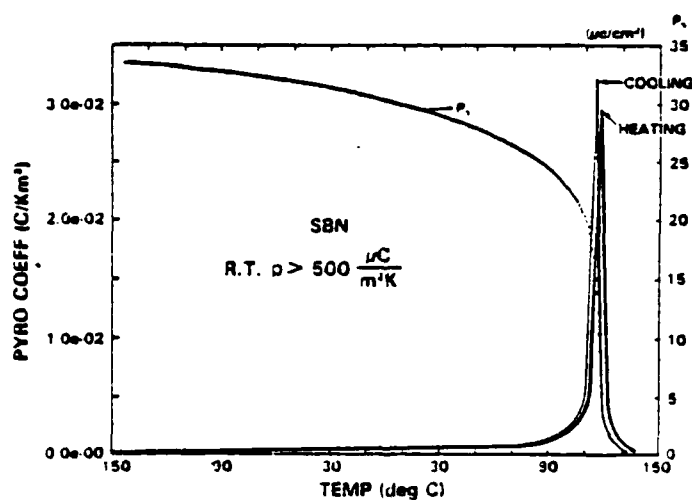


Figure 1. Thermal cycling of a dislocation free SBN-50 ( $T_c = 125^\circ\text{C}$  from dielectric peak)



# BASIC DISTRIBUTION LIST

Technical and Summary Reports

November 1979

<u>Organization</u>	<u>Copies</u>	<u>Organization</u>	<u>Copies</u>
Defense Documentation Center Cameron Station Alexandria, VA 22314	12	Naval Air Propulsion Test Center Trenton, NJ 08623 ATTN: Library	1
Office of Naval Research Department of the Navy 300 M. Quincy Street Arlington, VA 22217 ATTN: Code 471 Code 470	1 1	Naval Construction Battalion Civil Engineering Laboratory Port Hueneme, CA 93043 ATTN: Materials Division	1
Commanding Officer Office of Naval Research Branch Office Building 114, Section D 666 Summer Street Boston, MA 02210	1	Naval Electronics Laboratory San Diego, CA 92152 ATTN: Electron Materials Sciences Division	1
Commanding Officer Office of Naval Research Branch Office 536 South Clark Street Chicago, IL 60605	1	Naval Missile Center Materials Consultant Code 3312-1 Point Mugu, CA 92041	1
Office of Naval Research San Francisco Area Office One Hallidie Plaza Suite 601 San Francisco, CA 94102	1	Commanding Officer Naval Surface Weapons Center White Oak Laboratory Silver Spring, MD 20910 ATTN: Library	1
Naval Research Laboratory Washington, DC 20375 ATTN: Codes 6000 6100 6300 2627	1 1 1 1	Commander David W. Taylor Naval Ship Research and Development Center Bethesda, MD 20084	1
Naval Air Development Center Code 606 Warminster, PA 18974 ATTN: Mr. F. S. Williams	1	Naval Oceans Systems Center San Diego, CA 92132 ATTN: Library	1
		Naval Underwater System Center Newport, RI 02840 ATTN: Library	1
		Naval Postgraduate School Monterey, CA 93940 ATTN: Mechanical Engineering Department	1
		Naval Weapons Center China Lake, CA 93555 ATTN: Library	1

# BASIC DISTRIBUTION LIST (cont'd)

<u>Organization</u>	<u>Copies</u>	<u>Organization</u>	<u>Copies</u>
Naval Air Systems Command Washington, DC 20360 ATTN: Codes 52031 52032	1 1	NASA Lewis Research Center 21000 Brookpark Road Cleveland, OH 44135 ATTN: Library	1
Naval Sea System Command Washington, DC 20362 ATTN: Code 05R	1	National Bureau of Standards Washington, DC 20234 ATTN: Metals Science and Standards Division Ceramics Glass and Solid State Science Division Fracture and Deformation Division	1
Naval Facilities Engineering Command Alexandria, VA 22331 ATTN: Code 03	1	Director Applied Physics Laboratory University of Washington 1013 Northeast Fortieth Street Seattle, WA 98105	1
Scientific Advisor Commandant of the Marine Corps Washington, DC 20380 ATTN: Code AX	1	Defense Metals and Ceramics Information Center Battelle Memorial Institute 505 King Avenue Columbus, OH 43201	1
Army Research Office P. O. Box 12211 Triangle Park, NC 27709 ATTN: Metallurgy & Ceramics Program	1	Metals and Ceramics Division Oak Ridge National Laboratory P. O. Box X Oak Ridge, TN 37380	1
Army Materials and Mechanics Research Center Watertown, MA 02172 ATTN: Research Programs Office	1	Los Alamos Scientific Laboratory P. O. Box 1663 Los Alamos, NM 87544 ATTN: Report Librarian	1
Air Force Office of Scientific Research/NE Building 410 Bolling Air Force Base Washington, DC 20332 ATTN: Chemical Science Directorate Electronics & Materials Sciences Directorate	1 1	Argonne National Laboratory Metallurgy Division P. O. Box 229 Lemont, IL 60439	1
Air Force Materials Laboratory Wright-Patterson AFB Dayton, OH 45433	1	Brookhaven National Laboratory Technical Information Division Upton, Long Island New York 11973 ATTN: Research Library	1
Library Building 50, Room 134 Lawrence Radiation Laboratory Berkeley, CA	1	Office of Naval Research Branch Office 1030 East Green Street Pasadena, CA 91106	1
NASA Headquarters Washington, DC 20546 ATTN: Code RRM	1		

SUPPLEMENTARY DISTRIBUTION LIST A  
Electronic, Magnetic, and Optical Ceramics

032  
June 1980

Advanced Research Projects Agency  
Materials Science Director  
1400 Wilson Boulevard  
Arlington, VA 22209

Dr. Don Berlincourt  
Channel Products  
16722 Park Circle Drive W.  
Chagrin Falls, OH 44022

Dr. J. V. Biggers  
Pennsylvania State University  
Materials Research Laboratory  
University Park, PA 16802

Mr. George Boyer  
Sensor Systems Program  
Office of Naval Research  
Code 222  
Arlington, VA 22217

Professor R. Bradt  
Ceramics Section  
Materials Sciences Department  
The Pennsylvania State University  
University Park, PA 16802

Dr. Dean Buckner  
Piezo Products Division  
Gulton Industries  
P. O. Box 4300  
Fullerton, CA 92634

Dr. Robert Callahan  
Channel Industries  
339 Ward Drive  
Box 3680  
Santa Barbara, CA 93105

Professor L. E. Cross  
The Pennsylvania State University  
Materials Research Laboratory  
University Park, PA 16802

Mr. N. Gada  
Vice President for Engineering  
Erie Technological Products  
West College Avenue  
State College, PA 16802

Dr. Gene Haertling  
Motorola Corporation  
3434 Vassar, NE  
Albuquerque, NM 87107

Dr. W. B. Harrison  
Honeywell Ceramics Center  
1885 Douglas Drive  
Golden Valley, MN 55422

Dr. C. M. Stickley, V. P.  
The 30M Corporation  
7915 Jones Branch Drive  
McLean, VA 22102

Dr. L. L. Hench  
Department of Metallurgy  
University of Florida  
Gainesville, FL 32603

Dr. B. F. Rider  
Rockwell International  
400 Collins Road NE  
Cedar Rapids, IA 52406

Dr. F. Robert Hill  
Marine Resources  
755 Highway 17 492  
Fern Park, FL 32730

Dr. Bernard Jaffe  
232 Forbes Road  
Bedford, OH 44146

Dr. B. G. Koepke  
Honeywell, Inc.  
Corporate Research Center  
10701 Lyndale Avenue South  
Bloomington, MN 55420

Dr. R. Lapetina  
Eco Western Corporation  
2645 South 100 West  
Salt Lake City, UT 84115

Mr. G. LeBlond  
Naval Underwater Systems Center  
70101  
Newport, RI 02840

Dr. N. Perrone  
Code 474  
Office of Naval Research  
800 N. Quincy Street  
Arlington, VA 22217

Dr. Frank Recny  
General Electric Company  
Court Street  
Plant Building C  
Box 1122  
Syracuse, NY 13201

Dr. J. H. Rosolowski  
General Electric Company  
Research and Development Center  
P. O. Box 3  
Schenectady, NY 02301

Dr. P. L. Smith  
Naval Research Laboratory  
Code 6361  
Washington, DC 20375

Dr. R. W. Timme  
Naval Research Laboratory  
Code 3275  
Underwater Sound Reference Division  
P. O. Box 8337  
Orlando, FL 32806

Dr. Charles C. Walker  
Naval Sea Systems Command  
National Center #3  
2531 Jefferson Davis Highway  
Arlington, VA 20390

Dr. Paul D. Wilcox  
Sandia Laboratories  
Division 2521  
Albuquerque, NM 87115

The State University of New York  
at Alfred  
Material Sciences Division  
Alfred, NY

Dr. R. Rice  
Naval Research Laboratory  
Code 6360  
Washington, DC 20375

Professor R. Roy  
The Pennsylvania State University  
Materials Research Laboratory  
University Park, PA 16802

Dr. N. Tallan  
AFML Wright-Patterson AFB  
Dayton, OH 45433

Dr. H. E. Bennett  
Naval Weapons Center  
Code 3818  
China Lake, CA 93555

Dr. Michael Bell  
Inorganic Materials Division  
National Bureau of Standards  
Washington, DC 20234

Dr. R. Bratton  
Westinghouse Research Laboratory  
Pittsburgh, PA 15235

Dr. Joe Dougherty, Dir. Engr.  
Gulton Industries  
212 Durham Avenue  
Metuchen, NJ 08840

Dr. James Pappis  
Raytheon Co., Research Division  
28 Seyon Street  
Waltham, MA 02154

Dr. Perry A. Miles  
Raytheon Co., Research Division  
28 Seyon Street  
Waltham, MA 02154

Dr. P. E. D. Morgan  
Rockwell Science Center  
1049 Camino Dos Rios  
P. O. Box 1085  
Thousand Oaks, CA 91360

Dr. G. Ewell  
MS6-0163  
Hughes Aircraft Company  
Centinela & Teale Streets  
Culver City, CA 90230

Dr. David C. Hill  
Member Technical Staff  
Texas Instruments, Inc.  
Attleboro, MA 02703

Dr. S. K. Kurtz, V. P.  
Clairol, Inc.  
2 Blachley Road  
Stamford, CT 06902

Dr. Herb Moss  
RCA Laboratories  
Princeton, NJ 08540

Dr. R. E. Newnham  
Materials Research Laboratory  
The Pennsylvania State University  
University Park, PA 16802

Dr. Charles S. Sahagian, Chief  
EM Technology Branch, SSS Division  
HQ Rome Air Dev. Center (AFSC)  
Deputy for Electronic Technology  
Hanscom AFB, MA 01731

Dr. J. Smith  
GTE Sylvania  
100 Endicott Street  
Danvers, MA 01923

Dr. Wallace A. Smith  
North American Philips Laboratories  
345 Scarborough Road  
Briarcliff Manor, NY 10510

Mr. Raymond E. Sparks  
Technology Library R220  
Delco Electronics Division/GMC  
P. O. Box 1104  
Kokomo, IN 46901

Dr. Manfred Kann  
Senior Scientist, Prod. Dev.  
AVX Ceramics, P. O. Box 367  
Myrtle Beach, SC 29577

Mr. G. Goodman, Manager  
Corporation of Applied Research Group  
Globe-Union Inc.  
5757 North Green Bay Avenue  
Milwaukee, WI 53201

Dr. George W. Taylor  
Princeton Resources, Inc.  
P. O. Box 211  
Princeton, NJ 08540

Mr. John J. Thiermann  
Physics International  
2700 Merced Street  
San Leandro, CA 94577

Dr. D. Carson  
Code 7122  
Naval Ocean Systems Center  
San Diego, CA 92152

Dr. C. Hicks  
Code 631  
Naval Ocean Systems Center  
San Diego, CA 92152

Dr. R. Smith  
Code 7122  
Naval Ocean Systems Center  
San Diego, CA 92152

Professor R. Buchanan  
Department of Ceramic Engineering  
University of Illinois  
Urbana, Illinois 61801

Professor B. A. Auld  
Stanford University  
W. W. Hansen Laboratories of Physics  
Stanford, CA 94306

Dr. S. Musikant  
General Electric Co.  
3188 Chestnut Street  
Philadelphia, PA 19101

Dr. A. Gentile  
Hughes Research Laboratories  
3011 Malibu Canyon Road  
Malibu, CA 90265

Dr. J. Harrington  
Hughes Research Laboratories  
3011 Malibu Canyon Road  
Malibu, CA 90265

Professor E. Kino  
Stanford University  
Stanford, CA 94305

Dr. N. Macmillan  
Materials Research Laboratory  
The Pennsylvania State Univ.  
University Park, PA 16802

Mr. F. Markarian  
Naval Weapons Center  
China Lake, CA 93555

Mr. K.D. McHenry  
Yoneywell Corp. Tech. Center  
10701 Lyndale Avenue South  
Bloomington, MN 55420

Dr. R.R. Neurgaonkar  
Rockwell International Science Center  
1049 Camino Dos Rios  
PO Box 1085  
Thousand Oaks, CA 91360

Norton Company - Library  
Industrial Ceramics Division  
Worcester, MA 01606

James W. Pell  
Manager of Development  
Rohe Scientific Corporation  
2722 S. Fairview Street  
Santa Ana, CA 92704

Dr. R.C. Pohanka  
Room 619, Ballston Tower  
800 N. Quincy Street  
Arlington, VA 22217

Dr. R.A. Queeney  
126 Hammond Building  
The Pennsylvania State Univ.  
University Park, PA 16802

J.J. Rasmussen, Manager  
Applied Research Division  
Montana Energy and MHD R&D  
PO Box 3809  
Butte, Montana 59701

Dr. R. Ruh  
AFML, Wright-Patterson AFB  
Dayton, OH 45433

James Runt  
313 Steidle Bldg  
The Pennsylvania State Univ.  
University Park, PA 16802

Mr. G. Schmitt  
AFML, Wright-Patterson AFB  
Dayton, OH 45433

Dr. T. Sentementes  
GTE Sylvania  
100 Endicott Street  
Danvers, MA 01923

State University of New York  
College of Ceramics  
Alfred University  
Attn: Library  
Alfred, NY 14802

Dr. R.E. Tressler  
Ceramic Science Section  
226 Steidle Building  
The Pennsylvania State Univ.  
University Park, PA 16802

Eric Udd  
McDonnell Douglas Astron.  
5301 Bolsa Avenue  
Huntington Beach, CA 92647

Dr. T. Vasilos  
AVCO R & Adv. Dev. Division  
201 Lowell Street  
Wilmington, MA 01887

Mr. J.D. Walton  
Engineering Experiment Station  
Georgia Institute of Technology  
Atlanta, GA 30332

Mr. L.B. Weckesser  
Applied Physics Laboratory  
Johns Hopkins Road  
Laurel, MD 20810

Dr. N. Macmillan  
Materials Research Laboratory  
The Pennsylvania State Univ.  
University Park, PA 16802

Mr. F. Markarian  
Naval Weapons Center  
China Lake, CA 93555

Mr. K.D. McHenry  
Yoneywell Corp. Tech. Center  
10701 Lyndale Avenue South  
Bloomington, MN 55420

Dr. R.R. Neurgaonkar  
Rockwell International Science Center  
1049 Camino Dos Rios  
PO Box 1085  
Thousand Oaks, CA 91360

Norton Company - Library  
Industrial Ceramics Division  
Worcester, MA 01606

James W. Pell  
Manager of Development  
Rohe Scientific Corporation  
2722 S. Fairview Street  
Santa Ana, CA 92704

Dr. R.C. Pohanka  
Room 619, Ballston Tower  
800 N. Quincy Street  
Arlington, VA 22217

Dr. R.A. Queeney  
126 Hammond Building  
The Pennsylvania State Univ.  
University Park, PA 16802

J.J. Rasmussen, Manager  
Applied Research Division  
Montana Energy and MHD R&D  
PO Box 3809  
Butte, Montana 59701

Dr. R. Ruh  
AFML, Wright-Patterson AFB  
Dayton, OH 45433

James Runt  
313 Steidle Bldg  
The Pennsylvania State Univ.  
University Park, PA 16802

Mr. G. Schmitt  
AFML, Wright-Patterson AFB  
Dayton, OH 45433

Dr. T. Sentementes  
GTE Sylvania  
100 Endicott Street  
Danvers, MA 01923

State University of New York  
College of Ceramics  
Alfred University  
Attn: Library  
Alfred, NY 14802

Dr. R.E. Tressler  
Ceramic Science Section  
226 Steidle Building  
The Pennsylvania State Univ.  
University Park, PA 16802

Eric Udd  
McDonnell Douglas Astron.  
5301 Bolsa Avenue  
Huntington Beach, CA 92647

Dr. T. Vasilos  
AVCO R & Adv. Dev. Division  
201 Lowell Street  
Wilmington, MA 01887

Mr. J.D. Walton  
Engineering Experiment Station  
Georgia Institute of Technology  
Atlanta, GA 30332

Mr. L.B. Weckesser  
Applied Physics Laboratory  
Johns Hopkins Road  
Laurel, MD 20810

Dr. A. E. Clark  
Naval Surface Weapons Center  
White Oak Laboratory  
Silver Spring, MD 20910

Dr. Gordon Martin  
2627 Burgener  
San Diego CA 92110

Eric Udd  
McDonnell Douglas Astronautics  
5301 Bolsa Ave  
Huntington Beach CA 92647

Deborah Graves  
Ceramic Engineer  
Endevco  
Rancho Vie Jo Road  
San Juan Capistrano, CA 92675



Dr. David C. Hill  
Member Technical Staff  
Texas Instruments, Inc.  
Attleboro, MA 02703

Dr. S. K. Kurtz, V. P.  
Clairol, Inc.  
2 Blachley Road  
Stamford, CT 06902

Dr. Herb Moss  
RCA Laboratories  
Princeton, NJ 08540

Dr. R. E. Newnham  
Materials Research Laboratory  
The Pennsylvania State University  
University Park, PA 16802

Dr. Charles S. Sahagian, Chief  
EM Technology Branch, SSS Division  
HQ Rome Air Dev. Center (AFSC)  
Deputy for Electronic Technology  
Hanscom AFB, MA 01731

Dr. J. Smith  
GTE Sylvania  
100 Endicott Street  
Danvers, MA 01923

Dr. Wallace A. Smith  
North American Philips Laboratories  
345 Scarborough Road  
Briarcliff Manor, NY 10510

Mrs. Raymond E. Sparks  
Technology Library R220  
Delco Electronics Division/GMC  
P. O. Box 1104  
Kokomo, IN 46901

Dr. Manfred Kahn  
Senior Scientist, Prod. Dev.  
AVX Ceramics, P. O. Box 367  
Myrtle Beach, SC 29577

Mr. G. Goodman, Manager  
Corporation of Applied Research Group  
Globe-Union Inc.  
5757 North Green Bay Avenue  
Milwaukee, WI 53201

Dr. George W. Taylor  
Princeton Resources, Inc.  
P. O. Box 211  
Princeton, NJ 08540

Mr. John J. Thiermann  
Physics International  
2700 Merced Street  
San Leandro, CA 94577

Dr. D. Carson  
Code 7122  
Naval Ocean Systems Center  
San Diego, CA 92152

Dr. C. Hicks  
Code 631  
Naval Ocean Systems Center  
San Diego, CA 92152

Dr. R. Smith  
Code 7122  
Naval Ocean Systems Center  
San Diego, CA 92152

Professor R. Buchanan  
Department of Ceramic Engineering  
University of Illinois  
Urbana, Illinois 61801

Professor B. A. Auld  
Stanford University  
W. W. Hansen Laboratories of Physics  
Stanford, CA 94306

Dr. S. Musikant  
General Electric Co.  
3188 Chestnut Street  
Philadelphia, PA 19101

Dr. A. Gentile  
Hughes Research Laboratories  
3011 Malibu Canyon Road  
Malibu, CA 90265

Dr. J. Harrington  
Hughes Research Laboratories  
3011 Malibu Canyon Road  
Malibu, CA 90265

Professor G. Kino  
Stanford University  
Stanford, CA 94305